

# **Investigating the Role of USP9x and KrasG12D in Neural Stem Cell Proliferation and Development.**

**Caitlin R. F. Bridges,**  
*B.BMed.Sci (Hons)*

School of Sciences  
Science, Environment, Engineering and Technology  
Griffith University

Submitted in fulfilment of the requirements of the degree of  
Doctor of Philosophy

December 2015

<b>CONTENTS</b>	<b>Pages</b>
<b>LIST OF FIGURES.....</b>	<b>6</b>
<b>ABSTRACT.....</b>	<b>10</b>
<b>ABBREVIATIONS.....</b>	<b>12</b>
<b>ACKNOWLEDGEMENTS.....</b>	<b>15</b>
<b>1.0 CHAPTER ONE - GENERAL INTRODUCTION.....</b>	<b>17</b>
1.1 Neural Development.....	17
1.2 Neural / Cancer Stem Cell Hypothesis.....	19
1.3 Brain Cancer – Glioblastoma Multiforme .....	20
1.4 Gene Alterations determine GBM subtypes.....	22
1.5 Current Therapies used in treatment of brain cancer .....	24
1.6 Brain Cancer development in vivo .....	25
1.7 Dysregulation of cell cycle in cancer.....	27
1.8 G1 to S phase signalling pathways .....	29
1.9 The ubiquitin system .....	31
1.10 Regulation of proliferative brain cancer genes by ubiquitin .....	33
1.11 Ras signalling pathway.....	35
1.12 mTOR signalling pathway .....	37
1.13 PI3K signalling pathway .....	40
1.14 USP9x, Ubiquitin specific protease 9 X linked .....	42
1.15 USP9x and neural stem cells .....	43
1.16 USP9x and Cancer .....	44
1.16.a USP9x as a tumour suppressor .....	44
1.16.b USP9x as an oncogene .....	45
1.17 Broad project aims – Investigating the role of USP9x in brain cancer development .....	47
1.17.2 Aim 1: USP9x regulation of human neural stem cells .....	47
1.17.3 Aim 2: USP9x regulation of brain cancer cells, U-87 MG GBM cells .....	47
1.17.4 Aim 3: Investigating the consequence of USP9x deletion and co-activation of the KRasG12D oncogene in the developing forebrain.....	48
<b>2.0 CHAPTER TWO - MATERIALS AND METHODS</b>	
<b>2.1 Mammalian Tissue Culture.....</b>	<b>49</b>
2.1.1 Thawing stock cells from liquid nitrogen storage.....	49

2.1.2 Passage of Cells.....	49
2.1.3 Harvesting cells.....	49
2.1.4 Counting Cells for Seeding.....	49
2.1.5 ReNcell VM Cell Lines.....	50
2.1.6 Maintaining ReNcells VM.....	50
2.1.7 The Transducible lentiviral knockdown system.....	51
2.1.8 Real Time analysis of cultured cells using Xcelligence.....	51
2.1.9 MTT Assay.....	51
2.1.10 Inhibition of USP9X by WP1130.....	51
2.1.11 FLOW Cytometry Cell Cycle profile for ReNcell VM.....	52
2.1.12 Propidium Iodide Staining.....	52
2.1.13 Apoptosis Assays .....	52
2.1.14 Immunofluorescence – ReNcell VM cell differentiation .....	53
2.1.15 mTORC1 stimulation assay.....	53
2.1.16 Proteasomal inhibition – mTORC1 activity rescue experiments.....	53
2.1.17 Immunoprecipitation .....	54
2.1.18 Nucleofection of ReNcell VM cells .....	54
2.1.19 mTORC1 Plasmids .....	54
2.1.20 Maintaining U-87MG GBM cell lines .....	54
2.1.21 shRNA transduction of U-87MG cells.....	54
2.1.22 Lentiviral Plasmid Amplification for U-87MG .....	54
2.1.23 Cell Transduction for U-87MG. ....	55
2.1.24 293FT Viral Packaging Cell Line. ....	55
2.1.25 ViraPower Lentiviral Packaging .....	56
2.1.26 Transduction of U87MG GBM Cells. ....	56
2.1.27 USP9x siRNA interference in GBM cell lines .....	56
2.1.28 mTORC1 stimulation in USP9x depleted GBM cell lines. ....	57
2.1.29 Neurosphere dimensions.....	58
2.1.30 mTORC1 stimulation of Neurospheres.....	58
2.1.31 General Molecular Biology / Biochemistry Methods	
2.1.31.1 SDS PAGE and Western Blotting .....	58
2.1.31.2 Harvesting protein lysate .....	59
2.1.31.3 SDS PAGE preparation .....	59
2.1.31.4 Western Blotting preparation .....	59

2.1.31.5	<i>Immunoblotting and immunohistochemistry</i>	60
2.1.31.6	<i>Immunoblotting Procedure</i>	60
2.1.31.7	<i>Reprobing membrane</i>	62
2.1.32	<i>Animal Ethics</i>	62
2.1.33	<i>Genotyping Animals</i>	62
2.1.34	<i>In utero extraction – brain collection</i>	63
2.1.35	<i>Cryo-sectioning</i>	63
2.1.36	<i>Nissl Staining</i>	63
2.1.37	<i>Immunohistochemistry</i>	64
<b>3.0</b>	<b>CHAPTER THREE RESULTS – PUBLICATION</b>	
	<b>“USP9x regulation proliferation of neural progenitors primarily by mTORC1 signalling”</b>	
<b>3.1</b>	<b>Statement of Authorship</b>	<b>65</b>
<b>3.2</b>	<b>Introduction</b>	<b>66</b>
<b>3.3</b>	<b>Results</b>	<b>68</b>
3.3.1	<i>USP9X depletion results in reduced neural stem cell number</i>	69
3.3.2	<i>USP9X depletion does not result in morphological changes, apoptosis or differentiation of ReNcell VM</i>	68
3.3.3	<i>USP9X depletion results in G0/G1 cell cycle arrest</i>	78
3.3.4	<i>USP9X depletion in ReNcell VM cells reduces mTORC1 signalling</i>	83
3.3.5	<i>USP9X binds RAPTOR and regulates its levels</i>	86
3.3.6	<i>USP9X opposes proteasomal degradation of RAPTOR</i>	91
3.3.7	<i>USP9X null neurospheres have reduced neural progenitor proliferation but not stem cell self-renewal</i>	91
<b>3.4</b>	<b>Discussion</b>	<b>99</b>
<b>3.5</b>	<b>Supplementary Figures</b>	<b>104</b>
<b>4.0</b>	<b>CHAPTER FOUR RESULTS – USP9x depletion in U87MG GBM cells</b>	<b>106</b>
<b>4.1</b>	<b>Determining the effect of USP9x depletion from U-87 MG GBM Cells</b>	<b>106</b>
4.1.1	<i>Development of stable U-87 MG Cells with inducible USP9x knockdown</i>	106
4.1.2	<i>USP9x depletion from U87 MG GBM cells</i>	110
4.1.3	<i>mTORC1 activity in GBM cell lines following USP9x depletion</i>	112
<b>4.2</b>	<b>Discussion</b>	<b>116</b>

4.2.1	<i>Generation of inducible USP9x shRNA expression in U-87 MG GBM cells</i>	116
4.2.2	<i>mTORC1 signalling in GBM cells</i>	116
4.2.3	<i>Variation in mTORC1 activity in GBM cells</i>	117
<b>4.3</b>	<b>Supplementary Figures</b>	<b>119</b>
<b>5.0</b>	<b>CHAPTER FIVE RESULTS - Investigating the KrasG12D oncogene / Usp9x tumour suppressor nexus in neural progenitors</b>	<b>120</b>
<b>5.1</b>	<b><i>Determining the effect of KrasG12D activation in conjunction with Usp9x deletion on forebrain development</i></b>	<b>120</b>
5.1.1	<i>Generation of mice with activated KrasG12D and/or USP9x deletion in neural progenitors</i>	122
5.1.2	<i>Activation of KrasG12D results in peri-natal lethality</i>	124
5.1.3	<i>Activated KrasG12D results in gross morphological defects in the embryonic brain</i>	128
5.1.4	<i>KrasG12D expression disrupts the architecture of proliferative zones in late-but not mid-stage embryos</i>	134
5.1.5	<i>KrasG12D expression alters proportion of neural progenitors and neurons</i>	137
<b>5.2</b>	<b>Discussion</b>	<b>160</b>
5.2.1	<i>Mutant neural progenitors are sacrificed in vivo, in favour of intermediate progenitor expansion</i>	160
5.2.2	<i>mTORC1 activity and KrasG12D<sup>mutant</sup> signalling</i>	160
5.2.3	<i>Previous studies of KrasG12D activation in neural progenitors</i>	162
5.2.4	<i>KrasG12D<sup>mutant</sup> non-neural defects</i>	163
<b>5.3</b>	<b>Supplementary Figures</b>	<b>167</b>
<b>6.0</b>	<b>CHAPTER SIX – Conclusions and Future Directions</b>	<b>169</b>
<b>7.0</b>	<b>BIBLIOGRAPHY</b>	<b>170</b>
<b>8.0</b>	<b>APPENDIX – Submitted Manuscript</b>	<b>186</b>

## **LIST OF FIGURES**

### **1.0 CHAPTER ONE**

- Figure 1.1 Interkinetic Nuclear Migration of Polarised Neuroepithelial, Radial Glial and Basal Progenitors*
- Figure 1.2 Similarities between brain tumour initiating cells and neural stem cells*
- Figure 1.3 Altered gene expression leading to primary and secondary Glioblastoma development*
- Figure 1.4 Commonly mutated genes in GBM causing increased cell cycle progression.*
- Figure 1.5 Active immunity is effective in prolonging patient survival*
- Figure 1.6 Convergence of pathways involved in the maintenance of quiescence (G0 phase)*
- Figure 1.7 TGF- $\beta$  signalling transcribes G1-S phase inhibitors.*
- Figure 1.8 Cell Cycle and the proteins involved in G1 to S phase transition*
- Figure 1.9 Ubiquitin modification of substrates dictates fate.*
- Figure 1.10 Ras activation results in activation of multiple effector pathways including PI3K*
- Figure 1.11 mTOR complexes and signalling pathways*
- Figure 1.12 Akt regulation of downstream protein involved in other signalling pathways*
- Figure 1.13 PI3K signalling converging onto other signalling*

### **2.0 CHAPTER TWO**

- Figure 2.1 Representative packaging with virapower and lipofectamine*

### **3.0 CHAPTER THREE**

- Figure 3.1 USP9x depletion reduces ReNcells VM proliferation*
- Figure 3.2 USP9x depletion decreases density of ReNcells VM*
- Figure 3.3 Annexin V-Biotin Assay Dot Plot after 12hrs 1 $\mu$ M Dox addition and total Caspase 3 expression after 72hrs of 1 $\mu$ M Dox*
- Figure 3.4 USP9x depletion does not result in increased differentiation*
- Figure 3.5 No obvious increase in differentiation by immunofluorescence.*
- Figure 3.6 Immunofluorescence of differentiation markers, GFAP (Astrocytes),  $\beta$ -III tubulin (Neuron) over 9 days EGF and  $\beta$ FGF removal in presence of 1 $\mu$ M Dox*
- Figure 3.7 Loss of USP9x results in ReNcells VM accumulation in the G0/G1 phase of cell cycle*
- Figure 3.8 Expression of G1-S phase cell cycle proteins in USP9x depleted ReNcells VM after 24hrs, 36hrs and 72hrs of 1 $\mu$ M Dox addition.*

- Figure 3.9 mTORC1 activity and RAPTOR levels in ReNcells VM are dependent on USP9x*
- Figure 3.10 Proteasomal inhibition rescues USP9x-dependent p-S6 reduction after 15mins EGF/FGF stimulation*
- Figure 3.11 Reduction of RAPTOR expression in USP9x depleted ReNcells VM after EGF/FGF stimulation for 0, 5 and 15min.*
- Figure 3.12 USP9x binds RAPTOR in vivo and opposes its proteasomal degradation in neural progenitors*
- Figure 3.13. Representative reduction in neurosphere size in Usp9x KO*
- Figure 3.14. Reduction in diameter of E18.5 neurospheres in Usp9x KO compared to controls.*
- Figure 3.15. Increased expression of neuronal differentiation marker (NF160) in Usp9x KO E18.5 neurospheres.*
- Figure 3.16. mTORC1 activity is increased in Usp9x KOs at earlier time points.*
- Figure 3.17. mTORC1 activity remains repressed between 5min and 15min time course in ReNcells VM*
- Supplementary Figure 3.1 Investigating a physical association between USP9x and mTORC1 components in ReNcells VM*
- Supplementary Figure 3.2 Ectopic expression of mTORC1 plasmid in conjunction with USP9x plasmid expression*

#### **4.0 CHAPTER FOUR**

- Figure 4.1 U-87 MG cells express USP9x*
- Figure 4.2 FACS for GFP positive U-87 MG cells after lentiviral transduction failed to select a pure population*
- Figure 4.3 Single cell cloning isolated uniformly GFP-positive U-87 MG populations*
- Figure 4.4 Doxycycline inducible reduction in USP9x protein in U-87 MG cells after six days in culture*
- Figure 4.5 USP9x siRNA treatment fails to induce morphological changes in GBM cell lines*
- Figure 4.6 USP9x protein levels are reduced in GBM cell lines following 72hrs USP9x siRNA treatment.*
- Figure 4.7 mTORC1 activity in USP9x depleted GBM cell lines*

*Supplementary Figure 4.1 Densitometry of USP9x expression after six days 1 $\mu$ M Dox induction of USP9x shRNAs in U-87 MG cells*

## **5.0 CHAPTER FIVE**

- Figure 5.1 Generation of Kras/Usp9x<sup>mutant</sup> animals*
- Figure 5.2 Generation of Kras/Usp9x<sup>mutant</sup> embryos*
- Figure 5.3 Kras/Usp9x<sup>mutant</sup> genotype was not observed in weaned offspring*
- Figure 5.4 Kras/Usp9x<sup>mutant</sup> genotype is not observed in offspring*
- Figure 5.5 Kras/Usp9x<sup>mutant</sup> results in embryonic lethality*
- Figure 5.6 Kras/Usp9x<sup>mutant</sup> embryos are observed in the expected Mendelian ratios*
- Figure 5.7 Kras/Usp9x<sup>mutant</sup> mice display gross morphological defects*
- Figure 5.8 KrasG12D<sup>mutant</sup> embryos have the same phenotype as Kras/Usp9x<sup>mutant</sup> embryos*
- Figure 5.9 KrasG12D<sup>mutant</sup> have disrupted neural architecture at E17.5*
- Figure 5.10 Disrupted neural architecture of E17.5 KrasG12D<sup>mutant</sup> cortex*
- Figure 5.11 KrasG12D<sup>mutant</sup> has disrupted neural architecture at E16.5*
- Figure 5.12 Neural architecture is perturbed in E16.5 KrasG12D<sup>mutant</sup>*
- Figure 5.13 E16.5 KrasG12D<sup>mutant</sup> have cell debris in the ventricular space*
- Figure 5.14 KrasG12D<sup>mutant</sup> tissue fragility results in nonspecific and ubiquitous staining at E17.5*
- Figure 5.15 E14.5 KrasG12D<sup>mutant</sup> have increased ventricular space*
- Figure 5.16 Increased TBR2 and SOX2 expression in E16.5 KrasG12D<sup>mutant</sup> cortex*
- Figure 5.17 Beta-tubulin and G3PDH proteins are degraded in E16.5 KrasG12D<sup>mutant</sup>*
- Figure 5.18 Expression of neural markers in E14.5 KrasG12D<sup>mutant</sup>*
- Figure 5.19 Reduction in post-mitotic neurons at E14.5 in KrasG12D<sup>mutant</sup>*
- Figure 5.20 The number of intermediate progenitors at E14.5 in KrasG12D<sup>mutant</sup> is unchanged*
- Figure 5.21 The number of mitotic intermediate progenitors in E14.5 KrasG12D<sup>mutant</sup> is unchanged*
- Figure 5.22 Reduction in mitotic neural progenitors in E14.5 KrasG12D<sup>mutant</sup>*
- Figure 5.23 No neurospheres form from E16.5 KrasG12D<sup>mutant</sup>*
- Figure 5.24 Increased mean volume of neurospheres in E14.5 KrasG12D<sup>mutant</sup>*
- Figure 5.25 KrasG12D<sup>mutant</sup> neurosphere volume is initially increased*
- Figure 5.26 Increase in SOX2 expression in E14.5 KrasG12D<sup>mutant</sup> neurospheres*
- Figure 5.27 Reduced Ki67 in E14.5 KrasG12D<sup>mutant</sup> neurospheres*
- Figure 5.28 Reduction in mTORC1 activity in E14.5 KrasG12D<sup>mutant</sup> neurospheres*

*Supplementary Figure 5.1       $Kras/Usp9x^{mutant}$  genotype is not observed in offspring*

## ABSTRACT

All neural cell types of the brain are derived from neural progenitors (Götz and Huttner, 2005). Like all stem cells, neural progenitors / stem cells (NP/NSC) need to balance their capacity to self-renew, in order to maintain a stem cell pool, whilst maintaining the capacity to differentiate into neural and glial lineages. To achieve this balance NPs need to interpret multiple external signals arising from the stem cell niche or systemic circulation, and respond in a temporally and anatomically appropriate manner. This process occurs during both embryonic development of the brain as well homeostasis of NSCs in specialized niches in the adult. One protein ideally placed to coordinate NP/NSC responses to multiple signals and mediate rapid and quantitative responses is the deubiquitylating enzyme, USP9X. As a post-translational modifier USP9X can rapidly alter substrate levels and intracellular localisation without the need for gene transcription and translation. The balance between DUB and E3 ubiquitin ligase activity tightly regulates substrate levels. In addition, USP9X is highly expressed in NP/NSC *in vivo* and can regulate their responses *in vivo* and *in vitro*. The overarching aim of this project was to investigate the role of USP9X, if any, in the regulation of NP/NSC proliferation and by extension its putative role in brain cancer as either an oncogene or tumour suppressor.

In the first instance the effect of decreasing USP9x levels on the proliferation of a human neural stem cell line, ReNcell VM, was investigated. Depletion of USP9x protein levels by inducible shRNA interference in ReNcell VM, resulted in a significant and rapid reduction in cell number within 24hrs as determined using xCelligence real time analysis. This was not due to increased cell apoptosis, nor increased differentiation, but rather to an accumulation of cells in the G0/G1 phase of cell cycle. The accumulation of cells in G0/G1 phase, corresponded with reduced mTORC1 signalling as measured by decreased pS6 expression. Further investigation revealed that USP9X maintains the levels of RAPTOR, the defining mTORC1 scaffolding protein. In addition, the data show USP9X opposes the proteasomal degradation of RAPTOR in ReNcell VM cells. Using immunoprecipitation, we detected an interaction between endogenous Usp9x and Raptor in mouse embryonic day 16.5 (E16.5) brain lysates. Analysis of neurospheres isolated from E18.5 Usp9x KO mice revealed a reduction in sphere diameter, which not only supports a role for Usp9x in maintaining NP proliferation, but which phenocopies Raptor-null neurospheres. These data strongly implicate USP9x directly, in the regulation of mTORC1 signalling in the neural progenitors via stabilisation of RAPTOR. USP9X is the first DUB shown to directly bind and regulate RAPTOR.

USP9x has also been identified as an oncogene in lymphomas, chronic myeloid leukaemia and multiple myeloma (Schwickart et al., 2010) as well as a tumour suppressor in both pancreatic ductal adenocarcinoma and skin papilloma (Dupont et al., 2009). In the latter instance USP9X acts as tumour suppressor downstream of activated Kras (KrasG12D) where it rapidly progresses neoplastic cells into full adenocarcinoma, and promotes their metastases. As USP9x is known to have a role in neural stem cell regulation, the second aim of this thesis was to investigate if USP9x plays a role in brain cancer progression or development. Glioblastoma multiforme (GBM) is one of the deadliest brain cancers and initially, several GBM cells lines were obtained. To determine USP9x's role, if any, in GBM mTORC1 activity was investigated after USP9x depletion in the GBM lines. In contrast to ReNcell VM an increase in mTORC1 activity was observed indicating USP9x may suppress proliferative mTORC1 activity in some GBM tumours. This suggested USP9x may act as a tumour suppressor in GBM, similar to its role in KrasG12D mediated pancreatic cancer transformation (Pérez-Mancera et al., 2012). Therefore, a similar approach was taken to activate KrasG12D in conjunction with Usp9x deletion from the forebrain of mice to determine if the rate of tumour development was accelerated.

However, it was observed that activation of KrasG12D expression alone was sufficient to dramatically alter embryonic brain development. No offspring, with the active mutation, survived after birth. Analysis of late stage embryos revealed severely disorganised neocortical structure with no defined cortical layering consistent with the amplification of progenitor cells. Cerebral swelling and tissue fragility were also features in late stage embryos, and neurospheres could not be propagated. This result was somewhat surprising as previously, the activation of KrasG12D alone from neural progenitors results in glial tumour formation only after months (Ghazi et al., 2012, Holmen and Williams, 2005), which is reduced to weeks once on a background of tumour suppressor deletion.

Timely and controlled neural progenitor proliferation is crucial for appropriate progenitor expansion and differentiation. The data presented herein show that these processes can be strongly affected by disrupting substrate regulators, such as the post-translational modifying protein USP9x, or by the activation of major oncogenic proteins, such as KrasG12D.

## ABBREVIATIONS

2193 -	<i>USP9x targeted sequence See Materials and Method (2.1.5)</i>
4774 -	<i>USP9x targeted sequence See Materials and Methods (2.1.5)</i>
ASK1 -	<i>Apoptosis signal regulating kinase 1</i>
BLBP -	<i>Brain Lipid Binding Protein</i>
BMP -	<i>Bone morphic protein</i>
CDK -	<i>Cyclin Dependent Kinase</i>
CDKN2A -	<i>Cyclin-dependent kinase Inhibitor 2A</i>
CNS -	<i>Central Nervous System</i>
Cre –	<i>Cre recombinase, excises DNA between two loxP sites</i>
CTL –	<i>Cytotoxic T lymphocytes</i>
Dox –	<i>Doxycycline</i>
DUB -	<i>Deubiquitylating enzyme</i>
E2F1 -	<i>E2 factor 1</i>
EGF –	<i>Epidermal growth factor</i>
EGFR –	<i>Epidermal growth factor receptor</i>
ERK -	<i>Extracellular signal-regulated kinase</i>
FACS –	<i>Fluorescent activated cell sorting</i>
FGF –	<i>Fibroblast growth factor</i>
Floxed –	<i>Gene is flanked by loxP sites</i>
GBM -	<i>Glioblastoma Multiform</i>
GFAP -	<i>Glial fibrillary acidic protein</i>
GFP –	<i>Green Fluorescent Protein</i>
GSK3 -	<i>Glycogen synthase kinase-3</i>
HGF –	<i>Heparin growth factor</i>
KO -	<i>Knockout</i>
KD -	<i>Knockdown</i>

<i>Kras</i> -	<i>Kirsten Rat Sarcoma Viral Oncogene Homolog</i>
<i>KrasG12D</i> -	<i>Kirsten Rat Sarcoma Viral Oncogene Homolog Glycine to Aspartate at position 12</i>
<i>MAPK</i> –	<i>p38 mitogen activated protein kinase</i>
<i>MCL1</i> -	<i>Myeloid cell leukaemia sequence 1</i>
<i>MGMT</i> -	<i>O6methylguanine-DNA methyltransferase</i>
<i>mTOR</i> -	<i>Mammalian target of Rapamycin (Complex 1: mOTRC1, Complex 2 mTORC2)</i>
<i>NF1</i> -	<i>Neurofibromatosis 1</i>
<i>NP</i> -	<i>Neural Progenitors</i>
<i>NSC</i> -	<i>Neural Stem cells</i>
<i>PDA</i> -	<i>Pancreatic ductal adenocarcinoma</i>
<i>PDGFRA</i> -	<i>Platelet-Derived Growth Factor Receptor, Alpha Polypeptide</i>
<i>PH3</i> -	<i>Phospho-Histone 3</i>
<i>PI3K</i> -	<i>Phosphoinositide 3-kinase</i>
<i>PTEN</i> -	<i>Phosphatase and tensin homolog</i>
<i>Ras</i> –	<i>Rat Sarcoma Viral Oncogene homolog</i>
<i>Rb</i> –	<i>Retinoblastoma Protein (pRb phosphorylated form)</i>
<i>RTK</i> -	<i>Receptor tyrosine kinase</i>
<i>S6</i> -	<i>S6 protein (pS6 phosphorylated form)</i>
<i>S6K</i> -	<i>S6 Kinase (pp70S6K)</i>
<i>Scr</i> –	<i>Scrambled non targeting sequence (siRNA and shRNA)</i>
<i>SVZ</i> -	<i>Sub ventricular zone</i>
<i>TBR1</i> -	<i>T-Box Brain 1</i>
<i>TBR2</i> -	<i>T-Box Brain 2</i>
<i>TGF-β</i> –	<i>Transforming growth factor beta</i>
<i>TMZ</i> -	<i>Temozolomide</i>
<i>TP53</i> –	<i>Tumour protein p53</i>

*TSC* - *Tuberous sclerosis complex*  
*Ub* - *Ubiquitin*  
*USP9x* – *Ubiquitin Specific Protease 9, X linked*  
*VZ* - *Ventricular zone*  
*Wnt* – *Wingless and Integrase family / pathway*

#### NOMENCLATURE

*USP9x* – *Capitals, non-italic - Human USP9x protein*  
*USP9x* – *Capitals italic – Human USP9x DNA*  
*Usp9x* – *Lowercase, non-italic – Mouse Usp9x protein*  
*Usp9x* – *Lowercase, italics – Mouse Usp9x DNA*  
*KrasG12D* - *Non-italic, protein*  
*KrasG12D* - *Italic, DNA or modified allele*

## **ACKNOWLEDGMENTS**

### **A/Prof Stephen Wood**

I would like to thank my primary supervisor A/Prof Stephen Andrew Wood. He will cringe at the inclusion of his middle name.

Stephen, you have not only been a supervisor to me, but also a mentor, father, friend, sounding board and on many occasions, the man with the tissues ☺ I would have recommended that you had kept the receipt for taking on this PhD student, and traded in the goods a long time back. But I am incredible grateful that you didn't. I am sure that I have made a significant contribution to the percentage of grey hairs acquired over the past four years ( $N = 3$ ,  $P < 0.00000001$ ).

You have always been encouraging and so supportive. You always have an open door policy, which is rare and hard to come by. This extends not only to your students, which is also incredibly rare. I am so glad to have been under a caring wing and to be surrounded by someone who values the science, not who you know.

Sometimes I feel that I had lost my passion for research at multiple times during my PhD. In part because my reasons for embarking into neural science were becoming a distant memory I felt I could no longer grasp. The realisation that nothing I do in research can bring back a loved one who has passed from a neural disease seems obvious, but the fantasy was easier to live for. You changed my perspective on this which helped me claw through the final stages.

“If the cure to brain cancer is 20 years away, but you connect a dot that shortens that timescale by 5 years, that is still a significant contribution to the cure”

Thank you for getting me through ☺

### **Mum and Dad**

The amount of times I have annoyed you with my nonsense about my mice, my cells and my western blots.....There will be more of this to come I'm sure.

I am confident that you are at a point where you probably know a lot more about molecular biology than I do. The amount of presentations, theses, and posters that I have forced you to sit through extends beyond the number of phalanges on your hands and feet. Mum, I remember the first time I told you how my western blot failed, and you asked me why I was watching cowboy films at work anyway? Now, I come to you for advice regarding the amount of reduction in USP9x expression you feel you can observe visually, to determine if my densitometry reflects this assessment.

You have both been so supportive of me throughout these years. I have wanted to quit on multiple occasions, especially when experiments don't work, or they work transiently.....when it's a full moon and you don't look sideways at it. But you have both told me that it will pass. You will get through it. You have always told me that my PhD doesn't define me, and that I am not a quitter.

I am so lucky to have you both as parents and thank you so much for all your support through all the good times and the tearful ones. I love you more than anyone else in this world.

### **Mealz**

I hope that you are flying high. I wish that there were a way to bring you back to us. We miss you like crazy. I hope that there will be a way in the not too distant future to prevent anyone else so young from dying from such a horrible disease. I hope that I am apart of this contribution one day.

### **Wood Lab**

You guys are the best group. Susitha, you are genius. I have never met a man so talented at a lab bench. You are by far the best scientist that I have worked with, and in all honesty you are probably the best scientist that I have ever met. You are such a gentle soul, a dedicated worker and extremely quick witted guy. I am going to miss you incredibly. Devathri (Nana) I can't thank you enough for all your calmness, fruit and hugs. You have always been behind my cubicle to console me when analysis goes awry, Word decided to crash or you hear frustrated breathing during image analysis. You too are an amazing scientist, you pay so much attention to the fine and critical details which makes experiments almost perfect....okay perfect ☺. Mariyam, thank you for all your support inside and outside of the lab, again, thank you for your calmness in situations when I have got overly stressed. You have worked through problems step by step with me and helped suggest a lot of technical variations of certain protocols that I would not have considered if it weren't for you. They usually made all the difference to the outcome of some experiments.

### **JTV**

Mother hen, without you, all your chicks would be in a Bain Marie somewhere in Woolworths or Coles. You are the glue that held three lab groups together. You are always there for everyone, you give all, beyond anyone's expectations of a friend. You think of everyone expect for yourself. I have never met anyone as self-less as you. I am so excited to have finished along side you. The corks will be popping soon hopefully.

### **JPC**

The world works in mysterious ways. Peter Pan, you have taught me to laugh and feel safe again. You have given me an escape from my mind. You have taught me to do things for me, not only everyone else. You have given me nothing but love and care. Everything you do has the best of intentions. I love you.

## **1.0 CHAPTER ONE - General Introduction**

### ***1.1 Neural Development***

Neural progenitors arise from the highly polarised neuroepithelial cell layer of the embryonic neural plate of the developing embryo (Götz and Huttner, 2005). The cells of the neuroepithelia are neural stem cells which ultimately give rise to all neuronal and glial cell types within the CNS (Corbin et al., 2008, Tamai et al., 2007, Takanaga et al., 2009, Tohyama et al., 1992). Therefore, intricate control of their proliferation and fate is critical for the appropriate development of subsequent cell types. Proliferation and expansion of the neuroepithelial layer is initiated to establish the neural stem cell niche and prepare for differentiation into fate-restricted lineages, occurring later during the processes of neurogenesis and gliogenesis. The length of the G1 phase of the cell cycle plays an important role in the regulation of neuroepithelial fates and proliferation. If the G1 phase is short, symmetric division of the neuroepithelial cells prevails, resulting in neural stem cell (NSC) self-renewal and expansion of the population (Calegari and Huttner, 2003).

As embryogenesis progresses, the length of the G1 phase of the cell cycle is increased in neuroepithelial cells (Götz and Huttner, 2005), resulting in more asymmetric cell divisions and the generations of daughter cells with post-mitotic neuronal fates, that is, neurogenesis (Calegari and Huttner, 2003)(Figure 1.1). In the same process neuroepithelial cells can also transition into another type of neural stem cell namely, radial glial progenitors (Takahashi et al., 1995, Corbin et al., 2008). These cells share properties of both neuroepithelia and astroglia, expressing markers Nestin, SOX2 (both NSC markers), BLBP and GFAP (astrocyte markers). They extend their cell body from the apical ventricular zone to the basal lamina at the pial surface. Radial glial progenitors undergo mitosis at the apical surface, to give rise to neurons, astrocytes, radial glial progenitors (Götz and Huttner, 2005) or TBR2-positive intermediate basal progenitor cells (Malatesta et al., 2000) (Figure 1.1). Intermediate basal progenitors detach from the apical surface of the ventricular zone at the beginning of neurogenesis and migrate basally, forming the sub-ventricular zone. Here, they undergo a limited number of symmetric mitoses within the SVZ, giving rise to post-mitotic daughter neurons; the future neurons of the developing cortex (Figure 1.1).

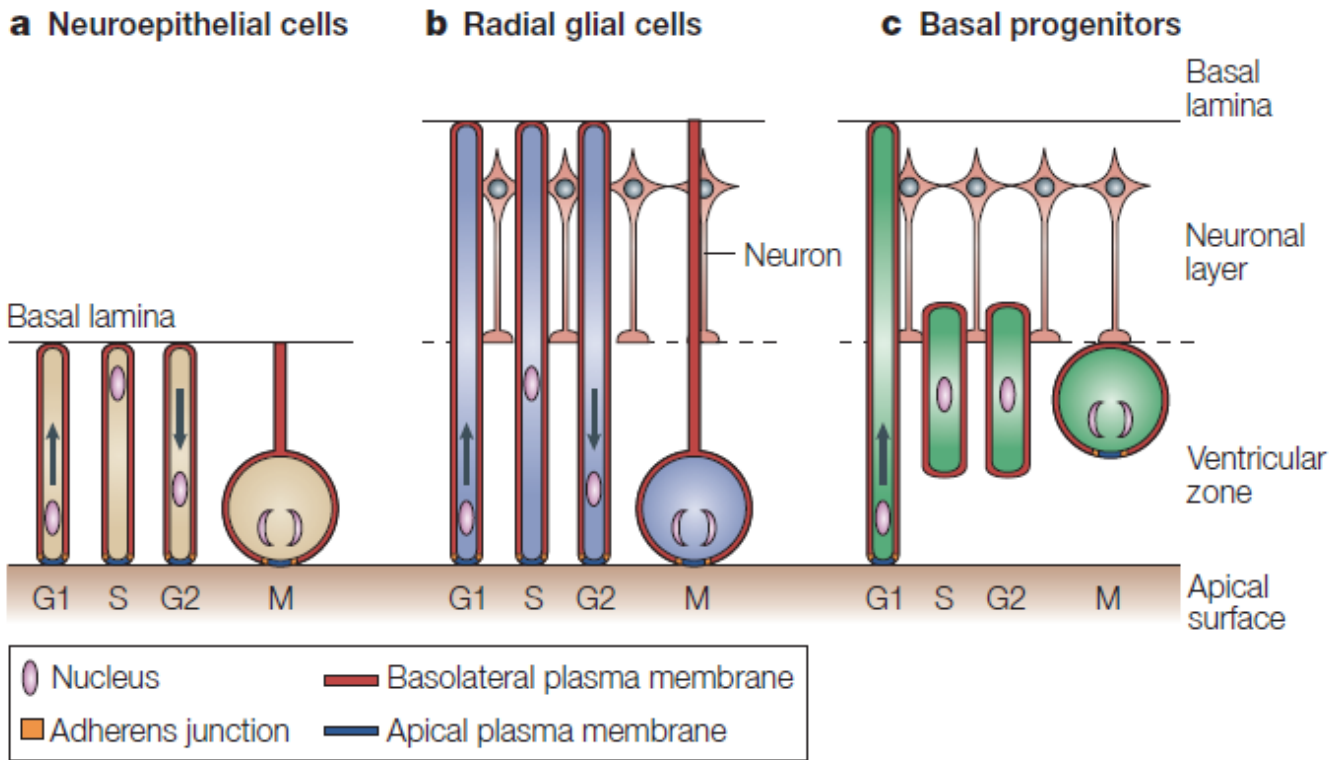


**Figure 1.1. Interkinetic Nuclear Migration of Polarised Neuroepithelial, Radial Glia and Basal Progenitors.** (A) In the neuroepithelial cells, the nucleus migrates along the entire apical-basal length during G1 phase, reaching the basal lamina during S phase and migrating back the apical axis during G2 Phase, only to divide at the apical surface (M phase). (B) In radial glia cells, nuclear migration that occurs during S phase ceases at the apical-basal boundary and returns to the apical membrane in G2, dividing at the apical membrane. (C) In basal progenitors, the nucleus migrates to the basal surface of the ventricular zone, as for radial glial progenitors, whilst detaching from the apical surface during S phase and G2 phase before dividing at the basal surface of the ventricular zone. (Gotz and Huttner 2005)(Reviewed by Gotz and Huttner, 2005, Licence # 3726830908686)

Considering that each neural progenitor cell type (neuroepithelia, radial-glia and intermediate) dictates not only their own proliferation and fate but those of their derivatives, mutations affecting cell division and proliferation can have a dramatic outcome on the composition, and therefore the function, of the brain. It is not unreasonable to suggest that mutations affecting early neural progenitors will have the greatest impact on terminally differentiated neural cell function. Dysfunction of neural progenitors occurs in a variety of neurodevelopmental disorder's including schizophrenia (Brown et al., 2014), epilepsy (Lugert et al., 2010) and mental retardation (Reif et al., 2006, Waldaun and Shetty, 2008). It is also common in the development of neural tumours. Neural tumour cells can propagate an entire tumour from one cell (Chen et al., 2012), just as a neural progenitor propagates an entire subset of neural cells in the brain (Götz and Huttner, 2005). Mutations of tumour suppressor genes and activation of

oncogenes including TP53, PTEN, c-myc, PDGFRA and EGFR, have been commonly reported in brain cancers such as GBM. These genes, when mutated in healthy neural, radial-glia, or astroglial progenitors, can lead to either the survival of quiescent cells or an uncontrolled cellular proliferation, by increasing progression through the cell cycle. These hyper-proliferative cells divide, expand and infiltrate healthy neighbouring neural tissues in an uncontrolled manner resulting in neural tumours.

There are many similarities between neural progenitors and brain cancer stem cells (Sandberg et al., 2013, Qiao et al., 2013). They can both proliferate, self-renew, differentiate and give rise to entire tissues, all through common signalling pathways including Notch, Wnt, mTORC1, pRb and p53 (Zohrabian et al., 2009, Albert et al., 2009). The difference being, that these processes and pathways become dysregulated or unable to be switched off in brain cancers. Therefore, understanding how stem cell propagation, proliferation and differentiation occurs in healthy neural progenitors and observing how the cell cycle and signalling pathways can be perturbed in brain cancer, is critical in comprehending how healthy neural progenitor cells become cancerous. This would assist the development of therapies that target the mutated neural progenitor of origin, which improves on the current method of treatments targeting the bulk of the tumour but not necessarily the cancer-initiating cell.

## **1.2 Neural / Cancer Stem Cell Hypothesis**

The cancer stem cell hypothesis has been a hot topic for several years. In theory the derivation of cancer can occur from a single mutated cell, whether this is a stem cell capable of giving rise to multiple cell types remains to be confirmed. Many types of cancer cells can metastasise from the primary site into other organs, where they proliferate and divide causing invasion into surrounding tissues. Aggressive brain cancer, on the other hand, does not metastasise outside the CNS, but may result from mutations in a population of stem cells creating cancer-like stem cells (Beghini et al., 2003, Qiang et al., 2009). Cancer-like stem cells have been isolated from GBM cell lines derived from patient tumours, creating a homogenous population of “cancer stem cells” and have been characterised as stem cells according to the presence of common neural stem cell markers (Beghini et al. 2003, Qiang et al. 2009). In these populations decreased expression of neuronal and astrocytic markers has been observed indicating these cells are undifferentiated (Qiang et al., 2009). However, it has been shown that the isolation of these “stem cells” alone is not always effective at recapitulating the tumour *in vivo*. One reason for this is the markers used to isolate “stem-cells” are simply upregulated or expressed within

the tumour cells, as cancer cells undergo frequent mutation. Instead the use of neurosphere forming assays from dissected tumour, to propagate true stem cells that are capable of self-renew, in conjunction with *in vivo* transplantation of the original tumour cells, has provided stronger evidence for the existence of glioma-initiating stem cells (Pavon et al., 2013). These cells give rise to a heterogeneous population of tumour cells, just as a neural stem cell gives rise to a heterogeneous population of neural cells, (Figure 1.2). The true determinant of defining a brain tumour initiating cell is its ability to recapitulate the original tumour *in vivo*.

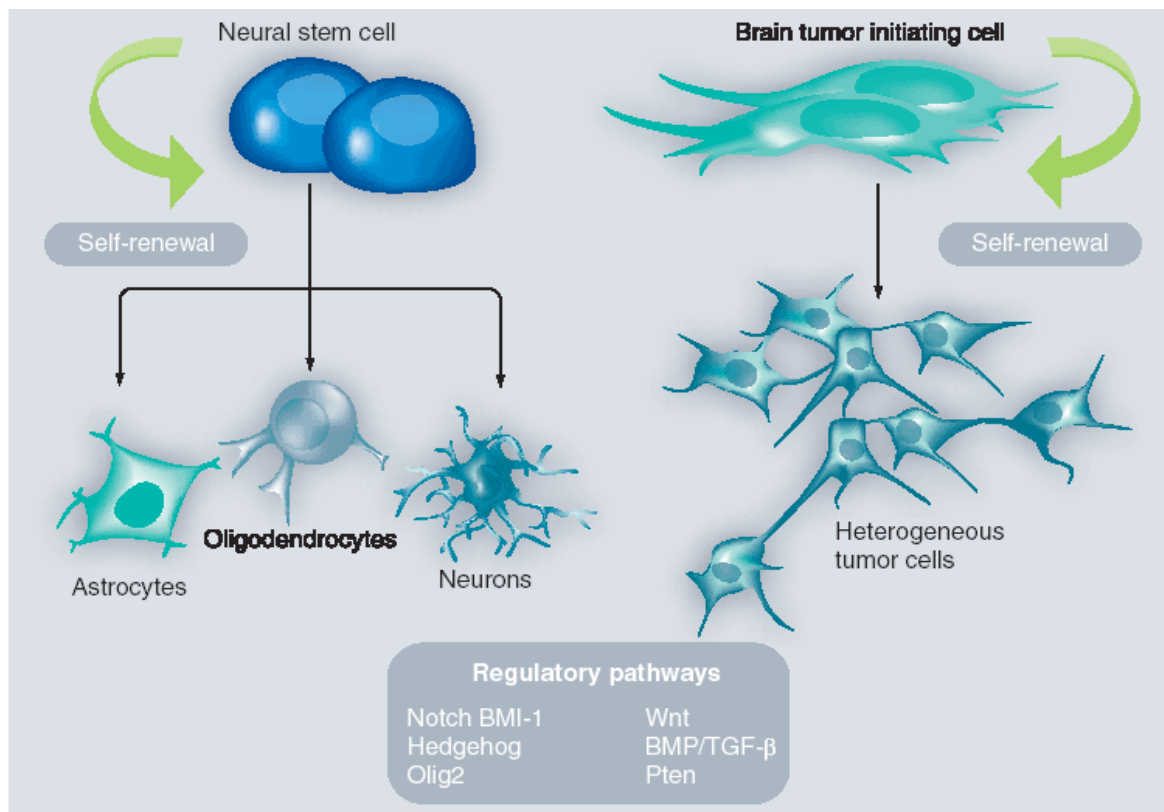


**Figure 1.2 Similarities between brain tumour initiating cells and neural stem cells.** Brain tumour initiating cells self-renew and give rise to heterogeneous tumour cells, just as neural stem cells self-renew and give rise to heterogeneous neural cells. They both have similar regulatory pathways including Wnt, Notch and TGF- $\beta$  (From *Future Neurology*. 2008;3(3):265-273 [http://www.medscape.com/viewarticle/578097\\_3](http://www.medscape.com/viewarticle/578097_3)).

### 1.3 Brain Cancer – GBM

Brain cancers arise from the transformation of different types of healthy neural cells, whether they are early progenitor populations or those further differentiated. The cell type a tumour arises from usually dictates how brain cancers are classified and is also becoming the basis for treatment design. Brain cancers are classified into ascending grades depending on their

severity, in accordance with the World Health Organisation. There are four grades of brain cancer, with a grade one tumour having the lowest malignancy, through to a grade four tumour, which has the highest malignancy and is most virulent (Chandrika, G et al., 2016). An example of a grade four tumour is Glioblastoma Multiforme (GBM) which develops either as a primary tumour, ‘*de novo*’, or a secondary, derived from a lower grade tumour (Figure 1.3), (Ohgaki and Kleihues, 2007). GBM accounts for approximately 69% of gliomas and 40% of all primary brain tumours making it the most frequent and malignant brain tumour (Ciammella et al., 2013, Martinez and Esteller, 2010). GBM has a survival rate of fewer than nine months (Carter et al., 2008). The poor prognosis is related to the high degree of infiltration and proliferation of the tumour (Biernat et al., 1997, Ueki et al., 1996). This is due to deletion of multiple tumour suppressors and/or activation of multiple oncogenes involved in cell cycle regulation, progenitor cell maintenance (Jin et al., 2004), projection outgrowth (Sierra et al., 2015) or epithelial to mesenchymal transition (Waldau and Shetty, 2008) all of which can be mutated in many brain cancers, not just GBM.

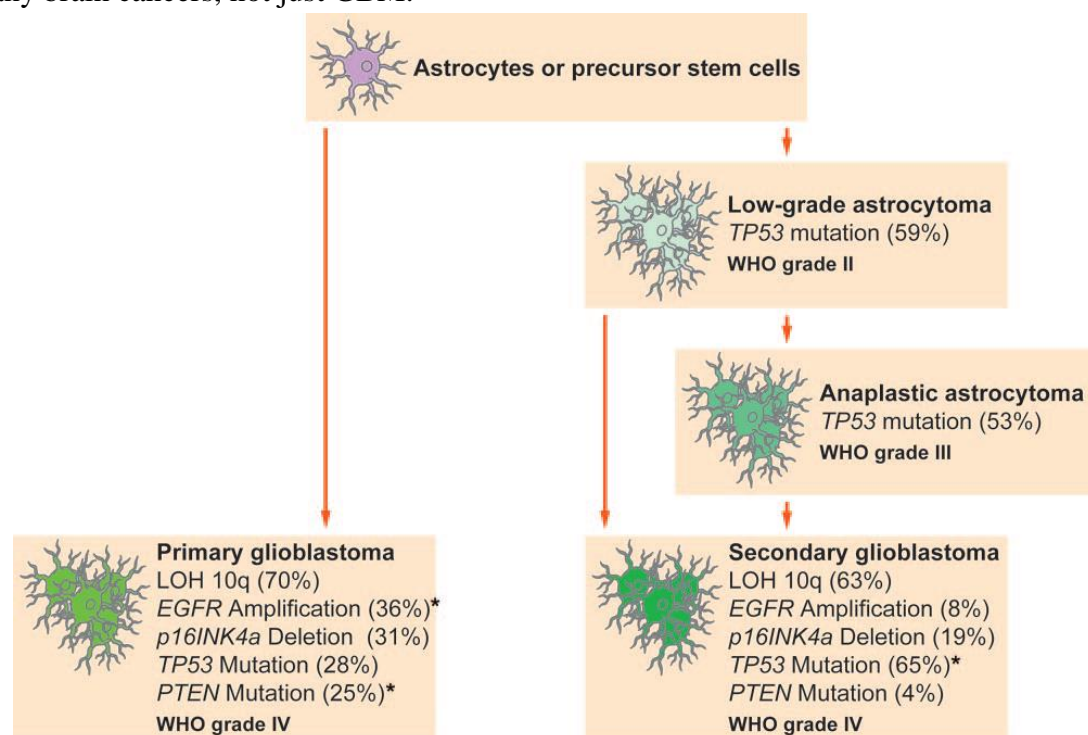


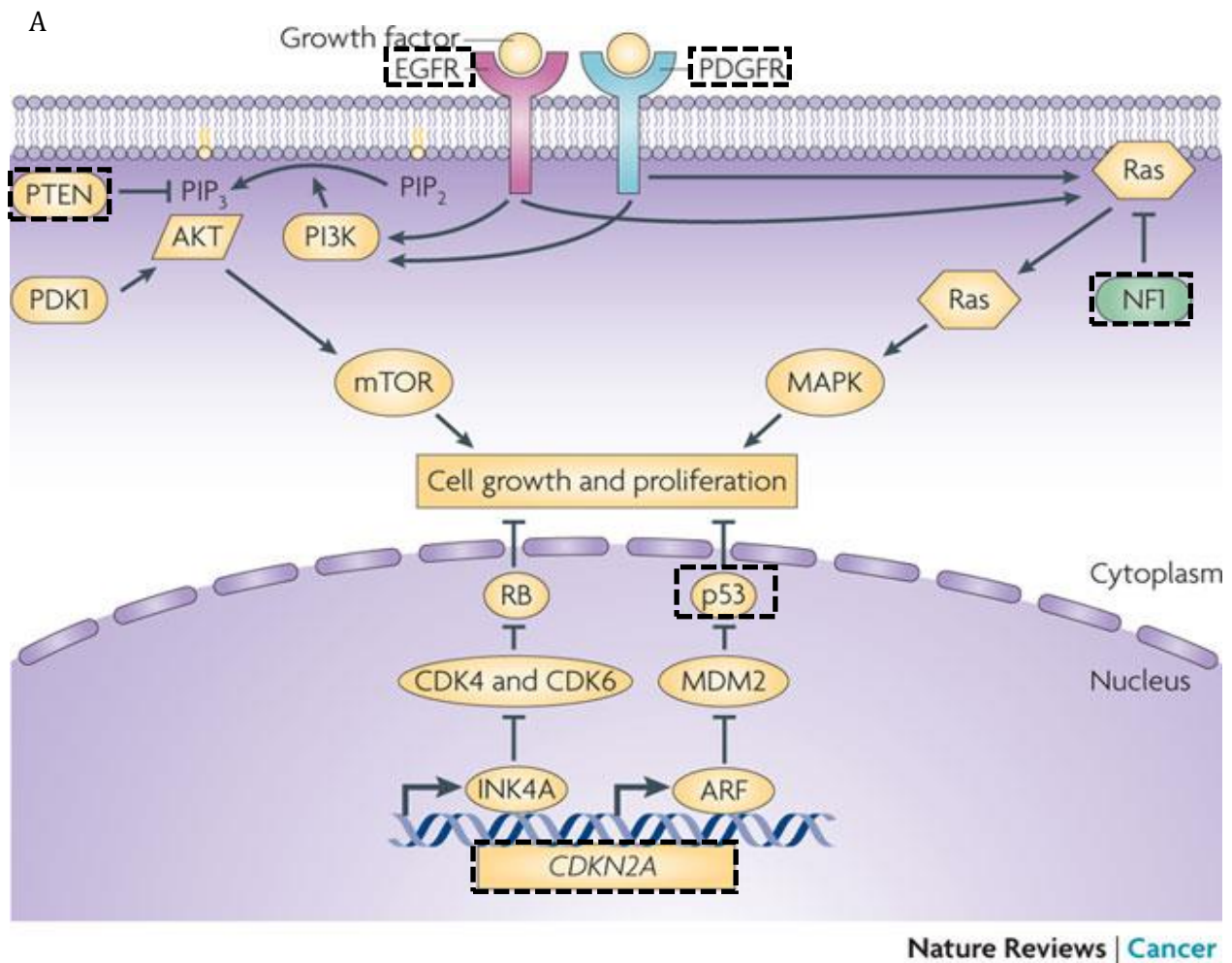
**Figure 1.3. Altered gene expression leading to primary and secondary Glioblastoma development.**

Astrocyte or progenitor stem cells can either undergo multiple spontaneous genetic alterations to develop primary GBM or gradual genetic alterations developing secondary GBM. Primary GBM has higher percentage of gene alteration in all genes listed, except TP53, as its alteration is the most common initial alteration leading to the disease. Both primary and secondary are classified as GBM based on their severity in accordance with WHO classification (Ohgaki and Kleihues, 2007)(Ohgaki and Kleihues, 2007, Licence# 3731050145774).

#### **1.4 Gene alterations determine GBM Subtypes**

There are four subtypes of GBM: Neural, Proneural, Mesenchymal and Classical, that have been categorised based on neural gene expression and mutation clustering studies (Verhaak et al., 2010). The mutated genes of each subtype can also be attributed to promote cell proliferation and cell cycle progression. The tumour suppressor, TP53, was the most frequently mutated gene in all subtypes of GBM except Classical, according to the cancer genome atlas research network 2008 (Verhaak et al., 2010). TP53 prevents progression into S phase until any DNA damage has been repaired. Inactivation of TP53 results in the progression of DNA damaged cells into S phase, as TP53 normally repressors CDK2/Cyclin E by the Cip/Kip family repressors, until repair is complete (Figure 1.4A,B). For Classical GBM, the most common mutations are amplification of the EGF receptor, and deletion of CDKN2A, which mutates the tumour suppressor, Retinoblastoma (Rb), preventing Rb from inhibiting G1-S phase progression (Figure 1.4B). Proneural GBM can be characterised by oncogenic PDGFRA alterations and p21<sup>Cip1</sup> (CDKN14) down regulation. Hyper-activation of PDGFRA results in hyper activation of Ras and PI3K pathways which lead to uncontrolled proliferative growth (Figure 1.4A). Normally p21<sup>Cip1</sup> inhibits Cyclin A-CDK2, Cyclin E-CDK2 and Cyclin D-CDK4/6. When p21<sup>Cip1</sup> is downregulated, this inhibition is lost and proliferation through these checkpoints prevails (Figure 1.4B). Both Neural and Mesenchymal subtypes have frequent mutations in PTEN, which normally inhibits PIP<sub>3</sub> signalling (Figure 1.4A), with the mesenchymal subtype also exhibiting an NF1 deletion (Verhaak et al., 2010). This study illustrates that GBM patients can be further categorised into well-defined subgroups, based on the expression patterns of integral pathways that promote the tumourigenesis and proliferative capacities of the GBM tumour. These findings may indicate why some GBM patients do not respond to generic cancer treatment schemes, and are also useful for predicting survival outcomes. However, there is also a need to understand what pathways those subtype mutations effect in healthy neural brain cells. Within each subtype mutation, there may be a cascade of overlapping pathways that contribute to the severity of resulting tumour grade. If specific proteins involved in those pathways can be identified and their interaction with other pathways predicted, then effective treatments may be developed. It is important to note that the identification of these subtypes is insufficient in predicting the rate of tumourigenesis, as patients with the same subtype of GBM may experience different rates of tumour progression and metastasis. Cell signalling and cell cycle progression are key processes that need to be investigated in both diseased and non-diseased neural progenitors, in order to understand how the microenvironment of a healthy niche is effected by the diseased population. This will allow

treatments to provide better stabilisation of the healthy population, but target the diseased population in patients, achieving better treatment and survival.



B

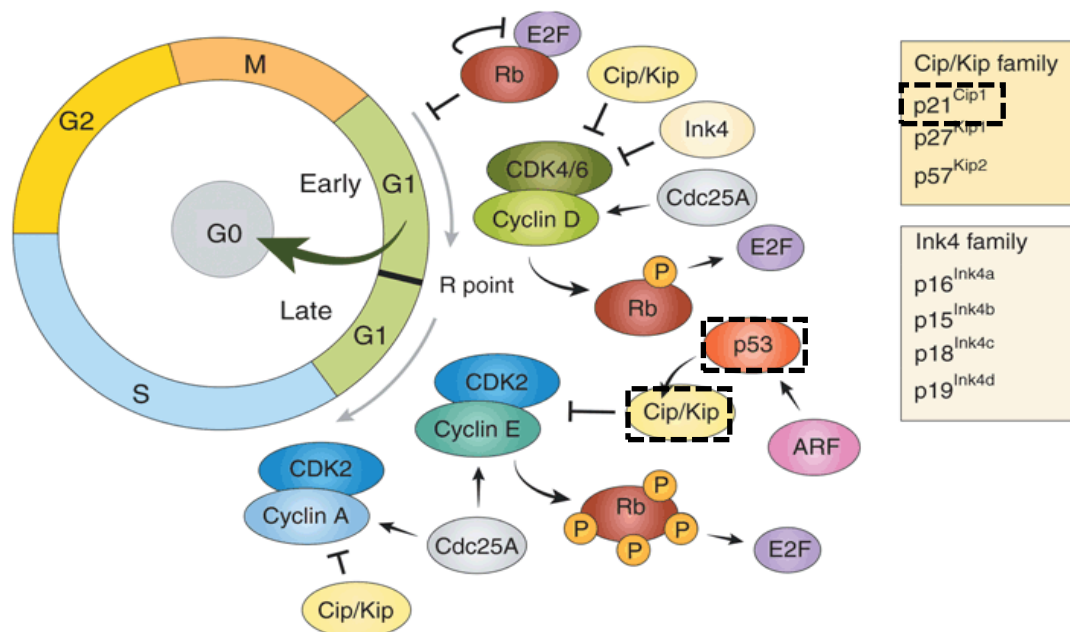


**Figure 1.4. Commonly mutated genes in GBM causing increased cell cycle progression.** (A) Amplification of EGF receptor, PDGFR and mTOR components as well as the inactivation or deletion of the tumour suppressors: CDKN2A, RB, TP53 and the Ink family genes result in increased proliferation, primarily at (B), the G0-S phase of the cell cycle at G0-G1 and G1-S phase checkpoints.

*For example, the p53 inactivation which is common to all except classical GBM, causes less inhibition of CDK2-Cyclin E and CDK4/6-Cyclin D by the Cip/Kip family of repressors resulting in uncontrolled progression from G1 into S phase and Early G1 into Late G1, respectively. This results in the hyper proliferation of a lot of brain cancers (Strauss et al., 2012, Huse and Holland, 2010). Progression through G1 phase and into S phase is determined transcription and translation of genes required for checkpoint progression, including cyclin E, CDK2, cyclin A and CDK 4/6, and for DNA replication. The transcription factor required for the transcription of these genes is E2F and can only be activated once released from retinoblastoma protein (Rb). Rb phosphorylation is required for E2F release is performed by the two complexes: cyclin D-CDK4/6 and cyclin E-CDK2. There are multiple inhibitors of S phase progression that belong to the two families listed, which are considered tumours suppressors. These include p15 (Ink4 family) and p21(Cip/Kip family) that inhibit cyclin d-CDK4/6 and cyclin E-CDK2 respectively. (Strauss et al., 2012). Huse and Holland, 2010 Licence# 3727280278230, (Strauss et al 2012 Licence# 3731060898183)*

### **1.5 Current Therapies used in Treatment of Brain Cancer**

Radiation therapy has been used for many years in the treatment of not only brain cancers, but other cancers also. There is a mild benefit for GBM from radiation treatment in which patients survival increases to 12.1 months with radiation therapy alone, to 14.6 months with combined treatment (Stupp et al., 2005). The standard procedure for treatment for GBM treatment is surgical extraction followed by treatment with temozolomide in parallel with 60Gy radiation and a final 6 weeks of continued temozolomide treatment (Friedman et al., 2000). Temozolomide is a DNA methylating drug that is distributed to all tissues including the CNS with low toxicity (Denny et al., 1994). Its effectiveness depends on the activity of the opposing O6-methylguanine-DNA methyltransferase (MGMT) which removes methyl from DNA, rescuing DNA replication in tumour cells (Friedman et al., 2000). Therefore patients with elevated MGMT activity in tumours are insensitive to TMZ, which has been a common problem, limiting the effect of the treatment.

Immunotherapy has been recently trialled in cancer treatment. It involves boosting the patient's own immune system to fight and attack the cancerous cells (Snook and Waldman, 2013). There are two types of immunotherapy that are currently being trialled in GBM treatments, namely Adoptive and Active Immunity. Adoptive immunity occurs by the *ex vivo* activation of patient lymphocytes, after their exposure to inactivated tumour proteins, into cytotoxic T lymphocytes (CTLs) (Vauleon E, 2010). The CTL are then re-injected into the patient. They are virulent and can target the patient's tumour more specifically and effectively then the patient's own immune

cells (Xu et al., 2012). Active immunity on the other hand, is when the patient produces their own CTLs *in vivo* (Figure 1.5). Patient tumour proteins are isolated and loaded onto immature dendritic cells isolated from blood and re-injected back into the patient. The dendritic cells are activated *in vivo* and stimulate the production of the patient's own CTLs targeted to the tumour. These CTLs attack any tumour protein they recognise. This method appears to have the most effective response in terms of patient survival so far with patients newly diagnosed with GBM having a survival range within 65-234 weeks compared to 0-58 weeks, after treatment (Bregya et al., 2013, Xu et al., 2012, Vauleon et al., 2010), however the effectiveness of this therapy depends on the patient's immune system and consequently variation in survival occurs.

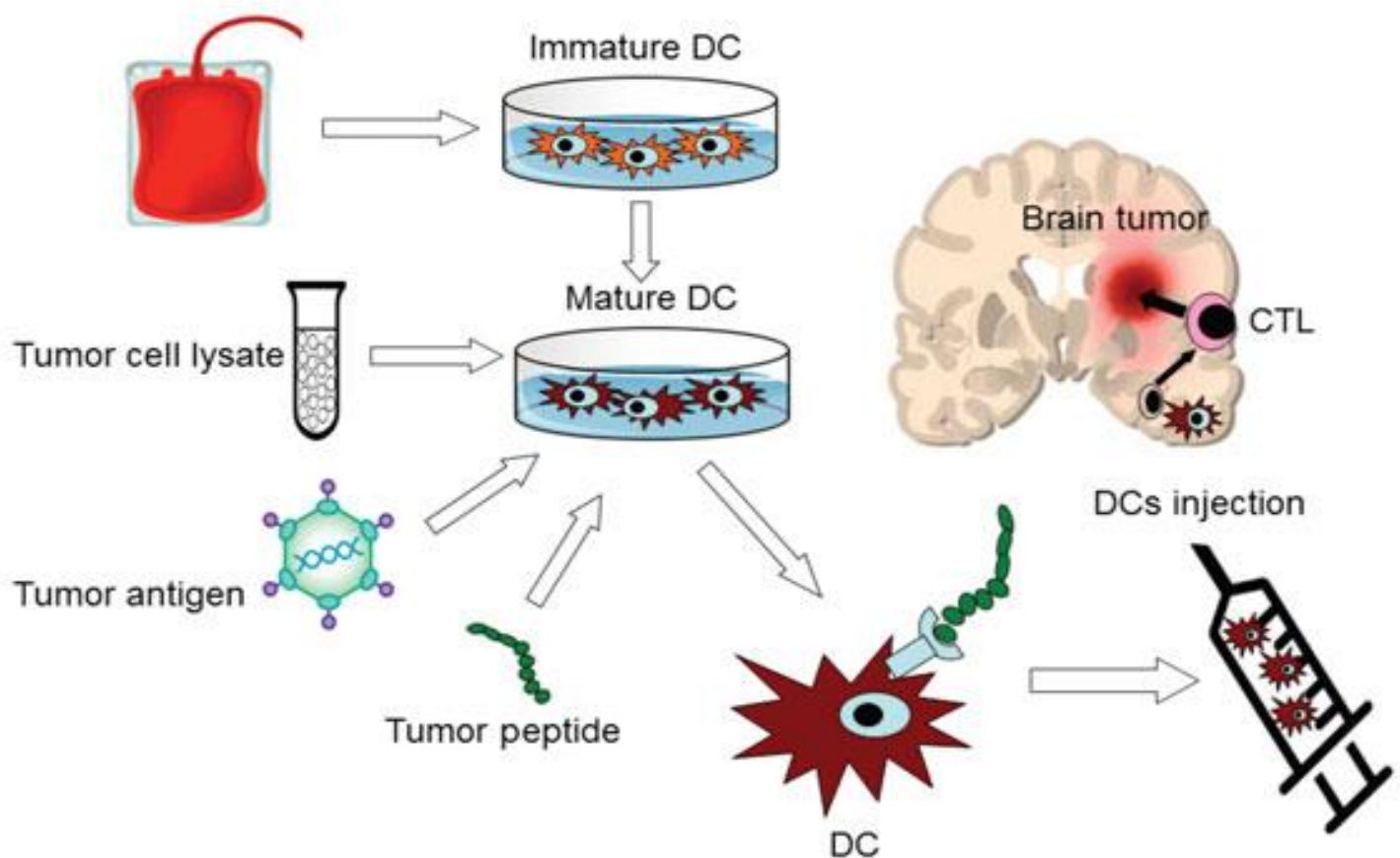


**Figure 1.5. Active immunity is effective in prolonging patient survival.** Immature dendritic cells are isolated from blood. Tumour protein extracted during surgery is used to produce tumour lysates, antigen and peptides that are loaded onto mature dendritic cells and reinjected back into the patient. The mature dendritic cells containing the tumour proteins will elicit lymphocyte conversion into

*cytotoxic T lymphocytes (CTLs). The CTLs are responsible for recognising the patient tumour protein and attack any remaining tumour tissues.(Etame, 2014, OncoLive)*

## **1.6 Brain Cancer Development In Vivo**

In order to further understand processes activated during neural tumorigenesis, identifying other genes contributing to the development of the disease has been approached using animal models. This is the only way to observe how tumor microenvironment influences the development of any disease, as simply extrapolating results from *in vitro* studies is not sufficient. Processes, such as the activation or inactivation of a signalling pathway *in vitro*, may remain unchanged *in vivo*, and not contribute to the development of the disease; the reverse is also true. Thus, *in vitro* studies eliciting significant results need to be confirmed *in vivo* prior to development of targeted therapies.

Steriotactic injection of brain cancer cell lines derived from patient tumours is one method used to induce murine brain tumours *in vivo*, and so doing, recapitulates the invasiveness of the tumour, in most cases (Behar et al., 2008). U-87 MG is a GBM cell line which has effectively recapitulated the original tumour of the 44 year old male from whom it was derived (Clark et al., 2010). This cell line has been used previously in the *in vitro* study of brain cancer and was thought to recapitulate the original tumour 28 days after transplantation in mice (Clark et al., 2010, Markiewicz-Zukowska et al., 2013, Shi et al., 2012, Behar et al., 2008), until recent findings suggest that there are some discrepancies regarding its reproducibility of the human disease *in vivo* (Jacobs, V et al., 2011). In comparison, the U251 cell line seems to initiate tumours comparable to the human GBM (Jacobs, V et al., 2011). None the less, U-87 MG steriotactic injections into mice have been used to study tumour formation, and despite some discrepancies regarding their efficiency to model the human disease, they are considered more effective than previous methods which involved isolating the “cancer-stem-cells” from patient tumours using stemness markers (such as CD133) and side population analysis are injected into mice, rarely mimic the original tumour (Broadley et al., 2011).

Alternatively the transformation of neural progenitor populations into gliomas *in vivo* has also been successful in mice (Uhrbom et al., 2005). Mutations in Ras signalling pathways have proven quite effective in generating infiltrative tumour models in mice. Ras signalling is critical for the maintenance of neural progenitors and also in brain cancer development, with

MAPK inhibitors, which oppose Ras signaling pathways, effectively reducing GBM cell proliferation *in vitro* (Zohrabian et al., 2009, Albert et al., 2009). The expression of genes involved in this pathway have been manipulated, in conjunction with other genetic alterations, to develop effective animal models of brain cancer (Uhrbom et al., 2005, Marumoto et al., 2009, Abel et al., 2009, Holland et al., 2000). The Kirsten rat sarcoma viral oncogene homolog (Kras) is a member of the Ras family and, when active, has been shown to be required for the maintenance of brain cancer (Holmen and Williams, 2005, Abel et al., 2009). In particular, mutant activation of Ras in the form KrasG12D, in conjunction with p53 deletion from neural progenitors of the SVZ, resulted in highly infiltrating gliomas (Ghazi et al., 2012). Using the same GFAP-Cre targeted KrasG12D activation in the SVZ, less infiltrative gliomas also developed (Abel et al., 2009), without the additional need of tumour suppressor deletion. This was also the case when KrasG12D was activated from radial glial progenitors, using BLBP-Cre mediated activation, in both embryonic and post-natal mice. Developing *in vivo* models of GBM and other brain cancers in which the underlying genetic alterations are known, allows researchers to identify major changes in cell cycle regulation and proliferation which arise.

### ***1.7 Dysregulation of the Cell Cycle in Cancer***

Cellular hyper-proliferation and dysregulation of the cell cycle are common attributes of all cancers, not only brain cancers. In healthy cells, cell cycle progression will not occur unless specific requirements, such as complete and accurate DNA replication and appropriate cell growth, are met. However, cancer arises from mutations in cell cycle checkpoints that control these requirements. There are four checkpoints in which mutations can occur and lead to cancer namely, G<sub>1</sub> to S; S to G<sub>2</sub>; G<sub>2</sub> to M and M to G<sub>1</sub>, (Figure 1.4B). Molecular control of cycle progression into and out of these phases is dictated by fluctuations in cyclin degradation and cyclin-dependent-kinase (CDK) activity. These cyclins and CDKs can be regulated by ubiquitin (Hershko and Ciechanover, 1998) which marks them and other cell cycle proteins for degradation by the proteasome. The length of G<sub>0</sub>/G<sub>1</sub> phase determines the period of cell growth before DNA replication begins, such that the longer cells remain in this phase, the fewer cycles they go through. Progression through G<sub>0</sub>/G<sub>1</sub> and into S phase is predominantly dependent on phosphorylation of the Retinoblastoma protein (Rb) which releases the transcription factor E2F1, which enhances transcription of cyclin D1 and cyclin E for S phase progression (Inoshita et al., 1999) (Figure 1.4B).

Cellular quiescence of cancer-initiating or cancer stem cells, is also thought to be a cause of failed therapy for GBM (Chen et al., 2012). Quiescence is the state in which a cell is no longer proliferating, but still receives signals to prevent the initiation of apoptosis. Quiescence is a characteristic known to be commonly possessed by stem cells. This is different from senescence whereby cells are no longer able to divide as they've reached their proliferative capacity (Hayflick, 1965). Senescent cells are unable to re-enter the cell cycle, however quiescent cells retain the ability to re-enter the cell cycle and proliferate upon re-addition of growth factors or other stimulants (Crescenzi et al., 1995).

The most common cell cycle entry point into quiescence (G0 phase) occurs within the G1 phase, when nutritional requirements are insufficient to continue through the cell cycle. Once optimal growth conditions and nutritional requirements are achieved, the cells will re-enter at the same restriction point from which they exited out of G1 phase (Pardee, 1974). Identifying a quiescent cell from a G1 phase cell may become crucial in preventing failed chemotherapies, as re-emergence of mutated quiescence cells into the cell cycle, is largely responsible for regression. It would be ideal to be able to isolate and target these cells specifically. It is difficult to distinguish a quiescent cell (G0) from those in G1 phase as both cell types exhibit changes involved with reduced growth and division. For example the two populations of cells would have the same amount of DNA content, that is '2N', as assessed by cell cycle analysis (Coller et al., 2006), they also show reduced BrdU incorporation as they are not highly proliferative (Kingsbury et al., 2005), they have reduced expression of genes required for chromatin assembly (Polo et al., 2004) and also have reduced spindle assembly proteins such as MAD2L1 (Coller et al., 2006). These changes simply identify G0/G1 populations from dividing phases: S and G2/M phase.

Quiescence can be induced by growth factor withdrawal, contact inhibition or prevention of cell adhesion (Coller et al., 2006). Although there are some differences, each mechanism of induction yields common changes in gene expression related to reduced proliferation or preparing for differentiation that occurs during quiescence (Coller et al., 2006). For example, the absence of M1-RR expression (Tay et al., 1991), accumulation of an E2F-p130 complex (Smith et al., 1996), downregulation of Chromatin Assembly Factor-1(CAF-1) (Polo et al., 2004), reduced ki67 expression as well as a reduction in mTORC1 activity (reduced p-S6 235/236 expression) are some common characteristics that distinguish G0 from G1 cells.

Multiple pathways are required for the initiation and maintenance of quiescence, including Wnt, PI3K, TGF- $\beta$  and as briefly mentioned above, mTOR. Wnt signalling is required in the HSC niche to prevent proliferation (Fleming et al., 2008), block differentiation (Kirstetter et al., 2006) and maintain quiescence (Li and Bhatia, 2011) to preserve the stem cell pool. Inhibition of the PI3K/Akt pathway results in fewer quiescent melanoma stem cells, with a greater population in G1 (Touil et al., 2013), indicating PI3K signalling is required to maintain cells in a quiescent state. TGF- $\beta$  signalling has also been shown to maintain the differentiation capacity and multipotency of HSCs *in vitro* whilst preventing their division, implicating TGF- $\beta$  in stem cell maintenance (Yamazaki et al., 2009). Lastly, deletion of genes that inhibit mTOR signalling result in increased stem cell proliferation (Zhang et al., 2006), which in time exhausts the stem cell pool (Li and Bhatia, 2011) indicating mTOR is also involved in maintaining stem cell quiescence, (Figure 1.6).

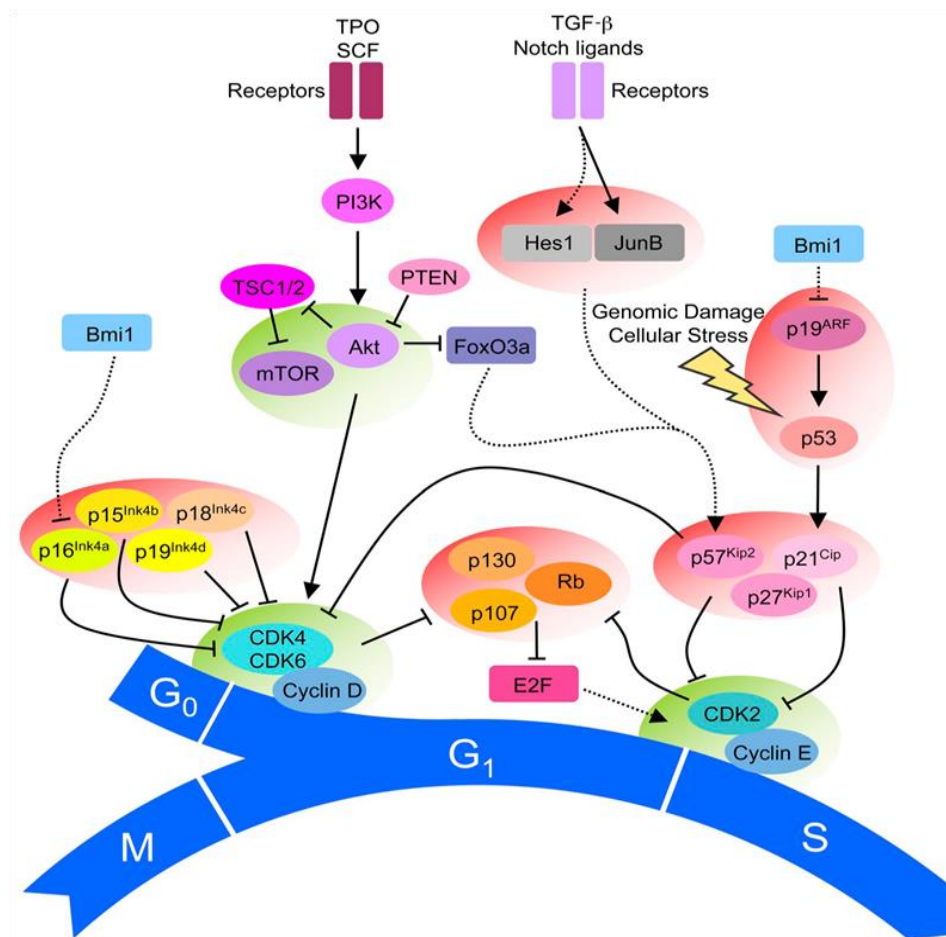


**Figure 1.6** Convergence of pathways involved in the maintenance of quiescence (G0 phase) and entrance into G1 and S phases. TGF- $\beta$ , Notch, mTOR and PI3K pathways converge to control cell cycle progression. TGF- $\beta$  ligands bind and promote p21 transcription which inhibits Cyclin E-CDK2 binding and Cyclin D-CDK4/6 binding and therefore entrance into S phase and into G1 phase

*respectively, thereby preventing both exit from quiescence and from G1 phase; Notch ligands have a similar effect. PI3K activates Akt which mediates activation of many downstream complexes including mTOR. mTOR activation ultimately activates S6 protein which promotes progression from G<sub>0</sub> into G<sub>1</sub> phase.*(Pietras et al., 2011) (Pietras et al 2011, JBC doi: 10.1083/jcb.201102131)

### **1.8 G1 to S Phase Signalling Pathways**

Genes encoding proteins controlling the G1 to S phase checkpoint are targets of major signalling pathways, including TGF- $\beta$ , Wnt, MAPK/ERK and PI3K/Akt/mTOR. These pathways can converge onto the same substrates which then mediate similar, although sometimes different roles within cells (Voskas et al., 2010). Therefore identifying changes in cell cycle proteins downstream of one signalling pathway doesn't indicate that that pathway is the only one regulating the substrate, as there will almost certainly be multiple feedback mechanisms involved (Voskas et al., 2010).

p15 and p21 are two tumour suppressor proteins, that prevent progression into S phase, and are directly transcribed downstream of TGF- $\beta$  signalling, (Figure 1.4B and 1.7). In TGF- $\beta$  signalling, the tyrosine receptor activation results in phosphorylation of Smad2/3 which recruits Smad4 before the complex enters the nucleus to mediate transcription of the CDK inhibitors. p15 prevents the interaction of Cyclin D with its corresponding kinase: CDK4, and p21<sup>Cip/Waf1</sup> prevents the formation of Cyclin E-CDK2, both outcomes leading to the inactivation of the respective CDK and halting progression from G1 phase (Meulmeester and Dijke, 2011), (Figure 1.4B and 1.7).

\

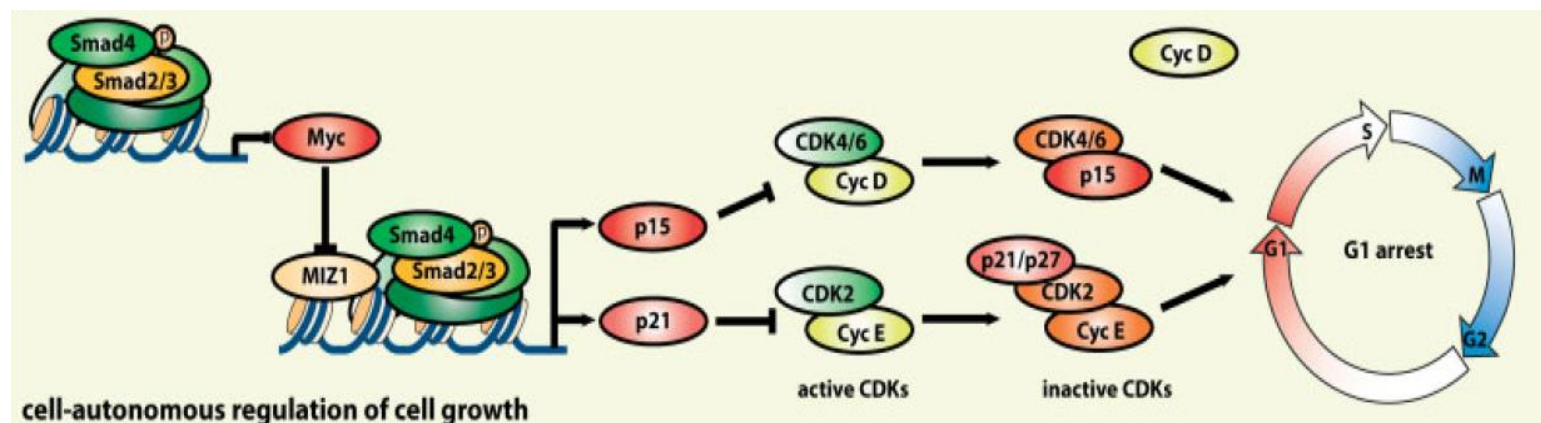


**Figure 1.7** *TGF- $\beta$  signalling transcribes G1-S phase inhibitors.* Upon binding of TGF- $\beta$ , there is co-receptor activation which phosphorylates R-Smad (Smad2/3) promoting dimerisation with Smad4 resulting in a transcription complex that enters the nucleus, mediating transcription of genes such as p21 and p15 (Meulmeester and Dijke, 2011, Licence# 3727410931105)

Activated Wnt signalling also positively correlates with cancer. In particular, Wnt signalling results in high  $\beta$ -catenin levels which activates transcription of cyclin D1 in many cancers (Chen et al., 2012). Wnt signalling has also been shown to increase cyclin D1 in conjunction with MAPK signalling (Diehl et al., 1998). Cyclin D1 is degraded by the proteasome upon ubiquitylation, although not exclusively (Germain et al., 2000), which was thought to be dependent on phosphorylation of threonine 286 by GSK-3 $\beta$  (Diehl et al., 1998). GSK-3 $\beta$  itself is regulated by phosphorylation through c-Akt, which is mediated by crosstalk between Ras/PI3K/Akt and Wnt pathways (Diehl et al., 1998) (Massague et al., 2004). Increased GSK-3 $\beta$  phosphorylation inhibits its kinase activity (Voskas et al., 2010, Vara et al., 2004), resulting in less Cyclin D1 phosphorylation and therefore, degradation. Despite this, mechanisms exist to remove ubiquitin molecules to prevent Cyclin D1 degradation. Ubiquitin-specific protease 2 (USP2) can remove ubiquitin from cyclin D1, stabilising it (Shan et al., 2009), but does not appear to do so for cyclin E or other D types cyclins indicating ubiquitin proteases can have specific cyclin targets. Other ubiquitin specific proteases may be involved in the regulation of Cyclin D1. Cyclin D1 is also positively regulated by AP-1 which in turn is positively regulated indirectly by apoptosis signal-regulating kinase 1 (ASK1), another ubiquitin ligase substrate (Hayakawa et al., 2010) and substrate of another ubiquitin specific protease, (Figure 1.8).

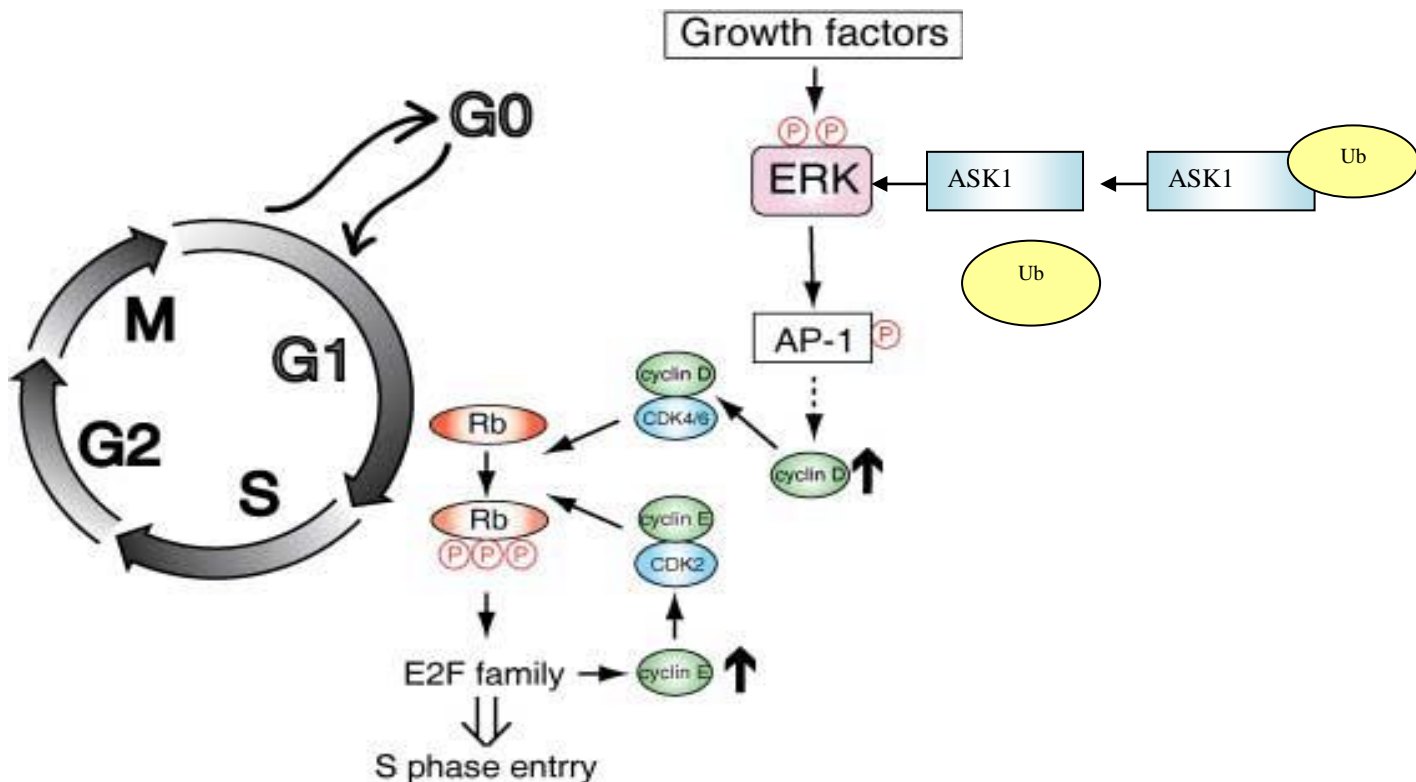


**Figure 1.8** *Cell Cycle and the proteins involved in G1 to S phase transition. G1 to S phase transition requires ERK MAP kinase pathway and regulation of retinoblastoma phosphorylation by CDK4/6-cyclin D complex. Activated ERK is required for AP-1 transcription complex (dimerised c-Fos and Jun) activation which promotes cyclin D transcription, which is critical for CDK4/6 complex formation to phosphorylate and deactivate retinoblastoma protein (Rb). Phosphorylated Rb activates E2F transcription factors that are required for transcription of the S phase cyclin, Cyclin E (modified from Hershko and Ciechanover, 1998)*

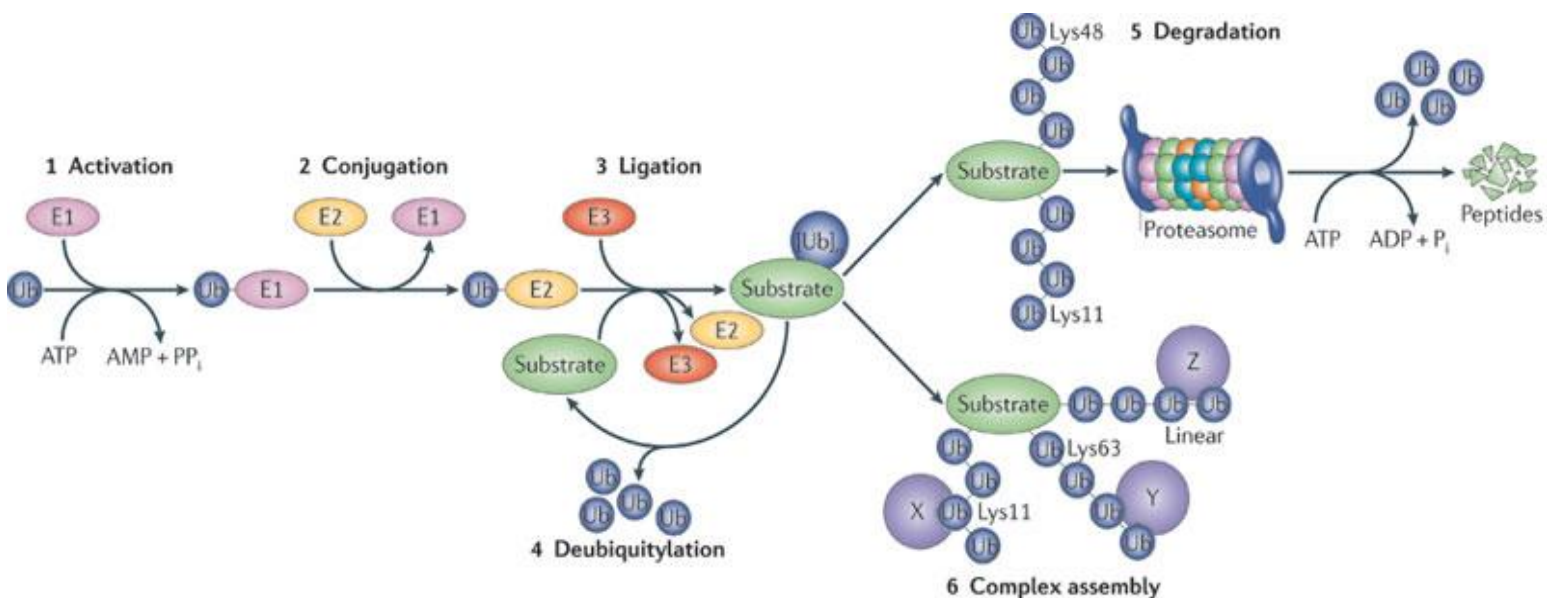
PI3K signalling has also been shown to inhibit p21<sup>Cip</sup>, p27<sup>Kip1</sup> and mTOR, promoting accelerated progression into S phase (Pietras et al., 2011). This indicates a convergence of pathways is necessary for intricate regulation of cell cycle substrates. These are just a few examples of pathways involved in the regulation of cell cycle proteins involved at the G1 to S phase transition.

### 1.9 The Ubiquitin System

Ubiquitylation is a postranslational modification that is required for most, if not all, cell functions including cell cycle control, cell signal transduction, membrane trafficking and DNA damage repair (Luise et al., 2011, Sacco et al., 2010). It involves the covalent addition of ubiquitin to protein substrates involving three enzymatic reactions requiring the activation,

carrying and final ligation of ubiquitin. The addition of ubiquitin to substrates regulates the distribution or activity of the substrate (Colland, 2010), can promote exportation of the substrate from the nucleus (Dupont et al., 2009) or, upon ubiquitin chain elongation, can promote substrate degradation by the 26S proteasome.

Ubiquitin is a highly conserved 76 amino acid polypeptide containing seven lysine residues, which enables it to take on diverse polyubiquitin chain structures, enabling functionally specific signalling (Pickart and Fushman, 2004). Ubiquitylation involves its activation by ubiquitin activating enzymes, E1, which uses ATP to form a thioester bond with the carboxy terminus of ubiquitin. The activated ubiquitin is then transferred to an E2 conjugating enzyme (Ramakrishna et al., 2011) in a transthiolation reaction (Bedford et al., 2011). The E2 enzyme, containing ubiquitin, forms a complex with an E3 ubiquitin ligase whereby ubiquitin is conjugated to the target protein's lysine residue, through isopeptide bond formation between the lysine residue and the C-terminal glycine 76 (Figure 1.9) (Pickart and Fushman, 2004, Bedford et al., 2011, Haglund and Dikic, 2005, Colland, 2010). E3 ubiquitin ligases are also known to interact with and add ubiquitin to targets through adaptor proteins (Fang et al., 2003). Just as phosphoryl groups are added by kinases and removed by phosphatases, ubiquitylation is reversed by very specific enzymes known as deubiquitylating enzymes (DUBs). With respect to proteosomal degradation, the polyubiquitin K48-linked chain (Chau et al., 1989) increases the efficiency for targeting the protein to the 26S proteasome for degradation. A protein substrate can escape this degradation if the polyubiquitin chain is removed by DUBs. This is one of the functions of USP9x (Schwickart et al., 2010). USP9x is a deubiquitylating enzyme that removes ubiquitin molecules from lysine residues of substrates to prevent degradation, promote substrate activation or alter localisation. It opposes E3 ubiquitin ligases which add monomers or polymers of ubiquitin to a molecule that mark it for both trafficking and degradation by the proteasome as reviewed by (Hershko and Ciechanover, 1998).



Nature Reviews | Molecular Cell Biology

**Figure 1.9 Ubiquitin modification of substrates dictates fate.** In the first step of the process, (1) Ubiquitin is activated by E1 enzyme in a reaction dependent of ATP. Secondly, (2) the activated ubiquitin is transferred to E2 enzyme which carries the ubiquitin to the E3 ligase which (3) adds ubiquitin to a lysine residue on the substrate. At this point, ubiquitin molecules can be removed by (4) deubiquitylating enzymes including USP9x, a ubiquitin specific protease. The addition of Ubiquitin molecules at lysine residue -48 or -11 results in their (5) degradation by the 26S proteasome. However when added linearly at lysine -11 or -63 promotes the substrates signalling pathway complex assembly. (Vucic et al 2011, Licence # 3731061268718)

### 1.10 Regulation of Proliferative Brain Cancer Genes by Ubiquitin

Genes required for the maintenance of healthy neural progenitors are also amplified or mutated in brain cancers. These include genes involved in progenitor self-maintenance, cell cycle and apoptotic regulators, some of which are regulated by the ubiquitin-proteasome system, making them substrates of both ubiquitin ligases and deubiquitylating enzymes. Genes specific for neural progenitor maintenance including Sox2 (Annovazzi et al., 2011, Ellis et al., 2004) and mTOR (Fan Q and Weiss W 2012) are regulated by ubiquitin (Baltus et al., 2009, Linares et al., 2014). Cell cycle suppressors such as p53, pRb, p27, p21, E2F1 (Vlachostergios et al 2012) and cell cycle promoters including Cyclin D1, Pescadillo and c-myc, are also all regulated by the ubiquitin-proteasome system.

SOX2 is highly expressed in the neural progenitors of the developing brain (Ellis et al., 2004) and its expression decreases upon differentiation as progenitors exit the cell cycle (Annovazzi et al., 2011). In brain cancer, high SOX2 expression correlates both with hyper proliferative regions in gliomas and the malignant grade, with high expression in glioma-derived

neurospheres. In contrast, low SOX2 expression is detected in terminally differentiated cells within neural tumours (Annovazzi et al., 2011). Nestin is a prominent marker of neural progenitors involved in their maintenance and, its expression decreases as differentiation proceeds. Glioblastoma cell clones that were characterised with high Nestin expression, gave rise to tumours faster, *in vivo*, than those with low Nestin (Lu et al., 2011).

mTOR signalling is involved in neural progenitor cell cycle and differentiation, and is commonly mutated in brain cancers (Kahn et al., 2014). Inactivation of mTORC1 signalling reduces neural stem cell proliferation (Cloëtta et al., 2013). mTORC1 signalling occurs in response to growth factor stimulation, by EGF/FGF/IGF/HGF, resulting in downstream activation of p-S6(s235/236). This promotes neural progenitors to exit the quiescent G0 phase and enter the G1-S phase (Eshleman, et al. 2002, Galan-Moya, E.M. *et al.* 2011, (Rodgers et al., 2014). Up regulation of EGFR is a common mutation amongst brain cancers and can lead to increased mTORC1 activation, promoting replication of brain cancer cells (Fan and Weiss 2012). Several components, including Raptor, S6K1 and S6K2, of the mTORC1 complex are regulated by the ubiquitin proteasome system (Gwaller et al., 2009, Hussain et al., 2013, Agrawal et al., 2012).

TP53 is a tumour suppressor commonly mutated in brain cancer. TP53 is required at both G0/G1 and G2/M cell cycle checkpoints, and is activated in response to DNA damage, as well as nutrient or growth factor deprivation (Vlachostergios, P et al, 2012). In its inactive state TP53 is bound by the E3 Ubiquitin ligase, Mdm2, which shuttles it into the cytoplasm and ubiquitylates it, resulting in its proteasomal degradation. However, phosphorylation of TP53 by kinases including ataxia telangiectasia mutated (ATM), AMP-activated protein kinase (AMPK) or casein kinase 1 (CK1), prior to binding Mdm2 result in TP53 stabilisation (Vlachostergios, P et al, 2012).

Cell cycle suppressor TP53/p21Cip1/Rb signalling is an essential component of Ras signalling, as knockdown of any of P53, p21Cip1 or Retinoblastoma protein (Rb) restores proliferative capacity following H-/N-/Kras cell cycle arrests. Ras signalling transmits mitogenic signals to cell cycle machinery, which converges onto Rb, resulting in its inactivation (Vlachostergios et al., 2012, Mittnacht and Olson, 1997). Rb is a tumour suppressor that, in its unphosphorylated form, associates with E2F1 preventing it from transcribing genes, cyclin D1 and cyclin E, which are required for entry into S phase

(Inoshita et al., 1999). Perturbations in pRb signalling, by CDKN2A deletion in brain cancers, can result in early entry into S phase. E2F1 is also regulated by ubiquitylation (Vlachostergios et al., 2012). The addition of ubiquitin by SCF SKP2 E3 ligase promotes E2F1 degradation and results in less G1-S phase progression (Galanti et al., 2008).

P27 and p21 are cyclin dependent kinase inhibitors that prevent entry into S phase. Both are ubiquitylated and their expression is reduced in many brain cancers (Piva et al., 1999, Pamarthy et al., 2007, Schiffer et al., 2002). P27 regulates activation of CyclinD-cdk4, Cyclin E-cdk2 and Cyclin A-cdk2 complexes at the G1-S phase checkpoint and itself is ubiquitylated by Skp2 (Schiffer et al., 2002), whereas p21 inhibits cdk2 and is ubiquitylated by the APC/cdc20 ligase (Amador et al., 2007). Degradation of these proteins result in the transcription of G1-S promoting proteins, such as Cyclin D1, resulting in premature entry into S phase, increasing proliferation.

Cyclin D1 acts as an oncogene in brain cancer (Wang et al., 2012) and is regulated directly by the SCF-FBX4- $\alpha$ crystallin E3 Ubiquitin ligase (Lin et al., 2006), but also indirectly via its phosphorylation by IKKa (Inhibitor of kappa B kinase alpha) which shuttles it into the cytoplasm where it is ubiquitylated and degraded by the proteasome. Positive regulation of Cyclin D1 can occur through the stabilisation of NF-kB via the ubiquitin proteasome system, which prevents differentiating glioma cells from becoming post-mitotic (Nogueira et al., 2011). As these cell cycle proteins, which can be regulated by ubiquitylation are mutated in brain cancers their potential stabilisation by DUBs, such as USP9x, is worth investigating in both healthy and transformed neural progenitors.

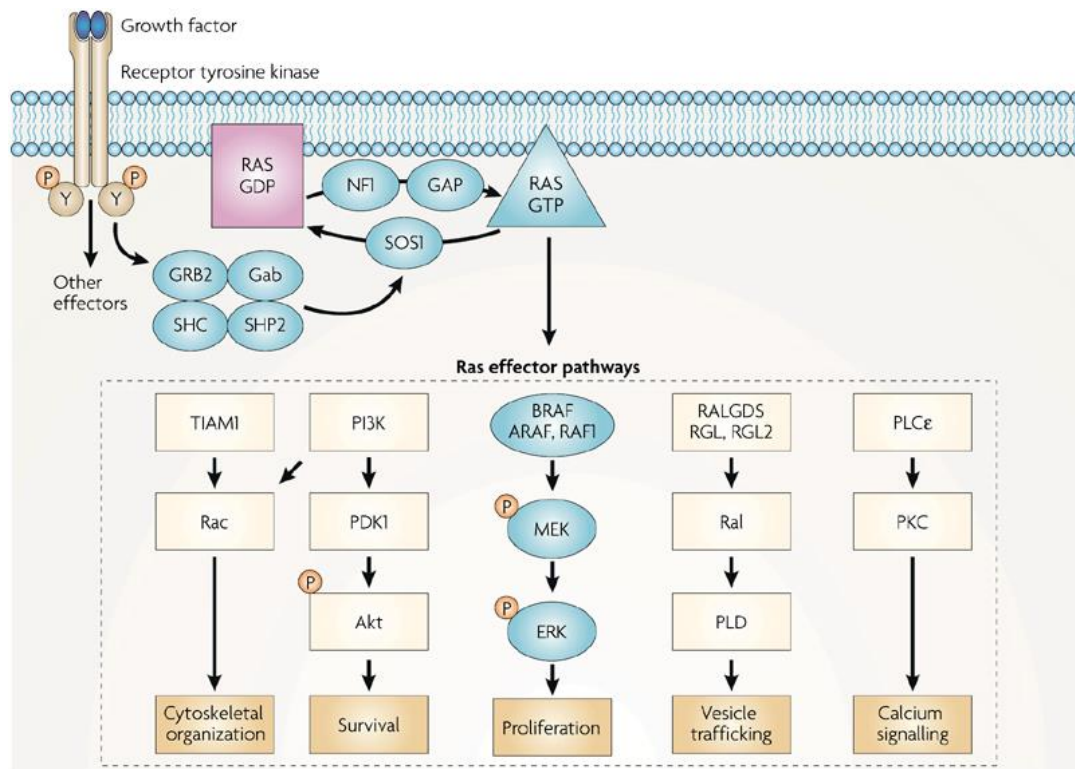
### ***1.11 Ras Signalling Pathway***

Ras signalling regulates many cellular functions including cell proliferation, apoptosis and differentiation (Molina and Adjei, 2006). Constitutive activation of Ras commonly occurs in cancers. Overexpression of growth factor ligands or receptors involved with receptor tyrosine kinase (RTK) activation, such as EGFR or PDGFR, occur in brain cancer increasing Ras activation and downstream signalling. Constitutive Ras activation by mutations in components of Ras/Raf/Erk (a.k.a MAPK) occurs in astrocytic gliomas and promotes the proliferation of astrocytic glioma *in vitro* (Guha et al., 1997) As mentioned, constitutive activation of oncogenic KRas has been used in the development of mouse models of GBM and other aggressive cancers (Ghazi et al., 2012, Liang et al., 2010, Pérez-Mancera et al.,

2012). Interestingly, KrasG12D mutations are not commonly observed in human brain cancer but occur in a variety of different cancers, promoting metastatic transformation in many cancer models (Pérez-Mancera et al., 2012, Fisher et al., 2001, Moon et al., 2014). Tumour suppressor deletion enhances the transformation of KrasG12D induced tumours in other cancers also. Of particular interest was the enhanced transformation in pancreatic cancer. Intermediate pancreatic tumours (PanIN) develop upon mutation of KrasG12D, however this rapidly progresses into the aggressive pancreatic ductal adenocarcinoma (PDA) upon deletion of USP9x (Perez-Mancera et al 2012), implicating USP9x as a tumour suppressor. The mechanism behind the transformation capacity by the deletion was attributed to the destabilisation of Itch (E3 ligase), which was reduced in PDA cells depleted of USP9x, yet no other USP9x substrates controlling cell apoptosis or proliferation were changed (Perez-Mancera et al 2012). Hence, investigating the transformation capacity of KRasG12D induced neural tumours into higher infiltrating ones by concurrently deleting *USP9x*, seemed worth pursuing.

Ras activation occurs upon the binding of a growth factor to its tyrosine kinase receptor, resulting in tyrosine autophosphorylation (Figure 1.9). This recruits Grb2, Shc, Gab2 and SHP-2 into a complex, which converts inactive Ras-GDP into active Ras-GTP. It is this active form of Ras that predominates in cancer (Molina and Adjei, 2006). Ras-GTP recruits Raf to the membrane, activates it, where it goes on to phosphorylate MAPK. MAPK then phosphorylates ERK which promotes activation of transcription factors, required for proliferation, survival and differentiation (Ward et al., 2012). Interplay between Ras signalling and other pathways that respond to growth factor activation, including the mTOR pathway, have been reported. mTOR Complex 1 includes the scaffolding and recruitment protein, Raptor. mTORC1 signalling is also activated in response to growth factors EGF/FGF and plays an important role in neural progenitor proliferation and quiescence. Ras signalling has been shown to be both activated and attenuated in response to mTOR Complex 1 signalling (Liang et al., 2010, Carracedo et al., 2008, Guha et al., 1997, Hoshii et al., 2012). Interplay can occur in a synergistic manner, and is largely cell context specific. For example, the hyperactivation of mTORC1 in lung cancer, by deletion of upstream inhibitors TSC1/2, results in increased Kras transformation (Liang et al., 2010). In murine T-cells, the inhibition of the mTORC1 component, Raptor, inhibits Kras-mediated proliferation (Hoshii et al., 2012, Guha et al., 1997). Ras-ERK1/2 has also shown to activate mTORC1 through its phosphorylation of Raptor. Cross-talk can occur between Ras and mTORC1 signalling. Upon the inhibition of one pathway, there can be a corresponding

upregulation of the other to counteract its effect and promote tumourigenesis. For example, inhibiting mTORC1 with Rapamycin in patient cancers, led to an upregulation of Ras-MAPK signalling (Carracedo, A et al 2008). USP9x has been shown to play a role in both mTORC1 signalling (Agrawal, P et al 2014) and in KrasG12D signalling (Pérez-Mancera et al., 2012). Based on the cross talk within these pathways, it is possible that USP9x plays a role in their signalling of neural progenitors.



Nature Reviews | Cancer

**Figure 1.10 Ras activation results in activation of multiple effector pathways including PI3K.** Tyrosine kinase receptor activation by growth factors such as EGF, FGF and IGF cause tyrosine autophosphorylation which activates Grb2/Gab/SHC/SHP2 complex which then activates SOS1. SOS1 converts Ras-GTP into Ras-GDP, opposing NF1 and GAP which mediate Ras conversion to its active GTP form. Ras-GTP activates Raf, which continues activation of MEK, which in turn activates ERK, which promotes genes required for proliferation. However, Active Ras can also directly bind and activate PI3K, to promote stimulation of this pathway required for cell survival, cell cycle progression and proliferation. (Schubbert et al 2007, Licence # 3731070141386)

## 1.12 mTOR Signalling Pathway

mTOR signalling is involved in the regulation of cell growth, metabolism, differentiation, proliferation (Agrawal et al., 2012, Fingar et al., 2004, Laplante and Sabatini, 2009). mTOR activation is required for the proliferation of both neural progenitors and brain cancer cells

(Galan-Moya et al., 2011, Eshleman et al., 2002). Hyperactivation of mTOR results in depletion of the stem cell pool (Castilho et al., 2009). There are two mTOR complexes, mTORC1 and mTORC2, that are thought to be involved in the regulation of different cellular functions, but can feedback and regulate the activity of each other. They are serine/threonine kinases and are defined by their unique binding partners. The mTORC2 complex includes its binding partner Rictor and functions predominantly in actin organisation and differentiation (Agrawal et al., 2012) (Figure 1.11). Activation of this complex is usually measured by the phosphorylation of Akt on Serine 473 (Agrawal et al., 2012). It is via pAkt that mTORC2 mediates other roles as a regulator of cell cycle progression, glycogen metabolism and protein synthesis, as well as as both a negative and positive feedback regulator of mTORC2 activity (Vara J et al 2004). The mTORC1 is the other complex and can be inhibited by the drug Rapamycin which has shown to be effective in reducing the growth of GBM cell lines *in vitro* (Arcella et al., 2013). In mTORC1, mTOR forms an association with Raptor, a recruitment and scaffolding protein (Nojima et al., 2003) to mediate regulation of cell growth, proliferation and protein synthesis (Figure 1.11). Activation of this complex is usually measured by the phosphorylation of S6 on Serine 235/236 or by the expression of the upstream kinase, P70S6K. mTORC1 components, Raptor, p-S6 and P70<sup>S6K</sup> mediate tight control of critical cell processes and fluctuate in response to cellular stress, such as hypoxia (Wolff et al., 2011), cell cycle changes, pH changes (Balgi et al., 2011) and nutrient deprivation/abundance (Khapre et al., 2014), in order to compensate for these changes.

mTORC1 has two immediate downstream targets: p70<sup>S6K</sup> and 4E-BP1 targets (Figure 1.11) (Hara et al., 1998). Firstly, mTORC1 can activate p70<sup>S6K</sup>, via phosphorylation, in turn activating S6 (Kawasome et al., 1998) to promote translation of mRNA encoding translation elongation factors and ribosomal proteins (Jefferies et al., 1997). mTORC1 phosphorylates its second downstream target: 4E-BP1 which frees eIF-4E (translation initiation factor) to promote protein translation. In terms of cell cycle, the activation of S6 and eIF-4E specifically have been shown to enhance progression from the quiescent G0 phase into G1 phase (Fingar et al., 2004). USP9x has been shown to negatively regulate mTOR signalling in mouse myoblast cells, leading to increased phosphorylated S6, indicating mTORC1 activation, upon *USP9x* depletion, coupled with an increase in myoblast differentiation (Agrawal et al., 2012). As mTORC1 regulates transition from G0 into G1 through S6 activation, depleting USP9x could promote this transition, resulting in a reduction of cells from the quiescent phase.

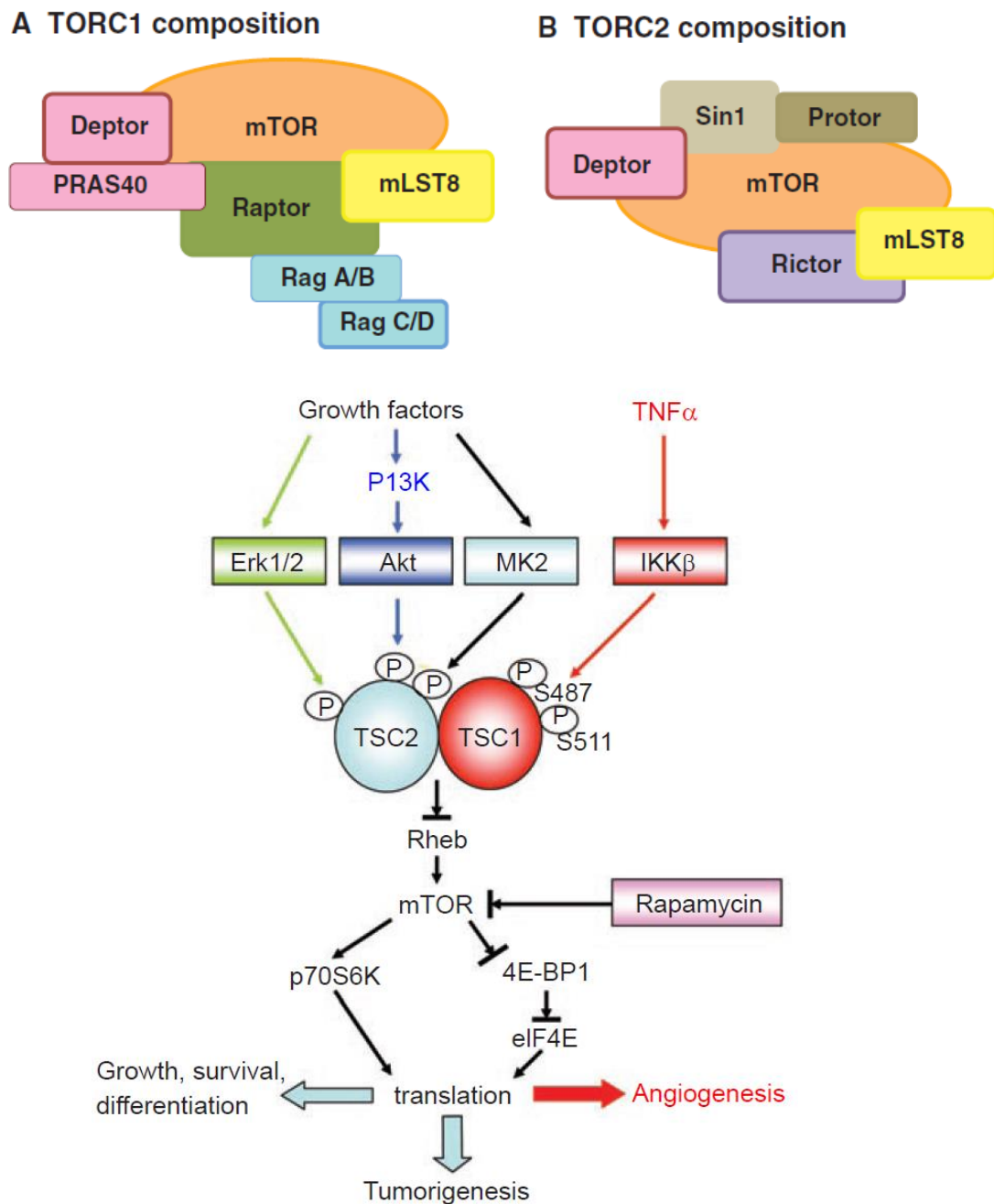


**Figure 1.11 mTOR complexes and signalling pathways.** The mTOR complexes are defined by the different proteins that they bind. mTORC1's major component is Raptor, whereas mTORC2's is Rictor. mTORC1 mediates the activation of p70<sup>SK6</sup> which activates S6 protein for translation of elongation factors and ribosomal proteins, whereas mTORC2 mediates the activation of Akt on serine473, which mediates processes involved in actin arrangement. (Russell et al., 2011) TSC1/2 complex inhibits Rheb which required for the activation of mTOR. When TSC2 is phosphorylated it can no longer inhibit Rheb, so Rheb activates mTOR. mTORC1 activates p70<sup>SK6</sup> which phosphorylates S6 to promote transcription of translation elongation factors, ribosomal proteins and transition from G0 in to G1 mTORC1 also activates 4E-BP1 which inhibits eIF4E. eIF4E has been also shown to promote G0 to G1 transition. (Wu and Zhou, 2007) (Licence # 3731070799491).

### 1.13 PI3K Signalling Pathway

Another pathway that links into the Ras and mTOR pathways, and has been reported to be mutated in cancer, is PI3K. Genes that are mutated within this pathway are mutated in GBM and neural caners. These include: PTEN and Ras which are both downstream of PI3K signalling (Wang et al., 2013, Castellano and Downward, 2011) or PI3K directly (Shayesteh et al., 1999, Ma et al., 2000). Phosphatidylinositol-3 Kinases (PI3K) are a class of kinase that phosphorylate phosphoipids on their inositol group (Fruman et al., 1998). Growth factors such as IGF, FGF and EGF bind their receptors and auto-phosphorylate tyrosine (Dilly and Rajala, 2008, Dey et al., 2010, Shah et al., 2006), recruiting PI3K to the intracellular membrane where it binds phosphotyrosine through its SH2 domain. This leads to the activation of PI3Ks catalytic subunit by which it converts PIP<sub>2</sub> to PIP<sub>3</sub>. PTEN is a phosphatase that catalyses the reverse reaction, preventing PIP<sub>3</sub> signalling, and has been found to be requently mutated in GBM (Wang et al., 1997). PIP<sub>3</sub> recruits PDK1 to the membrane which phosphorylates Akt on threonine 308. Akt then diverges to regulate substrates involved in cell cycle progression, survival and growth (Vara et al., 2004) (Figure 1.12).

For cell cycle progression, Akt inactivates GSK-3 $\beta$ , which prevents the downstream phosphorylation of  $\beta$ -catenin which is required for its degradation.  $\beta$ -catenin is then free to enter the nucleus, bind transcription factors and activate transcription of genes such as Cyclin D1. Akt also phosphorylates p21<sup>Cip/Waf1</sup> (Zhou et al., 2001) and p27<sup>Kip1</sup> (Viglietto et al., 2002, Shin et al., 2002), which mediate an inhibitory effect on cell cycle progression through association with CDK2, preventing CDK2-Cyclin E binding, which is required for progression into S phase. By phosphorylating p21<sup>Cip/Waf1</sup> and p27<sup>Kip1</sup> it localises them to the cytoplasm (Zhou et al., 2001, Shin et al., 2002, Viglietto et al., 2002), preventing its translocation into the nucleus so it can no longer interfere with cyclin E-CDK2 binding, losing its ability to inhibit cell cycle progression.

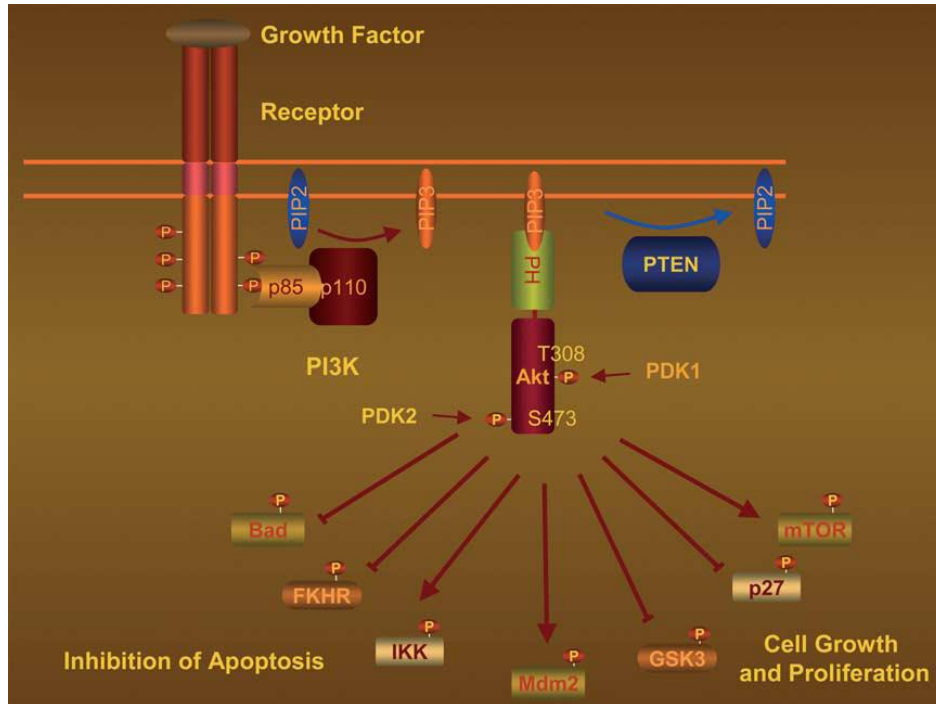


**Figure 1.12** *Akt regulation of downstream proteins involved in other signalling pathways. The activation of Akt occurs via the phosphorylation of threonine 308 and serine 473 by PDK1 and mTORC2 (with PDK2 when in the nucleus) respectively. Akt then goes on to activate substrates controlling regulation of checkpoint proteins, such as mdm2 and signalling pathway initiators like mTOR. It also inhibits cell apoptotic proteins, such as Bad, Wnt signalling proteins, as in GSK3 $\beta$  and cell cycle inhibitors such as p27. This demonstrates the multitude of substrates and processes that can be regulated by Akt. (Vara et al., 2004). (Vara et al 2007, Licence # 3731071104512)*

p-AktS473 is also regulated by activation of this pathway, where it can mediate control of cell growth and proliferation, independently, although, it commonly activates other pathways, such as mTORC1 (Figure 1.13). In the presence of growth factors, Akt phosphorylates the upstream mTORC1 inhibitor, TSC2 (Inoki et al., 2002) preventing its association with its binding partner TSC1. The TSC1/2 complex is active when growth factors are not present and inhibits Rheb, a GTPase that activates mTORC1 signalling under these circumstances, to promote protein synthesis.

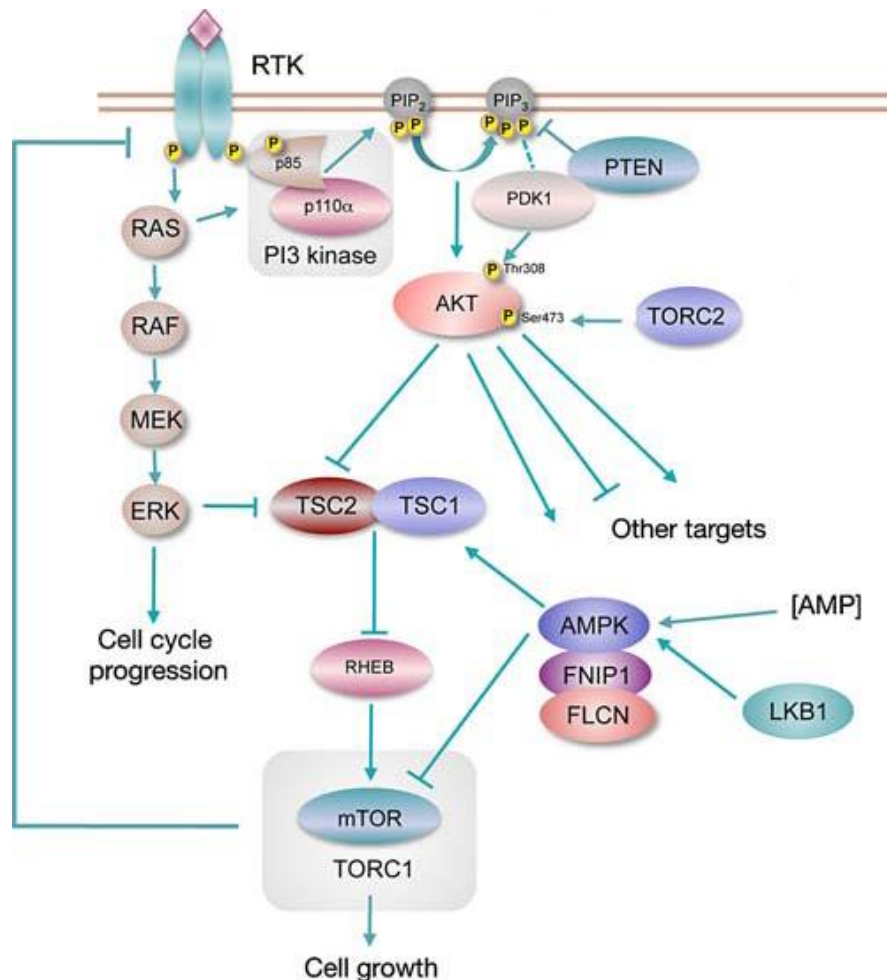


**Figure 1.13 PI3K signalling converging onto other signalling.** Tyrosine kinase receptors bind ligands such as EGFR, FGF and IGF which activate Ras and PI3K. Ras signalling promotes activation of Raf, MEK, and ERK downstream to promote activation of cell cycle progression proteins. Activation of PI3K converts PIP<sub>2</sub> to PIP<sub>3</sub>, (with PTEN phosphatase concurrently opposing this conversion) which activates PDK1. PDK1 phosphorylates Akt on threonine 308 which allows it to inhibit TSC2 through phosphorylation, preventing its binding with TSC1. TSC1/2 complex inhibits Rheb (a GTPase) in absence of growth factors. Rheb is a GTPase that activates mTOR1. (Knowles et al., 2009)( Licence # 3731071377400)

#### 1.14 USP9x, Ubiquitin Specific Protease 9 X linked

USP9x protein contains 2547 amino acids with a molecular weight of ~290kDa. It is involved in cell proliferation, signalling, self-renewal and substrate regulation (Dupont et al., 2009, Jolly et al., 2009, Li et al., 2011, Xie et al., 2012). It has been categorised as a stemness gene and shown to be both present and required for the maintenance of stem cell populations in developing organisms with expression decreasing as differentiation proceeds (Jolly et al., 2009). Its upregulation in mouse derived embryonic neural stem cells, resulted in an increased number of radial glial-like progenitors (Jolly et al., 2009). USP9x regulates the levels (Al-

Hakim et al., 2008, Nagai et al., 2009, Xie et al., 2012) or location (Dupont et al., 2009) of its substrates via deubiquitylation. USP9x itself is subjected to postranslational phosphorylation (Li et al., 2011). Substrates of USP9x can be involved in both tumour suppression and tumour cell survival (Schwickart et al., 2010, Dupont et al., 2009)

### **1.15 USP9x and Neural Stem Cells**

Usp9x is highly expressed in neural progenitors of the developing mouse brain (Stegeman et al 2013) and although its expression decreases in the adult, it remains highly expressed in regions of neurogenesis (Jolly et al., 2009). Fluctuations in its expression effect the neural organisation *in vitro* and *in vivo* (Jolly et al., 2009; Stegeman et al., 2013). Slight increases of Usp9x in neural progenitors, derived from embryonic stem cells, enhances their self-renewal capacity by promoting cell polarisation in highly proliferating radial clusters (Jolly et al., 2009). These radial clusters physiologically mimic the highly neurogenic apical and basal domain of polarised neural progenitors *in vivo*, where Usp9x is highly expressed apically, (Jolly et al., 2009). Usp9x is critical for neural development *in vivo*, as its deletion from neural progenitors of the mouse brain results in embryonic lethality (Stegeman et al., 2013). Nestin-Cre mediated deletion of *Usp9x* result in loss of the protein in developing brain from E10.5 onwards. This resulted in disruption in the organisation of neural progenitors of the cortical plate, ventricular and subventricular zones. There was also a reduction in neuronal projections from the neocortex to the cortical plate and the culture of embryonic hippocampal neurons confirmed a reduction in axonal outgrowth (Stegeman et al., 2013). This *in vivo* evidence demonstrates that Usp9x is required for the regulation of neural progenitors. Preliminary evidence from cultured human derived neural stem cells indicates that there is reduction in cellular proliferation after USP9x depletion, but no changes in differentiation. Taken together, this provides evidence that Usp9x is required for the neural progenitor maintenance, self renewal and proliferation both *in vitro* and *in vivo* (Jolly et al., 2009; Stegeman, et al 2009; Wood unpublished).

Usp9x plays a critical part in many signalling pathways including TGF- $\beta$ , Notch, Wnt, and mTOR signalling which regulate key processes including cell growth, proliferation, self-renewal and differentiation. The reduction in axonal outgrowth that was observed in the Usp9x<sup>-/-</sup> cultures was attributed to a reduction in TGF- $\beta$  signalling which normally promotes neuronal outgrowth. Usp9x has previously been shown to activate SMAD4 (Dupont et al., 2009), the TGF- $\beta$ /BMP secondary messenger, in multiple transformed cell lines, which promotes its

translocation into the nucleus. This promotes transcription of G1-S phase cell cycle inhibitors p21 and p15 which prevents proliferation (Dupont et al., 2009) and inhibits neurogenesis in neural development (Aigner and Bogdahn, 2008).

Usp9x has also been implicated in the Notch Signalling pathways by interacting with and stabilising the ubiquitin ligases Mindbomb-1 (Mertz et al., 2015), and Itch (Mouchantaf et al., 2006), which regulate Notch in the signal sending and receiving cell, respectively. Notch signalling is crucial for neural stem cell self-renewal, growth and proliferation (Aguirre et al., 2010). The interaction and stabilisation of  $\beta$ -catenin (Taya et al 1999), by Usp9x, has also implicated in promoting Wnt signalling, which is another critical pathway for neural stem cell growth and proliferation (Adachi et al., 2007). Increase  $\beta$ -catenin stability and signalling promotes its entry into the nucleus for transcription of cell cycle genes, such as cyclin D1 (Shutman et al., 1999) which promote cell proliferation at G1 – S phase. mTORC1 signalling is required for cell growth and cell cycle progression whereby the inactivation of mTORC1 results in reduced neural stem cell proliferation (Cloëtta et al., 2013). USP9x has recently been shown to interact with mTORC1 component, Raptor and p-mTOR but negatively regulates mTORC1 signalling in muscle myoblasts, whereby its depletion results in increased mTORC1 activity and an acceleration of myoblast differentiation (Agrawal et al., 2012). Therefore the regulation of neural progenitors by USP9x could involve multiple mechanisms

## **1.16 USP9x in Cancer**

### **1.16.a Usp9x as a tumour suppressor**

*Usp9x* has been suggested to be a tumour suppressor in pancreatic cancer (Pérez-Mancera et al., 2012). This study used a mouse model of pancreatic intraepithelial neoplasia (mPanIN), which is an intermediate in the development of pancreatic ductal adenocarcinoma (PDA) by expressing mutated KrasG12D in the developing pancreas. They then performed a sleeping beauty random transposon insertional mutagenesis screen in the developing pancreas to identify genes that reduced the latency of progression from mPanIN to PDA. This screen identified *USP9x* as the most common site for transposon insertion in the PDA tumours. The screen result was confirmed using Pdx1-cre mediated conditional deletion of *Usp9x*, and KrasG12D expression, specifically in the pancreas which demonstrated the very rapid development of pancreatic cancer from mPanIN (Pérez-Mancera et al., 2012). An interesting finding in human studies of PDA, was that there was poor prognosis for patients who had low *USP9x* mRNA expression after having undergone surgery to remove localised tumours (Pérez-

Mancera et al., 2012). This could also be seen in protein expression of USP9x from the PDA patient cell lines. This study strongly implicated USP9x as a tumour suppressor in the development of PDA. In addition, the sporadic expression of Pdx1-cre in the skin of these mice resulted in large papilloma as well as development of PDA, suggesting *Usp9x* may also act as a tumour suppressor in certain skin cancers (Perez-Mancera et al., 2012).

USP9x regulation of substrates such as ASK1, which mediates oxidative stress-induced cell death through activation of p38 MAPK and JNK pathways (Nagai et al., 2009) are also consistent with its role as a putative tumour suppressor. USP9x prevents ASK1 degradation through removal of ubiquitin (Nagai et al., 2009), increasing ASK1 availability to promote stress induced apoptosis and thereby opposing cell proliferation. USP9x also regulates the TGF- $\beta$  signalling pathway (Dupont et al., 2009) which promotes transcription of genes inhibiting G<sub>0</sub>/G<sub>1</sub> to S phase transition (Figure 1.7). These genes include p21 and p15 (Dupont et al., 2009) which repress cyclinD-Cdk4/6 and cyclinE-cdk2 (Figure 1.7). In early neoplasms, the signalling cascade has a growth inhibitory effect; reflective of the cyclin D-Cdk4/6 complex. In principle USP9x facilitation of TGF- $\beta$  signalling may also be consistent with a tumour suppressor role in some instances.

#### *1.16.b USP9x as an oncogene*

*USP9x* can also act as an oncogene. In blood cancers, USP9x acts as an oncogene and stabilises myeloid cell leukemia sequence 1 (MCL-1) through deubiquitylation, promoting tumour cell survival (Schwickart et al., 2010). Over expression of USP9x results in poor prognosis for patients. MCL1 is a member of the pro-survival BCL-2 family inhibiting mitochondrial-mediated apoptosis. This mechanism of cell death involves the activation of BH-3-only proteins, which further activates pro-apoptotic proteins Bax and Bak that are responsible for pore formation in the mitochondrial membrane, allowing release of cytochrome c (Hogarty, 2010). Bcl-2 family proteins, such as MCL1, can either sequester BH3-only proteins away, or, bind Bax and Bak preventing their dimerization and membrane pore formation (Li and Zhang, 2009). Stabilisation of MCL-1 by USP9x occurs through the removal of ubiquitin, added by the ubiquitin ligase Huwe1 which marks MCL-1 for degradation by the 26S proteasome (Schwickart et al., 2010). USP9x has also shown to increase the sensitivity of lung carcinoma cell lines to anti-apoptotic inhibitors and upon the exposure to ionising

radiation in lymphoma cells USP9x increases and enhances the stability of MCL-1, resulting in less cell death (Trivigno et al., 2012).

Further evidence supporting *USP9x* as an oncogene may lie in its role in the Wnt signalling pathway which maintains cell proliferation (Sacco et al., 2010, Tauriello and Maurice, 2010). USP9x stabilises the central protein involved in this pathway,  $\beta$ -catenin, (Voskas et al., 2010, Kaldis and Pagano, 2009, Tauriello and Maurice, 2010, Taya et al., 1999) thereby promoting its nuclear entry and transcription of cell cycle promoting genes, such as cyclin D1 (Colland, 2010) and hence stabilising an oncogenic/proliferative pathway. In the absence of Wnt ligand binding, a  $\beta$ -catenin destruction complex involving Axin-1, adenomatous polyposis coli (APC), casein kinase-1 (CK-1) and glycogen synthase kinase-3 (GSK-3), (Kaldis and Pagano, 2009, Tauriello and Maurice, 2010, Voskas et al., 2010) promotes the ubiquitylation of  $\beta$ -Catenin by  $\beta$ -TrCP which marks it for proteosomal degradation (Tauriello and Maurice, 2010). USP9x has been suggested to stabilise  $\beta$ -catenin by removing ubiquitin and disrupting the destruction complex near the APC and Axin-1 binding site (Taya et al., 1999).

The depletion of USP9x from brain tumour cell lines has been reported to reduce their growth *in vitro*. USP9x shRNA targeted depletion in a medulloblastoma cell line, DAOY-MB and two GBM cell lines, U118 and U87 resulted in reduced MTT activity and cell density *in vitro* (Cox et al., 2013). This provides supportive evidence that *USP9x* may act as an oncogene in the growth and proliferation of brain cancer cell lines prompting its further investigation in brain cancer development both *in vivo* and *in vitro*.

There is significant evidence for a requirement of USP9x in the maintenance, proliferation and growth of neural stem cells, as well as evidence for its role as either a tumour suppressor or an oncogene depending on cell context. This project is aimed at elucidating USP9x role in human neural stem cell regulation as well as identify its role as either a tumour suppressor or an oncogene in the development of brain cancer in an *in vivo* mouse model.

### ***1.17 Broad Project Aims – Investigating the role of USP9x in Brain Cancer Development***

Based on USP9x regulation of neural stem cell function and its role in human tumour progression this project aimed to precisely determine the role of USP9x in both healthy and diseased neural progenitors and identify the proliferative processes it regulates, using *in vitro* and *in vivo* approaches.

#### ***1.17.2 Aim 1: USP9x regulation of Human Neural Stem Cells***

1. Assess the effect USP9x depletion from the human NSC line ReNcell VM
2. Assess the effect of USP9x depletion on proliferation and cell cycle progression in ReNcell VM
  - a. Investigate the molecular mechanism behind changes proliferation and conduct cell cycle analysis
  - b. Investigate molecular changes at any affected cell cycle checkpoints
  - c. Investigate the activity of signalling pathways involved in affected checkpoints and screen for changes in expression of proteins involved in these pathways
  - d. Isolate the critical substrate of USP9x responsible for changes in proliferation or cell cycle
3. Investigate the possibility of USP9x depletion and cell death in ReNcell VM
  - a. Conduct cell apoptosis assays on USP9x depleted ReNcell VM
  - b. Investigate expression of cell apoptosis markers
4. Investigate the possibility of USP9x depletion causing increased differentiation
  - a. Investigate any changes in cell morphology and differentiation marker expression in USP9x depleted ReNcell VM

#### ***1.17.3 Aim 2: USP9x Regulation of Brain Cancer Cells, U-87MG GBM cells***

1. Confirm the USP9x is expressed and can be depleted from U-87MG GBM cells
  - a. Develop stable clones containing inducible USP9x shRNAs in ReNcells VM
  - b. Induce USP9x depletion and confirm a reduction in USP9x protein
2. Assess the effect of depleting USP9x from U-87MG GBM cells
  - a. Conduct proliferation and cell death assays
  - b. Investigate signalling pathways required in healthy USP9x ReNcells VM and compare differences in activation in these brain cancer cells

**1.17.4 Aim 3: Investigate USP9x Deletion and Activation of KrasG12D in the Developing Forebrain**

1. Develop animals with KrasG12D and *Usp9x* deletion from the forebrain
  - a. Obtain *KRasG12D* mice and breed them with USP9xfl/fl to develop *Kras/Usp9x* floxed females
  - b. Use *Kras/Usp9x* floxed females and mate with Emx-1Cre males
  - c. Allow *Kras/Usp9x* females to litter to give (a) *Kras/Usp9x* mutants), (a') *Kras/Usp9x* Cre- controls), (b) *KrasG12D* mutants (b') *KrasG12D* Cre- controls (c) *Usp9x* mutants (c') *Usp9x* Cre- controls)
2. Assess the effect of activating KrasG12D alone, compared to activation in conjunction with *Usp9x* deletion
  - a. Determine the time taken to develop, or amount of infiltration of tumours, in *KRasG12D*+/*USP9x*- compared with *KrasG12D*+ tumours.

## **2.0 CHAPTER TWO - MATERIALS AND METHODS**

### ***2.1 Mammalian Tissue Culture***

All cell culture was performed under sterile conditions in a class II biosafety tissue culture hood.

#### ***2.1.1 Thawing stock cells from liquid nitrogen storage***

Stock vials were obtained from liquid nitrogen stores and transferred on dry ice to -80°C freezer and thawed quickly by immersion in a 37°C water bath. Vial contents were transferred to 15ml Polypropylene tubes and 9mls of Maintenance Media was added drop wise to dilute DMSO with which cells were frozen. Cells were centrifuged for 5mins at 0.3rcf to generate a pellet, the solution was aspirated and cells were resuspended in Maintenance Media which was then transferred to flasks. Cells were maintained in incubators at 37°C with 5% CO<sub>2</sub>.

#### ***2.1.2 Passage of Cells***

Upon achieving confluence, media was aspirated and cells were washed with HBSS (life technologies). TrypLE (Life Technologies) of volume 1-2mls was then added to the flask and placed in the 37°C incubator for 5mins to allow cells to detach. Media was then added to dilute tryPLE, at least 1 in 10, and the cell suspension was transferred to 15ml polypropylene tube, which was then centrifuged at 0.3rcf for 5 minutes. Solution was then aspirated from cell pellet. Cells were resuspended in 1ml (for a small pellet that was just visible) and 3mls (for large pellet). Cells were then counted to establish cell number for seeding densities. Otherwise, cells were split at 1:2 ratio. In situations in which confluence had not been achieved during experiment, cells were split 1:1 into a new flask, to ensure cells were treated similarly.

#### ***2.1.3 Harvesting cells***

Media was aspirated from the flask and cells were washed once with HBSS. TrypLE (1-2mls) was added to the flask and incubated at 37°C for 5mins. Flasks were tapped to manually detach remaining cells from flask before media was added to dilute tryPLE. Cell solution was removed and transferred to 15ml polypropylene tubes which were then centrifuged for 5mins at 0.3rcf. From this stage, protocols for cell cycle analysis, annexin V-apoptosis, or cell

counting for seeding could be conducting. For western blotting, cell pellets were washed once in HBSS, re-centrifuged and the dry pellet collected for protein lysis and western blotting.

#### ***2.1.4 Counting cells for seeding***

A hemocytometer was used to count cells. 10µl of cell suspension was taken into 0.6ml eppendorf tube, to which 10µl trypan blue was added (1:1 ratio resulting in a dilution factor of 2). 10µl of solution was loaded onto one side of the hemocytometer. Cells within the four corner squares of the chamber were counted using Phase Contrast Olympus Microscope (CKX41) and the total cell number established.

#### ***2.1.5 ReNcell VM Cell Lines***

ReNcell VM are a cell line derived from the ventral mesencephalonic region of human fetal brain tissue that have been immortalised by retroviral transduction with v-myc oncogene (see product datasheet Millipore SCC010). Four ReNcell VM lines were incorporated in experiments. The two control lines that were used were wildtype untransduced ReNcell VM to control for the 'behaviour' of the untransduced cells and scrambled Scr ReNcell VM (which have been transduced with a lentiviral vector containing an shRNA with sequence: 5'ACTACCGTTGTTATAGGTGTTCAAGAGACACCTA TAACAACGGTAGT3' which has no homology to any known gene, including *USP9x*) to control for the transfection of the lentivirus. The two experimental lines used were both ReNcell VM that contain a *USP9x* shRNA, of which the expression is inducible upon Doxycyclin addition. The ReNcell VM 2193 line was transduced with a lentiviral vector containing shRNA of sequence: 5'GCTTGATCCTTCCCTGTTAAC3' targeted to *USP9x* (the first base pair being #2193 in the human *USP9x* sequence) and the ReNcell VM 4774 line was transduced with a lentiviral vector containing shRNA of sequence: 5'GCCATAGAAGGCACAGGTAGT3' targeted to *USP9x* (the first base pair being #4774 in the human *USP9x* sequence).

#### ***2.1.6 Maintaining ReNcell VM***

ReNcell VM Media was prepared as described (Donato et al., 2007). Maintenance media consisted of DMEMF12 (Life Technologies), 2mM L-Glutamine (Life Technologies), gentamicin 50ug/ml (Life Technologies), 1X B27 neural cell supplement mix (Life Technologies), 10Units/mL Heparin and was supplemented with 20ng/ml EGF (Chemicon Cat # GF144) and 20ng/ml bFGF (Chemicon Cat# GF003). For treatment, ReNcell VM

media (containing 20ng/ml EGF and 20ng/ml bFGF) was supplemented with 1 $\mu$ M Doxycyclin from a 1mM stock prepared from Doxycyclin Powder (Sigma D9891). Natural Mouse Laminin 1mg/ml (Life Technologies Cat# 23017-015) was diluted to 0.5mg/ml with UltraPure Distilled Water (Life Technologies) for a working solution. Flasks were coated, with Natural Mouse Laminin diluted to 20 $\mu$ g/ml with DMEM/F12 at least four, but up to twenty-four hours, prior to seeding/plating cells. Media was changed every two-three days, in which cells were washed HBSS (Life Technologies), and fresh supplemented media. Cells were passaged upon achieving 70-90% confluence using trypLE dissociation.

#### ***2.1.7 The transducible knockdown Lentiviral system***

Lentiviral system used is based on the doxycycline-inducible expression of silencing shRNAs (Brown et al., 2010). *USP9X*-targeting lentiviral vectors (2913 and 4774 Section 2.1.5) were transduced into ReNcell VM and U-87 MG GBM cells. Pools of EGFP-positive cells, which reflect high levels of shRNA expression were isolated by FACS. Cell lines were checked periodically to ensure EGFP expression was maintained in the population.

#### ***2.1.8 Real Time analysis of cultured cells using Xcelligence***

ReNcell VM cells were seeded in triplicate at 2000 cells/well of a 96well Xcelligence gold plate (E-Plate VIEW 96, Roche). The Xcelligence machine was started and paused 24hrs later, while Doxycycline was added to cells at a final concentration of 1 $\mu$ M. Xcelligence analysis was re-initiated and let run for up to 144hrs. For analysis, cell index was normalised to the reading prior to Dox treatment and cell indices were compared within treatment for each line.

#### ***2.1.9 MTT Assay***

ReNcell VM cells were seeded in triplicate at 2000 cells/well (for experiments up to 72hrs) or 500 cells/well (for experiments up to 168hrs – removal of Dox experiment) on a clear-based 96well plate (Nunc). At each timepoint, the MTT Reagent was added for 1-2hrs and incubated at 37°C prior to reading absorbance at 490nm.

### ***2.1.10 Inhibition of USP9X by WP1130***

Wildtype ReNcell VM cells were seeded at 2000 cells/well into a 96 well clear bottom plate. 24hrs later 5 $\mu$ M of WP1130 was added to cells, with 0.1% DMSO vehicle control. MTT assay was conducted for each of the following timepoints, 0hrs, 6hrs, 12hrs, 18hrs, 28hrs.

### ***2.1.11 FLOW Cytometry Cell Cycle profile for ReNcell VM***

Cells were seeded at 4-500000 cells/flask into T25 laminin coated flasks, containing Maintenance Media. The following day, media was refreshed with 1 $\mu$ M Doxycyclin supplemented media added to treatment flasks. Cells were maintained, split on day three of doxycycline treatment to ensure sub-confluence at day four. Cells were then harvested on the fourth day for Propidium Iodide staining and FLOW cytometry analysis.

### ***2.1.12 Propidium Iodide Staining***

Cells were harvested from flasks and pelleted before washing with 1  $\times$  HBSS and re-centrifugation for 5mins at 0.3rcf. HBSS was aspirated and cells were resuspended in 1ml HBSS. For fixation, 3mls of absolute ethanol was added (first 2mls added drop wise to prevent generation of aggregates) to HBSS/cell suspension. Cells were fixed at 4°C for one hour. Cells were then centrifuged at 0.4rcf for 5mins and solution aspirated. Pellet was washed with 1  $\times$  HBSS and centrifuged at 0.4rcf for 5mins. Tissue culture hood light was turned off before pellet was resuspended in 1ml of Propidium Iodide staining solution (3.8mM Sodium Citrate, 50ug/ml PI (Sigma P4170), in DPBS) due to light sensitivity of propidium iodide. 50 $\mu$ l of RNase A stock solution (10 $\mu$ g/ml RNase A (Roche Ref # 10109142001) in DPBS) was added to tubes. Tubes were wrapped in foil and stored at 4°C until FACS analysis was performed, by Dr. Bernedette Bellele, Eskitis Institute for Drug Discovery, Griffith University.

### ***2.1.13 Apoptosis Assays***

Cells were harvested 24hrs after doxycycline addition and centrifuged at room temperature for 5 mins at 0.4rcf before washing once with HBSS and then re-pelleted. At this point 400 $\mu$ l/sample of 1  $\times$  Binding buffer and 100 $\mu$ l/sample of Annexin V incubation reagents (10 $\mu$ l 10 $\times$  binding buffer, 10 $\mu$ L Propidium Iodide, 1 $\mu$ L Annexin V-biotin, 79 $\mu$ L UltraPure water; in darkness; on ice) were prepared and 10<sup>6</sup> cells were resuspended in Annexin incubation and left in darkness for 15mins at room temperature. 1 $\times$  Binding buffer was added

to suspension and cells were centrifuged as previously. Cells were then resuspended in 100µL streptavidin-PeCy7 conjugate buffer (Streptavidin-PeCy7 - 488 excitation, 767 emission - in 100µL 1× binding buffer) and incubated in darkness for 15mins at room temperature. 400µL binding buffer then added to samples and processed by flow cytometry within 1 hr, by Dr. Bernadette Bellette.

#### ***2.1.14 Immunofluorescence – ReNcell VM cell differentiation***

ReNcell VM cells were seeded in triplicate at 500 cells/well into a 96 well plate and replaced with 1µM Doxycyclin media after 24hrs. ReNcell VM cells were differentiated by EGF/FGF withdrawal. After 9 days culture, media was removed, cells were washed and fixed with 4% PFA in DBPS for 5mins, washed twice, blocked and permeabilised with 0.2% Triton X-100, 3% goat serum in DBPS for 45mins-1hr at room temperature, washed twice and incubated with primary antibodies (either goat anti-mouse GFAP 1/500, mouse anti-βIII tubulin 1/200 or rabbit anti-S100β 1/200 (all from abcam), rabbit anti-USP9x 1/200 (Bethyl)) for 1hr at room temperature, before washing as above and addition of secondary antibodies (either goat anti-mouse 1/500 or anti-rabbit 1/500). Dapi staining was used at 1/5000, to identify nuclei.. Immunofluorescence was observed on Olympus IX-70.

#### ***2.1.15 mTORC1 stimulation assay***

ReNcell VM cells were treated with 1µM doxycycline for 24hrs or 72hrs to induce USP9x depletion. Media was then replaced with media lacking EGF/FGF (1µM Dox) and cultured for 24hrs to deplete mTORC1 and mTORC2 activity, causing cells to enter quiescence. After 24hrs (i.e. 0min timepoint) cell lysate was harvested for western blotting by adding RIPA lysis buffer (150mM NaCl, 1.0% Triton X-100, 0.5% sodium deoxycholate, 0.1% sodium dodecyl sulphate, 50mM Tris, pH 8.0. Stock solution of 10% deoxycholate solution was prepared and kept in dark as advised by protocol. 20µl/mL Protease and 20ul/mL phosphatase inhibitor was added to prevent protein degradation.) and mechanically scraping. For 5min and 15min timepoints, EGF/FGF media was incubated for these times prior to protein lysis using RIPA buffer mix. Lysates were prepared for western blotting.

#### ***2.1.16 Proteasomal inhibition – mTORC1 activity rescue experiments***

‘4774’ ReNcell VM cells were seeded at 10<sup>5</sup> cells/well into a 6 well plate and treated with 1µM doxycycline for 72hrs, at which time EGF/FGF was removed in preparation for

mTORC1 stimulation assay. 18hrs after, 25nM Expoxomicin (0.1% DMSO as a control) was added to inhibit the proteasome and by the 24<sup>th</sup> hour, EGF/FGF stimulation was conducted (as per mTORC1 stimulation experiment materials and methods above).

#### ***2.1.17 Immunoprecipitation***

Immunoprecipitation was conducted using the Co-Immunoprecipitation kit in accordance with manufacturer's instructions (Thermo Pierce Scientific). 0.5mg of ReNcell VM cell lysate was precipitated with 3µg USP9x antibody and precipitated proteins run on SDS PAGE gel and subjected to western blot analysis.

#### ***2.1.18 Nucleofection of ReNcell VM cells***

Nucleofection of ReNcell VM cells was conducted using Lonza Amaxa Cell Line Nucleofector Kit V in accordance with manufacturer's instructions (Lonza).  $2 \times 10^6$  ReNcell VM cells were transfected with between 2µg and 4µg of purified plasmid DNA. Cells were monitored for pDESTEGFP or pmax-GFP controls to determine transfection efficiency as determined by the percentage of cells expressing EGFP from control plasmids.

#### ***2.1.19 mTORC1 Plasmids***

The following mTORC1 plasmids were obtained from Addgene: myc-mTOR (Addgene #1861) and Ha-Raptor (Addgene #8513) and Ha-S6K1 (Addgene #8984). Plasmid maps can be found in Appendix. These were expanded and purified for transfection into ReNcells VM.

#### ***2.1.20 U-87 MG GBM Cell lines***

U-87 MG GBM cell lines were received as a kind gift from Dr. Adrian Medeeniya, Griffith University. U-87 MG cells were transduced with lentiviral DNA vectors, as described for ReNcell VM experiments (Section 2.1.7).

#### ***2.1.21 Maintaining U-87 MG GBM cell lines***

U-87 MG cells were maintained in media consisting of: 10% FBS (Life Technologies), 1.5% PenStrep (Life Technologies) in DMEM-F12 (Life Technologies) and refreshed every 2-3 days depending on confluence. U-87 MG cells achieve confluence when ~60% of the culture flask was covered. If cells were left for longer period, spheres formed due to contracting and

detaching from bottom of flask. Upon achieving confluence, cells were passaged using trypLE (Life Technologies) dissociation. N.B. Other GBM cell lines later obtained were routinely cultured as per U-87 MG culturing.

#### ***2.1.22 shRNA transduction of U-87 MG cells***

U-87 MG cells were transduced with the same *USP9x* and control lentiviral vectors as for ReNcells VM, ie. 'Scr', '2193' and '4774' shRNA constructs. Stock plasmids were transformed, expanded and confirmed before proceeding to transfection and transduction, in which GFP expression was monitored for successful transfection, before FACS sorting to obtain homogenous populations.

#### ***2.1.23 Lentiviral Plasmid Amplification for U-87 MG***

Plasmids were amplified as per routine laboratory protocols. JM109 E. coli cells were transformed with plasmid DNA using the heat shock method and were grown on Ampicillin or Kanamycin plates as described (Froger and Hall, 2007). Plasmid minipreps were performed by alkaline lysis as described (Birnboim and Doly, 1979). Plasmid midi-preps were performed using Qiagen Midi Prep Kit (25) Cat# 12143 as per the manufacturer's instructions. Plasmid integrity was determined using restriction enzyme digestion (Sambrook et al., 1989)

#### ***2.1.24 Cell Transduction***

##### ***2.1.24.1 293FT viral packaging cell line***

293FT cells were thawed as previously described in 2.1.1 and maintained in 10% FBS in DMEMF12. Viral packaging cell line 293FT cells were obtained from Dr. Lyndal Mason (Griffith University, Eskitis Institute, QLD, Australia) and used to produce viral supernatant according to manufacturer's instructions, (Life Technologies). Cells were cultured in DMEM high glucose (Invitrogen) supplemented with 10% FBS (Bovogen), 0.1mM MEM Non-Essential Amino Acids (NEAA) (Invitrogen), 6mM L-Glutamine (Invitrogen,) and 1mM MEM Sodium Pyruvate Solution (Invitrogen,). No antibiotics were incorporated in media as ViraPower packaging step 5 (Invitrogen, ViraPower Lentiviral Expression Systems, 2006) recommends no antibiotics for viral packaging.

#### **2.1.24.2      *ViraPower Lentiviral Packaging***

293FT cells were transfected with plasmid DNA for viral packaging according to manufacturer's instructions (Invitrogen, 2006 'ViraPower Lentiviral Expression Systems'). Viral supernatant was collected after three days and centrifuged at 3000rpm for 15mins to pellet debris. Supernatant was aliquoted into cryovials and stored at -80 degrees until required for transduction.

#### **2.1.24.3      *Transduction of U-87 MG GBM cells***

The transduction of U-87 MG cells was performed according to Manufacturer's instructions (Invitrogen, 2006 'ViraPower Lentiviral Expression System Manual') and successfully transduced GFP+ cells were clonally sorted into a 96 well plate for Scr, 2193 and 4774 constructs. The yield achieved for wells containing single GFP+ cells was less than 10%. Clones were expanded until all cells were GFP+.

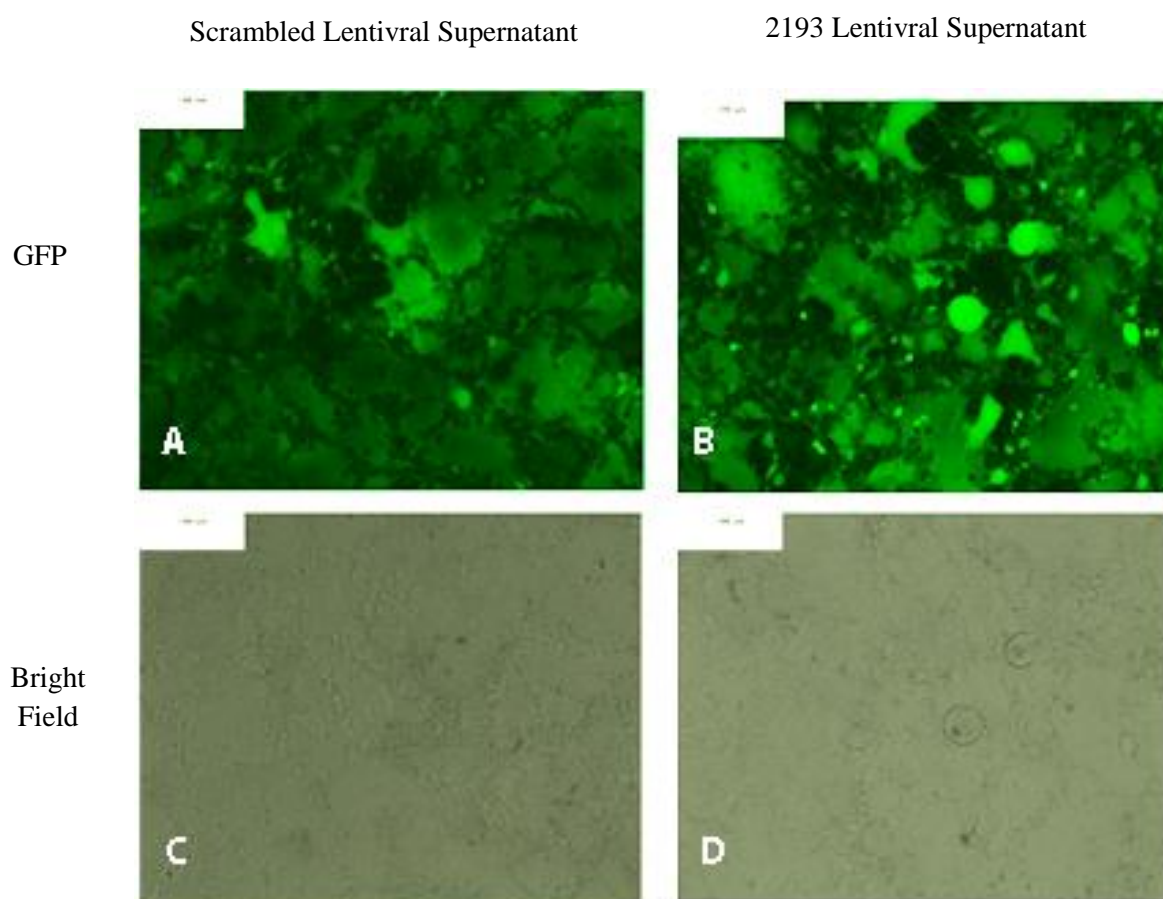


**Figure 2.1** *Representative packaging with virapower and lipofectamine. 24hrs after packaging of Lentivirus into 293FT (viral packaging cell line). 293FT cells transfected with*

*Scrambled DNA (A GFP positive cells, C Bright field) and 2193 DNA (B GFP positive cells and D Bright field). 100µm scale bar magnification.*

#### **2.1.25 Culturing of GBM cell lines U118, U-87 MG, U251,D645,D270**

Five mycoplasma free GBM cell lines were obtained from Dr. Andrew Boyd at the Queensland Institute for Medical Research, Brisbane. They were U118, U-87 MG, U251, D645, D270 and have all been classified and routinely used as GBM grade tumour cells. Cells were grown and cultured in maintenance medium consisting of 10% FBS, 1-2% PenStrep in DMEMF12, and stock vials were made and frozen in liquid nitrogen.

#### **2.1.26 USP9x siRNA interference in GBM cell lines**

USP9x siRNA interference was conducted using Thermo Scientific DharmaFECT Transfection Protocol (Thermo Scientific) in accordance with the manufacturer's instructions. A pool of four USP9x siRNAs was used to knockdown USP9x and were obtained from Millenium Science (SMARTpool ON-TARGETplus USP9x siRNA Cat# L-006099-00-0005 5nmol) as well as non targeting scrambled control siRNA (ON-TARGETplus Non-targeting Pool Cat# D-001810-10-05 5nmol). siRNAs were prepared to 5µM stock solutions and final transfection concentration was 25nM in accordance with manufacturer's recommendations. The GBM cells were seeded at 75000 cells/well into a 6 well plate. Prior to transfection 1600µL of complete media was added in preparation for the addition of the 400uL of siRNA mix. For each well, tube 1 was prepared containing 10µL of 5µM stock siRNAs was diluted with 190µL of Serum-Free OptiMEM media (Life Technologies), and tube 2 was prepared containing: 10µL of DharmaFECT (Millenium Science) diluted in Serum-Free OptiMEM media. Each tube was incubated for 5mins at room temperature prior to their combination for 20mins at room temperature. USP9x siRNA and control siRNA mixtures were added dropwise to each well of each GBM cell line. After 72hrs, wells were collected for western blot expression or prepared for mTORC1 activity stimulation.

#### **2.1.27 mTORC1 stimulation in USP9x depleted GBM cell lines.**

Following 72hrs post transfection of USP9x and control siRNAs, mTORC1 stimulation was conducted in the same manner as for ReNcells VM (Section 2.1.15). However, as FBS is used to provide necessary mitogens, starvation and stimulation was achieved removal and addition of FBS.

### ***2.1.28 Neurosphere cultures – For USP9xKO and KrasG12D Spheres***

Neurosphere isolation and propagation was conducted as previously described (Homan, et al., 2013). Briefly, embryos were extracted and dissected in cold sterile Hanks solution ( $10\times HBSS$ ). Cortex was removed and placed in digestion mix 1:1 PAP (L15 Media, 30U/mL papain, 0.24mg/ml cysteine, 40 $\mu$ g/ml DNase, filter sterilised): Ovomuroid (L15 media, 0.86mg/ml ovomucoid trypsin inhibitor, 0.5mg/ml BSA, 40ug/ml DNase, filter sterilised), mechanically digested and incubated at 37°C for 45mins, prior to neutralisation with ovomucoid. Tissue was homogenised with a flame polished pipette, settled for 3mins before washing through GlutaMax-DMEMF12 and centrifuging at 1.0rpm. Remaining cells were resuspended in neurosphere culture media before transferring into flasks. Spheres were passaged every four days as necessary by collecting all spheres, resuspending in 1ml Versene, centrifuging before resuspending cells in 0.5mL of 1:20 ratio of  $10\times$  TrypLE: Versene and incubating for 15mins. Ovomuroid (0.5mL) was added to neutralise the reaction for 5mins before homogenising with fire polished glass pipette. Cells were washed through GlutaMax-DMEMF12 and centrifuged at 1.0rpm before resuspension into Neurosphere media (DMEMF12-GlutaMax, 2% B27, 20ng/ml hEGF, 20ng/ml bFGF, 1% PenStrep) and passaged into new flasks.

### ***2.1.29 Neurosphere dimensions***

Prior to each passage four or five fields of view were photographed in order to count the number of spheres, measure sphere diameter and volume. During each passage, dissociated cells were counted in triplicate in order to establish the number of dissociated cells and the number of cells / sphere. The diameter of each sphere was ruled, the volume was calculated using the ‘volume of a sphere’ formula:  $\frac{4}{3} \times \pi \times (\text{diameter}/2)^3$ . The number of cells/neurosphere was calculated by: # dissociated cells / # of neurospheres per field of view.

### ***2.1.30 mTORC1 stimulation of Neurospheres***

Neuropheres in EGF/FGF media were collected by from flask suspension and centrifuged at 1.0rpm for 5mins to pellet spheres. Spheres were then resuspended in EGF/FGF deficient media for 24hrs before being resuspended in 1mL of EGF/FGF media for 0, 5 15, 25 mins for USP9x KO spheres and 0, 10, 20, 30 mins for KrasG12D before collection for western blotting.

## **2.1.31 General Molecular Biology / Biochemistry Methods**

### **2.1.31.1 SDS PAGE and Western Blotting**

#### **Reagents and Solutions**

RIPA Lysis Buffer: (150mM NaCl, 1.0% Triton X-100, 0.5% sodium deoxycholate, 0.1% sodium dodecyl sulphate, 50mM Tris, pH 8.0. Stock solution of 10% deoxycholate solution was prepared and kept in dark as advised by protocol. 20 $\mu$ l/mL Protease and 20 $\mu$ l/mL phosphatase inhibitor was added to prevent protein degradation.), SDS Lysis buffer: (20% glycerol, 1% SDS, 10mM Tris pH 7.4, dH<sub>2</sub>O to 20mL, 20 $\mu$ l/mL Protease Inhibitor was added to prevent protein degradation.), 2  $\times$  SDS PAGE loading buffer (100mM Tris pH 6.8, 4% SDS, 20% glycerol, dH<sub>2</sub>O to 20mL, Bromophenol Blue ~20-30 $\mu$ l, Prior to use 100mM DTT was added to reduce disulphide bonds), SDS Running buffer (precast gels): (50mL 20 $\times$  NuPAGE SDS Running buffer (Invitrogen cat# NP0002), dH<sub>2</sub>O to 1 litre). Transfer Buffer 2 $\times$  (28.8g Glycine, 6.1g Tris, 200mL methanol, dH<sub>2</sub>O to 1 litre), Blotting Buffer (3g Tris, 8.8 NaCl, 0.1% Tween, Adjust pH to 7.4 using HCl), Blocking Buffer (5% skim milk in blotting buffer (above)). Antibodies were diluted in blocking buffer and incubated on membrane. 10 $\times$  TBS: (24.23g Tris, 80.06g NaCl, dH<sub>2</sub>O to 1 litre, adjust pH to 7.4-7.6), TBS Tween: (1M TBS, 1mL Tween 20, 900mL dH<sub>2</sub>O), Ponceau S Stain Solution (0.1% Ponceau S and 1% acetic acid in 500ml milliQ water.)

### **2.1.31.2 Harvesting protein lysate**

At timepoint of interest, cells were harvested by either cell scraping or TripLE to generate cell pellet. Pellet was washed twice with HBSS to remove excess media. RIPA lysis buffer (containing protease and phosphatase inhibitors) was added to pellet, cells were resuspended and vortexed to disrupt membranes. DNA was sheared by repeated passage through a 27G needle. Lysates were spun for 10mins at max speed (21,130rcf) in Eppendorf 5424 Benchtop Centrifuge at 4 degrees. Supernatant was transferred to a clean Eppendorf tube and BCA estimation conducted as per manufacturer's instructions (Pierce Thermo Scientific).

### **2.1.31.3 SDS PAGE preparation**

The reducing agent Dithiothreitol (DTT) was added to 2  $\times$  SDS PAGE loading buffer at final concentration of 100mM, to reduced disulphide bonds. The required volume of samples (as calculated using BCA estimation) along with an equal volume of 2  $\times$  SDS PAGE loading buffer was added to 1.5ml Eppendorf tubes. Tubes were then heated for 5 minutes at 95°C, to denature inaccessible disulphide bonds. Samples were either stored at -80°C or loaded

directly onto relevantly prepared percentage casted-gels. 4µl of Protein ladder (Thermo Scientific Cat# SM1811) was loaded into the first lane of gels. Samples were run at 150V for 60mins, with gels immersed in MES NuPAGE Running buffer (Invitrogen Cat #NP0002). Gels were then prepared for Western Blotting.

#### **2.1.31.4 Western Blotting preparation**

Western blotting was conducted as previously described (Stegeman et al., 2013) and in accordance with manufacturer's instructions (BioRad). Antibodies used are listed in the table below.

#### **2.1.31.5 Immunoblotting and immunohistochemistry**

<b>Primary Antibody (&amp; Protein molecular weight)</b>	<b>Company</b>	<b>Dilution **</b>	<b>Raised in</b>
β-Catenin 88-94kDa	Sigma Cat#C2206	1/1000	Rabbit
Cyclin D1 36kDa	Cell Sig Tech Cat#2922	1/1000	Rabbit poly
Cyclin E (HE12) 48-56kDa	Cell Sig Tech Cat# 4129	1/1000	Mouse IgG1 mono
Cyclin A (BF683) 55kDa	Cell Sig Tech Cat #4656	1/2000	Mouse IgG2b mon.
Cleaved Caspase-3 (Asp175) 17,19kDa	Cell Sig Tech Cat# 9661	1/1000	Rabbit
Caspase-317, 19, 35kDa	Cell Sig Tech Cat# 9662	1/1000	Rabbit poly
Mcl-1 L.40kDa S. 32kDa	Santa Cruz Cat# sc-819	1/500	Rabbit poly
N term. USP9x Sww2/1 ~290kDa	Affinity Purified*	1/2000	Rabbit
USP9x C terminal ~290kDa	Bethyl Lab. Cat# A301-351A	1/2000	Rabbit
p-S6(ser235/236) XP 32kDa	Cell Signalling Technologies	1/2000	Rabbit
S6	Cell Signalling Technologies	1/2000	Rabbit
p-mTOR	Cell Signalling Technologies	1/800	Rabbit
mTOR	Cell Signalling Technologies	1/2000	mouse
Raptor	Cell Signalling Technologies	<b>1/800</b>	Rabbit
Rictor	Cell Signalling Technologies	1/800	Rabbit
P70S6K	Cell Signalling Technologies	1/500	Rabbit

p-Akt(S473)	Cell Signalling Technologies	1/1000	Rabbit
Akt	Cell Signalling Technologies	1/2000	Rabbit
TBR1	Abcam	1/200	Rabbit
TBR2	Abcam	1/200	Rabbit
KrasG12D	NewEast	1/25	Mouse
SOX2	Abcam	<b>1/200</b>	Rabbit
BLBP	Millipore	1/200	Rabbit
PH3	Abcam	1/200	Rabbit
$\beta$ III tubulin	Abcam	1/250	Rabbit
PAX6	Abcam	1/1000	Rabbit
S100 $\beta$	Abcam	1/250	Mouse
E2F1	Millipore	1/1000	Rabbit
p-Rb	Cell Signalling Technologies	1/1000	Rabbit
Rb	Cell Signalling Technologies	1/2000	Mouse
<b>Loading Controls</b>			Rabbit
G3PDH~38kDa	TREVIGEN Cat# 2275-PC-100	1/10000	Rabbit IgG mono
$\beta$ -tubulin~50kDa	Sigma-Aldrich Prod # T0198	1/1000	Mouse IgG1 mono
<b>Secondary Antibody</b>	<b>Company</b>	<b>Dilution</b> **	<b>Raised in</b>
Goat anti Rabbit HRP conjugate	Millipore Cat# AP 132P	1/5000	Goat IgG poly
Goat anti Mouse HRP	Millipore Cat# AP 124P	1/5000	Goat IgG poly

\* by colleague of Dr. Stephen Wood as per Kanai-Azuma et al 2001., \*\* in 5% skim milk in blotting buffer

#### 2.1.31.6 Immunoblotting Procedure

Primary antibody was added to membrane and incubated overnight at 4°C. The following day the membrane was washed three times with blotting buffer and the secondary antibody added and incubated for two hours at room temperature. Membrane was then washed three times with blotting buffer before ECL Chemiluminescent substrate (Millipore, Cat # WBKLS0500) was added and membrane visualised at VersaDoc Imaging station and band expression was normalised against loading control antibody expression.

### 2.1.31.7 Reprobing membrane

After visualisation, membrane was washed for 15 minutes with TBSTween, re-blocked for 10 minutes at room temperature. Procedure was repeated (Section 2.1.31.6).

### 2.1.32 Animal Ethics

Animals ethics was granted for this project under ESK10/12 and ESK04/13. Animals for KRasG12D × Emx1 Cre experiments were approved under ESK09/14. All experiments were carried out in accordance with the ethical approval.

### 2.1.33 Genotyping Animals

PCR was used to determine the genotypes of animals for breeding and resulting litter progeny. Animals for breeding and their weaned progeny, were ear notched at 3 weeks and genotyped. For embryonic extractions, tail tips were collected during dissection and genotyped for KRasG12D<sup>lox</sup>, USP9x<sup>lox</sup>, Emx-1-Cre, using REDExtract-N-Amp Tissue PCR Kit (Sigma) in the following reaction:

PCR Reaction	Volume/ Reaction (uL)
Red Mix	7.5
Fwd Primer	0.95
Rev Primer	0.95
Extraction Buffer	0.95
Neutralisation Buffer	0.95
Water	1.7
DNA sample	2

In order to confirm the presence of the USP9x ‘floxed’ cassette in progeny, primers detecting the Neo cassette added to intron 3 as a part of the loxP modification and has been used previously (Stegeman et al., 2013). Therefore, animals positive for the ‘Neo’ amplicon indicated the presence of a floxed USP9x sequence and termed ‘Neo positive’. The primer sequences have an annealing temperature of 60 degrees, producing a 400bp amplicon with their sequence:

*Neo<sup>f</sup>*                      5'-tgctcctgccgagaaagtatccatcatggc-3'

*Neo<sup>r</sup>*                      5'-cgccaagctcttcagcaatatcacgggtag-3'

The presence of the modified *KrasG12D* allele was detected by primers that flank the LoxP site of the ‘STOP’ sequence and the modified *KrasG12D* sequence. Primers sequences were designed according to *NCI Mouse Repository* and have been previously described (Jackson et

al., 2001). The forward primer ‘recognises the beginning of the downstream LoxP site flanking the ‘*STOP*’ modification, behind the *Kras* allele. The reverse primer ‘*Kras006*’ recognises part of the manipulated *KrasG12D* sequence, further downstream from the final LoxP site. The primer sequences have an annealing temperature of 55 degrees (but needed to be continuously modified), with the amplicon producing a band of 550bp, and have the following sequence below. Animals positive for the *KrasG12D* sequence have the modified *KrasG12D<sup>lox</sup>* gene.

*Kras005<sup>f</sup>*      5'-agctagccaccatggcttgagtaagtctgca-3'  
*Kras006<sup>r</sup>*      5'-cctttacaagcgagactgtaga-3'

The modification of the *Emx-1* allele to include the DNA enzyme, Cre recombinase, downstream of the *Emx-1* gene was detected using forward and reverse primers flanking the sequence of Cre recombinase. These primers have an annealing temperature of 53 degrees and produced an amplicon of 203bp, (primers sequence below).

*Emx-1Cre<sup>f</sup>*      5'-tgatgaggttcgcaagaacc-3'  
*Emx-1Cre<sup>r</sup>*      5'-ccatgagtgaacgaacactgg-3'

The *Sry* gene is located on the Y chromosome, and is used to identify male embryos (Stegeman et al., 2013). Detection of *Sry* used the following primers flanking the region of the SRY gene:

*SRY<sup>f</sup>*              5'-gaggcacaagttggcccagcag-3'  
*SRY<sup>r</sup>*              5'-ggttcctgtcccactgcagaag-3'

Animals that were ‘*KrasG12D*’, ‘*Neo*’ and ‘*Cre*’ positive meant they were of the genotype: *KrasG12D<sup>lox</sup>/Usp9x<sup>lox</sup>/Cre<sup>+</sup>* and expected to express the mutant form of *KrasG12D*, on the background of *Usp9x* deletion in the forebrain. Animals that were ‘*KrasG12D*’ and ‘*Cre*’ positive only expressed *KrasG12D* from the forebrain and animals that were ‘*Neo*’ and ‘*Cre*’ positive only had *USP9x* deleted from the forebrain.

### **2.1.33 In utero extraction – brain collection**

Pregnant mothers were sacrificed using CO<sub>2</sub> asphyxiation and embryos were extracted. Embryonic heads were removed prior to taking tails for PCR. For western blotting, the brain was isolated and the cortices extracted for protein lysis using RIPA lysis buffer containing protease inhibitors. For immunohistochemistry, macro-dissection was conducted on heads to remove surrounding meninges. Brains were fixed in 4% PFA for 2.5hrs prior to transfer into 15% sucrose in PBS. Heads were transferred into increasing sucrose gradients (15%, 30%,

30%:OCT, OCT) after two days, or upon 'floating'. Heads were then mounted in OCT blocks and stored at -80 degrees until sectioning.

#### ***2.1.34 Cryo-sectioning***

OCT blocks were mounted onto chucks and sectioned at 10µm thickness onto SuperFrost glass slides using a Leica CM3050 S Cryostat. Slides were dried for 2-3hrs at room temperature and frozen at -20 degrees, or taken for Nissl or Immunohistochemistry staining.

#### ***2.1.36 Nissl Staining***

Sections were washed in Xylene (2 × 3min) to remove OCT on tissue slides, rehydrated in 100% alcohol (2 × 3min each), Stained with 0.1% Cresyl Violet in 0.2% in Acetate Buffer (4-15mins), rinsed in water to remove stain, washed in 70% ethanol, dehydrated in 100% ethanol (2 x 3min), cleared in Xylene (2 times) and mounted in DePex, drying in fume hood. Images were captured on Olympus BX-50 microscope.

#### ***2.1.37 Immunohistochemistry***

Antigen retrieval was conducted on tissue slides using sodium citrate buffer (10mM sodium citrate, 0.05% tween pH6.0), and heating to 95-100% in water bath (Shi et al., 1993). Slides were then encircled with silicon grease, washed 1×15min PBS 0.02% azide, 1x4 min 1% SDS in PBS to permeabilise, 3 × 5min PBS 0.02% azide, 1 x 15min BSA in PBS 0.02% azide to block, before adding primary antibodies overnight at 4C (Rabbit anti TBR1 1/200 - abcam, Chicken anti TBR2 1/200 - abcam, mouse anti PH31/200, rabbit anti PH3 1/500 – abcam, mouse anti KrasG12D 1/100 – NewEast, rabbit anti BLBP1/500 – Millipore, ). The following day slides were washed in high salt PBS (2 × 5min), PBS 0.02% Azide (1 × 5min) and biotin anti rabbit was either added, or secondaries (goat anti mouse 594 1/2000, goat anti rabbit 594 1/1000, goat anti rabbit 488 1/1000, goat anti mouse 1/1000 488, rabbit anti biotin 1/1000) were added for 1hr room temperature. Sections were washed high salt PBS (2 × 5min), PBS 0.02% Azide (1 × 5min) and streptavidin anti biotin was added (Streptavidin 488) or sections were stained with DAPI and cover slips were mounted using Anti-fade Gold DAPI (Life Technologies). Immunofluorescence was observed and images captured using confocal. Image J was used to analyse densities of immunofluorescence images.

### **3.0 CHAPTER THREE - USP9X deubiquitylating enzyme maintains RAPTOR protein levels, mTORC1 signalling and proliferation in neural progenitors.**

#### **3.1 STATEMENT OF AUTHORSHIP**

The work presented in this chapter is based on a submitted manuscript (see Appendix A) as well as additional data. The majority of the work, in both the manuscript and chapter, was performed by the candidate, Caitlin Bridges. Data generated by other authors is clearly identified throughout the chapter. Caitlin Bridges also wrote the original draft of the manuscript and worked with others on subsequent drafts.

Name of Candidate:

I hereby certify that the above statement of contribution to this chapter is correct.

Signed:

Date:

Name of Supervisor:

I hereby certify that the above statement is an accurate reflection of the candidate's contribution to the manuscript and thesis chapter.

Signed:

Date:

## **Chapter 3 - USP9X deubiquitylating enzyme maintains RAPTOR protein levels, mTORC1 signalling and proliferation in neural progenitors.**

### **3.2 Introduction**

The proliferation, self-renewal and differentiation of neural stem cells (NSCs), and their closely related derivatives, neural progenitors (NPs), in both the developing and adult nervous systems, are tightly controlled by both extrinsic and intrinsic signals. Extrinsic signals, derived from the stem cell niche or embryonic organising centres, need to be recognised, relayed internally, coordinated and interpreted to ultimately produce a precise cellular response. Cell polarity, adhesion, cycle length and migration all influence the response to extrinsic signals. Concerning the cell cycle, the G0 and G1 phases are particularly involved in dictating the fate of a NP (Blomen and Boonstra, 2007). Specifically, it is the length of the G1 phase that regulates progenitor differentiation. Cells that linger in these phases have increased longevity and retain the capacity to self-renew (Blomen and Boonstra, 2007). Multiple extrinsic signals influence NP cell cycle progression and the intracellular mammalian target of rapamycin (mTOR) pathway responds to many of these growth factors by coordinating an appropriate RNA and protein synthesis response and, as such, is a major regulator of G0/G1 cell cycle progression. mTOR is an ubiquitous protein kinase found in two complexes, mTORC1 and mTORC2. The mTORC1 complex, which consists of mTOR, regulatory-associated protein of mTOR (RAPTOR) and mammalian lethal with SEC13 protein 8 (MLST8), responds to growth factor stimulation and links this, along with nutrient availability, to cell growth and division (Fingar et al., 2004, Dibble and Manning, 2013). In particular, mTORC1 response to growth factor stimulation is required for cell cycle progression through the G1 phase of the cell cycle (Fingar et al., 2004).

mTOR is a critical regulator of NSC/NP function *in vivo* and *in vitro* balancing self-renewal, proliferation, differentiation and maturation (Magri and Galli, 2012). Dysregulation of mTOR signalling gives rise to neurodevelopmental disorders (Scheffer et al., 2014, Dibbens et al., 2013). Hyperactivation of the mTOR pathway, due to loss of function mutations in the TSC1 and TSC2 genes, upstream inhibitors of mTOR, gives rise to Tuberous Sclerosis Complex (TSC). TSC is characterized by benign malformations comprised of aberrantly proliferating non-malignant cells of the tissue of origin. In the brain, these lesions are ectopic neurogenic compartments with enhanced proliferation of NPs and their subsequent premature differentiation (Magri and Galli, 2013). Conversely loss of mTORC1 function results in

decreased NP proliferation. Deletion of RAPTOR, an essential protein of the mTORC1 complex, from NPs of the dorsal telencephalon leads to decreased proliferation but not loss of self-renewal capacity (Cloëtta et al., 2013). Similarly, these cardinal features are seen in *ex-vivo* cultures of murine NSC/NPs grown as free-floating aggregates, called neurospheres, lacking mTORC1 function: inhibition of mTORC1 signalling in neurospheres, by addition of rapamycin, also decreased proliferation of NPs without affecting the self-renewing capacity of the NSCs (Sato et al., 2010). Therefore, mTOR signalling needs to be tightly balanced to maintain homeostasis in NPs.

Another protein well placed to integrate extrinsic signals with the intrinsic responses of NPs, is the ubiquitin-specific protease 9 located on the X-chromosome (USP9X). USP9X is a deubiquitylating enzyme highly expressed in adult and embryonic NPs *in vivo*, and *in vitro* (Murtaza et al., 2015). Altering *Usp9x* expression levels affects NP function. Moderately increased *Usp9x* expression in mouse embryonic stem cell-derived NPs *in vitro* promotes their self-renewal leading to a large increase in the number of NPs (Jolly et al., 2009). Conversely, Nestin-*cre* mediated deletion of *Usp9x* from all NPs of the mouse central nervous system disrupted their organisation in the ventricular and sub-ventricular zones and results in peri-natal lethality (Stegeman et al., 2013). Deletion of *Usp9x* from the dorsal telencephalon only, is compatible with post-natal survival, but results in a dramatic 75% reduction in adult hippocampal size, suggesting NP proliferation is reduced (Stegeman et al., 2013). Mutations in human USP9X are associated with several neurodevelopmental disorders including X-linked intellectual disability and autism (Homan et al., 2014). In addition, mutations in Doublecortin that specifically disrupt its ability to interaction with USP9X, result in lissencephaly and severe epilepsy, further highlighting the importance of USP9X function for normal brain development (Friocourt et al., 2005).

Recently, *Usp9x* has been implicated in mTOR signalling in C2C12 mouse muscle myoblasts (Agrawal et al., 2012). Knockdown of USP9x in these cells increased mTORC1 activity (Agrawal et al., 2012). Epitope pull-down assays showed that *Usp9x* associated with mTOR, as well as RAPTOR and RICTOR, signature proteins of the mTORC1 and mTORC2 signalling complexes, respectively (Agrawal et al., 2012). However altered expression of USP9x did not affect the level of mTOR protein in HEK293 cells. Here, we show that USP9X is a potent regulator of the mTORC1 signalling in NP/NSCs. Decreasing USP9X levels resulted in a rapid arrest of cultured NPs in G0/G1 of the cell cycle. Further we show

that USP9X binds RAPTOR in the developing brain and maintains RAPTOR levels in cultured NPs suggesting RAPTOR is a critical USP9X substrate.

### 3.3 Results

#### *USP9X depletion results in reduced neural stem cell number*

To directly test the role, if any, of USP9X in NPs we altered its levels in the immortalized human neural progenitor cell line, ReNcell VM. To deplete USP9X in these cells, lentiviral vectors with doxycycline-inducible expression of shRNAs directed against *USP9X* were generated (Drabsch et al., 2007). The lentiviral vector also expressed *EGFP*, which was used to identify and FACS purify, successfully transduced pools of cells, for subsequent experiments. Two independent shRNAs (2193 and 4774, indicating the position of the first base pair of the shRNA in the *USP9X* open reading frame) efficiently depleted USP9X and these cell lines were chosen for future experiments. Induction of a scrambled shRNA, as well as the addition of doxycycline, had no effect on USP9X protein levels (Figure 3.1A). Partial loss of USP9X was evident 24 hours after doxycycline addition in 2193 and 4774 cells, and reached maximal levels by 72 hours (Figure 3.1A). To examine the effect of USP9X depletion on ReNcell VM and determine the time of maximum effect, cells were analyzed using the xCELLigence system, which measures electrical impedance, and so is proportional to cell number, in real time. Analysis of two biological replicates revealed that the cell index of ReNcell VM cells expressing *USP9X* shRNAs (2193 and 4774) plateaued approximately 20 hours after doxycycline addition (Figure 3.1B; Data generated by Dr MC Tan). In 2193 and 4774 cells the decrease in cell index reached statistical significance ( $p < 0.05$ ) at 34 hours and 28 hours, respectively. At 24 hours USP9X protein levels were not yet fully depleted (Figure 3.1A). These data indicate that ReNcell VM NPs are particularly sensitive to reduced USP9X levels.

#### *USP9X depletion does not result in morphological changes, apoptosis or differentiation of ReNcell VM*

The xCELLigence cell index, which measures electrical impedance, does not distinguish between effects on cell proliferation, morphology or cell death. Therefore we examined the effect of *USP9X* knock-down on these functions. No changes in ReNcell VM morphology were observed but a clear reduction in the cellular density of USP9X depleted ReNcell VM could be distinguished at 72 hours after doxycycline treatment (Figure 3.2). An MTT

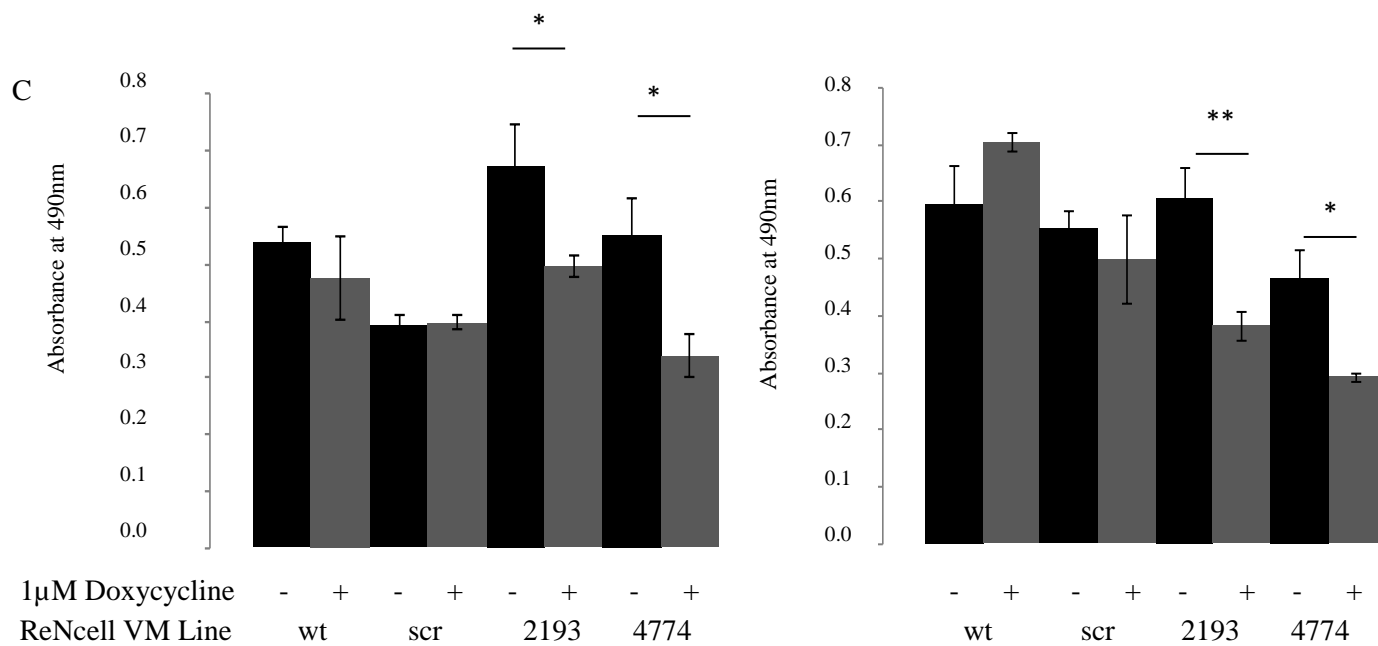
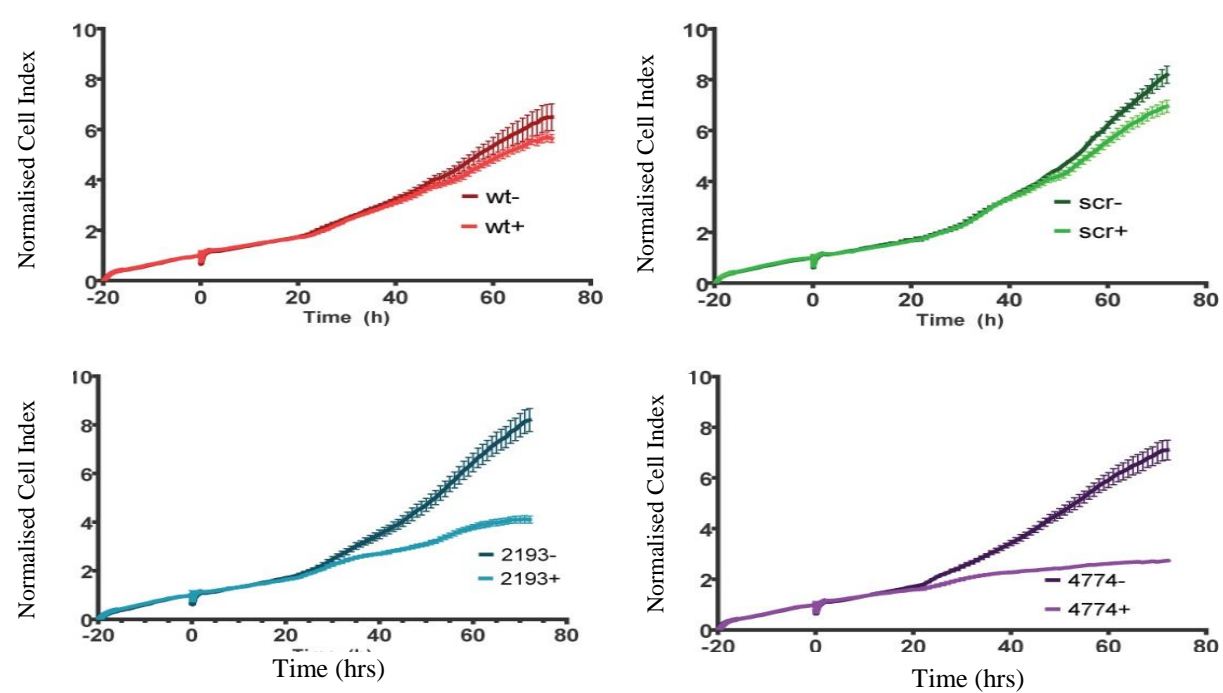
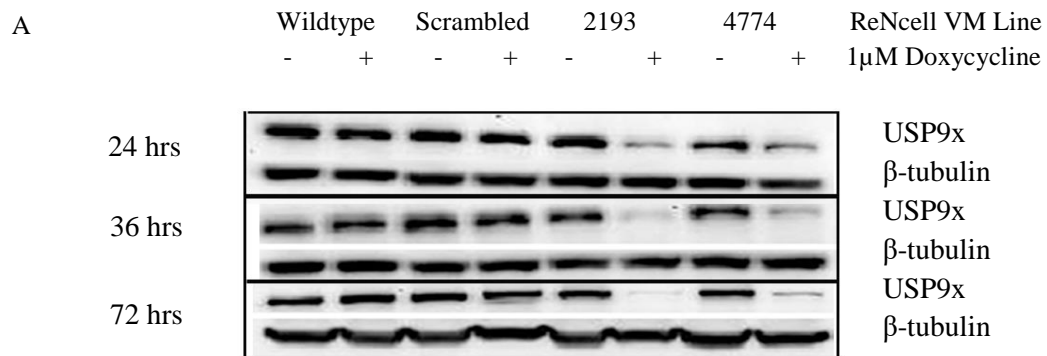


**Figure 3.1. USP9x depletion reduces ReNcells VM proliferation.** (A) Doxycycline treatment depleted USP9X protein levels after 24hrs, 36hrs and 72hrs in ReNcell VM cells harbouring USP9X-targeted shRNA (2913 and 4774) but not a nonsense shRNA (Scrambled) or non-transduced cells (Wildtype). Blot representative of multiple biological replicates. Gels were run under the same experimental conditions. Usp9x and  $\beta$ -tubulin proteins at expected molecular weights. (B) (Data generated by Dr MC Tan) Reduced Cell index of ReNcell VM cells following addition of 1 $\mu$ M Doxycycline (0 hr). xCELLigence real-time measurement of increasing electrical impedance plotted on “Y axis” (“Normalised Cell Index”). Cell Index of doxycycline treated (+) ‘2193’ RenCell VM cells differed significantly from non-treated after 34 hours ( $p < 0.05$ ), 35 hours ( $p < 0.01$ ) and 36 hours ( $p < 0.001$ ). After 72hrs, the cell index was approximately 50% of untreated 2193 cells. For ‘4774’ cells, the cell index differed significantly at 28 hours  $p < 0.05$ , 29 hours  $p < 0.01$  and 30 hours  $p < 0.001$  after treatment. After 72hrs, the reduction in cell index was approximately 61% that of untreated 4774 cells. Analysis was obtained by plotting t-values of the two way ANOVA analysis (versus time). Error bars represent standard deviation. wt: wildtype, scr: scrambled, +: 1 $\mu$ M doxycycline treated, -: No doxycycline (C) MTT Assay analysis of RenCell VM cells after (i) 48 hours and (ii) 72 hours treatment with 1 $\mu$ M doxycycline showing reduction in proliferation in USP9X knock-down cells. \*  $p < 0.05$ ; \*\*  $p < 0.01$ . Error bars = standard error of the mean.

proliferation assay confirmed the reduction in cell numbers in USP9X depleted ReNcell VM after 48 and 72 hours doxycycline treatment (Figure 3.1C). Analysis of both Annexin V (Figure 3.3A,B) and cleaved caspase 3 (Figure 3.3C) indicated there was no increase in apoptosis, after 12 and 72 hours doxycycline treatment, respectively. Immunoblot analysis failed to detect any change in the level of the astrocytic marker GFAP or neuronal marker  $\beta$ III-tubulin, indicating that loss of USP9X did not induce the differentiation of ReNcell VM cells to post-mitotic cell fates (Figure 3.4, data generated by Dr MC Tan). By immunofluorescence there was not obvious increase in differentiation after 9 nine days in culture (Figure 3.5), nor after both EGF and FGF were removed from media for the same period (Figure 3.6). An enlargement / splaying of the USP9x depleted cells seemed to occur over the nine days most probably due to the reduced number of cells (Figure 3.5 and 3.6). These data demonstrate that loss of USP9X decreases proliferation of ReNcell VM cells and does not alter their morphology, cell death or differentiation.

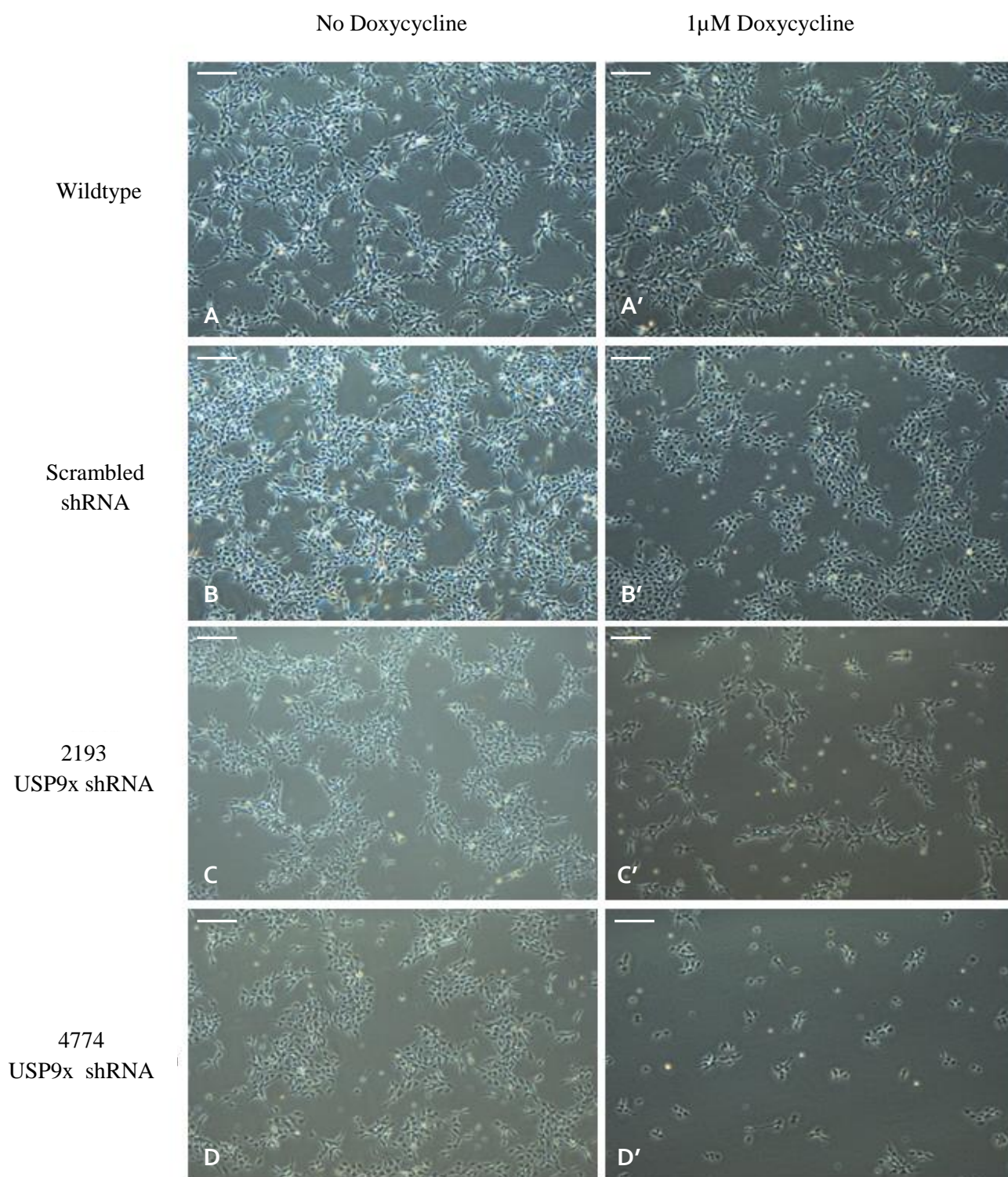
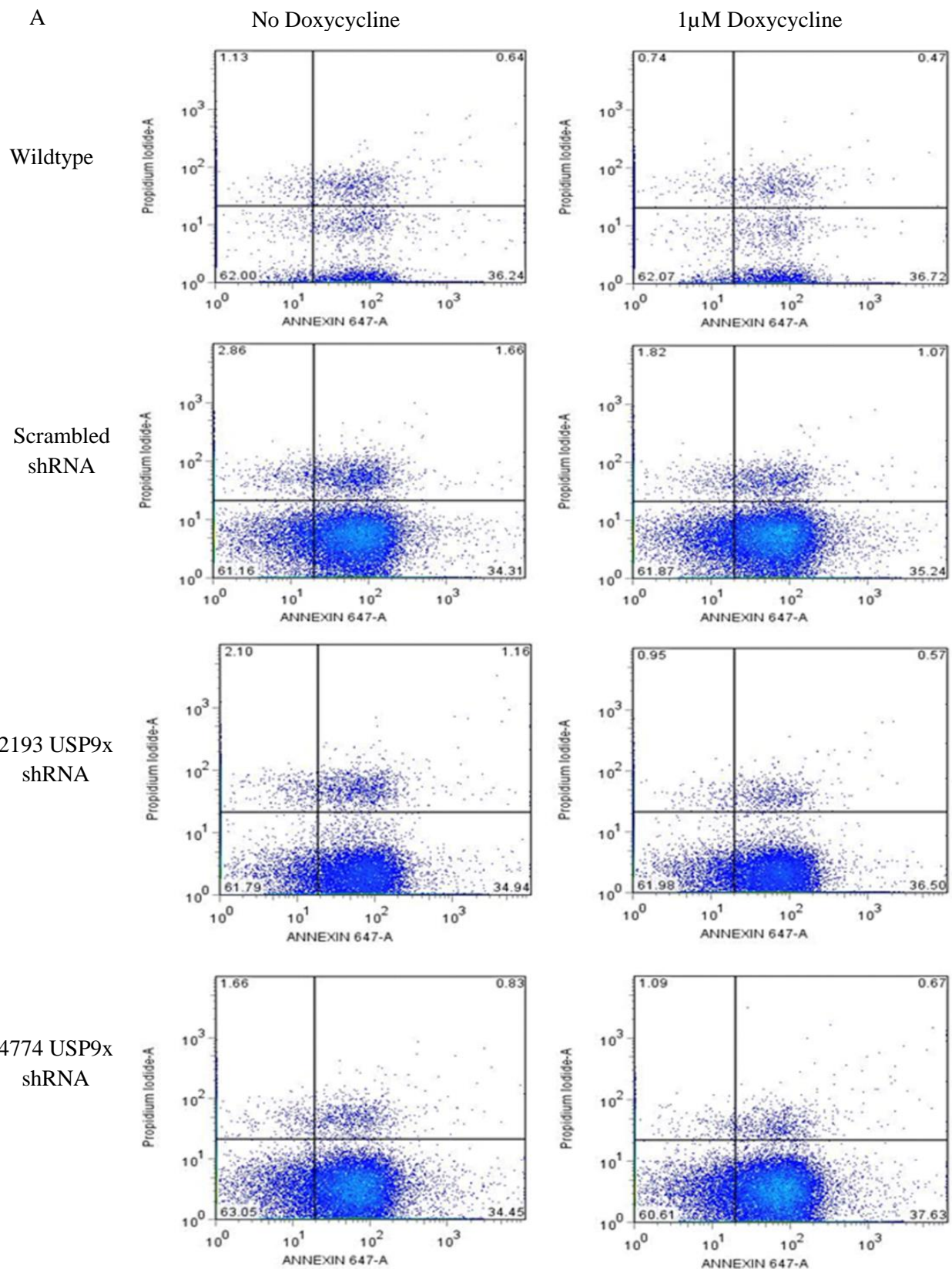


**Figure 3.2 USP9x depletion decreases density of ReNcells VM.** Phase contrast micrographs of Wt (A, A'), Scr (B, B'), 4774 (C, C') and 2193 (D, D') after 72hrs treatment with 1 $\mu$ M Doxycyclin (A',B',C',D') to induce USP9x shRNA expression. There is reduced cellular density for 2193 (C') and 4774 (D'). Scale bar represents 100 $\mu$ m in length.



**B**

	Early Apoptotic Population (%)		
ReNcell VM	No Doxycycline	1uM Doxycycline	Increase (%)
Wildtype	36.24	36.72	0.48
Scrambled	34.31	35.24	0.93
2193	34.94	36.5	1.56
4774	34.45	37.63	3.18

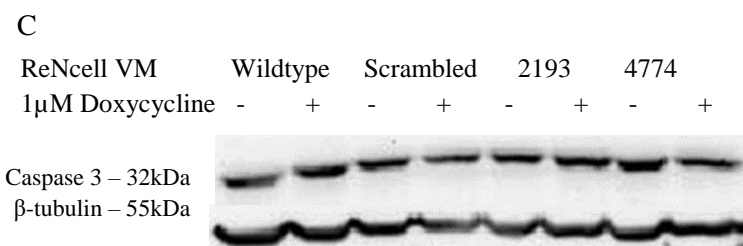


**Figure 3.3 Annexin V-Biotin Assay Dot plot after 12 hours 1 $\mu$ M Dox addition and total Caspase 3 expression after 72hrs 1 $\mu$ M Dox addition.** (A) Dot Plot of untreated 'No Doxycycline' and treated '1 $\mu$ M Doxycycline' ReNcells VM after 12 hours Shown are Viable in lower left quadrant, Early Apoptotic in lower right quadrant (Annexin V Biotin/Streptavidin APC 647-A positive), Late Apoptotic in upper right quadrant (Annexin V Biotin/Streptavidin APC 647-A positive and Propidium Iodide positive). Cells were treated with 1 $\mu$ M Doxycycline for 12hrs before collecting for analysis of Early Apoptotic events. Analysis courtesy of Dr. Bernadette Bellette. Values in quadrants represent percentage of cells in each quadrant. Change in percentage of early apoptotic cells after treatment are as follows: Wildtype (0.48%), Scrambled (0.93%), 2193 (1.56%) and 4774 (3.18%). (B) Tabulated Dot-Plot Data of Early apoptotic population in USP9x depleted ReNcells VM. (C) Western Blot of Caspase 3 in ReNcells VM after 72hrs 1 $\mu$ M Dox addition. No increase in Caspase 3 expression in USP9x depleted ReNcells is observed. This is not thought to be the cause for the increase in percentage of cell in G0/G1 and reduced proliferation in USP9x depleted ReNcells VM.

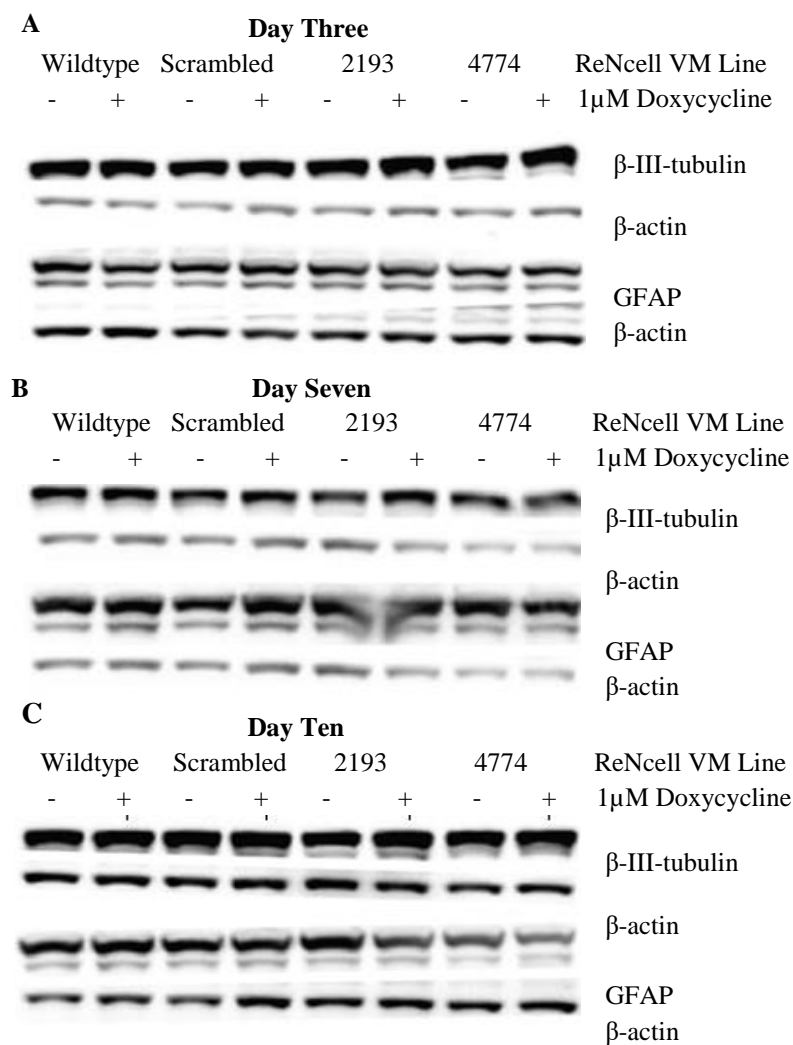


**Figure 3.4 USP9x depletion does not result in increased differentiation.** Immunoblotting of ReNcells VM after (A) three, (B) seven and (C) ten days of 1 $\mu$ M Doxycycline treatment for the expression of differentiation markers Beta-III-Tubulin and GFAP. No obvious increase in expression was observed in the USP9x depleted ReNcells VM. Beta-Actin was used as a loading control. (Data in this figure generated by Dr MC Tan).

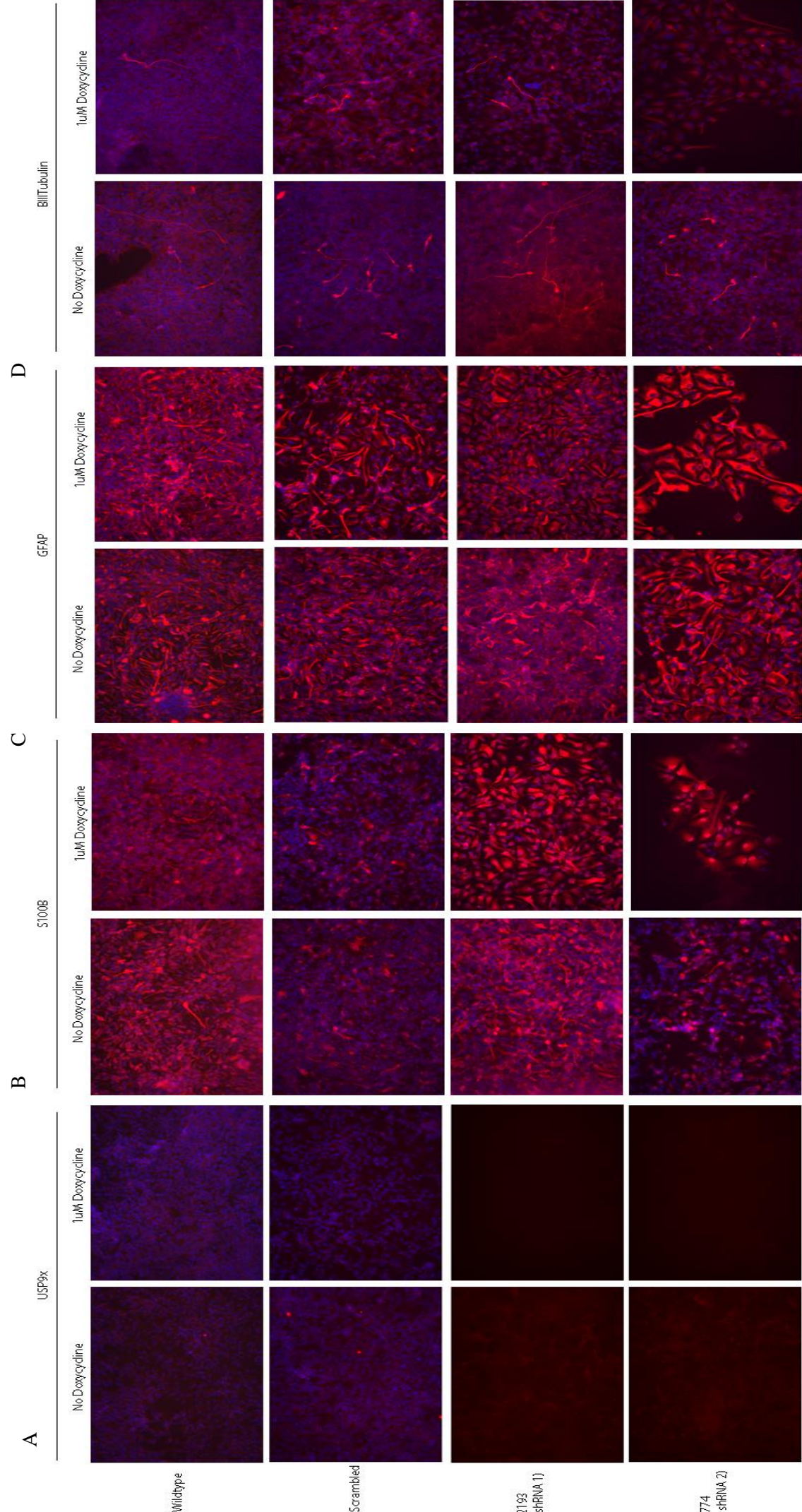


**Figure 3.5 No obvious increase in differentiation by immunofluorescence.** Immunofluorescence of differentiation markers,  $\beta$ III-tubulin (Neuron), USP9x (Neuron), GFAP (Astrocytes),  $\beta$ III-tubulin (Neuron). USP9x to show reduction after 9 days after 1 $\mu$ M Doxycycline. (A) After 1 $\mu$ M Dox treatment for nine days, 2193 and 4774 cells have reduced USP9x expression as expected. (B) The intensity of  $\beta$ III-tubulin expression varies in each ReNcell VM line/population. For Wildtype and 2193 untreated, there is high expression both cytoplasmic and nuclear, which becomes more intense in 2193 Dox treated cells. For Scrambled and 4774 there is low expression both cytoplasmic and nuclear, but becomes more intense in 4774 Dox treated cells. (C) GFAP is expressed in cytoplasm of ReNcells VM after 9 days 1 $\mu$ M Dox treatment. (D)  $\beta$ III-tubulin expression is strong in cellular/neural processes of all ReNcells VM lines in absence of 1 $\mu$ M Dox. After treatment, wildtype ReNcell morphology remains similar to untreated, but different to scrambled, 2193 and 4774 cells due to lower confluency.

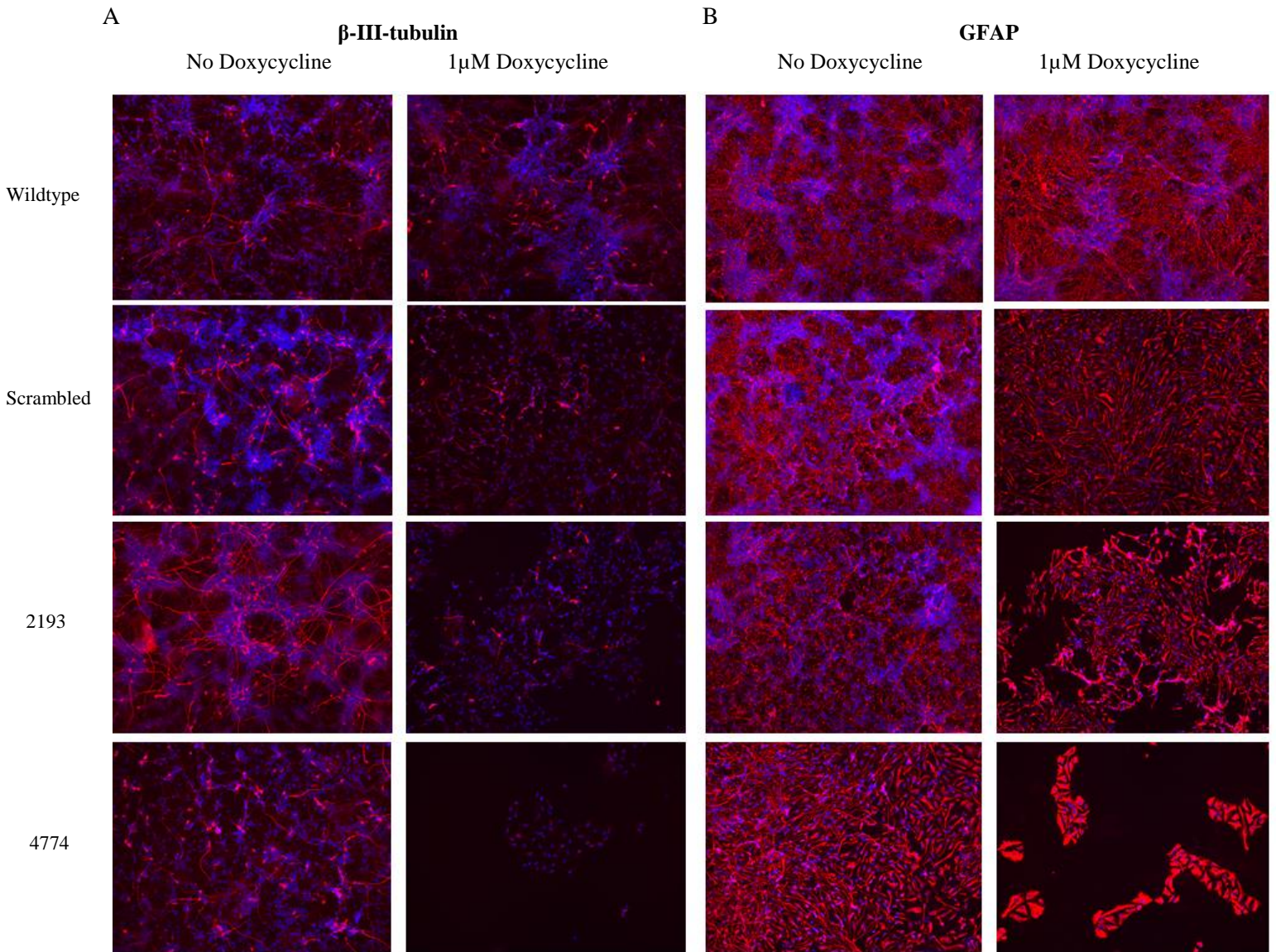
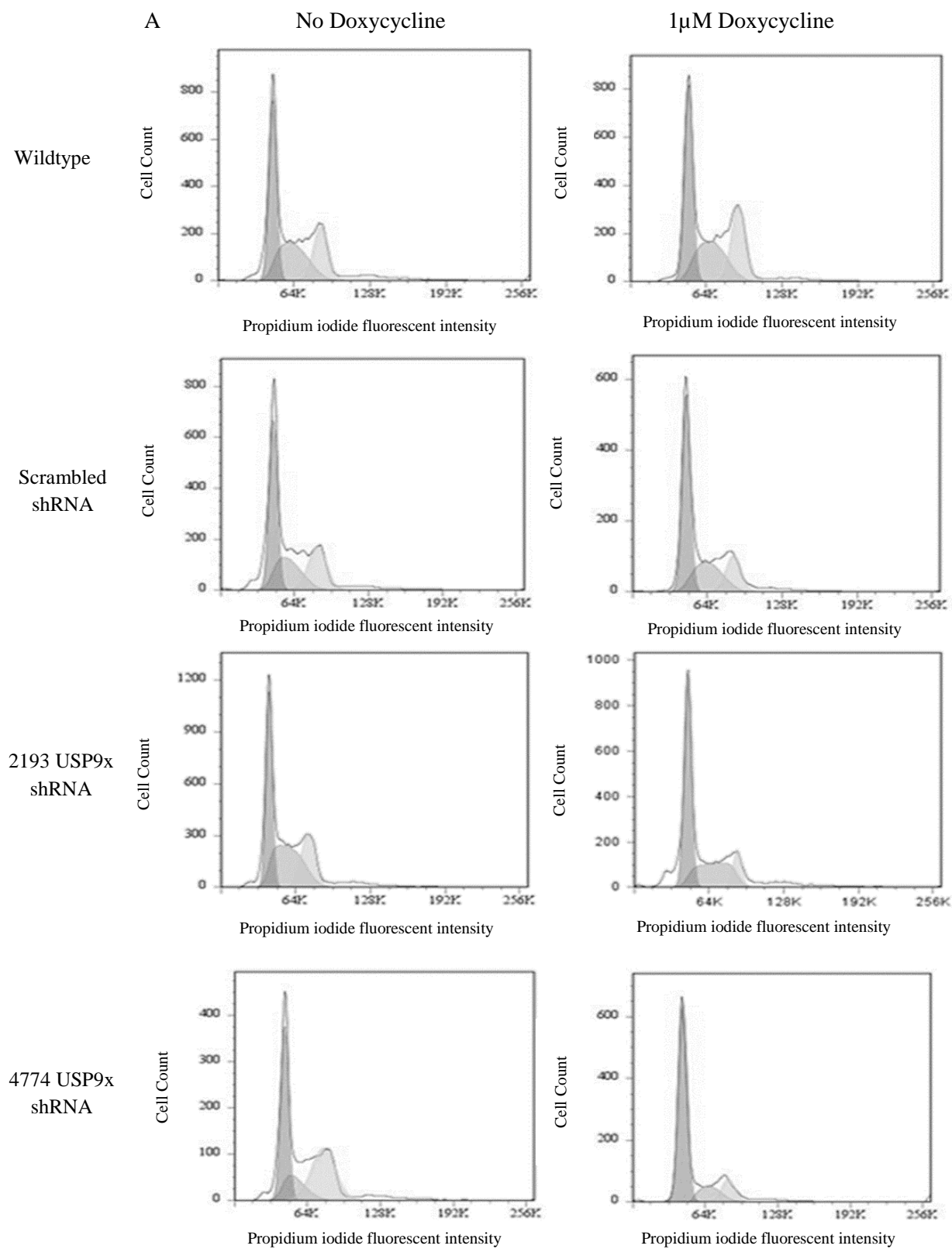


**Figure 3.6 Immunofluorescence of differentiation markers, GFAP (Astrocytes),  $\beta$ III-tubulin (Neuron) over 9 days EGF and bFGF removal in presence of 1 $\mu$ M Doxycycline.** (A) After nine days of EGF/FGF withdrawal,  $\beta$ III-tubulin is highly expressed in the neuronal processes of the ReNcells in untreated cells. For all Dox treated cells, except the Wildtype, there are fewer processes (B) After 9 days EGF/FGF removal, all treated and untreated ReNcells express GFAP. Difference in morphology of GFAP positive and  $\beta$ IIItubulin ReNcells VM is possibly due to the low confluency as the Scrambled control treated also exhibits different morphology to USP9x depleted 2193 and 4774 Dox treated ReNcells.

### *USP9X depletion results in G0/G1 cell cycle arrest*

To investigate if USP9X depletion affected ReNcell VM cell cycle, flow cytometric profiling of cellular DNA content was conducted. Knock down of USP9X resulted in an increase in cells at the G0/G1 stage of the cell cycle 72 hours after doxycycline treatment (Figure 3.7). Over three biological replicates the average increase in cells in G0/G1 following USP9X depletion was 12.6%  $\pm$  6.3 ( $p=0.0134$ ) for “2913” and 22.91%  $\pm$  8.9 ( $p=0.0065$ ) for “4774” cells. There was no statistically significant alteration in wildtype or scrambled shRNA cells exposed to doxycycline. Removal of doxycycline from the culture medium resulted in restored levels of USP9X and ReNcell VM proliferation (data not shown). These data indicated that USP9X is required for progression of ReNcell VM cells through G0/G1 and/or progression into S-phase. To investigate the molecular mechanism contributing to the accumulation of cells in G0/G1 phase we examined, by immunoblot, the levels of various proteins facilitating the G1/S phase transition. A decrease in the phosphorylated form of retinoblastoma protein (pp-Rb<sup>S780</sup>) was detected in USP9X depleted cells, but only after 72 hours of doxycycline treatment. No consistent changes in other proteins including Cyclin D1 or E2F1 were observed at any stage of the time course (Figure 3.8). Immuno-precipitation was performed to investigate if there was a physical interaction between USP9x and either pRb, E2F1 or Cyclin D1. However no interaction was observed (data not shown). As the cell index of USP9X depleted ReNcell VM cells plateaued at 24 hours in the xCELLigence assay this suggested that decreases in pp-Rb<sup>S780</sup> were unlikely to be the mechanism initiating the G0/G1 arrest.



**B**

ReNcellVM	Percentage (%) in G0/G1	
	No Doxycycline	1 $\mu$ M Doxycycline
Wildtype	38.64	36.01
Scrambled	41.08	49.42
2193 USP9x shRNA 1'	37.9	57.67
4774 USP9x shRNA 2'	38.16	68.01

**Figure 3.7. Loss of USP9x results in ReNcell VM cell accumulation in the G0/G1 phase of cell cycle.** (A) Flow cytometric analysis of ReNcell VM cells after 72 hours of doxycycline treatment. Representative of three biological replicates. (Cell samples prepared by Caitlin Bridges, Flow analysis performed by Dr B Bellette) (B) Quantitation of percentage of cells in each cell cycle phase in (A). ReNcell VM cells accumulate in G0/G1 in 2913 and 4774 cells treated with 1 $\mu$ M doxycycline.

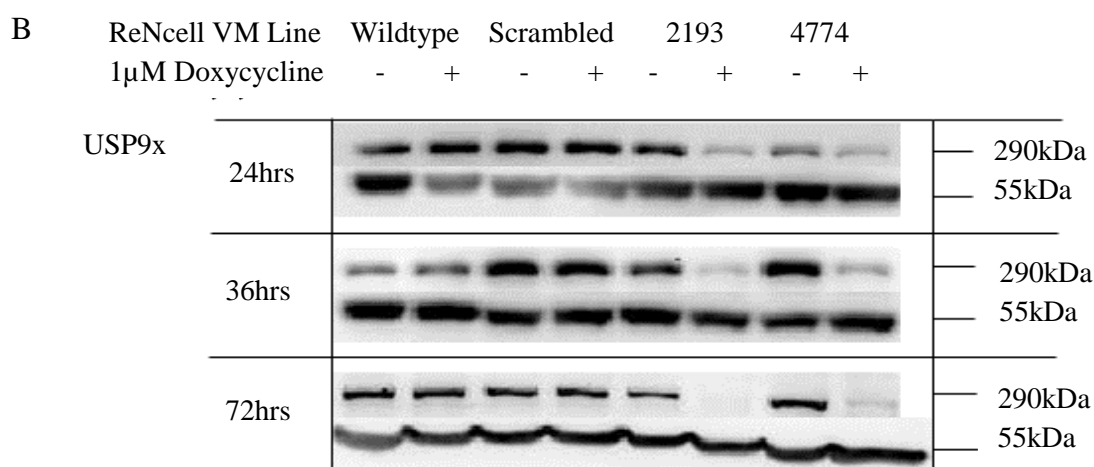
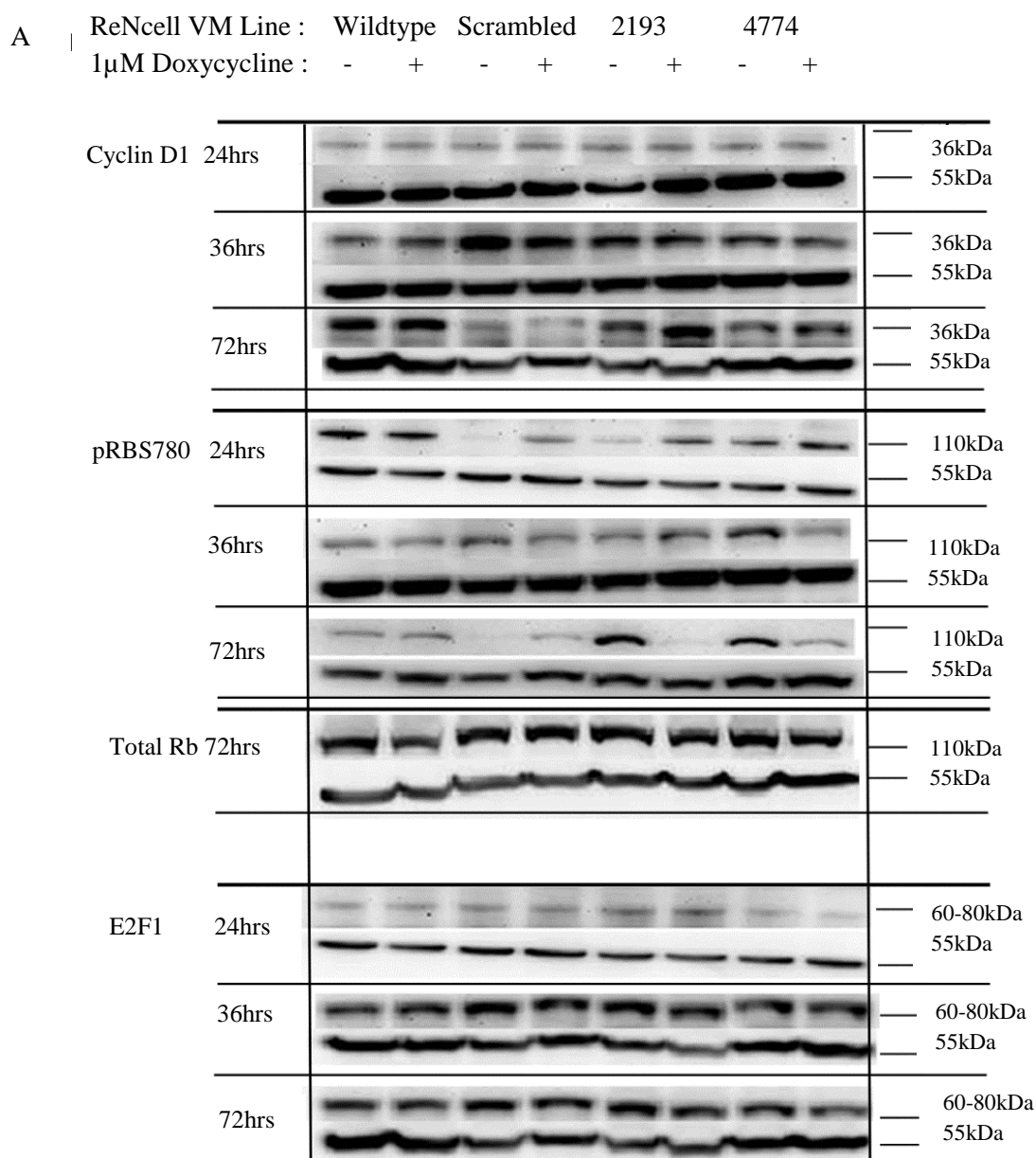


**Figure 3.8 Expression of G1-S Phase cell cycle proteins in USP9x depleted ReNcells VM after 24hrs, 36hrs and 72hrs of 1 $\mu$ M Doxycycline addition. (A) No consistent change in**

*Cyclin D1, E2F1 of Total Retinoblastoma (Rb) protein expression in USP9x depleted cells was observed. Reduction of phosphorylated Rb (S780) in USP9x depleted ReNcells VM occurs after 72hrs treatment. (B) Significant for 4774 USP9x depleted ReNcells VM.  $P < 0.05$ . Loading control Beta-Tubulin was used in each blot.*

### *USP9X depletion in ReNcell VM cells reduces mTORC1 signalling*

It has recently been reported that USP9X interacts with the mTOR signalling pathway (Agrawal et al., 2012), a major regulator of progression through the G1 phase of the cell cycle. mTOR exists in two complexes, mTORC1 and mTORC2, and the activity of each pathway is measured by the phosphorylation of their substrates, S6 and Akt, respectively (Rodgers et al., 2014, Agrawal et al., 2012, Leontieva et al., 2014, Leontieva et al., 2012). In the absence of growth factor stimulation, cells arrest in G0. However, re-addition of growth factors promptly activates mTOR signalling. Therefore we examined the activation of mTOR in ReNcell VM cells, by the re-addition of EGF and FGF, in the presence and absence of USP9X. ReNcell VM cells were exposed to doxycycline for 72 hours for maximal knock down of USP9X, and a further 24 hours in the absence of EGF and FGF to cause G0 arrest. Upon the reintroduction of EGF and FGF there was a rapid increase in pS6 levels, dependent on the presence of USP9X (Figure 3.9A). A failure to induce pS6, in the absence of USP9X, was observed in each of six biological replicates, with a reduction in Raptor expression observed in four of the six biological replicates (Figure 3.9C). There were no obvious or consistent alterations in pAKT, total S6 or total AKT protein levels across the biological replicates (Figure 3.9A, and data not shown), nor was there any change in mTORC2 component, Rictor, or p-mTOR or t-mTOR expression (Figure 3.9C). To determine if the decreased mTORC1 signalling occurred with similar kinetics to the observed cell index plateauing (Figure 3.1B) upon USP9X depletion, we examined pS6 protein levels following 24 hours doxycycline treatment. A similar decrease in pS6 levels in the absence of USP9X was detected at this earlier time point (Figure 3.9B) suggesting this may account for the plateauing cell index detected in the xCelligence assay.

The levels of pS6 are increased by inhibition of the proteasome in wildtype cells (Figure 3.10A) suggesting it may be regulated by ubiquitylation. Therefore, we sought to determine if the reduction in p-S6 observed in USP9x depleted cells could be rescued by proteasomal inhibition, and found this was the case (Figure 3.10B). Interestingly there was also an increase in the expression of the kinase that phosphorylates S6 protein, pp70S6K, after proteasomal inhibition. This indicates that USP9x is involved in preventing the proteasomal degradation of p-S6, possibly through upstream regulators of the S6 protein, such as pp70S6K, or further upstream regulators such as Raptor, which had been observed in multiple biological replicates (Figure 3.11). These data suggest that USP9x's deubiquitylating activity regulates a step or steps, in the mTORC1 signalling cascade.

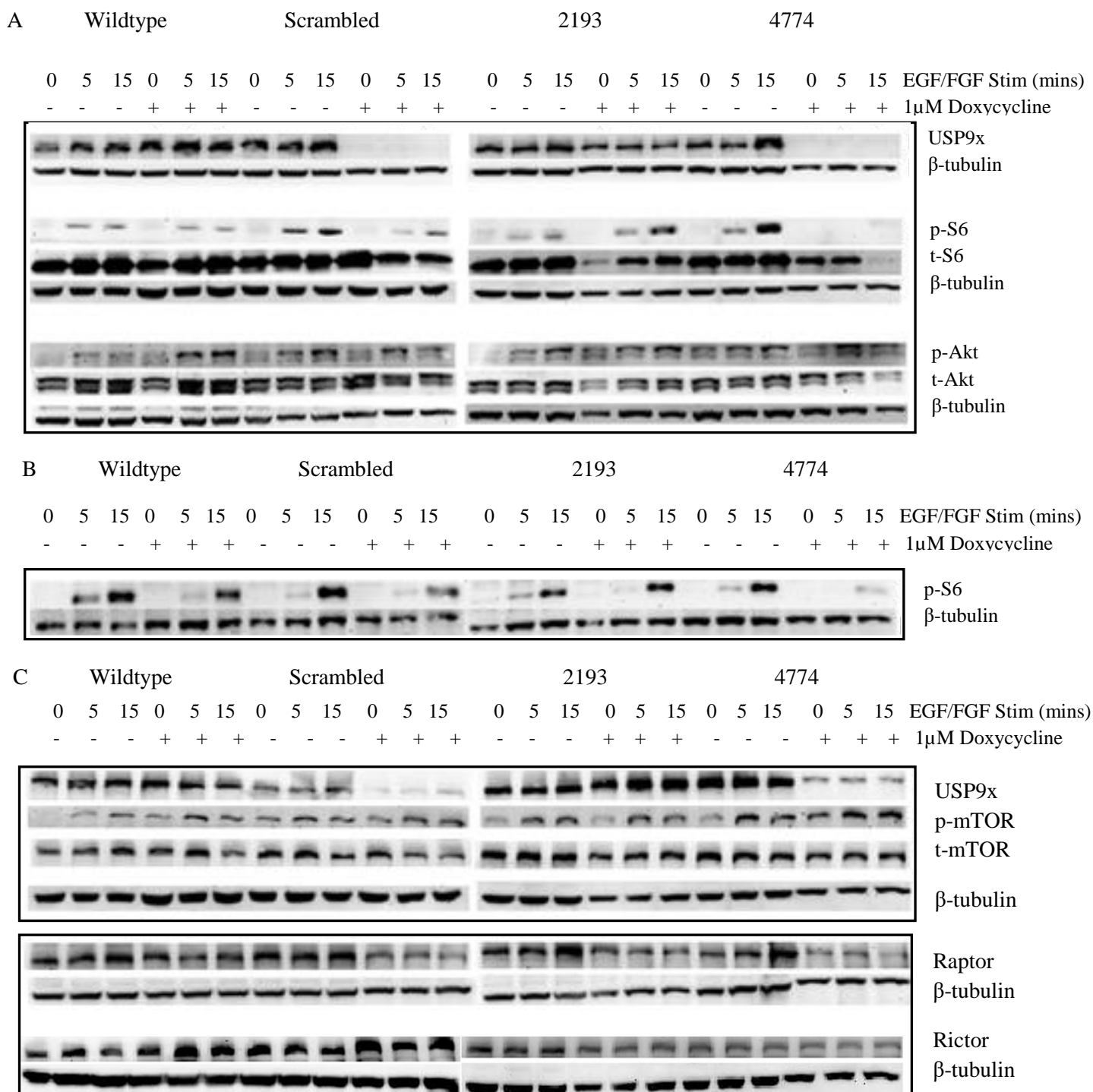


**Figure 3.9. mTORC1 activity and RAPTOR levels in ReNcell VM cells are dependent on USP9X.** (A) Immunoblot analysis of growth factor induction of mTORC1 and mTORC2 pathways in absence of USP9X. USP9X was depleted from 2193 and 4774 cells by 72 hours exposure to doxycycline before growth factors (EGF/FGF) were removed from ReNcell VM medium 24 hours prior to protein collection (0 minutes) and then 5 and 15 minutes after re-addition of EGF/FGF. Both pS6 and pAkt levels increased upon exposure to EGF/FGF (compare 0 to 5 and 15 min) indicating both mTORC1 and mTORC2 pathway activation, respectively. However, the extent of induction was markedly reduced in the absence of USP9X (compare plus and minus Dox at 5 and 15 mins in 2193 and 4774). Total S6 and Total AKT were not affected by USP9X depletion. Representative of multiple biological

repeats. **(B)** Diminished mTORC1 activation in ReNcell VM cells, as determined by p-S6 levels, was evident after only 24 hours doxycycline treatment, consistent with the xCELLigence data. **(C)** RAPTOR protein levels are decreased in ReNcell VM cells with depleted USP9X (2193 and 4774 plus doxycycline). Phospho-, Total mTOR and Rictor levels were unaffected by the absence of USP9X. Representative of multiple biological replicates.

### *USP9X binds RAPTOR and regulates its levels*

RAPTOR is the major scaffolding protein of the mTORC1 complex and also binds p70S6 kinase (Hara et al., 2002, Nojima et al., 2003). The level of RAPTOR protein is reportedly regulated by ubiquitylation (Hussain et al., 2013, Choi et al., 2014) raising the possibility that USP9X maintains mTORC1 signalling by opposing RAPTOR degradation in the ubiquitin-proteasome system. To determine if USP9X and RAPTOR interact, immunoprecipitation was performed on lysate from the frontal cortex of wild-type embryonic mouse brains, as these are enriched for NPs. A clear interaction between endogenous USP9X and RAPTOR proteins was detected, as was a weaker interaction with p70S6K in both E16.5 (Figure 3.12A, data obtained by Mr S Premarathne) and E14.5 (not shown) tissue. Interestingly, no interaction between USP9X and mTOR was detected under these conditions. Also no endogenous interaction within ReNcell VM cells could be established (Supplementary Figure 3.1), which is similar to results from cultured HEK293 and C2C12 cells (Agrawal et al., 2012). This may be due to a weak interaction and therefore overexpression of both mTORC1 plasmids with USP9x plasmids in ReNcell VM cells was attempted as for other reports (Agrawal et al., 2012). However due to the low transfection efficiency into ReNcell VM cells, high levels of expression were not achieved (Supplementary Figure 3.2).

Loss of USP9X correlated with decreased levels of RAPTOR (Figure 3.9 and 3.11). To further investigate the relationship between these proteins, USP9X was transiently over-expressed in HEK293 cells (due to low transfection efficiency of ReNcell VM cells). Increased levels of USP9X resulted in increased RAPTOR but did not alter the level of other mTORC1 pathway components including mTOR, total S6 or phosphor-S6 (Figure 3.12C, data from Dr L Jolly). Over-expression of three USP9X mutations, which are associated with human intellectual disability but do not affect their deubiquitylating activity (Homan et al., 2014), also increased RAPTOR levels (Figure 3.12C).

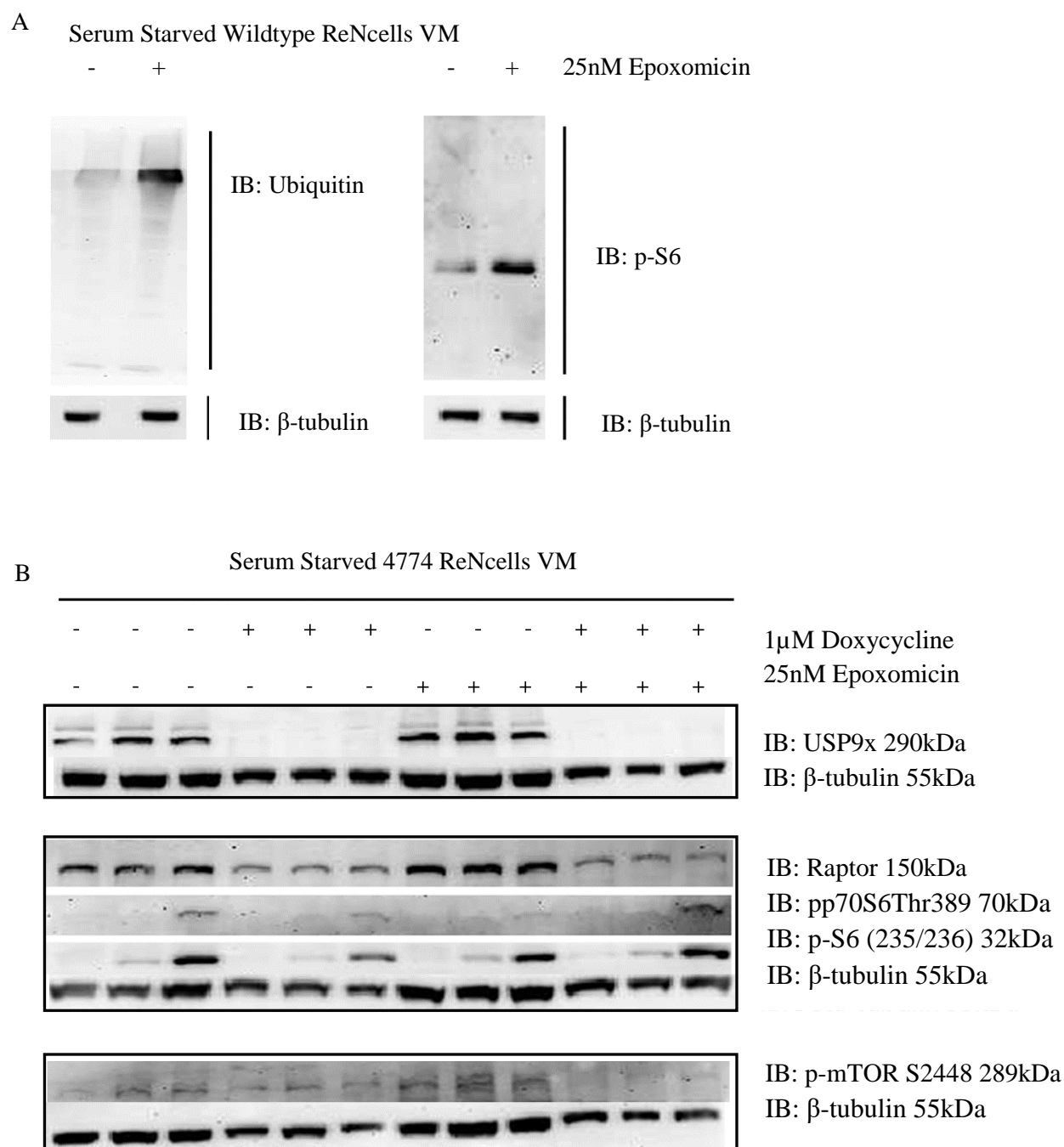


**Figure 3.10. Proteasomal inhibition rescues USP9x-dependent p-S6 reduction after 15min EGF/FGF stimulation.** (A) Proteasome inhibition by 25nM Epoxomicin for 6hrs after EGF/FGF starved Wildtype ReNcells VM increases ubiquitin and p-S6 expression (B) Inhibition of proteasome by 25nM Epoxomicin for 6hrs rescues p-S6 degradation after EGF/FGF stimulation for 5min and 15min in USP9x depleted ReNcells VM and increases phosphorylated S6 kinase expression, pp-70S6K (Thr389), 70kDa).

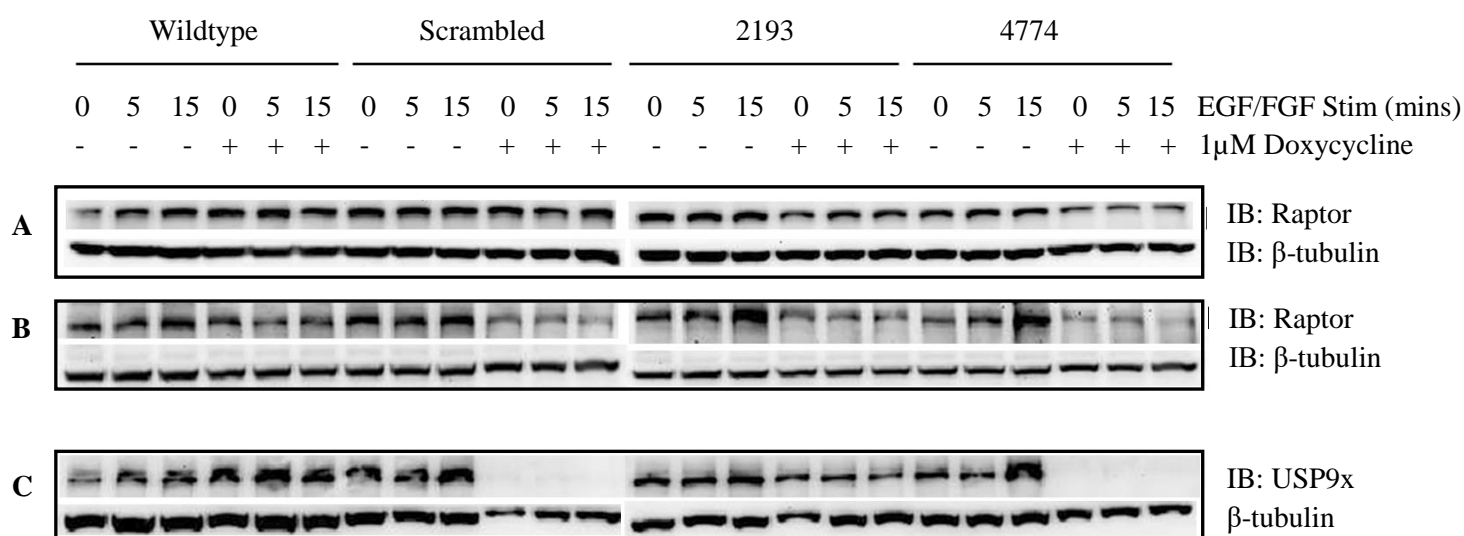


**Figure 3.11. Reduction of RAPTOR expression in USP9x depleted ReNcells after EGF/FGF stimulation for 0, 5 and 15min. (A) and (B) Two biological replicates of EGF/FGF stimulation experiment demonstrating reduction in RAPTOR protein levels in USP9X depleted ReNcell VM cells. (C) Representative reduction of USP9X depletion after 72hrs doxycycline treatment. Panel (A) and Panel (C) are from the same biological replicate.**

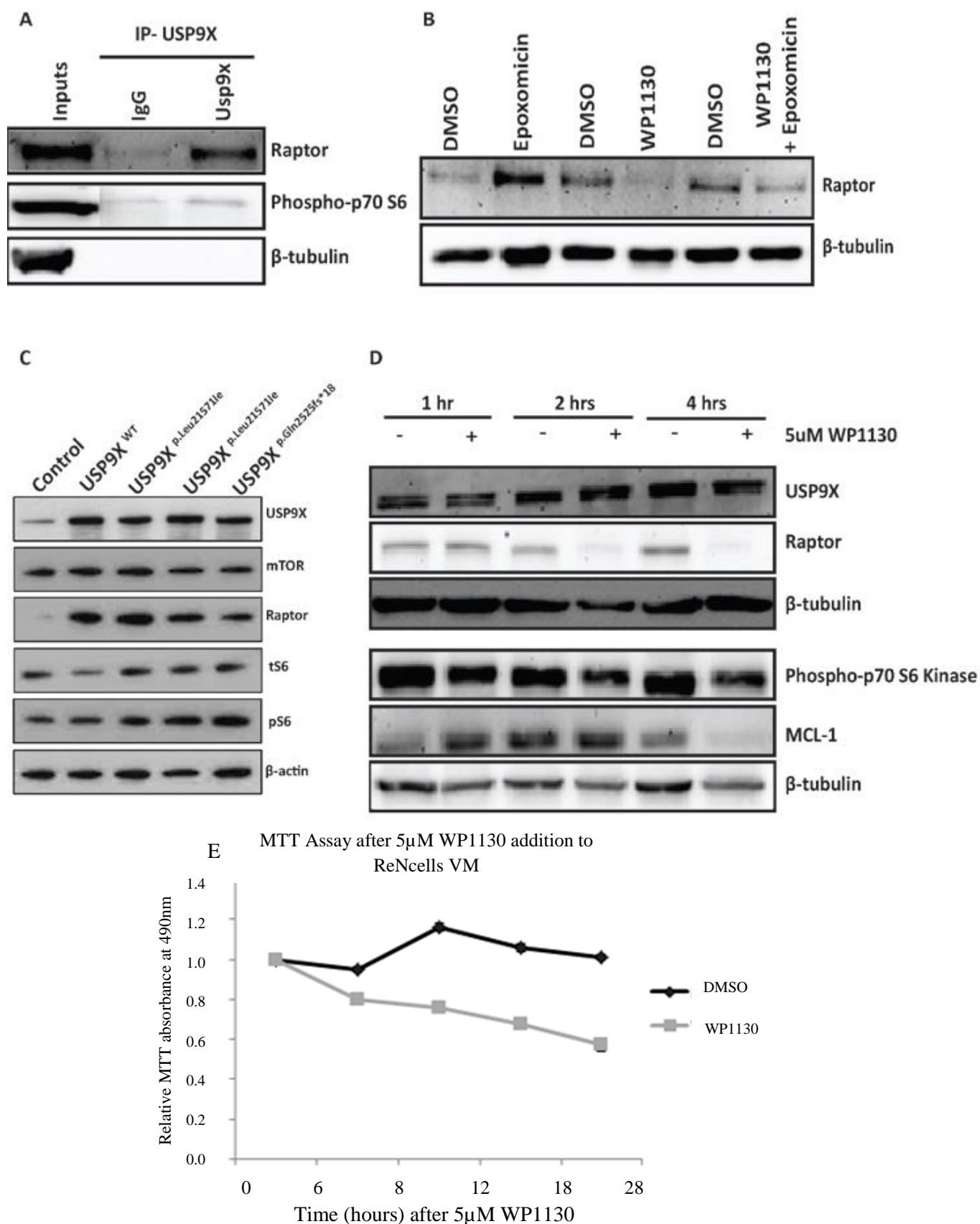


**Figure 3.12 USP9X binds Raptor in vivo and opposes its proteasomal degradation in neural progenitors.** (A) Endogenous USP9X immunoprecipitated endogenous Raptor from E16.5 mouse brain (frontal cortex only to enrich for NPs). An interaction with phospho-p70S6 kinase was also detected. Similar results were obtained from E14.5 frontal cortex. (B)

*RAPTOR* protein levels are regulated by proteasomal inhibition (epoxomicin) and inactivation of USP9X deubiquitylating activity (WP1130) in ReNcell VM. Proteasomal inhibition following 4 hours exposure to 25nM epoxomicin resulted in increased RAPTOR levels. Inhibition of USP9X DUB activity with 5µM WP1130 for 4 hours resulted in decreased RAPTOR. Treatment of ReNcellVM cells for 4 hours with WP1130 followed by 4 hours of epoxomicin resulted in intermediate levels of RAPTOR. DMSO was used as the vehicle control for each experiment. Final concentrations of DMSO were – 0.0025% for epoxomicin; 0.00005% for WP1130; 0.00255% for WP1130 + Epoxomicin. (C) USP9X over-expression increased RAPTOR protein levels. Proliferating HEK293T cells were transiently transfected with empty vector, full length USP9X (wt) or one of three USP9X variants, which do not affect enzymatic activity but are associated with human intellectual disability. Cell lysates were collected 24 hours later. Immunoblot analysis identified increased RAPTOR protein but mTOR, total and Phospho-S6 were unaffected. (D) Chemical inhibition of USP9X deubiquitylating activity leads to a rapid depletion of RAPTOR protein. ReNcell VM cells were treated with 5µM WP1130 and analysed by immunoblot. WP1130 does not deplete USP9X protein levels over 4 hours but results in almost complete loss of RAPTOR by 2 hours. Phospho-p70S6 kinase levels were not affected. Levels of the USP9X substrate MCL1 were depleted after 4 hours. (E) WP1130 treatment causes reduction in ReNcell VM proliferation as early as 6hrs and continues over 28hrs. Proliferation was measured by MTT absorbance. Significant reduction in MTT absorbance was observed after 6hrs, 12hrs, 18hrs and 28hrs treatment.  $P < 0.05$ . (Data from panels A,B,D from S. Premarathne; C Dr L. Jolly; E by candidate C. Bridges)

The above loss- and gain-of-function approaches, in human ReNcell VM cells and HEK293T cells, respectively, identified a direct correlation between USP9X and RAPTOR protein levels but they do not indicate if USP9X's deubiquitylating activity is required. Recently a small compound, WP1130, has been identified which inhibits USP9X DUB activity, but does not affect USP9X protein level (Peterson et al., 2015). In addition, WP1130 rapidly inhibits USP9X within hours (Figure 3.12D), compared with days for RNA knock-down approaches and thereby circumvents possible induction of compensatory DUB expression (Peterson et al., 2015). The addition of WP1130 to proliferating ReNcell VM cells under normal culture conditions, in the presence of EGF and FGF, resulted in a rapid decrease in RAPTOR protein levels after as little as 2hrs, but had no effect on p70S6K (Figure 3.12D, data from Mr S Premarathne). As reported by others, WP1130 did not affect the level of USP9X protein, but did deplete another USP9X substrate, MCL1 (Schwickart et al., 2010) after 4 hours, indicating USP9x activity was reduced. After 6hrs there was a corresponding decrease in MTT proliferation which continued over 28hrs, which correlates with the shRNA induced USP9x depleted in the ReNcells VM. This provides evidence that the inhibition of USP9X's deubiquitylating activity by WP1130, leads to a rapid decrease in RAPTOR protein, coupled with a corresponding decrease in proliferation in ReNcell VM cells.

#### *USP9X opposes proteasomal degradation of RAPTOR*

The above data are consistent with USP9X opposing the degradation of RAPTOR in the ubiquitin-proteasome system. To directly examine this, we measured RAPTOR levels in ReNcell VM cells treated with the proteasome inhibitor, epoxomicin (Meng et al., 1999). Epoxomicin treatment for 4 hours increased RAPTOR levels (Figure 3.12B lane 2, data from S Premarathne) suggesting it is subject to proteasomal degradation in ReNcell VM cells. As shown previously, inhibition of USP9X deubiquitylating activity by WP1130 resulted in depleted RAPTOR levels (Figure 3.12B lane 4). The combination of epoxomicin and WP1130 resulted in intermediate levels of Raptor protein compared with epoxomicin or WP1130 alone (Figure 3.12B, compare lane 6 with 2 and 4). These data are consistent with USP9X's deubiquitylating activity opposing degradation of RAPTOR by the proteasome.

#### *USP9X null neurospheres have reduced neural progenitor proliferation but not stem cell self-renewal.*

(A detailed analysis of USP9x deletion on neurosphere proliferation and expansion was performed by Dr L Jolly, see Figure 5 submitted manuscript Bridges et al (Appendix A).

However, a pilot study was completed by the candidate Caitlin Bridges and is described below).

The mTORC1 pathway is well known to regulate murine NP proliferation. Inactivation of mTORC1 signalling in NPs *in vivo*, by conditional Nestin-*cre* mediated deletion of the *Raptor* gene in mouse brains, resulted in reduced NP proliferation. When mTORC1 signalling is inhibited in NSC/NPs cultured *ex-vivo* as neurospheres, the reduced NP proliferation manifested as a reduction of neurosphere size (Cloëtta et al., 2013). Previous data indicated deletion of USP9x results in reduced sphere size and sphere-forming capacity (data generated by L Jolly, Figure 5, submitted manuscript). This suggested there may be, as in ReNcell VM, a similar reduction of mTORC1 activity, as Raptor null neurospheres have reduced sphere size, number and a diminished sphere forming capacity (Cloëtta et al., 2013). To determine if mTORC1 signalling is reduced in the absence of USP9x, E18.5 neurospheres were harvested and propagated over 3 passages, before undergoing growth factor (EGF/FGF) withdrawal and re-addition to induce mTORC1 activity.

First the reduction in the number of cells per sphere, sphere diameter and sphere forming capacity of E18.5 USP9x KO neurospheres, was confirmed. Over three passages, there was a reduction in sphere size (Figure 3.13) and significantly smaller neurosphere diameter (Figure 3.14). The expression of differentiation markers was investigated and loss of Usp9x did not increase expression of the astrocytic marker (GFAP), however a slight increase in NF160 expression was observed (Figure 3.15), suggesting an increased proportion of neuronal cells (Figure 5, Submitted manuscript).

The phenotype of smaller neurospheres (Figure 3.13, 3.15 and Figure 5 submitted manuscript) and reduced NP proliferation but not their self-renewal, is shared with both Raptor null or rapamycin treated neurospheres (Cloëtta et al., 2013) and suggests that Usp9x may also be required to regulate mTORC1 function in NPs in neurospheres. To further investigate, the level of p-mTOR expression was measured in Usp9x KO neurospheres over three passages and a slight reduction in p-mTOR expression was observed but only at passage 3 (Figure 3.16). This provided preliminary evidence that mTORC1 activity may be perturbed in Usp9x KO neural progenitors. To further investigate this, mTORC1 activity was assessed after EGF / FGF stimulation of the Usp9x KO and control neurospheres. Interestingly, instead of a reduction in phospho-S6 (mTORC1 activity) in Usp9x KO an increase was

observed, with higher expression of the phosphorylating kinase p70S6K at earlier time points (Figure 3.16). This potentially indicated that mTORC1 activity initially peaks in Usp9x KO, but may not be able to be sustained over time. This raised another possibility that we had not considered in the ReNcell VM cells that the increase, and eventual decrease, in mTORC1 activity may differ in ReNcell VM cells and NPs in neurospheres. An initial peak in mTORC1 activity after EGF / FGF stimulation in ReNcell VM cells may occur rapidly, but we have only observed the decline in mTORC1 activity by collecting samples at 5min and 15mins. Therefore, to more precisely define the time of activation samples were collected following EGF / FGF stimulation at 0, 5, 7, 9, 12 and 15mins. Analysis by immunoblot confirmed that there was still reduced mTORC1 activity in USP9x depleted ReNcell VM cells during these time points (Figure 3.17).

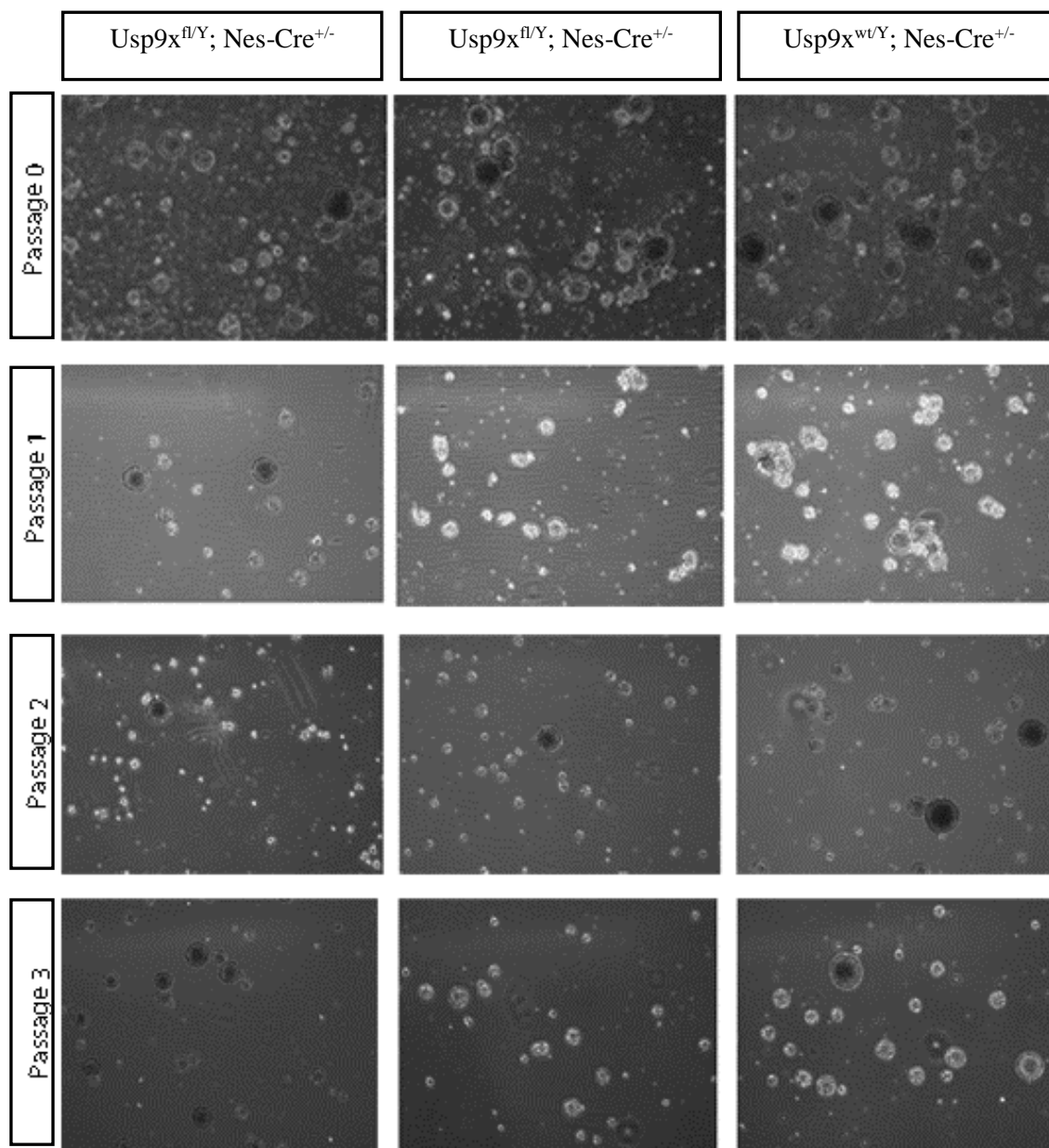


**Figure 3.13. Representative reduction in neurosphere size in Usp9x KO.** Bright Field Microscopy of E18.5 Neurospheres over three passages. 2 Usp9x KO compared to 1 control. No neuronal differentiation, sphere attachment nor projectional outgrowth occurs in 2 USP9x KO cultures compared to 1 Nestin-Cre control. Usp9x<sup>fl/Y</sup>; Nestin-Cre<sup>+/-</sup> (KO) and Nestin-Cre<sup>+/-</sup> (CON).

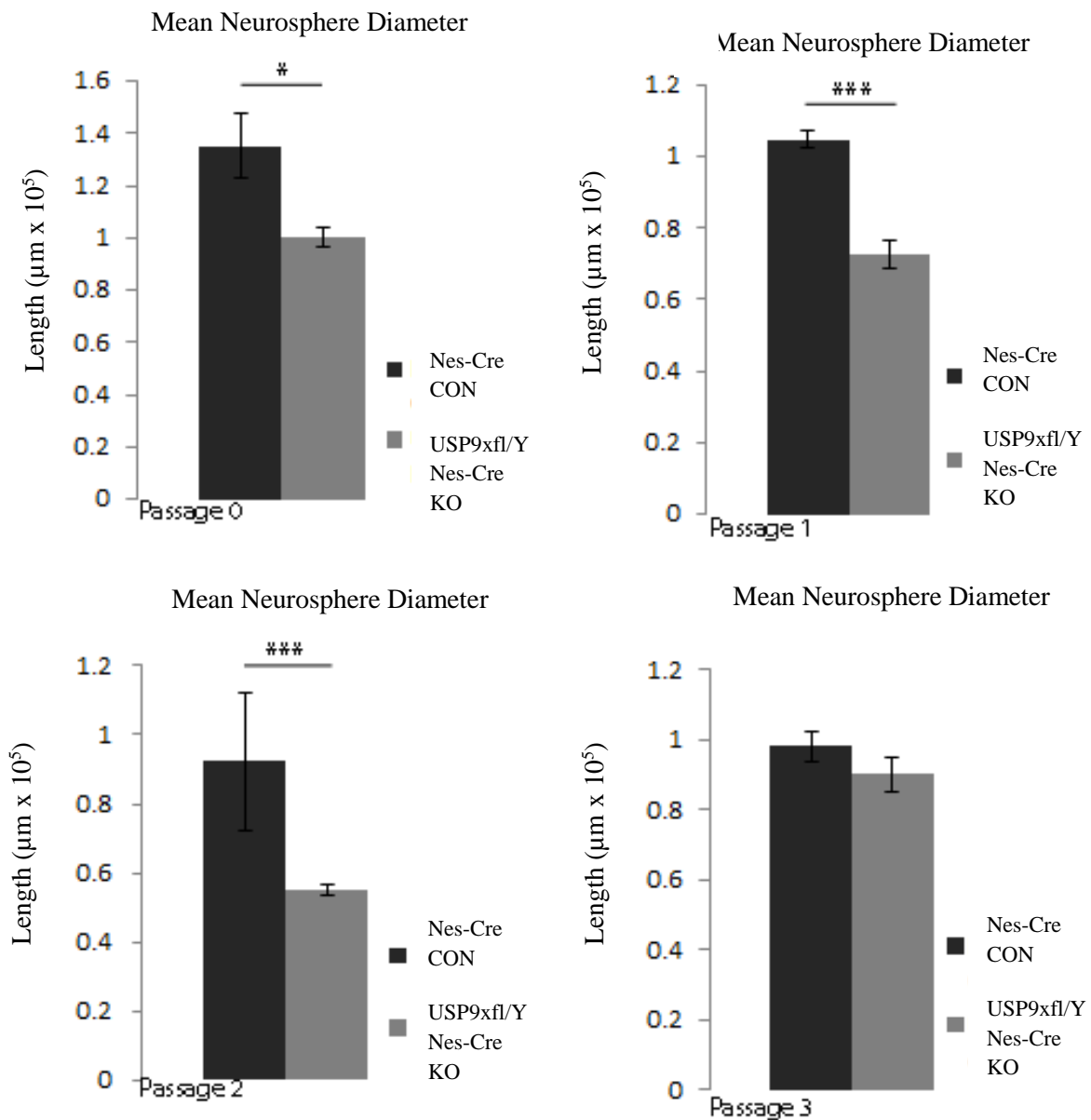


**Figure 3.14. Reduction in diameter of E18.5 neurospheres in *Usp9x* KO compared to controls.** Graphical representation of the mean reduction in *Usp9x* KO compared to the control (CON) after passage 0 (A), passage 1 (B) and passage 2 (C). \*P<0.05 and \*\*\*P<0.0001. Pooled 2 KO vs. 1 CON. *Usp9xfl/Y; Nes-Cre+/-* (KO) and *Nestin-Cre* (CON)

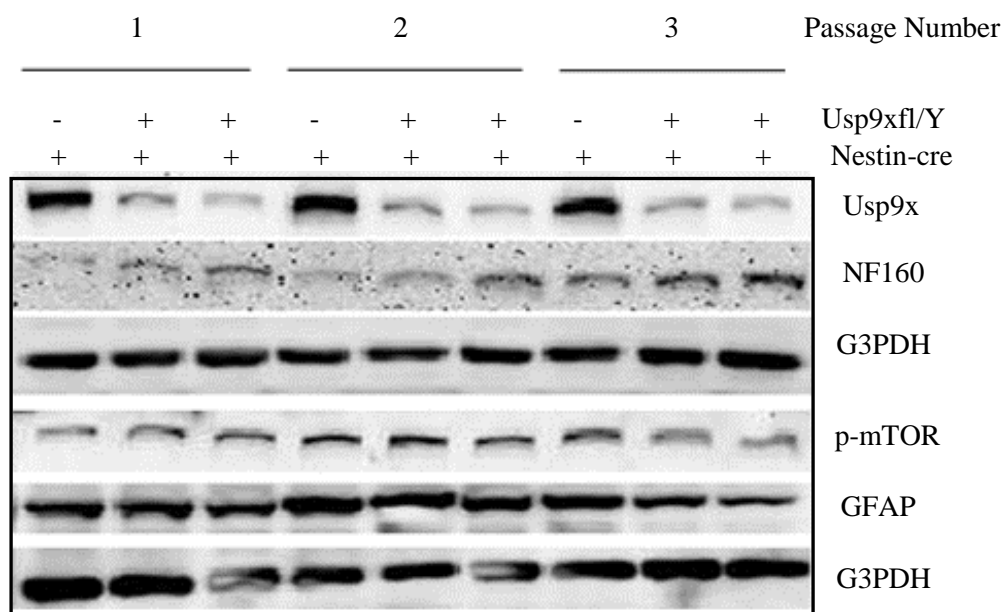


**Figure 3.15. Increased expression of neuronal differentiation marker (NF160) in Usp9x KO E18.5 neurospheres.** Western Blot analysis on whole neurospheres after passage one, two and three show reduced Usp9x expression in Usp9x KO. Expression of neural differentiation markers, NF160 (neuron), GFAP (astrocyte) as well as p-mTOR protein was investigated. There was a progressive increase in NF160 and possible decrease in p-mTOR expression with increasing passage in Usp9x KO. G3PDH, was used as a loading control.

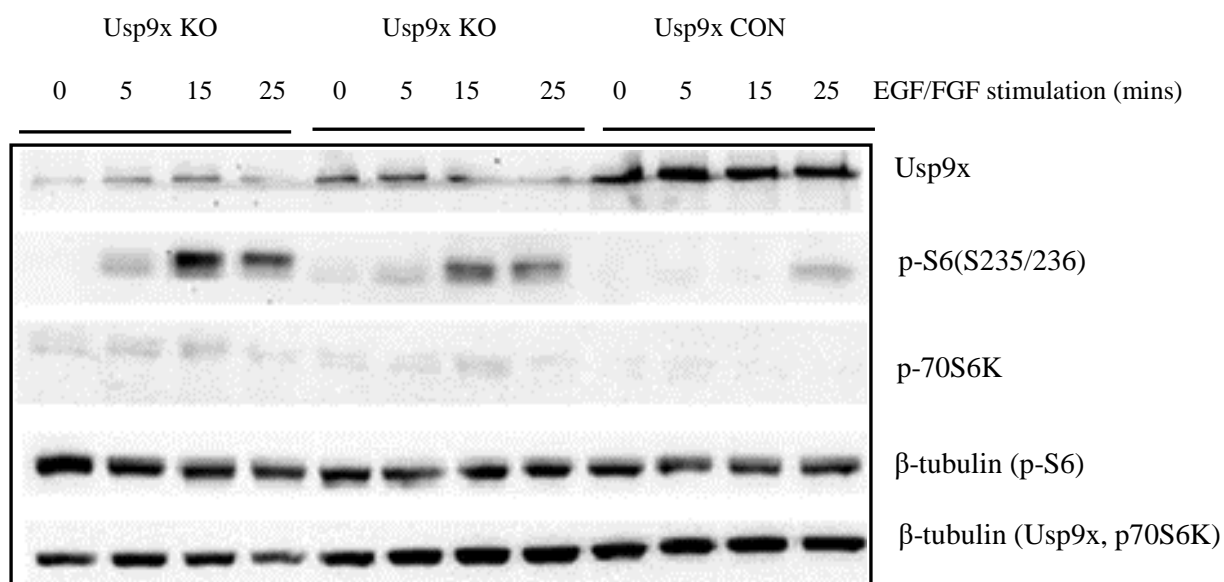


**Figure 3.16. mTORC1 activity is increased in Usp9x KOs at earlier timepoints.** Western Blotting of E18.5 EGF/FGF stimulated Neurospheres after passage three. Usp9x is reduced in Usp9x KO compared to the control. P-S6 expression is increased in Usp9x KO after 5mins, 15mins and 25mins compared to the control. P70S6k expression is higher across all time points in Usp9x KO compared to the control.

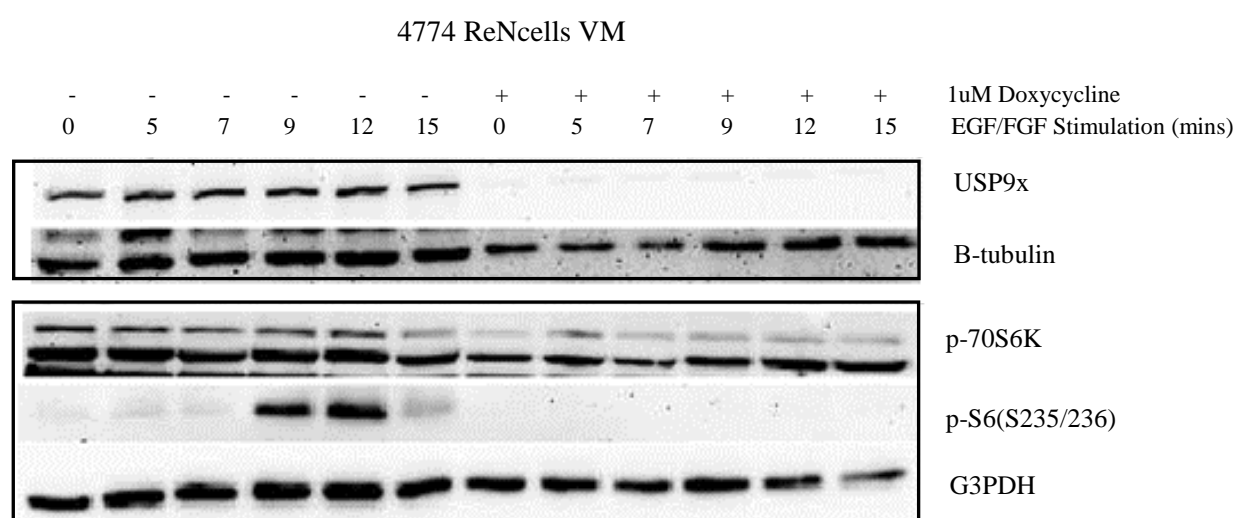


**Figure 3.17. mTORC1 activity remains repressed between 5min and 15min timecourse in ReNcells VM.** In USP9x depleted ReNcells, no initial spike in mTORC1 activity at earlier, and frequent time points after EGF/FGF activation, as there was for Usp9x KO Neurospheres. Reduced Usp9x expression after 1uM Doxycycline treatment. There is a reduction in the expression of mTORC1 activity proteins, p-S6(S235/236), P70S6K in USP9x KD ReNcells, compared to controls. G3PDH was used as a loading control.

### 3.4 Discussion

*USP9X* is a putative “stem-ness” gene that is highly expressed in, and regulates the function of NPs both *in vivo* and *in vitro* (Jolly et al., 2009, Stegeman et al., 2013). Previously, increased expression of *Usp9x* was shown to regulate NP self-renewal by promoting apical-basal cell polarity and altering the architecture of NP cultures derived from mouse embryonic stem cells (Jolly et al., 2009). Here we show *USP9X* is also required to maintain proliferation of the human NP line ReNcell VM, in a cell autonomous manner, and this probably mediated via facilitating mTORC1 pathway signalling.

Inducible knock down of *USP9X* demonstrated that ReNcell VM cells are exceptionally sensitive to *USP9X* depletion. Within 24 hours of initiating *USP9X* knock-down, proliferation of the ReNcell VM cells halted (Figure 3.1B) despite the presence of mitogenic quantities of EGF and FGF. Considering that *USP9X* protein levels were not completely depleted at this time (in some experiments *USP9X* was only 50% depleted) and, that ReNcell VM have a cell cycle time of approximately 30 hours, this indicates that even partial depletion of *USP9X* results in a rapid and comprehensive arrest of proliferation. Although apoptosis can quickly alter cell numbers, and the anti-apoptotic protein Mcl1 is a *USP9X* substrate in some cellular contexts (Schwikart et al., 2010), no alterations in Annexin V or cleaved caspase 3 levels were detected, indicating no increase in apoptosis (Figure 3.3 A,B and C). Nor did *USP9X* depletion promote the differentiation of ReNcells VM to post-mitotic neuronal or glial lineages (Figure 3.4-3.6). Instead the NPs accumulated in the G0/G1 phase of the cell cycle (Figure 3.7). This rapid response was not due to alterations in G1/S checkpoint proteins, although a delayed decrease in pRb levels was observed (Figure 3.8). Retinoblastoma protein (Rb) is phosphorylated by Cyclin D1-CDK4/6 and Cyclin E-CDK2, which converts it to its inactive form, pRb<sup>(S780)</sup>. When active, Rb is bound to the transcription factor E2F, preventing E2F from mediating transcription (Bertoli et al., 2013). Once Rb is phosphorylated to form pRb<sup>(S780)</sup>, it releases E2F, allowing it to transcribe genes required for entry into S phase. When *USP9x* was depleted from ReNcell VM, a reduction in pRb<sup>(S780)</sup> was observed (Figure 3.8), which could indicate either that there is more Rb bound to E2F, despite the total expression of Rb being unchanged, (Figure 3.8), or that *USP9x* directly regulates p-Rb<sup>(S780)</sup> expression, as *USP9x* has a retinoblastoma binding site within its sequence. Therefore the reduction in p-Rb<sup>(S780)</sup> may result from its direct destabilisation. This was preliminarily investigated with no interaction between *USP9x* and p-Rb<sup>(S780)</sup> observed, data not shown.

The mTOR pathway regulates progression through the G0/G1 stage of the cell cycle (Fingar et al., 2004) and Usp9x influences mTORC1 and mTORC2 pathway activity in the C2C12 mouse myoblast cell line (Agrawal et al., 2012). Here we show that USP9X is required for mTORC1, but not mTORC2, activity in ReNcell VM human NPs. The depletion of USP9X levels, loss of mTORC1 signalling, as indicated by failure to induce p-S6, and ReNcell VM cell-cycle arrest, all occurred with very similar kinetics strongly suggesting these NPs rely on USP9X-dependent mTORC1 activity for proliferation. The reduction in mTORC1 signalling in USP9x depleted ReNcells VM is clear, by the consistent reduction in p-S6 levels after 72hrs and 24hrs. Six biological replicates were conducted of the EGF/FGF stimulation experiments and every time, p-S6 expression was reduced in the USP9x depleted cells.

S6 kinases, in particular, p70S6K which phosphorylates S6 to p-S6<sup>(S235/236)</sup>, are known to be ubiquitinated and degraded by the proteasome (Wang et al., 2008). P70S6K was reduced in USP9x depleted ReNcells VM, and expression was restored in USP9x depleted ReNcells VM after proteasomal inhibition, including the expression of its target, p-S6<sup>(S235/236)</sup> (Figure 3.10B). Interestingly, P70S6K mediates mTOR phosphorylation at Ser-2448 (Abraham and Chiang, 2005). However, in the USP9x depleted ReNcells VM, p-mTOR was not reduced (Figure 3.9), when P70S6K was (Figure 3.10B), and only a slight physical interaction between USP9x and P70S6K could be established in vivo, (Figure 3.12A). Therefore, if it were the case that P70S6K causes p-mTOR reduction, which is leading to the reduction in mTORC1 signalling in both the mouse and the cells, it would be expected that this would be evident in the less complex ReNcell VM system, but there was not a reduction in p-mTOR expression in USP9x depleted ReNcells VM, (Figure 3.9).

Post-translational modification of mTOR proteins, including by ubiquitylation, allow the mTOR pathway to respond rapidly to changing extra-cellular signals. Both p-mTOR and RAPTOR are targeted for proteasomal degradation by poly-ubiquitylation (Hussain et al., 2013, Ghosh P et al., 2008). Raptor protein is an mTORC1 scaffolding and recruitment protein, enhancing mTORC1 signalling upon phosphorylation of Ser863, which promotes phosphorylation on other sites to initiate mTORC1 cascade (Foster et al., 2010). It is known to be ubiquitinated by DDB1-CUL4 (Hussain et al., 2013). Here we present several lines of evidence identifying the canonical mTORC1 scaffold protein, RAPTOR, as a probable USP9X substrate in NP/NSCs. Firstly, we show that endogenous USP9X and RAPTOR proteins co-immunoprecipitate from mouse embryonic brain tissue enriched for NPs (Figure

3.12A). USP9X did not interact with mTOR under the same conditions. The much weaker interaction detected between USP9X and phospho-p70S6K may be direct or indirect via RAPTOR, which binds phospho-p70S6K to recruit it to the mTORC1 complex (Nojima et al., 2003). The absence of any alteration in phospho-p70S6K levels following the inhibition of USP9X activity (Figure 3.12D), suggests USP9X does not directly regulate phospho-p70S6K, but this doesn't negate the possibility that USP9X regulates Raptor, upstream, which leads to the downstream increase in phospho-p70S6K after proteasomal inhibition (Figure 3.10B), as phospho-p70S6K is known to be regulated by Raptor (Nojima et al., 2003).

Second, inducible USP9X-specific shRNA-mediated knockdown (Figure 3.9 and 3.11), and transient over-expression (Figure 3.12C) of full length USP9X resulted in a concomitant decrease and increase in RAPTOR protein, respectively. Interestingly, the inhibition of the proteasome, after inhibiting USP9X activity by using the chemical WP1130, which rapidly inhibits USP9X's deubiquitylating activity but does not deplete USP9X protein levels, restored RAPTOR protein levels (Figure 3.12B). In this case a clear and rapid loss of RAPTOR was observed (Figure 3.12D). The near complete depletion of RAPTOR protein within 2 hours strongly suggests that USP9X regulation occurs at the post-translational level. This is supported by the observation that the loss of MCL-1, a bona fide USP9X substrate, occurred only after 4 hours in the same experiment (Figure 3.12D). However, as WP1130 inhibition is not restricted to USP9X, we cannot rule out the possibility that other DUBs, in addition to USP9X, might also regulate RAPTOR stability.

An obvious hypothesis is that USP9X's deubiquitylating activity opposes RAPTOR's degradation at the proteasome. Data presented (Figure 3.12B) confirmed that inhibition of the proteasome increased RAPTOR protein levels in ReNcell VM cells as observed in HEK293T cells, and that inhibiting the proteasome, in the absence of USP9X activity partially rescued RAPTOR levels, but only in HEK293 cells, not ReNcells VM.

USP9X is the first deubiquitylating enzyme shown to directly interact with, and stabilize, components of the mTOR pathway namely, RAPTOR. Although another deubiquitylating enzyme, UCH-L1 has been shown to impact upon mTORC1 signalling it does so indirectly by affecting assembly of the mTORC1 complex. Unlike USP9X, UCH-L1 has no effect on the protein levels of mTOR complex components including RAPTOR.

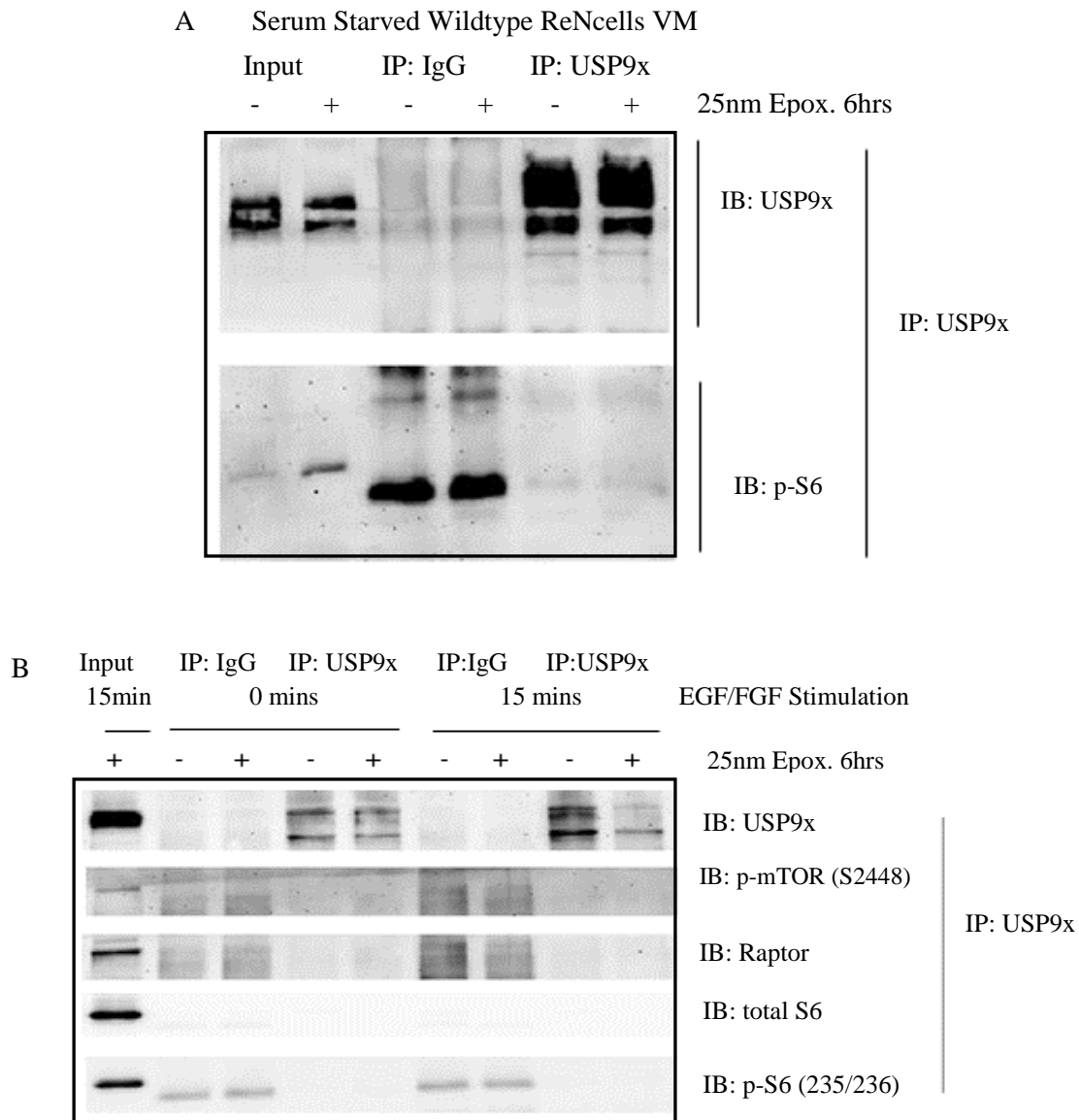
USP9X's regulation of mTOR signalling appears to be very cell context specific. Variation in mTORC1 activity between cell types may be attributed to external influences. For example, the variability in p-S6 and S6K1 expression in murine liver tissue collected from control mice at the same time of day was attributed to feeding habits of the animal (Khapre et al., 2014). Similarly slight changes in pH (Balgi et al., 2011) as well as hypoxic conditions (Wolff et al., 2011) can influence the magnitude of mTORC1 activation. Therefore, different external factors may dictate the level of mTORC1 activity that can be stimulated even in the same cell type. Recently it was shown in C2C12 muscle myoblasts that epitope-tagged USP9X weakly associated with mTOR and both RAPTOR and RICTOR in HEK293T cells and its depletion in C2C12 myoblasts accelerated their differentiation to myotubes (Agrawal et al., 2012). In contrast to our results in NPs, Usp9x depletion from C2C12 cells led to increased mTORC1 activity, in response to growth factor stimulation. Interestingly, while Usp9x depletion in C2C12 cells altered the downstream mTORC1 and mTORC2 effectors, pS6 and pAKT, respectively, no alteration in the levels of the upstream proteins mTOR or RAPTOR, were detected. Therefore, in C2C12 myoblasts, the regulation of mTOR signalling by Usp9x may be indirect. Cell context specific roles of USP9X have also been observed in other systems (Cox et al., 2014, Perez-Mancera et al., 2012, Schickart 2010). Although Usp9x has been identified as a putative “stemness” gene / protein (Van Hoof et al., 2006), decreasing Usp9x levels does not overtly diminish the proliferation of other progenitor/stem cells including, embryonic stem cells (Nagai et al., 2009), T-cell progenitors (Park et al., 2013) or pancreatic progenitors (Perez-Mancera et al., 2012). In contrast, the data presented here indicates that both cultured human NPs and, those in mouse neurospheres, are particularly sensitive to USP9X levels.

mTOR signalling is a major regulator of NP function in both development and disease (Magri and Galli, 2012). Our data reveals the phenotype of Usp9x null neurospheres is very similar to that reported for rapamycin treated and Raptor depleted neurospheres (Cloëtta et al., 2013) and is therefore consistent with Usp9x stabilisation of Raptor in mouse NPs as well. Loss of either Usp9x or Raptor resulted in smaller neurospheres but did not affect their capacity for serial passage indicating they affected proliferation of NPs without affecting the self-renewal capacity of the sphere-initiating NSC. Likewise rapamycin treatment of neurosphere cultures resulted in reduced NP proliferation (and reduced neurosphere size) without affecting the stem cell state (Sato et al., 2010), and rapamycin delivery to the adult sub-ventricular zone neurogenic niche specifically depleted the transiently amplifying NPs but not the stem cell

population (Paliouras et al., 2012). Indeed, the loss of *Usp9x* resulted in more neurosphere initiating stem cells at each passage raising the possibility that NSCs acquired quiescence in *Usp9x*'s absence. These data are consistent with retention of transiently amplifying NPs in the G0 stage of the cell cycle, a phenomenon reported for adult neural stem cells exposed to rapamycin (Paliouras et al., 2012). However, once inhibition has been removed, stimulation with growth factors restores mTORC1 signalling (Paliouras et al., 2012). The reason we observe an increase in mTORC1 activity after growth factor stimulation in the *Usp9x* KO neurospheres, beyond that of the controls, may be due to the combined effect of the small sphere size and a compensatory mechanism, as overall mTORC1 activity is suppressed in E12.5 neural progenitors, *in vivo* (data not shown). There were more of the sphere forming cells, i.e the transient amplifiers, plus the size of the neurospheres were smaller which meant that there was an increased surface area for the EGF / FGF to enter the spheres and initiate the mTORC1 activity faster. In conjunction with this, the peak in the *Usp9x* KO neurospheres may also be a compensatory mechanism to activate all the available remaining mTORC1 components from the stimulating EGF/FGF available. Up regulation of all available mTORC1 proteins may be activated in response to the EGF/FGF stimulation in a positive feedback manner, hence the reason an early peak in p-S6 is observed initially, but quickly declines, as it may not be sustainable in the *USP9x* KO spheres.

As *Usp9x* regulates brain development in mice (Stegeman et al., 2013) and is associated with several human neurodevelopmental disorders (Brett et al., 2014, Homan et al., 2014) the precise role of *Usp9x* in NPs and stem cells warrants further investigation. Across all systems; the ReNcell VM, the cortical brain lysates, the neural progenitors of the *USP9x* KOs and the *USP9x* KO neurospheres, we have shown that *USP9x* plays a role in mTORC1 signalling.

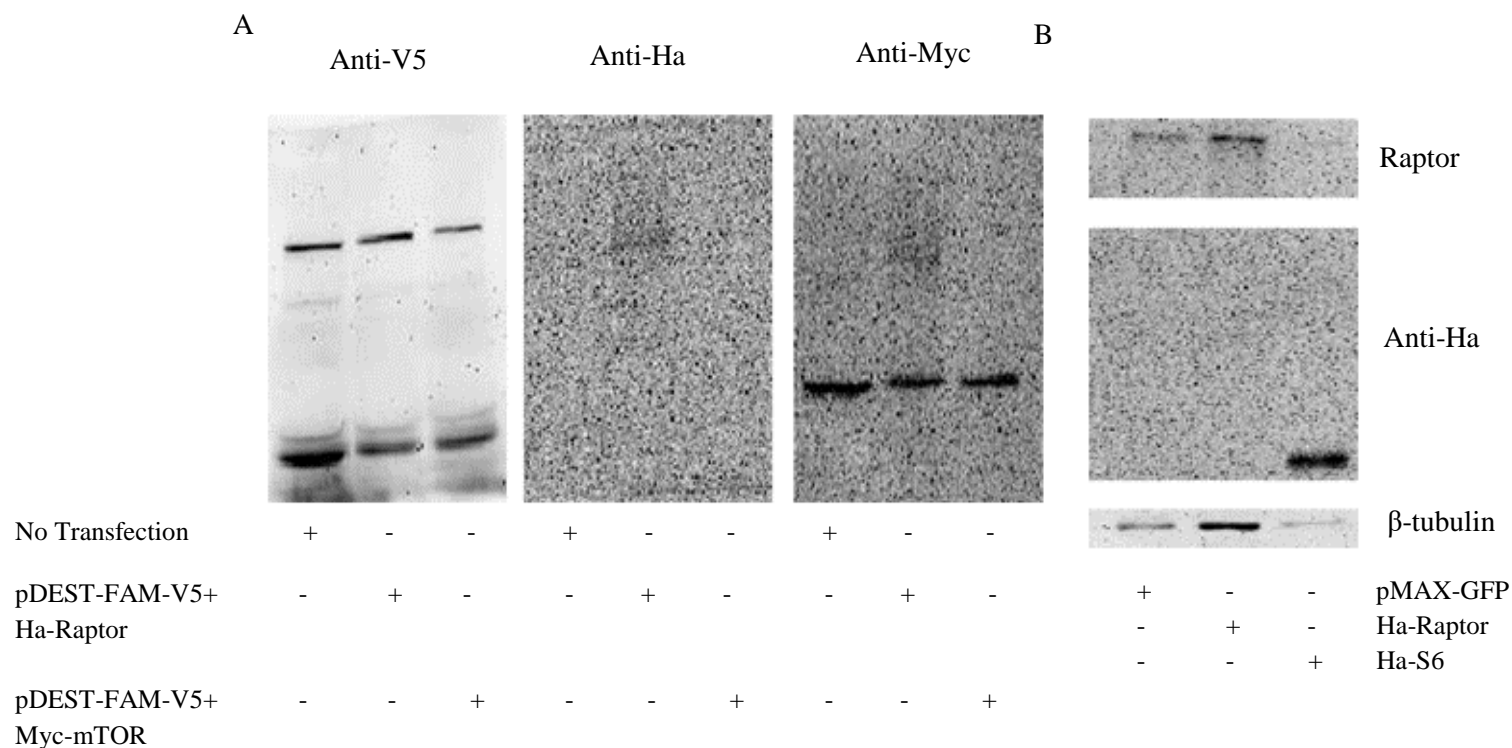
### 3.5 Supplementary Figures



**Supplementary Figure 3.1 Investigating a physical association between USP9x and mTORC1 components in ReNcells VM** (A) IP with USP9x antibodies precipitated USP9x in both presence and absence of epoxomicin. No interaction with p-S6 was detected under these conditions. (B) Neither the presence of epoxomicin or growth factor stimulation promote interaction between USP9x and mTORC1 components in ReNcell VM cells.



Wildtype ReNcells VM



**Supplementary Figure 3.2 Ectopic expression of mTORC1 plasmid in conjunction with Usp9x plasmid expression.** (A) V5-tagged USP9x, HA-tagged Raptor and Myc-tagged mTOR plasmids were transiently transfected into ReNcell VM cells in order to investigate the interaction between mTORC1 components and USP9x. Western Blotting for epitope tag expression after nucleofection showed non-specific Anti-V5 expression but no band of the expected molecular weight. In addition a similar banding pattern was detected in cells transfected with the pMAX-GFP control plasmid. (B) In a separate experiment, ReNcells VM we again transfected with Ha-Raptor and Ha-S6 in isolation, and faint but specific expression of Ha-tag antibody in Ha-Raptor expressed cells.



## **4.0 CHAPTER FOUR RESULTS – USP9x and Glioblastoma Multiforme In Vitro**

### **4.1 Determining the effect of USP9x depletion from U-87 MG GBM Cells**

*USP9x* has been implicated as both a tumour suppressor in pancreatic ductal adenocarcinoma (Perez-Mancera et al., 2012) and an oncogene in lymphoma and multiple myeloma (Schwickart et al 2010). Data presented in Chapter 3 indicates that USP9X facilitates cell cycle progression in immortalised ReNcell VM neural stem cells. ReNcell VM cells however, are not cancer cells despite being immortalised and proliferating rapidly. They are derived from foetal brain tissue and preferentially differentiated into astroglia *in vivo* (Donato et al., 2007). Hence, the results in ReNcell VM cells raise the possibility that USP9x may function as an oncogene in glial-derived tumours such as GBM. Therefore USP9x's role in GBM derived cell lines was investigated. In these initial studies, U-87 MG GBM cells, which recapitulate the tumour *in vivo*, were studied (Clark et al., 2010, Markiewicz-Zukowska et al., 2013, Shi et al., 2012) and *USP9x* shRNA constructs were incorporated to study the effect of USP9x knockdown on U-87 MG cell proliferation in an *in vitro* GBM model.

#### **4.1.1 Development of stable U-87 MG Cells with inducible USP9x knockdown**

Prior to knocking down USP9x, it was important to establish whether *USP9x* is expressed in U-87 MG cells. Immunoblot analysis, of three biological replicates, readily detected USP9x protein at the correct molecular weight of approximately 290kDa in U-87 MG cells (Figure 4.1).

To better study the effect of decreased USP9x protein levels on U-87 MG cell function, stable cell lines containing the same doxycycline-inducible shRNA lentiviral vectors, as used in the ReNcell VM cells (Chapter 3) were generated. The lentiviral vectors were packaged as described (Section 2.1.24). and added to the parental U-87 MG cells for 24hrs. Forty-eight hours after transduction GFP-positive cells, indicating successful transduction, were isolated by fluorescence-activated cell sorting (FACS) as described (Section 2.1.11). Surprisingly, the resultant cultures contained less than 10% GFP-positive cells, as determined by eye, despite gating the FACS for high GFP expression, (Figure 4.2). Hence, single cell clonal sorting was performed, on the previously sorted GFP positive cells. The cells were sorted into 96 well plates in order to obtain single cells, containing the shRNA constructs, that could be expanded (Figure 4.3). After expanding the clones, GFP positive cells across wells were pooled to minimise clonal variation and these pools were used for experimentation.

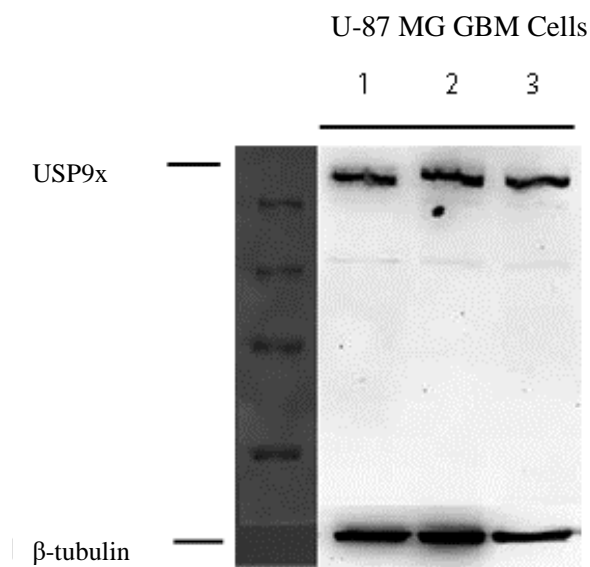


**Figure 4.1** *U-87 MG cells express USP9x. Immunoblot analysis of USP9x expression from triplicate (1, 2, 3) biological replicates of wildtype cultured U-87MG cells. USP9x expression was investigated and is clearly expressed in the cells. Beta-tubulin was used as a loading control indicates protein present across all samples.*

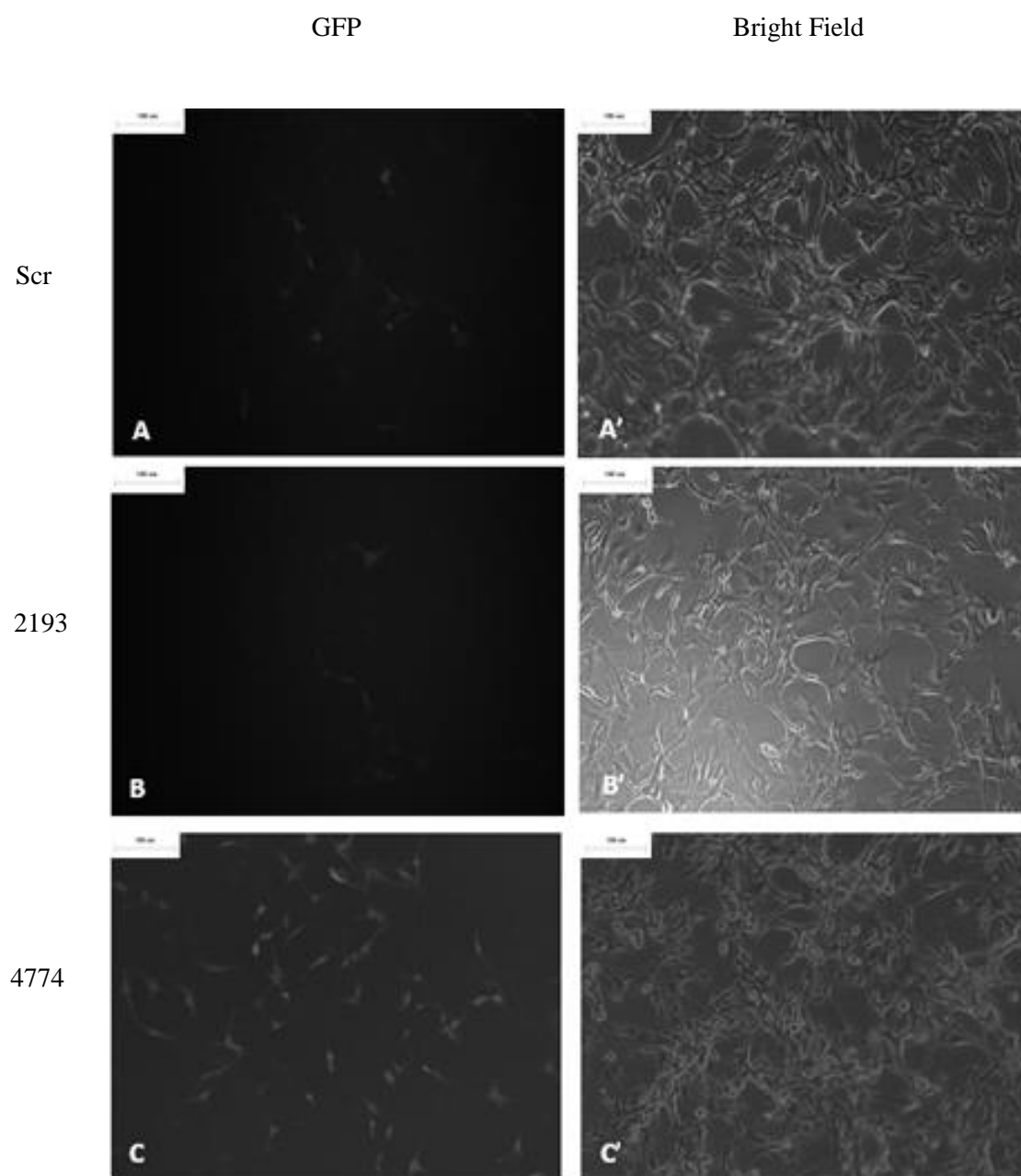


**Figure 4.2.** FACS sorting of GFP positive U-87 MG cells after lentiviral transduction failed to select a pure population. GFP (A,B,C) and bright field (A',B',C') images of U-87 MG cells transduced with lentiviral vectors containing shRNA including Scrambled (A, A'), 2193 (B, B') and 4774 (C, C'). 100 $\mu$ m scale bar.

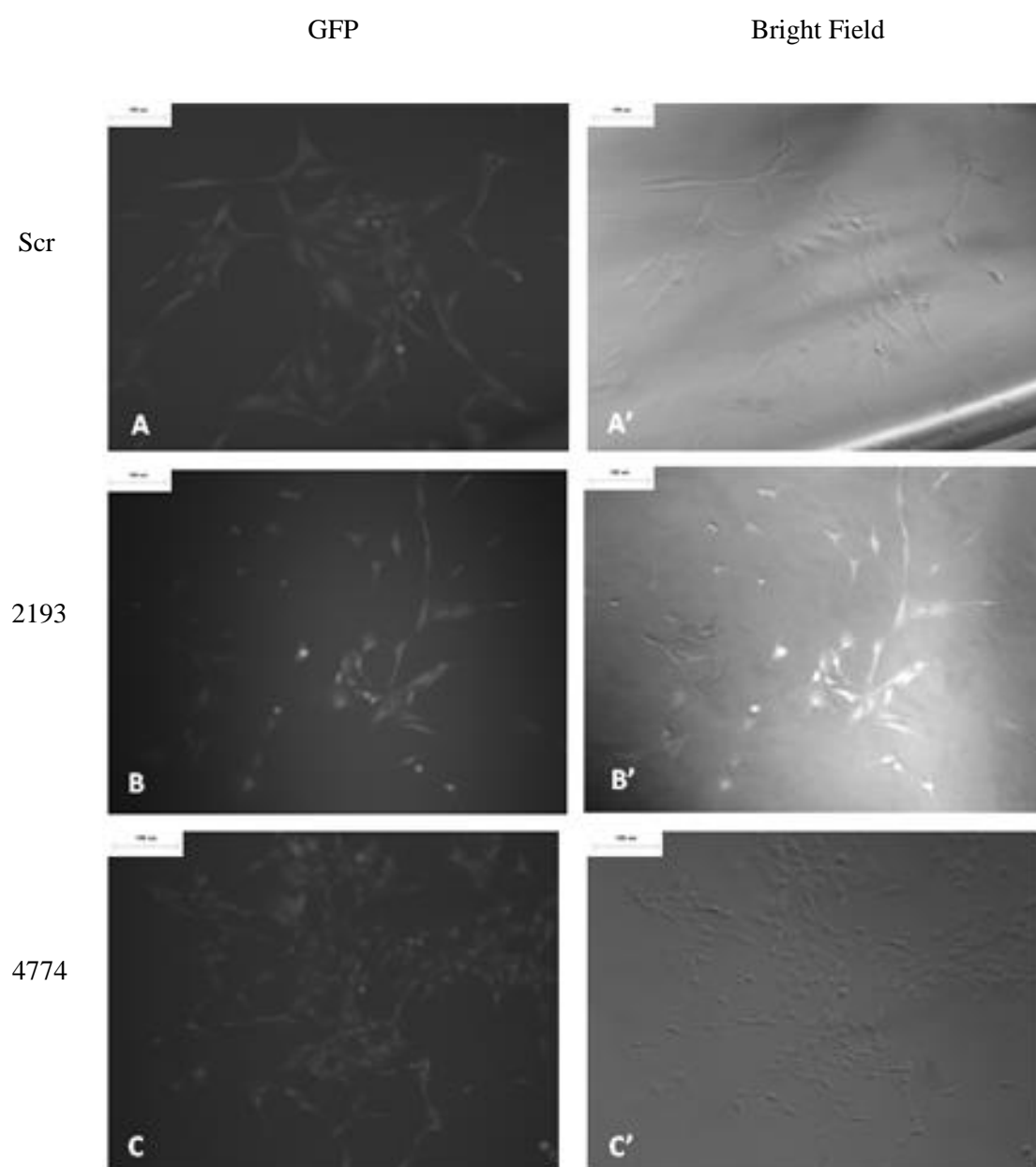


**Figure 4.3.** *Single cell cloning isolated uniformly GFP-positive U-87 MG populations. GFP (A, B, C) and Brightfield (A', B', C') images of U-87 MG cells transduced with lentiviral sectors Scrambled (A, A'), 2193 (B, B') and 4774 (C,C'). 100 $\mu$ m scale bar.*

#### **4.1.2 *USP9x depletion from U-87 MG GBM cells.***

To determine the kinetics of USP9x protein depletion, transduced U-87 MG cells were exposed to 1µM Doxycycline for 144hrs, as previously described for ReNcell VM cells. Doxycycline induced a reduction in *USP9x* expression and morphological changes in 2193 U-87 MG cells (Figure 4.4 and Supplementary Figure 1.0). The cells decreased in size, developed long, thin, “neural-like” projections and eventually detached from the culture surface. Doxycycline had a less dramatic effect on the morphology of 4774 U-87 MG cells although a decrease in cell number was observed (Figure 4.4 C,C’). Immunoblotting analysis revealed that after 144hrs, a 72% and 14% reduction in USP9x protein was observed for 2193 and 4774 +Dox cultures respectively (Figure 4.4B and Supplementary Figure 4.1). The greater reduction of USP9x protein in 2193 +Dox cultures may explain the more dramatic phenotype compared to 4774 +Dox cultures, (Figure 4.4A).

Optimisation experiments were initiated to quantify cell numbers (Xcelligence), and cell cycle analysis. However, at this time it was discovered that all the transduced U-87 MG cell lines were highly contaminated with mycoplasma. Antibiotic treatment was not an option as the infection was too prominent. Therefore, further analysis of the 2913 and 4774 U-87 MG lines was discontinued.

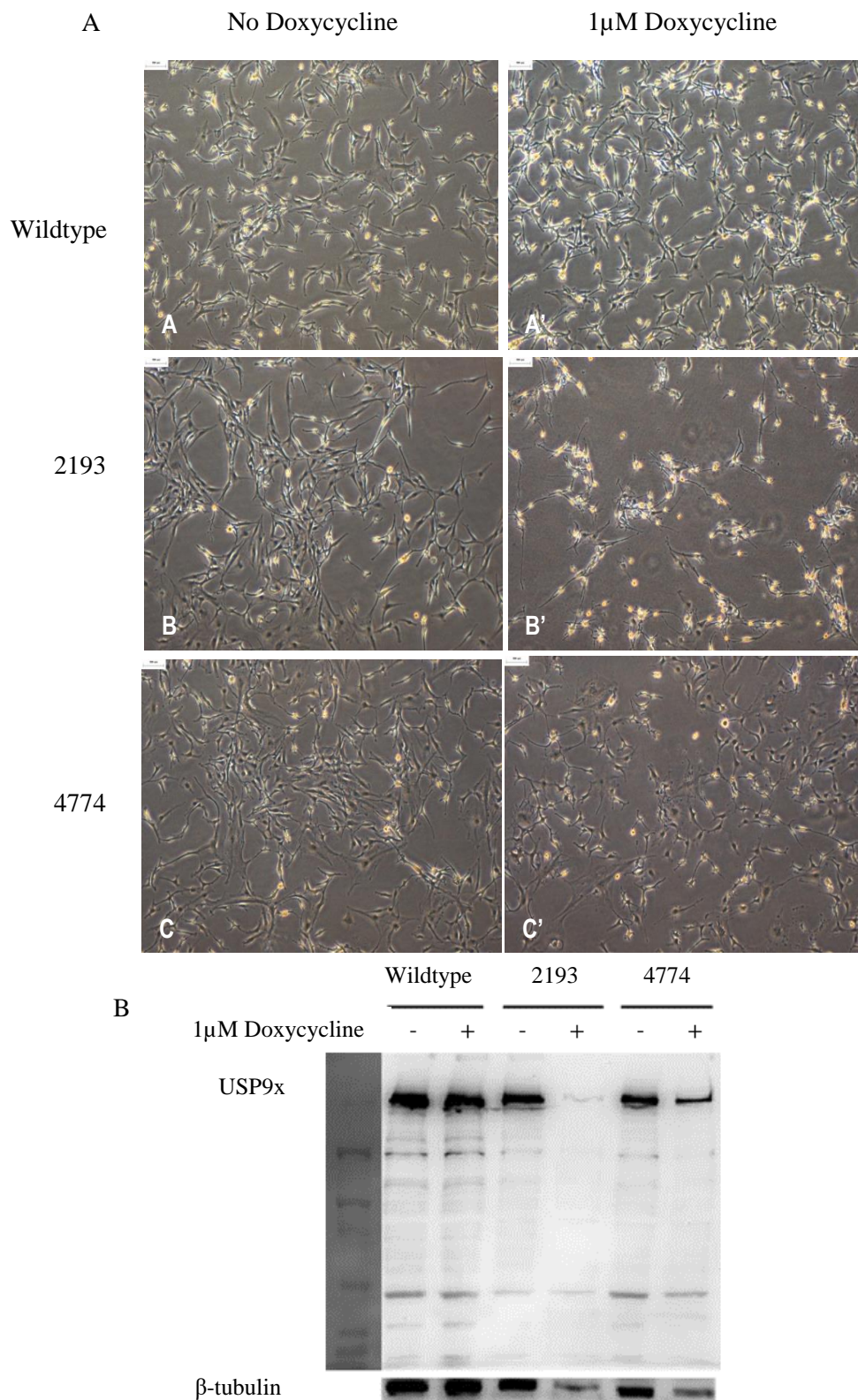


**Figure 4.4 Doxycycline inducible reduction in USP9x protein in U-87 MG cells after six days in culture.** (A) Untransduced wildtype U-87 MG cells with (A') and without 1  $\mu$ M doxycycline (A). U-87 cells transduced with USP9x 2193 and 4774 shRNA lentiviral vectors and six days with (B', (C')) and without (B), (C) 1 $\mu$ M Doxycycline. (B) Immunoblot analysis of USP9x protein level confirms depletion in the presence of 1 $\mu$ M Doxycycline in 2193 and 4774 U-87 MG cells. USP9x expression was normalised against Beta-tubulin loading control.

#### ***4.1.3 mTORC1 activity in GBM cell lines following USP9x depletion***

To continue the investigation of USP9x regulation on GBM cell lines, five mycoplasma-free cell lines were obtained (a generous gift from Dr. Andrew Boyd at the Queensland Institute for Medical Research, Brisbane). During this time USP9X's regulation of mTORC1 activity in ReNcell VM cells had been preliminarily established. As mTORC1 activation has been reported to enhance the tumorigenic capacity of neural tumours, it was appealing to determine the status of mTORC1 activity in GBM cell lines, which are of high virulence. In addition, incorporating multiple GBM cell lines in the mTORC1 analysis after USP9x knockdown, would provide a broader indication of how USP9x affects mTORC1 activity in that tumour type. To knockdown USP9x in five GBM cell lines the direct addition of USP9x siRNAs were used. Pooled USP9x-targeted siRNAs were obtained from Sigma and consisted of a mix of four siRNAs specific for, and validated to deplete, USP9x. A Scrambled siRNA was used as a control.

Treatment of GBM cell lines with USP9x-directed siRNA after 40hrs revealed no dramatic change in morphology (Figure 4.5) and by 72hrs, resulted in negligible USP9x protein in all five GBM cell lines (Figure 4.6 and 4.7). Induction of mTORC1 activity was conducted as for ReNcell VM cells by re-addition of serum 24 hours after its removal (Materials and Methods, Section 2.1.15) and mTORC1 activation determined by immunoblot analysis of p-S6(S235/236) levels (Figure 4.7). In three of the GBM cell lines, D270, U118 and U251, higher levels of p-S6 induction was observed in USP9x depleted cells (Figure 4.7). (This was confirmed in a biological replicate). In U-87 MG and D645 cells the depletion of USP9X had no effect on serum-stimulated induction of pS6 levels, as the slight increase in D645 cells could not be replicated (Figure 4.7). Interestingly, both U-87 MG and D645 cells expressed significantly higher levels of pS6 even at 0min, after 24 hours serum-starvation.

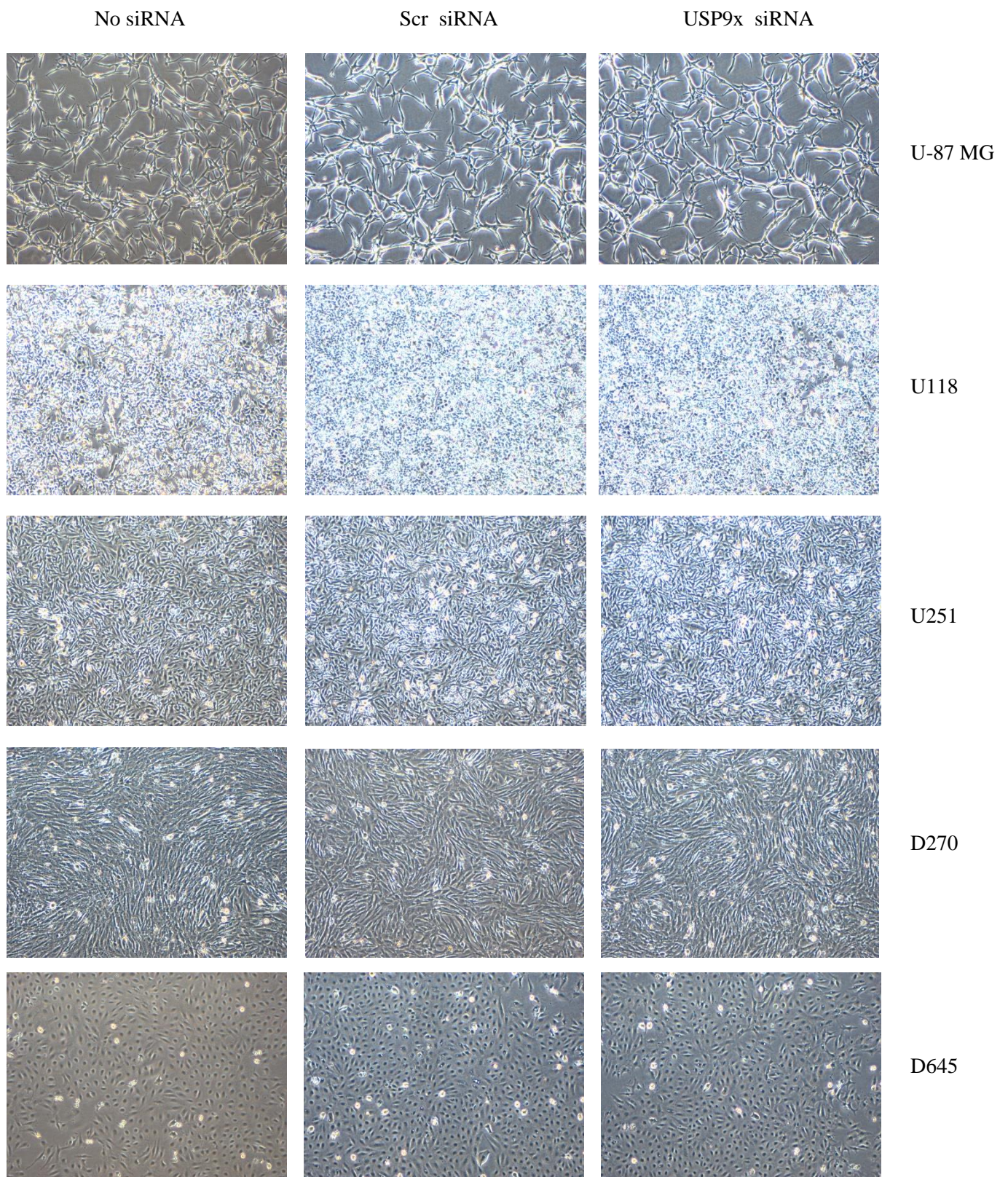


**Figure 4.5** *USP9x siRNA treatment fails to induce morphological changes in GBM cell lines. GBM cell lines were imaged 40 hours after addition of USP9x-specific siRNA. Untransfected and Scr siRNA transfected controls displayed similar morphology and density as USP9x siRNA treatment GBM cell lines.*



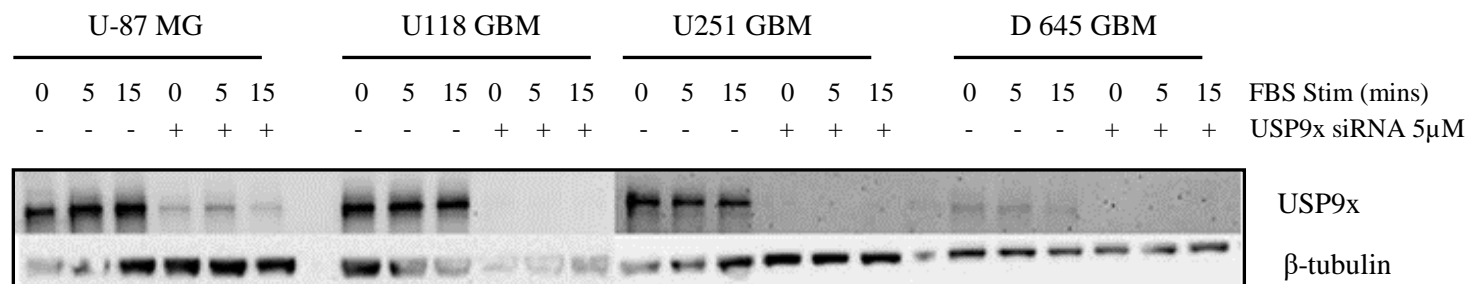


**Figure 4.6.** *USP9x protein levels are reduced in GBM cell lines following 72hrs USP9x siRNA treatment. Total USP9x protein levels were clearly reduced in the 4 GBM lines, following treatment with USP9x siRNAs. Beta-Tubulin was used as a loading control. Beta-Tubulin staining saturation occurred for U118 GBM cells, however obvious reduction of USP9x protein is clear.*

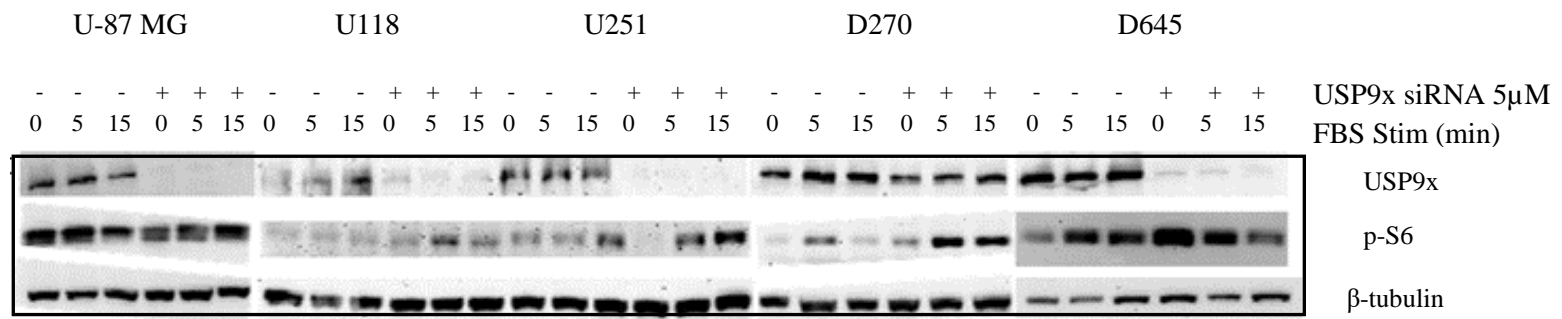


**Figure 4.7 mTORC1 activity in USP9x depleted GBM cell lines.** USP9X levels were reduced in U-87 MG, U118, U251, D645 and D270 cell lines. Phospho-S6 expression increased in U118, U251 and D270 GBM cell lines. Reduction in phospho-S6 expression was observed in D645, but could not be repeated. No obvious increase in U-87 phospho-S6 expression. Beta-tubulin was used as a loading control.

## **4.2 Discussion**

A number of technical issues prevented the generation of U-87 MG cell lines containing vectors from which expression of *USP9X* shRNAs can be induced. A number of troubleshooting approaches will be presented in the first section of this discussion, before the second section discussing implications of *USP9X* depletion on mTORC1 signalling in GBM cells.

### **4.2.1 Generation of inducible *USP9x* shRNA expression in U-87 MG GBM cells**

The detection of GFP expression in some U-87 MG cells following exposure to lentiviral supernatant indicates a successful transduction. However, technical problems arose when establishing a pure population of GFP-positive cells as this could not be achieved by bulk sorting of the total transduced population. Eventually clonal pools were established, and *USP9x* shRNA induction was successful (Figure 4.4B, Supplementary Figure 2.0). However the magnitude of the *USP9x* depletion for the 2193 and the 4774 pools of U-87 MG cells was varied ranging from 74% reduction in 2193 and 14% in 4774 pools. Although we had seen some variation in *USP9x* knockdown in 2913 and 4774 for the ReNcells VM, the magnitude was not great. The greater variation observed in the GBM lines, may have been due to the presence of GFP negative cells within the 4774 pool.

The change in morphology of the U-87 MG cells after *USP9x* depletion was quite dramatic (Figure 4.4A) even after three days in culture (data not shown). Interestingly, such a dramatic phenotype was not observed in the mycoplasma-free U-87 MG cells using *USP9x* siRNA induction (Figure 4.5). This may have been attributable to the mycoplasma infection. However, the source of the cells also varied: QIMR lab versus Eskitis lab, which may also be a contributing factor.

### **4.2.2 mTORC1 signalling in GBM cells**

mTORC1 activity is required for cell growth, proliferation and cell cycle progression in healthy, non-transformed neural progenitors. Its expression is low during times of quiescence, as in G0 phase of cell cycle. Once stimulated by growth factors, activity increases and prompts progression through G1 and into S phase of cell cycle (Fingar et al., 2004). mTORC1 activity has been reported to be upregulated in multiple cancer types, including aggressive brain cancers such as GBM (Yamada et al., 2014). In GBM cells lines, the inhibition of mTORC1 activity significantly reduced proliferation of lines including U-87 and

U118 (Eshleman et al., 2002, Gulati et al., 2009), with a corresponding reduction in P70S6K, which suggests mTORC1 targeting for therapies may be a promising lead. As USP9x reduced the proliferation of immortalised neural stem cells, ReNcell VM, through reduced mTORC1 signalling, we anticipated there may also be a reduction in mTORC1 activity in GBM cells after USP9x is depleted. If this were to be the case, USP9x could potentially be incorporated as another target to reduce GBM cell proliferation, instead of targeting mTORC1 signalling directly. However, we instead provide preliminary evidence that there was a corresponding increase in mTORC1 activity in the majority of GBM cell lines after USP9x was depleted, but observed no increase in cellular proliferation (Figure 4.5). This indicates that the USP9x depletion may exacerbate any already elevated mTORC1 activity that exists prior to serum starvation.

However, as mTORC1 activity was not measured prior to serum starvation and stimulation, the initial activity for these cells in our conditions is not known. Instead activity after serum starvation (time 0min) was measured and was high in controls for U-87 MG cells, as well for USP9x depleted U-87 MG, D645 and D270. High levels of mTORC1 activity during periods of nutrient deprivation may indicate that the GBM cells have adapted compensatory mechanisms in order to remain cycling. The variation in mTORC1 activity across the cell lines may reflect the responsiveness of the original tumour and its adaptability to stress conditions. The five GBM cell lines were derived from five different patients and the way in which their tumour adapt to stressors may be different, their response to treatments (which induce stress upon the tumour cells) may also be affected by the ability of their tumours to adapt to stressors such as nutrient deprivation, as for the U-87MG cells which have high mTORC1 activity, despite lack of nutrients although their tumours all categorised as GBM originally.

#### **4.2.3 Variation in mTORC1 activity in GBM cells**

Variations in mTORC1 activity can occur between different cell types. A reduction of USP9x in ReNcells VM, causes a reduction in mTORC1 activity, whereas it causes an increase in C2C12 muscle myoblasts and GBM cells. If the molecular target of USP9x is Raptor for both the C2C12 and ReNcells VM, then the depletion of USP9x would result in more Raptor degradation, and therefore reduced downstream mTORC1 signalling, which make sense in our slowly proliferating USP9x depleted ReNcells VM. However, this is counterintuitive for the C2C12 myoblasts, as there was increased phosphor-S6 expression after USP9x depletion

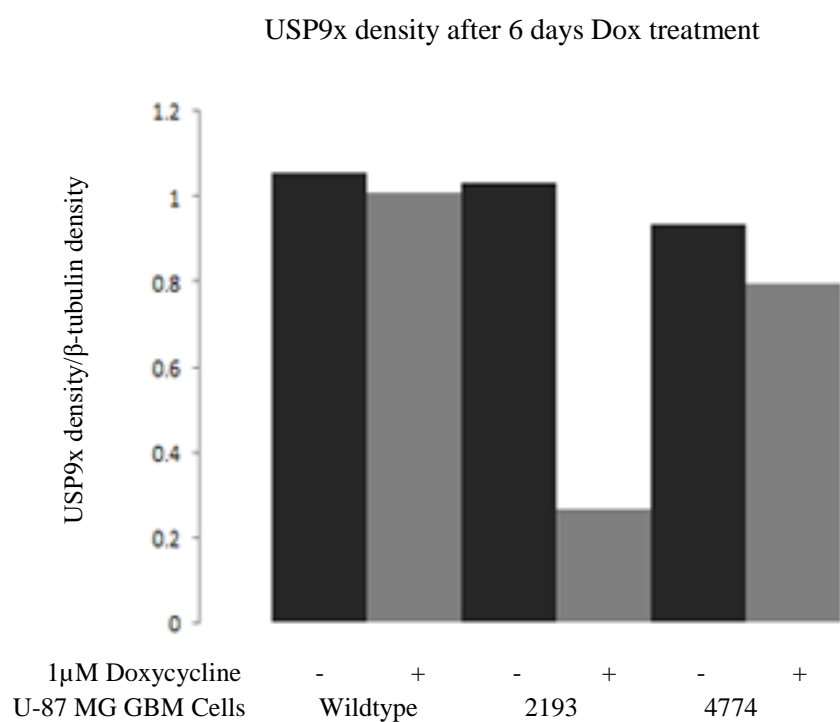
(Agrawal et al., 2012). The ReNcells VM and C2C12 cells are both progenitors, however exhibit opposite responses to USP9x depletion, despite an effect being mediated within the same pathway (mTORC1). ReNcells VM are a neural cell type, whereas C2C12 cells are muscular. This difference alone may be the reason for the variation, but does not explain why mTORC1 activity is increased if Raptor and p-mTOR are the primary targets of USP9x. If the depletion of USP9x resulted in the hyperubiquitylation of a negative regulator of mTORC1 signalling, such as the TSC1/2 complex, then the degradation of this complex would result in the hyperactivation of mTORC1 signalling which would explain Agrawal's results. This could be another target in C2C12 cells, that is not a target in ReNcells VM purely because the C2C12 are a muscular lineage and the ReNcells, as neural lineage.

GBM cells and ReNcells VM are both neural, and still the mTORC1 response is opposite after USP9x depletion, which may come down to the tumorigenic properties of the GBM cells. The molecular target of USP9x in the GBM cells could be different to that of the ReNcells VM and C2C12 muscle myoblasts. The molecular target of USP9x may be a protein regulating the TSC1/2 complex, as loss of this complex has been reported in GBM to cause hyperactivation of mTORC1 signalling (Yamada et al., 2014). Raptor and p-mTOR may not be the only targets of USP9x for the C2C12 and GBM cells.

The immortalisation of the ReNcells VM with the v-myc oncogene may play a role in the differing response compared to the C2C12 and GBM cells after USP9x depletion. Immortalisation with v-myc allows cells to continually proliferate, but inhibiting mTORC1 activity with rapamycin has been shown to reduce c-myc activity in leiomyoma cells (Babcock et al., 2013), and in our system if USP9x diminishes mTORC1 activity, this may be the cause of the reduced proliferation in the ReNcells VM and was not further investigated.

Another possibility may come down to environmental mTORC1 activity is known to fluctuate based on slight changes in environmental conditions, such as in response to pH changes, metabolic changes, availability of oxygen, including cell-cell contact mediating growth inhibition (Khapre et al., 2014, Balgi et al., 2011, Wolff et al., 2011). Therefore, are all three cell types require different biological conditions, both in vitro and in vivo, environmental factors would influence their biological mTORC1 activity.

### 4.3 Supplementary Figures



**Supplementary Figure 4.1. Densitometry of USP9x expression after 6days 1μM Doxycycline induction of USP9x shRNAs in U-87 MG cells. Reduction of 74% and 14% of USP9x protein in 2193 and 4774 +Dox cultures respectively.**

## **5.0 CHAPTER FIVE – Investigating the *KrasG12D* oncogene / *Usp9x* tumour suppressor nexus in neural progenitors**

### ***5.1 Determining the effect of *KrasG12D* activation in conjunction with *Usp9x* deletion on forebrain development***

The *KrasG12D* mutation is frequently detected in a variety of human cancers including pancreatic (Pérez-Mancera et al., 2012), colorectal (Moon et al., 2014), and lung (Sasaki et al., 2011, Fisher et al., 2001). This mutation results in neoplastic cellular transformation. The activation of other oncogenes or deletion of tumour suppressors, in conjunction with *KrasG12D* expression, enhances metastatic progression of low grade tumours into higher, more aggressive grades (Fisher et al., 2001, Perez-Mancera et al., 2012, Moon et al., 2014). For example, the loss of the tumour suppressor p53, in conjunction with *KrasG12D* activation, accelerates the transformation of both astroglial progenitors (Ghazi et al., 2012) and intermediate pancreatic cancer cells (Morton et al., 2010) into high grade gliomas and pancreatic ductal adenocarcinoma, respectively. *Usp9x* deletion in conjunction with *KrasG12D* activation in the pancreas also results in the greatly accelerated progression of pancreatic ductal adenocarcinoma from intermediate stage pancreatic cancer, implicating *USPX* too as a tumour suppressor (Pérez-Mancera et al., 2012).

Whilst the specific *KrasG12D* mutation is not common in human brain tumours, the hyperactivation of Ras signalling, mediated through receptor tyrosine signalling cascade, is (*The Cancer Genome Atlas Research, 2008*) Activation of Ras signalling enhanced glioma progression to the aggressive brain cancer, GBM, *in vivo*, (Marumoto et al., 2009, Holland et al., 2000, Abel et al., 2009). In this instance the combined activation of either H-ras or K-ras, in conjunction with tumour suppressor depletion and/or additional oncogenic activation, resulted in GBM development (Holland et al., 2000, Marumoto et al., 2009). Well characterised murine studies have shown that the activation of *KrasG12D* alone, within mid-gestation stage neural progenitor populations of the subventricular zone (SVZ) leads to the development of infiltrating intermediate grade gliomas with a latency of approximately two and a half months post-natal (Abel et al., 2009, Munoz et al., 2013, Ghazi et al., 2012). This time frame is reduced upon tumour suppressor deletion or additional oncogenic activation.

*USP9x* has been implicated as a tumour suppressor, acting secondary to *KrasG12D* initiated transformation of intermediate stage pancreatic intraepithelial neoplasia (PanIN), accelerating

progression into final stage pancreatic ductal adenocarcinoma (PDA) (Pérez-Mancera et al 2012). This study showed that USP9X dramatically shortened cancer latency such that at 3 months all *KrasG12D* mice presented with early stage PanIN whereas the large majority of mice expressing *KrasG12D* and also null for *Usp9x* were in final stage PDA (Pérez-Mancera et al., 2012). As well as transforming pancreatic epithelial cells loss of *Usp9x* also promoted resistance to anoikis, suggesting an additional role in metastasis. Importantly, the loss of *Usp9x* alone had no affect on normal pancreatic development in this mouse model (Pérez-Mancera et al., 2012).

One role of USP9x in the regulation of neural progenitors is to enhance neural stem cell self-renewal and proliferation, at least *in vitro* (Jolly et al., 2009 and data in Chapter 3). These data are somewhat at odds with the role of *USP9X* as a tumour suppressor in PDA. However, they are consistent with reports of *USP9X*'s oncogenic role in other cancers, including lymphomas (Schwickart et al., 2010) and small cell lung cancer (Sun et al., 2011) where its increased expression promotes tumourigenesis. The ability of a protein to act as both oncogene and tumour suppressor is however, not unique to *USP9X* and a context-specific role for *USP9X* has been investigated in established pancreatic cancer cell lines (Cox et al., 2014).

Loss of *Usp9x* alone in neural progenitors does not lead to tumour development (Stegeman et al., 2013). To date a single study has identified *Usp9x* as a common insertion site in a subset of GBM in a mouse insertional mutagenesis model (Koso et al., 2012). However, there was no report on whether the transposon insertion enhanced or inhibited *Usp9x* expression or function. Therefore, what role, if any, *USP9X* plays in the transformation of neural gliomas into advanced stage gliomas, especially on a *KrasG12D* activated background, remains to be resolved. Therefore the aim of the experiments described herein was to determine if *KrasG12D* has the ability to promote the development of gliomas and, whether deleting *USP9x* promotes tumourigenesis to an aggressive brain cancer such as GBM, analogous to the *KrasG12D* / *Usp9x* interaction in PDA. To investigate this we activated oncogenic *KrasG12D*, in conjunction with *Usp9x* deletion (Stegeman et al., 2013), in neural progenitors of the embryonic mouse forebrain.

### 5.1.1 Generation of mice with activated *KrasG12D* and/or *Usp9x* deletion in neural progenitors.

A number of mouse strains were generated to investigate the interaction, if any, of *KrasG12D* activation and *Usp9x* deletion in neural progenitors. Expression of the *KrasG12D* mutation can be conditionally induced in a tissue and/or time specific manner in mice. In these mice (Jackson et al., 2001) the *KrasG12D* mutation has been introduced into one of the *Kras* alleles. In addition to the G12D mutation in *Kras*, the targeting vector included a *Lox-STOP-Lox* cassette upstream of *Kras* preventing transcription from this allele. Upon expression of Cre recombinase, the *Lox-STOP-Lox* cassette is deleted and results in *KrasG12D* expression under control of the endogenous *Kras* promoter. It should be noted that inheritance of the *Lox-STOP-Lox* / *KrasG12D* modification on both *Kras* alleles results in embryonic lethality, due to no *Kras* expression. Therefore the *KrasG12D* mice are maintained as heterozygotes, which appear normal (Jackson et al., 2001). (The *KrasG12D* mice were a kind gift from Dr Patrick Humbert, Peter MacCallum Cancer Centre, Melbourne). The generation of the “floxed” *Usp9x* mice, *Usp9x<sup>fl/fl</sup>* females and *Usp9x<sup>fl/Y</sup>* males has been reported previously (Stegeman et al., 2013, Pérez-Mancera et al., 2012). In these mice, exon 3 of *Usp9x* is deleted upon expression of Cre recombinase, which results in loss of the *Usp9x* protein (Stegeman et al., 2013, Pérez-Mancera et al., 2012) to produce *Usp9x<sup>-Y</sup>* males and *Usp9x<sup>-/+</sup>* females. *Usp9x* is an X chromosome-linked gene and so wildtype males are *Usp9x<sup>+Y</sup>* and *Usp9x* negative males designated *Usp9x<sup>-Y</sup>*.

To activate *KrasG12D* expression and delete *Usp9x*, mice were crossed with *Emx1-cre* mice, which express Cre recombinase in neural progenitors of the forebrain from E9.5 (Stegeman et al., 2013, Guo et al., 2000, Shinozaki et al., 2004). *Emx-1* expression occurs specifically in the developing dorsal telencephalon, cortex, olfactory bulbs and hippocampus (Shinozaki et al., 2004, Guo et al., 2000). The following specific mouse strains were bred to generate loss of *Usp9x* from, and activate *KrasG12D* expression in, the forebrain (Figure 5.1). The specific gene alterations can be found in (Figure 5.2).

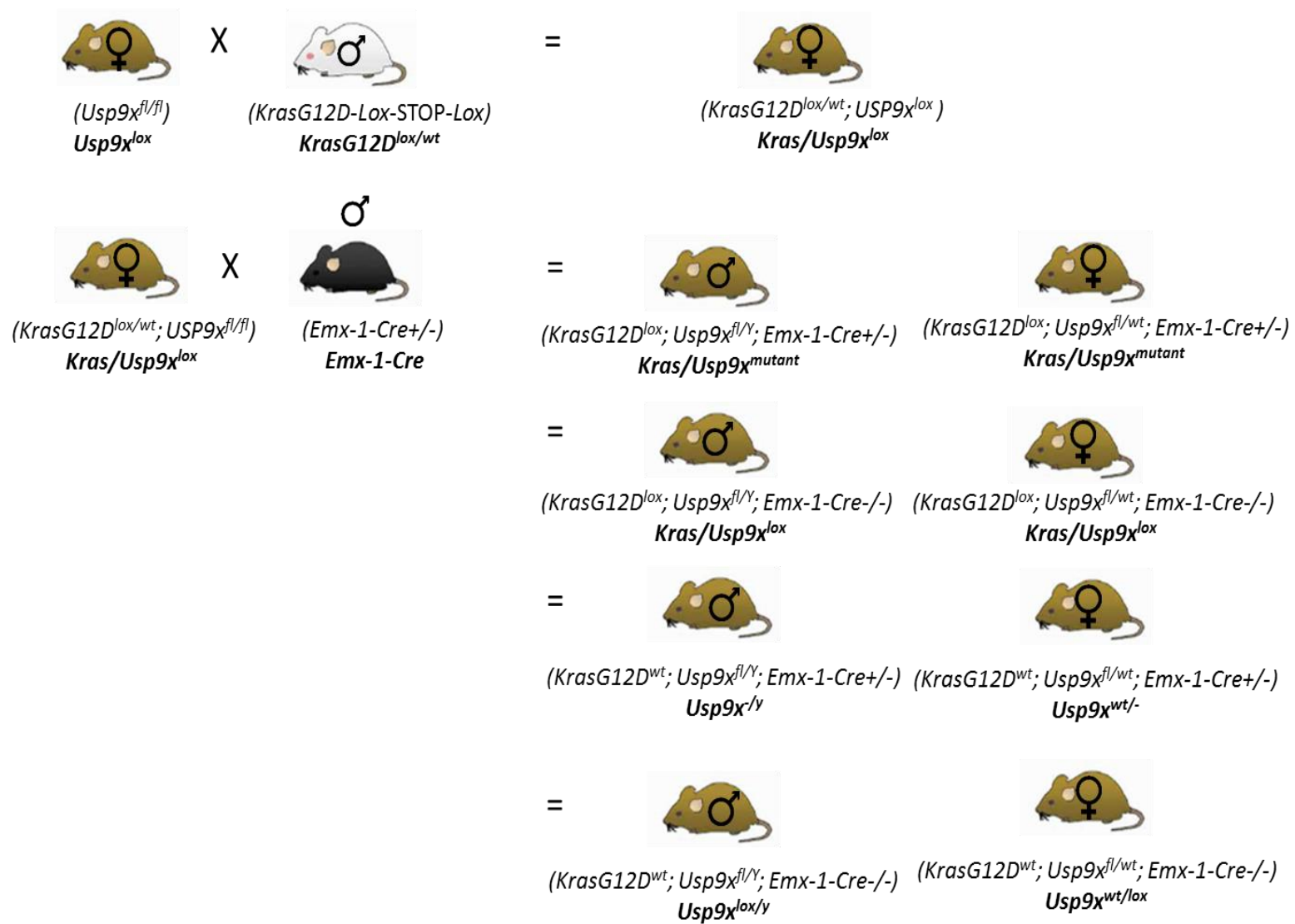


**Figure 5.1 Generation of *Kras/Usp9x<sup>mutant</sup>* animals.** Mating scheme to generate mice used to investigate role of *Kras* activation and *Usp9x* deletion in neural progenitors. Heterozygous *KrasG12D-Lox-STOP-Lox* (referred to hereafter as *KrasG12D<sup>lox/wt</sup>*) mice were mated to *Usp9x<sup>fl/fl</sup>* or *Usp9x<sup>fl/wt</sup>* (referred to hereafter as *Usp9x<sup>lox</sup>*) females to produce *KrasG12D<sup>lox/wt</sup>;Usp9x<sup>lox</sup>* females (referred to hereafter as *Kras/Usp9x<sup>lox</sup>*)

females). The *Kras/Usp9x<sup>lox</sup>* females were mated with *Emx-1-Cre* males to produced *KrasG12D<sup>lox/wt</sup>; Usp9x<sup>lox/lox</sup>; Emx-1-Cre+/-* (referred to hereafter as *KrasG12D<sup>mutant</sup>*).

### 5.1.2 Activation of *KrasG12D* results in peri-natal lethality

Genotyping of weaned litters from *Kras/Usp9x<sup>lox</sup>* x *Emx1-Cre* matings revealed that no *Kras/Usp9x<sup>mutant</sup>* nor *KrasG12D<sup>mutant</sup>* offspring were produced. Mendelian mode of inheritance predicted that 25% should be *Kras/Usp9x<sup>mutant</sup>*, (Figure 5.3) which was not observed. This raised the possibility that mice had not inherited the *KrasG12D<sup>lox</sup>/Usp9x<sup>lox</sup>* genotype. The inheritance of *KrasG12D<sup>lox</sup>/Usp9x<sup>lox</sup>* as well as *KrasG12D<sup>lox</sup>* was investigated and inheritance was lower for both with 5.15% and 6.19% inheritance, respectively instead of the 50% expected (Figure 5.3). PCR (Figure 5.4) was used to confirm full genetic inheritance (Supplementary Figure 5.1).

These data suggested that the *Kras/Usp9x<sup>mutant</sup>*, and possibly the *KrasG12D<sup>mutant</sup>*, genotype resulted in peri-natal lethality. This was supported by the analysis of stillborn P0 mice from *Kras/Usp9x<sup>mutant</sup>* litters. Two stillborn pups from one litter (denoted P1 and P2) and three stillborn pups from another (denoted 'd3', 'd4' and 'd5') were collected and genotyped. All five pups were positive for *KrasG12D<sup>lox</sup>* and Cre, with 'P2' (Figure 5.5 A and B), 'd4' (Figure 5.4 C) and 'd5' (Figure 5.4 C) also positive for *Usp9x<sup>lox</sup>*. These data indicate that *Kras/Usp9x<sup>mutant</sup>* and *KrasG12D<sup>mutant</sup>* genotypes may be embryonic lethal.

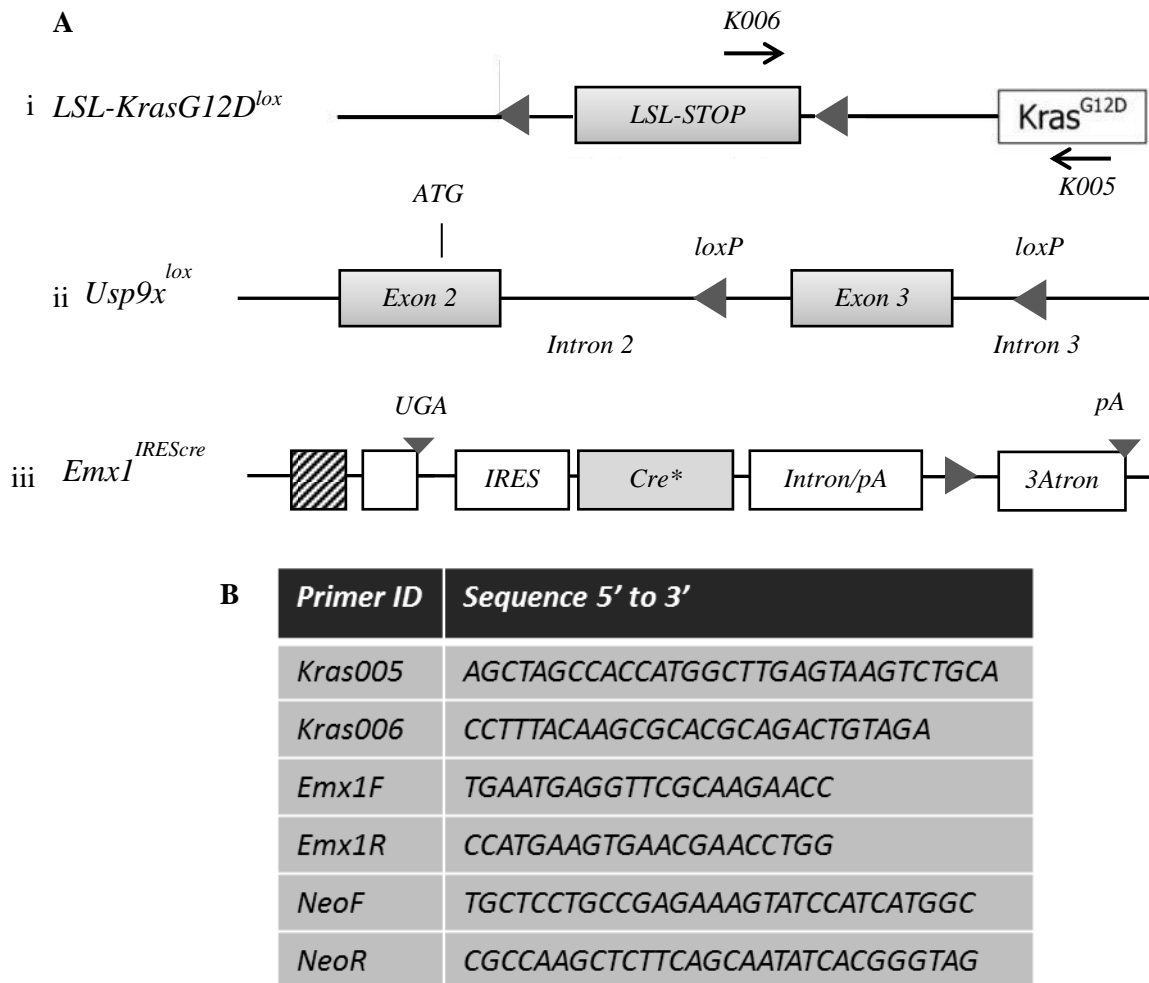


**Figure 5.2 Generation of *Kras/Usp9x<sup>mutant</sup>* embryos. (A) Ai Modification of *Kras*, *Usp9x* and *Emx-1* alleles in mice used to generate *KrasG12D/Usp9x* mutations within the forebrain. *KrasG12D<sup>lox</sup>* is created by incorporating a *STOP* sequence flanked by two *LoxP* sites, preventing the activation of the mutant allele. Primers K005 and K006 (B) were used to identify the presence of this allele. Upon expression of *Emx-1* at E9.5 during embryonic brain development, *Cre* gene will be expressed and will promote the recombination of the *LoxP* sites, on the *Kras* allele, resulting in excision of the *STOP* sequence and commence driving mutant *Kras* (*KrasG12D*) expression from E9.5-E10. Aii Generation of the *Usp9x<sup>lox</sup>* allele as previously described (Stegeman et al., 2013) which incorporates *loxP* sites flanking exon 3 of *Usp9x*. NeoF and NeoR primers (B) are used to detect this modification within the *Usp9x* allele. Aiii Generation of the *Emx-1-Cre IRES* allele which initiates the expression of *Cre* recombinase from E9.5 in cells expressing the *Emx-1* gene. Primers *Emx-1F* and *Emx-1R* were used to detect this modification (B). (Willaime-Morawek, et al. 2006), (NCI Mouse Repository), (Stegeman, et al 2013)**

Number of Weaned mice										
Litter	i Number of pups	ii <i>Kras/Usp9x</i> <sup>mutant</sup> Obt/Exp	iii <i>KrasG12D</i> <sup>mutant</sup> Obt/Exp	iv <i>KrasG12D</i> <sup>lox</sup> / <i>Usp9x</i> <sup>lox</sup> Obt/Exp	v <i>KrasG12D</i> <sup>lox</sup> Obt/Exp	vi <i>Usp9x</i> <sup>lox</sup> <i>Emx-1-Cre</i> Obt/Exp	vii <i>Usp9x</i> <sup>lox</sup> Obt/Exp	viii <i>Emx-1-Cre</i> Obt/Exp	ix Negative Obt/Exp	Totals
1	8	0/2	0/4	0/4	0/4	4/4	2/8	2/4	0/0	8
2	10	0/2.5	0/5	0/5	1/5	7/5	2/10	0/5	0/0	10
3	10	0/2.5	0/5	0/5	0/5	3/5	2/10	2/5	3/0	10
4	10	0/2.5	0/5	0/5	1/5	3/5	2/10	3/5	1/0	10
5	10	0/2.5	0/5	2/5	0/5	3/5	0/10	5/5	0/0	10
6	10	0/2.5	0/5	0/5	1/5	3/5	0/10	2/5	4/0	10
7	11	0/2.75	0/5.5	0/5.5	2/5.5	4/5.5	1/11	4/5.5	0/0	11
8	9	0/2.25	0/4.5	0/4.5	0/4.5	9/4.5	0/9	0/4.5	0/0	9
9	9	0/2.25	0/4.5	0/4.5	0/4.5	7/4.5	1/9	0/4.5	1/0	9
10	10	0/2.5	0/5	3/5	1/5	2/5	1/10	0/5	3/0	10
Average	9.7	0/2.425	0/4.85	0.5/4.85	0.6/4.85	4.6/4.85	1.1/9.7	1.8/4.85	1.2/0	9.7
Total	97	0/24.25	0/48.5	5.0/48.5	6/48.5	46/48.5	11.34/97	18/48.5	12/0	97
Percentage of expected	100	0/25%	0/50%	5.15%/50%	6.19%/50%	47.42%/50%	11.69/100%	18.55%/50%	1200%/0%	100

**Table 5.3. *Kras/Usp9x*<sup>mutant</sup> genotype was not observed in weaned offspring.** A total of ten litters producing 97 weaned animals were examined. The number of animals obtained per litter is shown in the second column (i). For each genotype (ii – ix), the number obtained number is a ratio of the number expected, based on calculated Mendelian genetic ratios. There were no surviving offspring for (ii) *Kras/Usp9x*<sup>mutant</sup> or (iii) *KrasG12D*<sup>mutant</sup>. It was expected that 25% of animals in each litter should be *Kras/Usp9x*<sup>mutant</sup> and 50% should be *KrasG12D*<sup>mutant</sup>. The inheritance of the two floxed allele without cre (iv) *KrasG12D*<sup>lox</sup>/*Usp9x*<sup>lox</sup> and (v) *KrasG12D*<sup>lox</sup> was expected to be 50%, but were 5.15% and 6.19% respectively. The inheritance of (vi) *Usp9x*<sup>lox</sup> and Cre was as expected (50% and 47.42% observed). For (vii) *Usp9x*<sup>lox</sup> and (viii) *Emx-1-Cre* alone prediction of inheritance was difficult as these alleles were expected to be inherited in conjunction with either *Kras* or *Usp9x*, for (viii) *Emx-1-Cre* or with *Kras*, for (vii) *Usp9x*<sup>lox</sup>. Hence the predictions were calculated based on inheritance of the floxed alleles alone in which 100% inheritance was expected for (vii) *Usp9x*<sup>lox</sup> and 50% inheritance for (viii) *Emx-1-Cre*. It was not expected that there would be animals in which no modified allele was inherited, however 12 animals were obtained (ix).

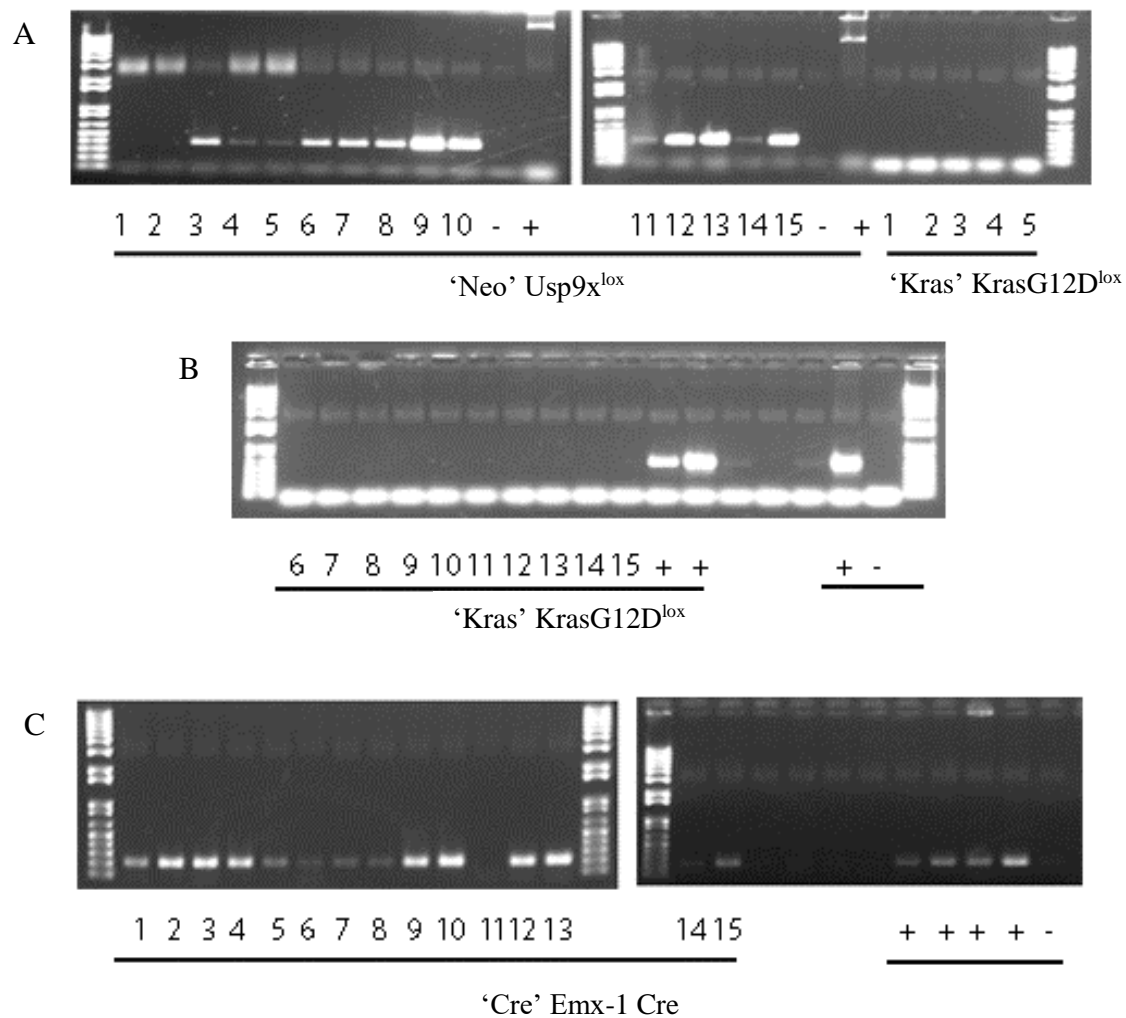


**Figure 5.4** *Kras/Usp9x<sup>mutant</sup> genotype is not observed in offspring. Representative genotyping by PCR for Usp9x<sup>lox</sup> 'Neo', KrasG12D<sup>lox</sup> 'Kras' and Emx-1-Cre 'Cre' for the first fifteen (1-15) weaned mice. (A) genotyping for Usp9x floxed, (A-B) genotyping for KrasG12D floxed and (C) genotyping for Emx-1-Cre. A total of 97 post-natal offspring were genotyped.*

### 5.1.3 Activated *KrasG12D* results in gross morphological defects in the embryonic brain

To determine to which developmental stage *Kras/Usp9x<sup>mutant</sup>* pups were viable, embryos were extracted prior to birth, from E18 to E20. Genotyping detected '*KrasG12D<sup>lox</sup>*' together with '*Usp9x<sup>lox</sup>*' and '*Cre*' in the expected Mendelian ratios at each stage tested. It was anticipated that 25% of the embryos per litter would inherit all three modified alleles, and on average 34% of embryos per litter did so, (Figure 5.6 Table B). Embryos inheriting the '*KrasG12D<sup>lox</sup>*', and '*Emx-1-Cre*' alleles rarely occurred without '*USP9x<sup>lox</sup>*' inheritance, due to the breeding with homozygous *Usp9x<sup>fl/fl</sup>* mothers, (Figure 5.6 Table C). Both males and females embryos that had the mutant genotype were analysed as the potency of mutation may be similar, as X chromosome inactivation could mean the wildtype *Usp9x* is inactivated in some of the female embryos' cells. This was the case during the development of PDA in *KRas* activated and *Usp9x* deleted mice where tumour frequency in females was the same as males (Perez-Mancera et al., 2012). Therefore, the same may apply for the development of neural tumours, whereby the *Kras<sup>mutant</sup>/Usp9x<sup>-/+</sup>* females may be just as potent as the *Kras<sup>mutant</sup>/Usp9x<sup>-Y</sup>* males. However, as the *KrasG12D<sup>mutant</sup>* was so dramatic in males and females, the additive effect of *Usp9x* deletion was not further investigated.

Upon dissection at E18.5, some embryos were obviously paler, suggesting poor overall body vascularisation and, they also appeared to have severe cerebral swelling, (Figure 5.7 A, B). Genotyping established that all such embryos were *Kras/Usp9x<sup>mutant</sup>* (Figure 5.7 C). Interestingly, the phenotype was not dependent on the deletion of *Usp9x*, as *Usp9x<sup>lox</sup>* negative embryos had the same phenotype, raising the possibility that activation of the *KrasG12D* mutation alone was causative. To directly test this *KrasG12D<sup>lox</sup>* and *Emx-1-Cre* animals were mated. Embryo genotyping at E17.5 confirmed that inheritance of the *KrasG12D* allele alone correlated with the phenotype including both cerebral swelling and pale colouring. Next, embryonic extractions were conducted at E14.5 and E16.5 to determine the earliest developmental stage at which a morphological defect could be observed. Pale embryos were observed at each stage (E14.5, E16.5 and E17.5). However, at E14.5, (Figure 5.8 Aiii), no cerebral swelling was obvious but it was evident at E16.5 (Figure 5.8 Aii) and E17.5 (Figure 5.8 Ai). Interestingly, this phenotype has not been reported in other studies activating *KrasG12D* in neural progenitors (Marumoto et al., 2009, Holland et al., 2000, Abel et al., 2009). Therefore the effect of *KrasG12D* activation on neural progenitors was further investigated.

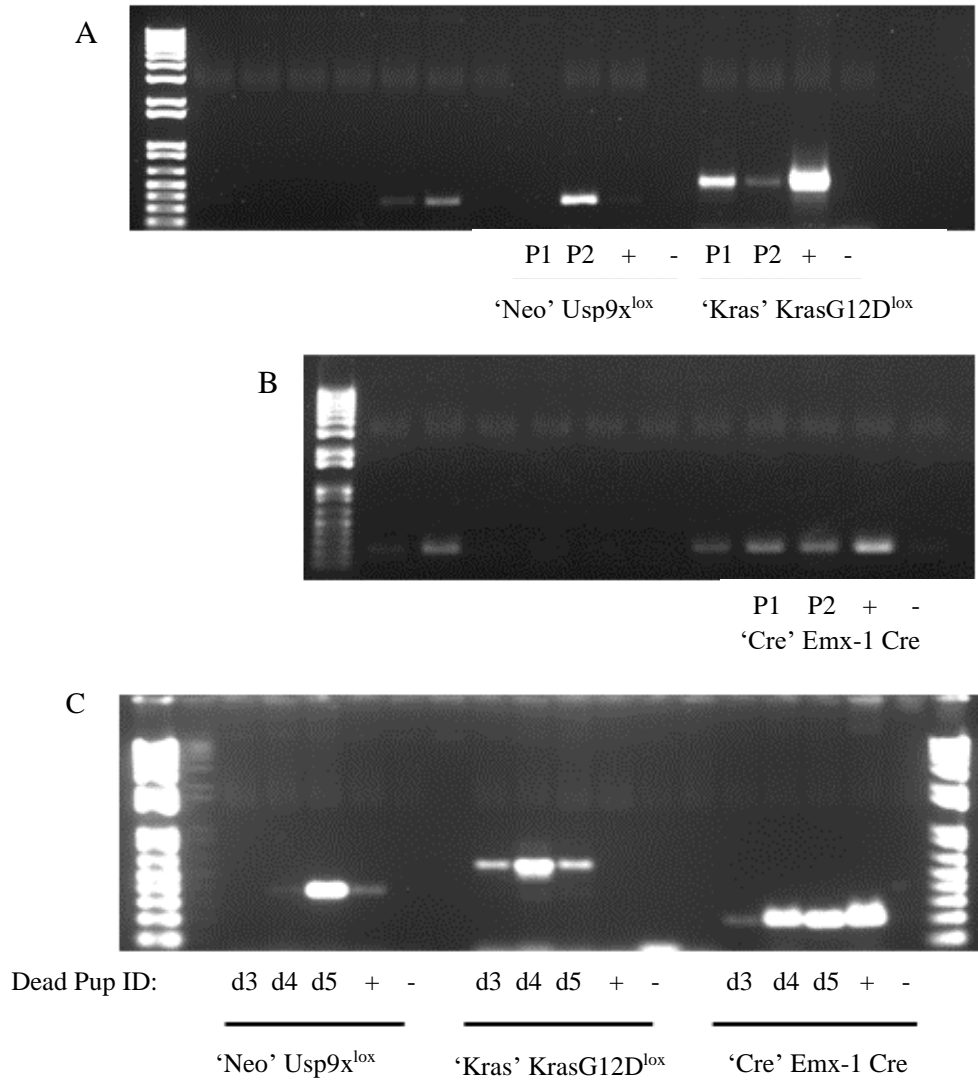


**Figure 5.5 *Kras/Usp9x*<sup>mutant</sup> results in embryonic lethality.** *Kras/Usp9x*<sup>mutant</sup> pups were born, but did not survive. These P0 stage pups were collected during birthing and analysed for *KrasG12D*<sup>lox</sup>, *Usp9x*<sup>lox</sup> and *Emx-1-Cre* genotypes. P0 stage pups were collected from different litters. (A-B) Litter one: (P1 and P2) and (C) Litter two: (d3, d4, d5). 'P2', 'd4' and 'd5' were positive for all three genotypes, indicating they were *Kras/Usp9x*<sup>mutant</sup>, but all were positive *KrasG12D*<sup>lox</sup> and *Emx-1-Cre*, indicating they were *KrasG12D*<sup>mutant</sup>. This prompted the investigation of *Kras/Usp9x*<sup>mutant</sup> in embryos. A total of 5 still born mice were analysed.

A The number of embryos inheriting each allele				
Litter	#embryos	Emx-1-Cre	KrasG12D <sup>lox</sup>	Usp9x <sup>lox</sup>
1	8	4	3	1
2	10	4	0	7
3	10	6	0	8
4	10	10	6	10
5	10	7	6	7
6	10	10	6	10
7	11	7	6	7
8	9	9	5	9
9	9	9	4	9
10	11	5	6	7
11	12	7	8	10
12	11	7	8	9
Average	10.08333	7.083333333	4.833333333	7.833333333
Total	121	85	58	94

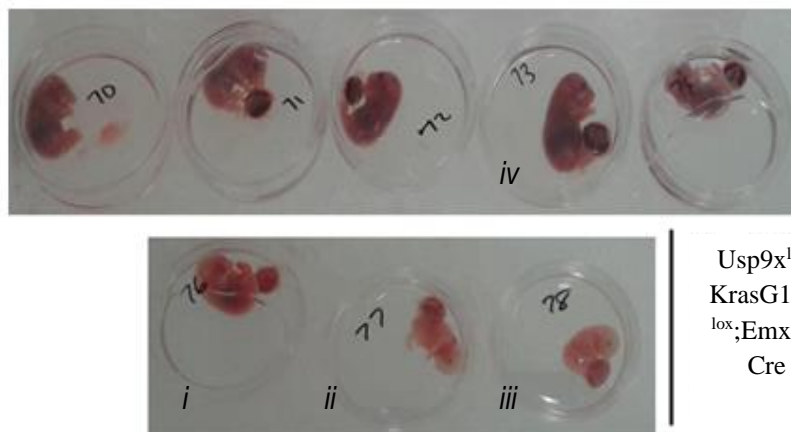
B Number of <i>Kras/Usp9x<sup>mutant</sup></i> embryos						
Litter	Number of pups	Expected	Expected %	Number of <i>Kras/Usp9x<sup>mutant</sup></i> Obtained	Ratio of Obtained	% of Ratio Obtained
1	8	2	25	0	0	0
2	10	2.5	25	0	0	0
3	10	2.5	25	0	0	0
4	10	2.5	25	6	0.6	60
5	10	2.5	25	3	0.3	30
6	10	2.5	25	6	0.6	60
7	11	2.75	25	5	0.454545	45.45454545
8	9	2.25	25	5	0.555556	55.55555556
9	9	2.25	25	4	0.444444	44.44444444
10	11	2.75	25	2	0.181818	18.18181818
11	12	3	25	5	0.416667	41.66666667
12	11	2.75	25	6	0.545455	54.54545455
Average	10.08333	2.520833333	25	3.5	0.347107	34.1540404
Total	121	30.25		42	4.098485	

C Number of <i>KrasG12D<sup>mutant</sup></i> embryos						
Litter	Number of pups	Expected	Expected %	Number of <i>KrasG12D<sup>mutant</sup></i> obtained	Ratio of Obtained	% of Ratio Obtained
1	8	4	50	2	0.25	25
2	10	5	50	0	0	0
3	10	5	50	0	0	0
4	10	5	50	0	0	0
5	10	5	50	0	0	0
6	10	5	50	0	0	0
7	11	5.5	50	0	0	0
8	9	4.5	50	0	0	0
9	9	4.5	50	0	0	0
10	11	5.5	50	0	0	0
11	12	6	50	0	0	0
12	11	5.5	50	0	0	0
Average	10.1	5.04	50	0.167	0.021	2.1
Total	121	60.5		2	0.25	

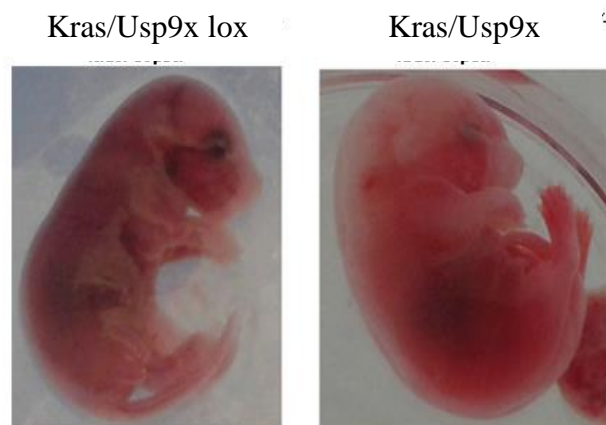
**Table 5.6.. *Kras/Usp9x<sup>mutant</sup>* embryos are observed in the expected Mendelian ratios.** Embryos between stages E18-E20 were collected and analysed for inheritance of *KrasG12D<sup>lox</sup>*, *Usp9x<sup>lox</sup>* and *Emx-1-Cre* by PCR. (A) The number of embryos inheriting each allele is shown for the twelve litters collected. The expected number and percentage of embryos per litter was calculated to be 2.5 and 25% respectively, for the inheritance of all three alleles (B) and 5.0 and 50% respectively for the inheritance of both *KrasG12D<sup>lox</sup>* and

*Emx-1-Cre (C). The number and percentage of embryos obtained per litter calculated and compared to the expected numbers. The average number of embryos per litter that were positive for all three alleles was 3.5, with a percentage of 34.15% (B). This was greater on average than the expected numbers. The average number of embryos per litter that were positive for KrasG12D<sup>lox</sup> and Emx-1-Cre alone was only 0.167 with a percentage of 2.1% (C). KrasG12D<sup>lox</sup> was rarely observed without Usp9x<sup>lox</sup> and Cre. A total of 121 embryos were extracted for these studies.*

A



B



C

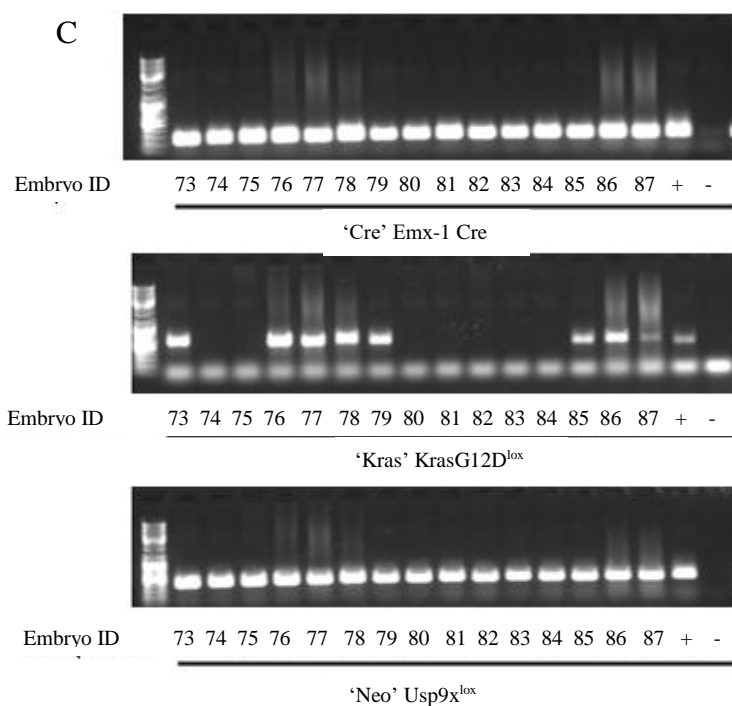


**Figure 5.7 *Kras/Usp9x<sup>mutant</sup>* mice display gross morphological defects.** (A) Representative phenotype of *Kras/Usp9x<sup>mutant</sup>* which are pale, and have cerebral swelling at E18.5. (B) Higher magnification of swollen heads of *Kras/Usp9x<sup>mutant</sup>* at E18.5 (C) Genotyping of E18.5 embryos confirms the mutant phenotype observed (Ai, ii and iii) which correlates with *Kras/Usp9x<sup>mutant</sup>* genotype. Interestingly embryo 73 was also positive for all three alleles, but did not show a dramatic phenotype (Aiv). Total number of embryos analysed was 121, of which 42 were of the *Kras/Usp9x<sup>mutant</sup>* genotype.

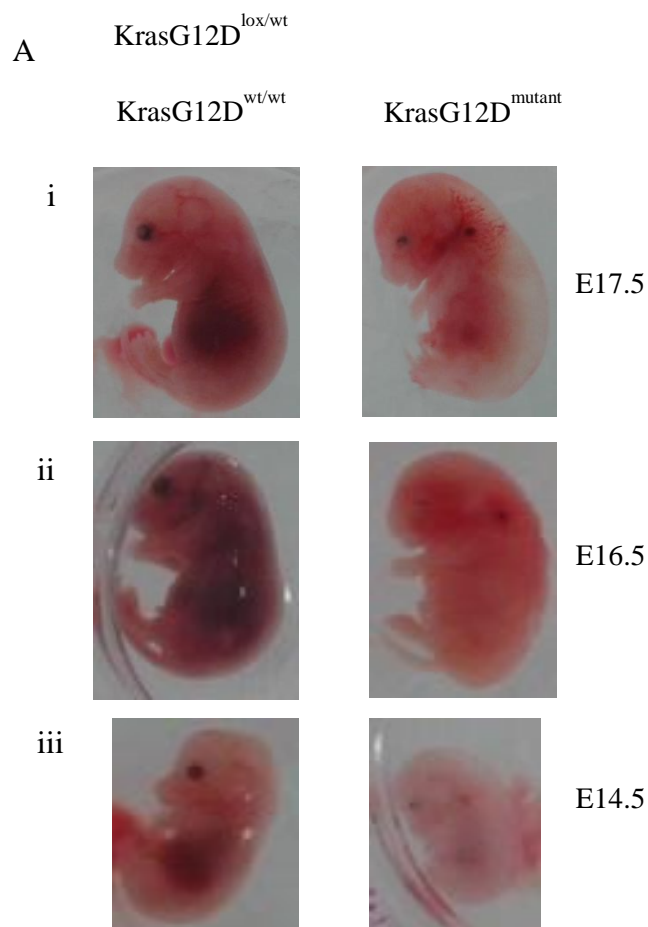


**Figure 5.8. *KrasG12D<sup>mutant</sup>* embryos have the same phenotype as *Kras/Usp9x<sup>mutant</sup>* embryos**  
 (A) Representative phenotype of *KrasG12D<sup>mutant</sup>* embryos at (i) E17.5, (ii) E16.5 and (iii) E14.5. Embryos at all stages were pale throughout entire body, especially the viscera. E16.5 and E17.5 embryos presented with cerebral swelling, which was not consistently observed in E14.5 embryos.

#### ***5.1.4 KrasG12D expression disrupts the architecture of proliferative zones in late- but not mid-stage embryos***

To refine the analysis of the effect *KrasG12D* expression on the organisation of the brain, Nissl staining was conducted on embryos at E17.5 (Figure. 5.9, and 5.10). It was immediately apparent upon cryostat sectioning that the E16.5 and E17.5 *KrasG12D*<sup>mutant</sup> brains were extremely fragile making it difficult to preserve tissue organisation. However E14.5 *KrasG12D*<sup>mutant</sup> brains responded to fixation and sectioning similarly to wildtype. Sections that could be obtained from E17.5 *KrasG12D*<sup>mutant</sup> embryos exhibited ventricular disorganisation, low cellular packing density and poor neural architecture (Figure 5.9Aiii, Biii, Ciii) and (Figure 5.10A, Ai, Aii), and E16.5 (Figure 5.11 Aiii, Biii, Ciii) and (Figure 5.12A, B, C and D). Higher magnification of the ventricular regions of *KrasG12D*<sup>mutant</sup> brains (Figure 5.13A, B, C and D) detected cellular debris in the ventricles, and the lack of a contiguous cell layer bordering the ventricle, which was not observed in controls (Figure 5.13A', B' and C'). Interestingly at E17.5 and E16.5 the ventricles were poorly defined and almost absent in *KrasG12D*<sup>mutant</sup> (Figure 5.11A, B, C and D) and (Figure 5.12A, B, C and D). The lack of a defined ventricular space, an expansion in cortical size and poorly defined cortical layers, is consistent with hyper-proliferation of NPs (Katayama et al., 2011). Hence, a marker of mitosis, phosphor-histone 3 (PH3) staining was conducted on E17.5 sections to determine the percentage of cells undergoing mitosis in the mutants. However, due to the lack of tissue integrity in *KrasG12D*<sup>mutant</sup> the PH3 staining was inconclusive (Figure 5.14Bii). In controls PH3 staining was restricted to the ventricular zone as expected.

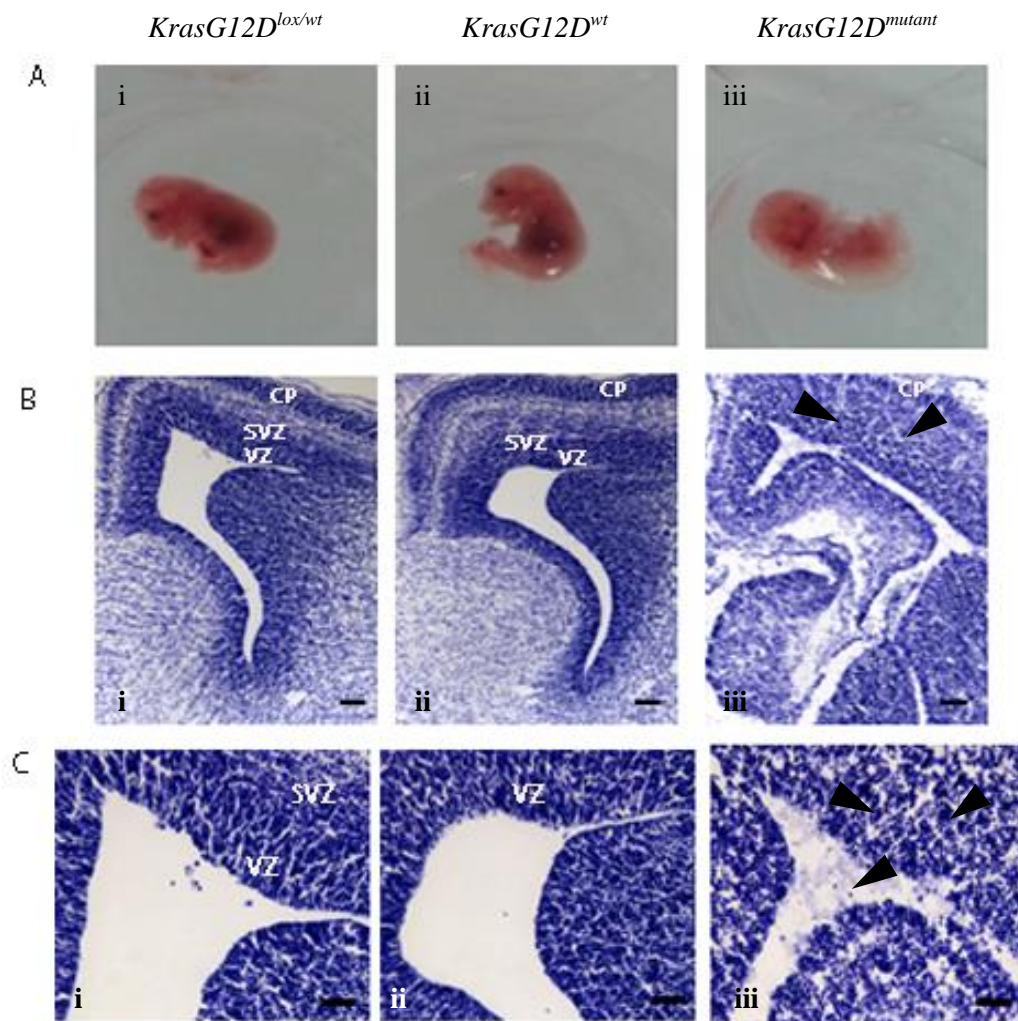


**Figure 5.9. *KrasG12D<sup>mutant</sup>* have disrupted neural architecture at E17.5.** (A) Gross morphology of E17.5 embryos. *KrasG12D<sup>mutant</sup>* (Aiii) is paler than control littermates and has cerebral swelling. (B) Nissl staining of *KrasG12D<sup>mutant</sup>* (Biii) embryos revealed abnormal architecture with disorganised ventricular region and poor distinction between VZ and SVZ, compared to controls (Bi and Bii). (C) *KrasG12D<sup>mutant</sup>* (Ciii) presence of cell “debris” in ventricular space (arrow-head). Scale Bar represents 50μm. A total of 1 E17.5 *KrasG12D<sup>mutant</sup>* embryo and 3 controls were stained with Nissl. CP – cortical; SVZ – subventricular zone; VZ – ventricular zone.

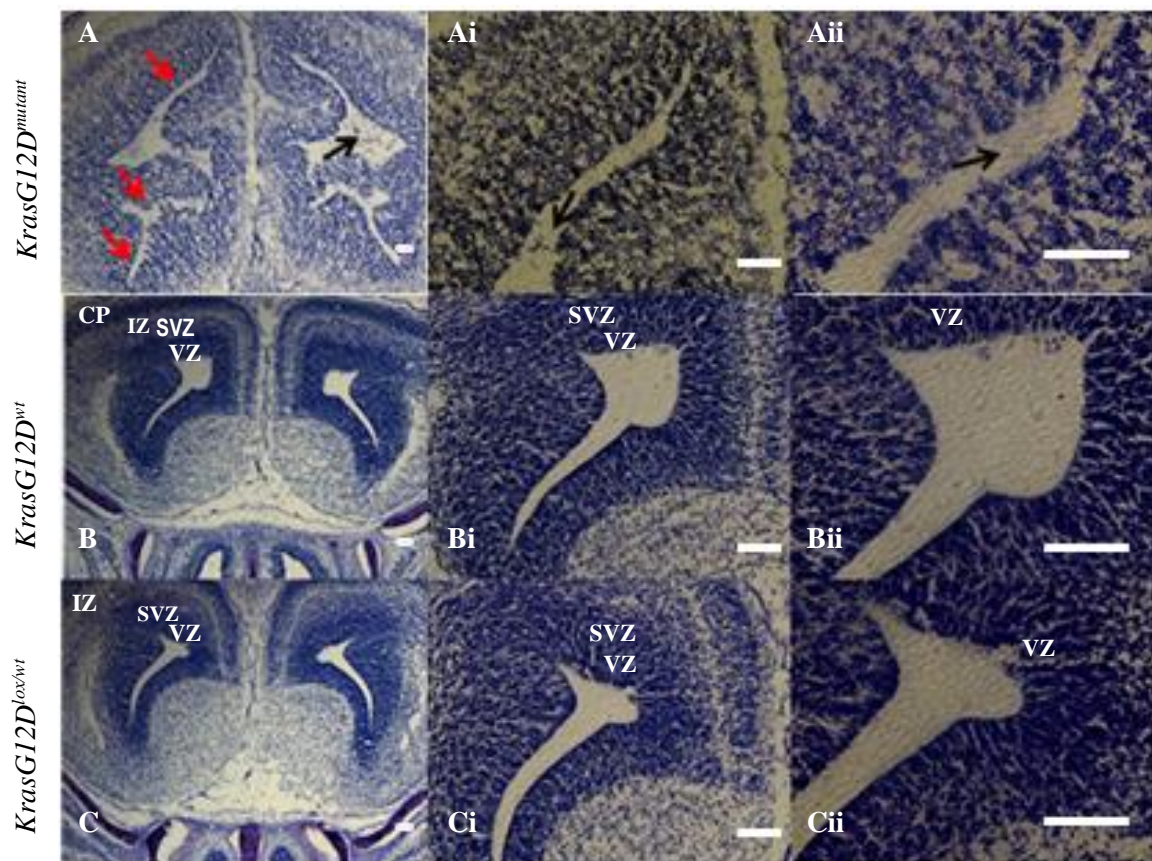


**Figure 5.10. Disrupted neural architecture of E17.5 *KrasG12D<sup>mutant</sup>* cortex.** *KrasG12D<sup>mutant</sup>* forebrain (A, Ai, Aii) has poor ventricle architecture, loosely packed cells and poor cortical layer definition. Multiple branched ventricle structures develop (arrowed red). *KrasG12D<sup>mutant</sup>* ventricles contain debris at “ventricular zone” (Ai and Aii) (arrowed black). *KrasG12D<sup>lox/wt</sup>* and *KrasG12D<sup>wt</sup>* controls have well defined ventricular structure. Scale bar represents 50 $\mu$ m. A total of 1 E17.5 *KrasG12D* mutant and 3 controls were stained. CP- cortical plate; SVZ – subventricular zone; VZ – ventricular zone; IZ – intermediate zone.

### 5.1.5 *KrasG12D* expression alters proportion of neural progenitors and neurons

Nissl staining revealed that the ventricular regions of *KrasG12D*<sup>mutant</sup> at E17.5 and E16.5 lacked a clear demarcation between the VZ, SVZ and IZ evident in *KrasG12D*<sup>lox</sup> and *KrasG12D*<sup>wt</sup> controls. This raised the possibility that *KrasG12D* mutant brains were comprised mainly of a homogeneous cell population. As *Emx-1-Cre* activates *KrasG12D* expression in the NPs, the mutation may promote progenitor expansion at the expense of differentiation. However, at E14.5 *KrasG12D*<sup>mutant</sup> brains displayed a normal overall architecture, at least as can be determined by Nissl staining, although the ventricular space was larger compared to controls (Figure 5.15Ai, Bi and Ci). These observations indicate that sometime between E14.5 and E16.5, neural progenitor proliferation is perturbed resulting in an expansion of either neural progenitors or another neural cell population causing the dramatic phenotype at E16.5 and E17.5. As immunohistochemistry was ineffective in determining cell types in later embryonic *KrasG12D*<sup>mutant</sup> due to tissue fragility (Figure 5.14Aii and Bii) the expression of neural markers was investigated by western blotting.

Protein lysate from E16.5 *KrasG12D*<sup>mutant</sup> cortex was analysed for the expression of apical neural progenitors (PAX6 and SOX2), radial progenitors (BLBP), intermediate neural progenitors (TBR2) (Figure 5.16), post-mitotic neurons (TBR1), proliferating progenitors (PH3) as well as an antibody specific to the *KrasG12D* mutant protein (Figure 5.17), to determine the cell types present. An increase in the expression of SOX2 and TBR2 was detected in *KrasG12D*<sup>mutant</sup> samples (Figure 5.16) but there was no change in markers of radial progenitors, PAX6 (Figure 5.16) and BLBP (Figure 5.16 and 5.17), although BLBP was stronger at a higher molecular weight in mutants (Figure 5.16). These data suggested an expansion of intermediate progenitors. There was a reduction in TBR1 expression (Figure 5.17) indicating the number of post-mitotic neurons was reduced in mutants as well as a slight reduction in mitotic PH3 expression, although staining was quite weak and largely inconclusive (Figure 5.17). An attempt was made to confirm the expression of the mutant *KrasG12D* protein using a G12D specific antibody, however some of the mutants, by PCR and phenotype, did not express it while some of the controls did (Figure 5.17). Thus it was

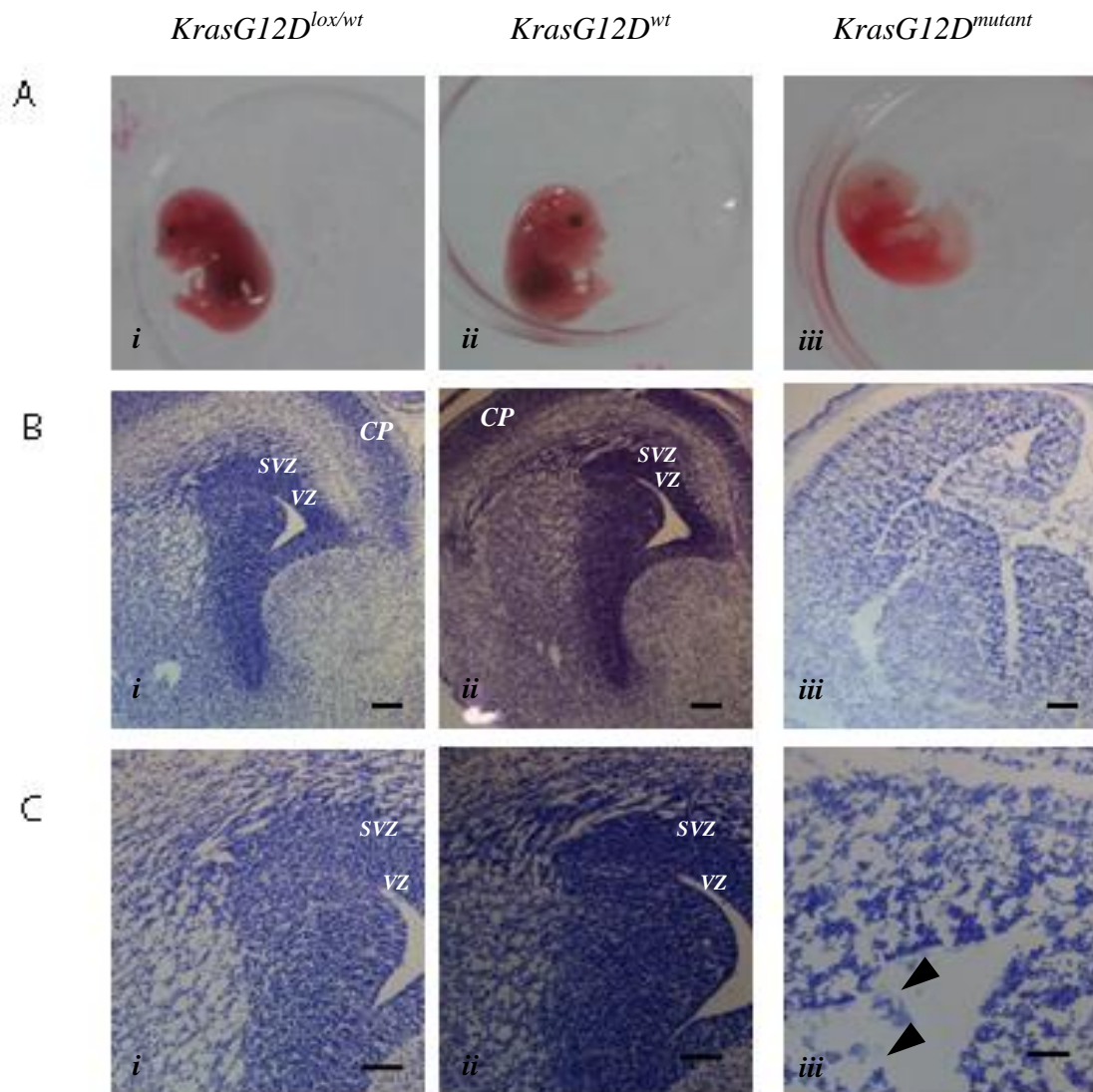


**Figure 5.11. *KrasG12D<sup>mutant</sup>* has disrupted neural architecture at E16.5.** E16.5 brains were sectioned and stained with Nissl to observe morphology of *KrasG12D<sup>mutant</sup>* brain. (A) As for stage E17.5, E16.5 *KrasG12D<sup>mutant</sup>* (Aiii) embryos were noticeably paler, had obvious cerebral swelling and tissue fragility and cerebral swelling. *KrasG12D<sup>lox/wt</sup>* (Ai) and *KrasG12D<sup>wt</sup>* (Aii) controls. (B) Representative Nissl staining of the disorganised neural tissue with poorly defined ventricular and subventricular zones in *KrasG12D<sup>mutant</sup>* (Biii) compared to *KrasG12D<sup>lox/wt</sup>* (Bi) and *KrasG12D<sup>wt</sup>* (Bii) controls. (C) Higher magnification of sections in (B) indicating cellular debris in ventricular space of *KrasG12D<sup>mutant</sup>*. Scale Bar represents 50µm. A total of 4 *KrasG12D<sup>mutant</sup>* and 2 *KrasG12D<sup>lox/wt</sup>* and 1 *KrasG12D<sup>wt</sup>* were stained with Nissl. CP- cortical plate; IZ- intermediate zone; SVZ – subventricular zone; VZ- ventricular zone.

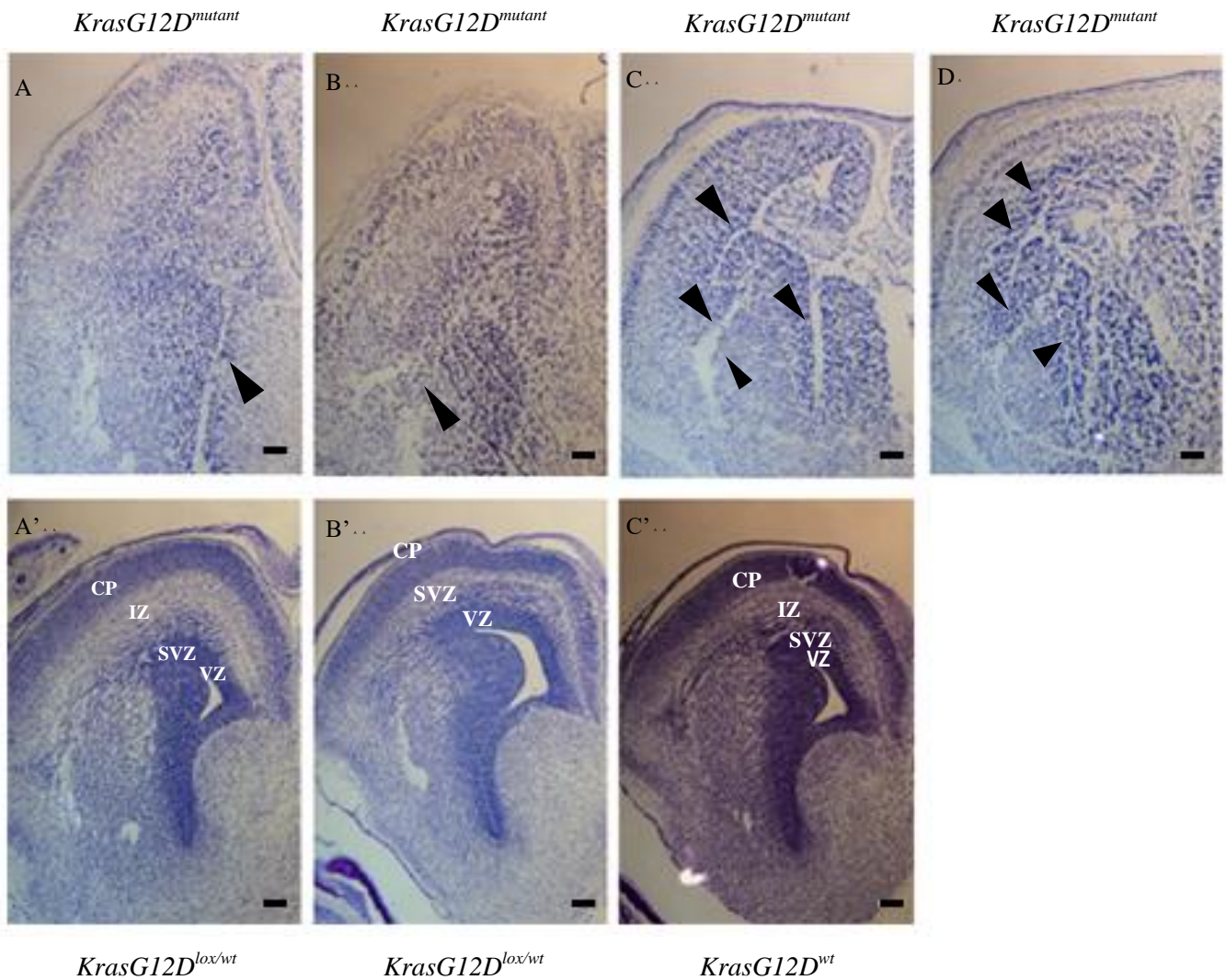


**Figure 5.12. Neural architecture is perturbed in E16.5 *KrasG12D<sup>mutant</sup>*.** Nissl staining of the right ventricular region of four E16.5 *KrasG12D<sup>mutant</sup>* (A, B, C, and D) displaying disorganised and undefined ventricular architecture in comparison with controls *KrasG12D<sup>lox/wt</sup>* (A' and B') and *KrasG12D<sup>wt</sup>* (C'). Multiple ventricle branching is prominent in two (C and D) of four *KrasG12D<sup>mutant</sup>*. E16.5 *KrasG12D<sup>lox/wt</sup>* and *KrasG12D<sup>wt</sup>* controls (A', B' and C') have well defined ventricular architecture and structure. A total of 4 *KrasG12D<sup>mutant</sup>*, 2 *KrasG12D<sup>lox/wt</sup>* and 1 *KrasG12D<sup>wt</sup>* were examined. Scale bar represents 50µm. CP- cortical plate; IZ-intermediate zone; SVZ – subventricular zone; VZ- ventricular zone.

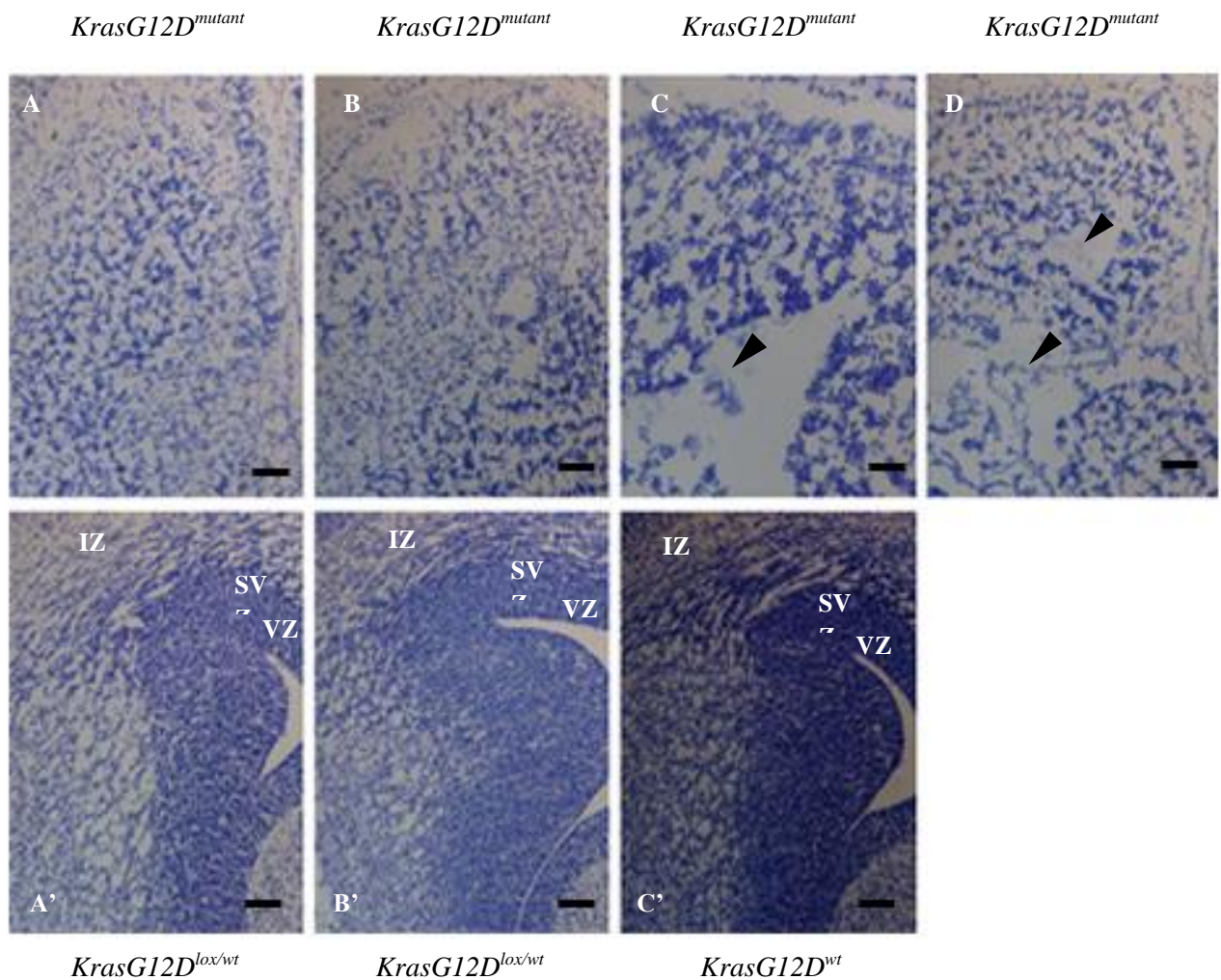


**Figure 5.13. E16.5 *KrasG12D<sup>mutant</sup>* have cell debris in the ventricular space.** Nissl Staining of four *KrasG12D<sup>mutant</sup>* (A, B, C, D) and *KrasG12D<sup>lox/wt</sup>* and *KrasG12D<sup>wt</sup>* controls (A', B' and C'). Higher magnification of *KrasG12D* mutants and controls from **Figure 5.10**. Arrow heads indicate cellular debris leaking into ventricular space of the *KrasG12D<sup>mutant</sup>*. A total of 4 *KrasG12D<sup>mutant</sup>*, 2 *KrasG12D<sup>lox/wt</sup>* and 1 *KrasG12D<sup>wt</sup>* were analysed. Scale bar represents 50µm. SVZ – subventricular zone; VZ – ventricular zone; IZ – intermediate zone.

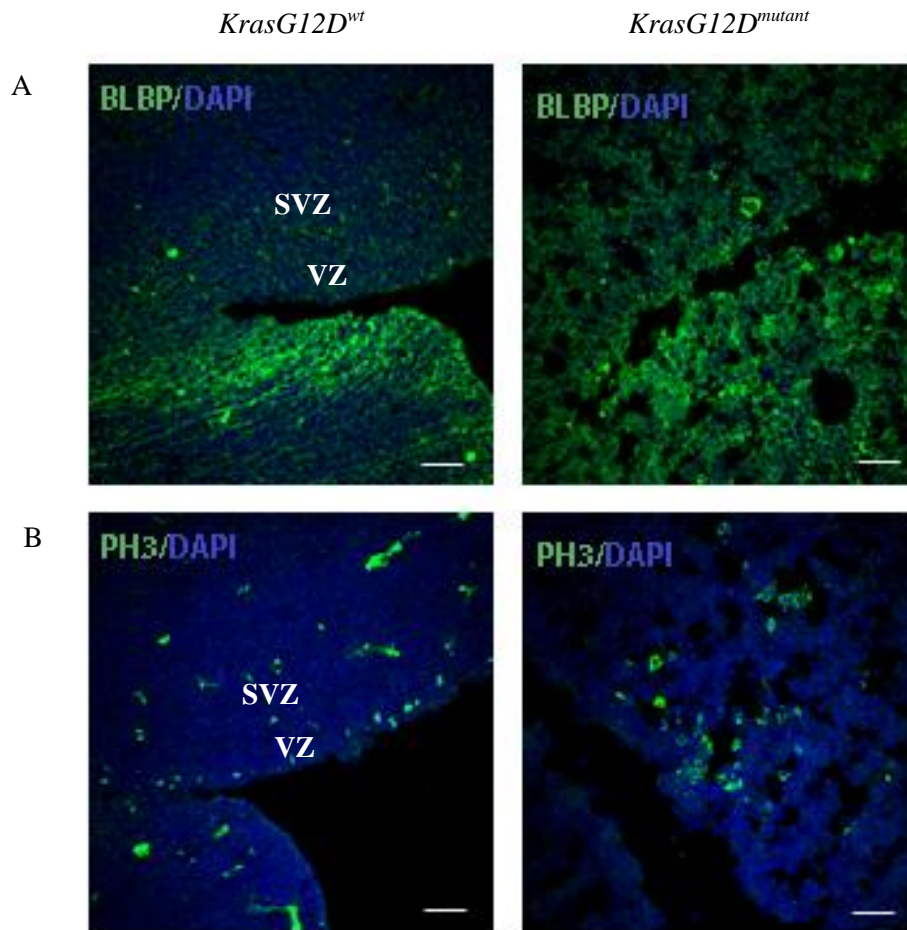


**Figure 5.14.** *KrasG12D<sup>mutant</sup> tissue fragility results in nonspecific and ubiquitous staining at E17.5.* E17.5 brain sections were stained with BLBP, a marker of radial glia progenitors as well as the mitotic marker, PH3. (A) Defined BLBP staining in E17.5 cortex of *KRasG12D<sup>wt/wt</sup>* control radial glia progenitors (Ai), which is undefined, ubiquitous, nonspecific and mis-localised in *KrasG12D<sup>mutant</sup>* (Aii). PH3 positive neural progenitor cells line ventricular zone in *KrasG12D<sup>wt/wt</sup>* controls (Bi). In *KrasG12D<sup>mutant</sup>* PH3 staining is displaced from ventricular neural progenitors (Bii). Scale bars represent 50 μm. A total of 1 E17.5 *KrasG12D<sup>mutant</sup>* embryos and 1 control were stained for BLBP and PH3. SVZ – subventricular zone; VZ – ventricular zone

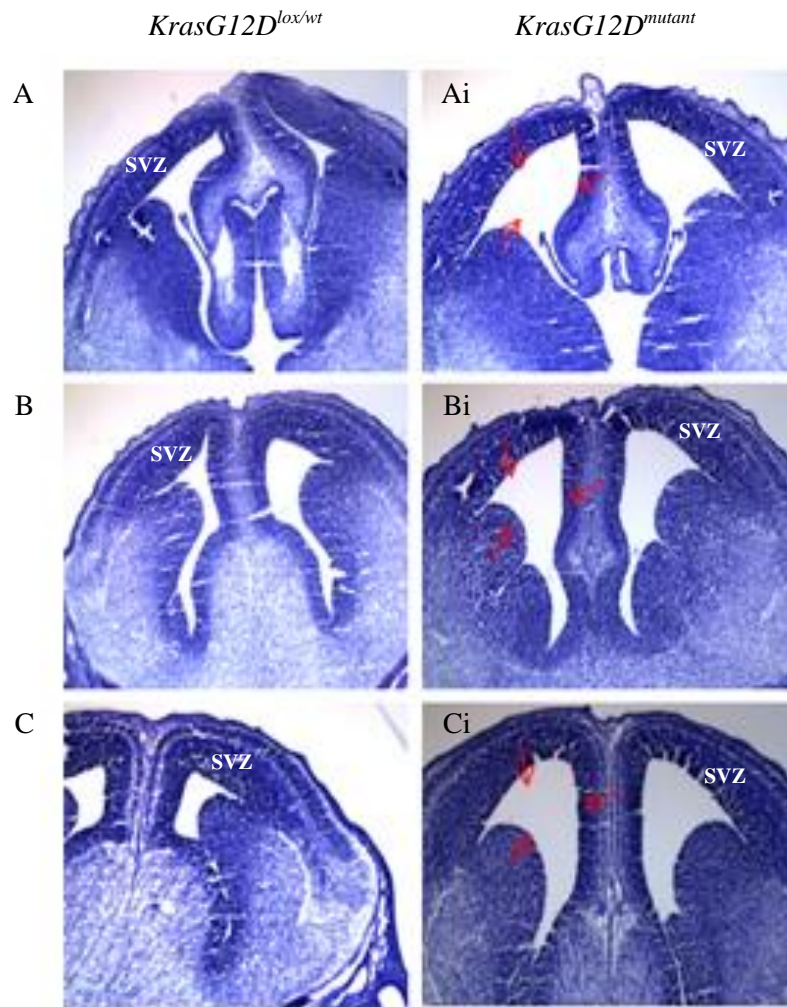


**Figure 5.15. E14.5  $KrasG12D^{mutant}$  have increased ventricular space.** Nissl staining of E14.5  $KrasG12D^{mutant}$  (A', B' and C') show an increase in ventricular space (red arrows), compared to  $KrasG12D^{lox/wt}$  (A and B) and  $KrasG12D^{wt}$  (C) controls but the cellular architecture of  $KrasG12D^{mutant}$  is normal. Total of 3  $KrasG12D^{mutant}$  and 2  $KrasG12D^{lox/wt}$  and 1  $KrasG12D^{wt}$  were used. SVZ – subventricular zone.

concluded that the antibody was not specific. Coomassie staining of membranes was included to confirm that similar levels of protein were present (Figure 5.16) as the commonly used loading controls, beta-tubulin and GAPDH could not be detected (data not shown). Similarly (Figure 5.17) beta-tubulin and GAPDH protein levels were much reduced or almost absent in the *KrasG12D* samples. However the detection of equal amount of BLBP in these samples suggests this was not due to overall protein degradation or failure to load protein as BLBP staining was detected across all samples (Figure 5.16 and 5.17). Overall, these data suggests that in E16.5 *KrasG12D<sup>mutant</sup>* there is an expansion of intermediate progenitors at the expense of post mitotic neurons, with the caveat that normal loading controls were not informative. In addition, the embryonic stage this expansion of intermediate progenitors begins in the mutant cortex remained unclear. Therefore the expression of neural markers at a stage in which cortical architecture is still normal, that is E14.5, was investigated.

At E14.5 there was no consistent change in BLBP expression in *KrasG12D<sup>mutant</sup>*, (Figure 5.18), nor was there any consistent increase in SOX2 or TBR2, although staining may be inconclusive. No reduction in TBR1 expression was observed at this stage (Figure 5.18). This indicated that the intermediate progenitor population, as determined by TBR2 and SOX2 in E16.5s, was not the predominant cell population in *KrasG12D<sup>mutant</sup>* E14.5 cortex. To further investigate the cell populations present at E14.5 immunofluorescence was conducted to investigate expression of neural markers in localised regions of the mutant cortex. The expression of the post mitotic neuronal marker, TBR1, intermediate neural progenitor marker, TBR2, and mitotic marker, PH3, were assessed. The expression of TBR1 in *KrasG12D<sup>mutant</sup>* (Figure 5.19A,B) was significantly reduced in comparison to *KrasG12D<sup>lox/wt</sup>* and *KrasG12D<sup>wt</sup>* controls indicating that there were fewer post-mitotic neurons at this stage in the mutants. Immunofluorescence revealed no difference in TBR2 expression in *KrasG12D<sup>mutant</sup>* (Figure 5.20A and Ai). Co-staining for TBR2 and PH3 was also conducted to determine if the number of “proliferating” intermediate progenitors (TBR2+/PH3+) was altered at E14.5 in mutants, preceding the increased intermediate progenitor population expansion detected at E16.5. However, the average number of TBR2+ /PH3+ double positive cells in *KrasG12D<sup>mutants</sup>* was unchanged (Figure 5.21A and Ai). This indicated that at E14.5, the *KrasG12D<sup>mutant</sup>* intermediate progenitors were proliferating at a similar rate to controls. To determine if the apical neural progenitors of the mutants were also proliferating at a similar rate, PH3 staining was investigated at the ventricular region of the E14.5 cortex.

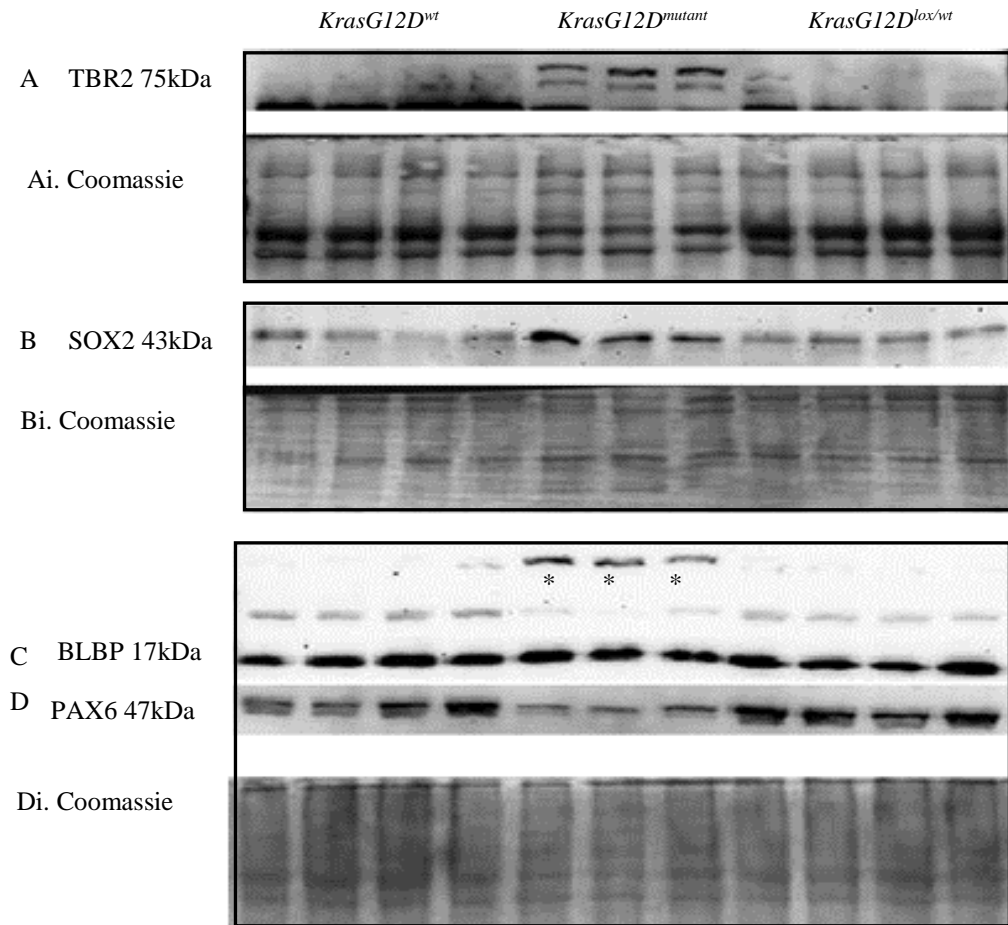


**Figure 5.16. Increased TBR2 and SOX2 expression in E16.5 *KrasG12D<sup>mutant</sup>* cortex.** Western blotting was conducted on E16.5 brain lysate for the expression of neural progenitor markers SOX2 and PAX6, radial glia progenitor marker, BLBP and intermediate neural progenitor marker, TBR2. The expression of TBR2 and SOX2 is increased in E16.5 *KrasG12D<sup>mutant</sup>* cortical lysates (A and B). BLBP expression at expected size is unchanged, but runs at a higher molecular weight in *KrasG12D<sup>mutant</sup>*. Reduced PAX6 expression was observed in mutant samples (D lower band). Coomassie Stains were used to show equal protein loading as housekeeping loading controls were degraded in *KrasG12D<sup>mutant</sup>* lysates. *KrasG12D<sup>mutant</sup>* (*Kras*+, *Cre*+), *KrasG12D<sup>lox/wt</sup>* (*Kras*+, *Cre*-), *KrasG12D<sup>wt</sup>* (*Kras*-, *Cre*-). A total of 3 *KrasG12D<sup>mutant</sup>*, 4 *KrasG12D<sup>lox/wt</sup>* and 4 *KrasG12D<sup>wt</sup>* were used for analysis.

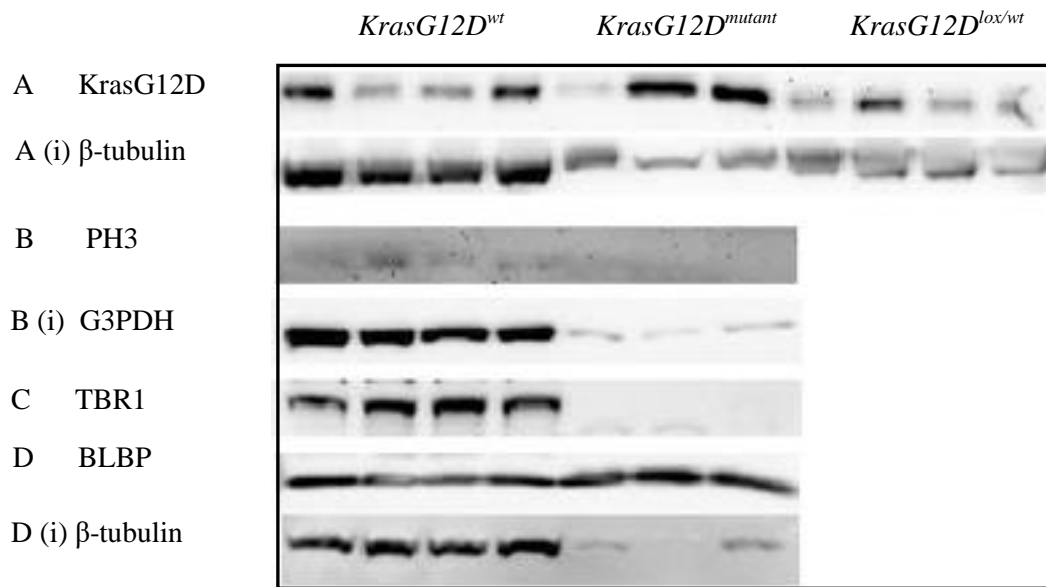


**Figure 5.17. Beta-tubulin and GAPDH proteins are degraded in E16.5 *KrasG12D<sup>mutant</sup>*.** Immunoblot of E16.5 cortical brain lysates probed for (A) *KrasG12D*, (B) *PH3*, (C) *TBR1* and (D) *BLBP*. (A) *KrasG12D* antibody is not specific for *KrasG12D<sup>mutant</sup>* protein, as it also binds to *KrasG12D<sup>lox/wt</sup>* and *KrasG12D<sup>wt</sup>* protein at high levels indicating it is a pan Ras antibody. (B) *PH3* expression faint in all samples, but lower in *KrasG12D<sup>mutant</sup>* compared to *KrasG12D<sup>wt</sup>* controls (C) *TBR1* expression is low in *KrasG12D<sup>mutant</sup>* compared to *KrasG12D<sup>wt</sup>* controls (D) *BLBP* expression was strong in both *KrasG12D<sup>wt</sup>* and *KrasG12D<sup>mutant</sup>* despite degraded beta-tubulin loading control (di). There is degradation of beta-tubulin (di) and GAPDH (bi) loading controls in *KrasG12D<sup>mutant</sup>* samples. A total of 3 *KrasG12D<sup>mutant</sup>*, 4 *KrasG12D<sup>wt</sup>* and 4 *KrasG12D<sup>lox/wt</sup>* were used in analysis.

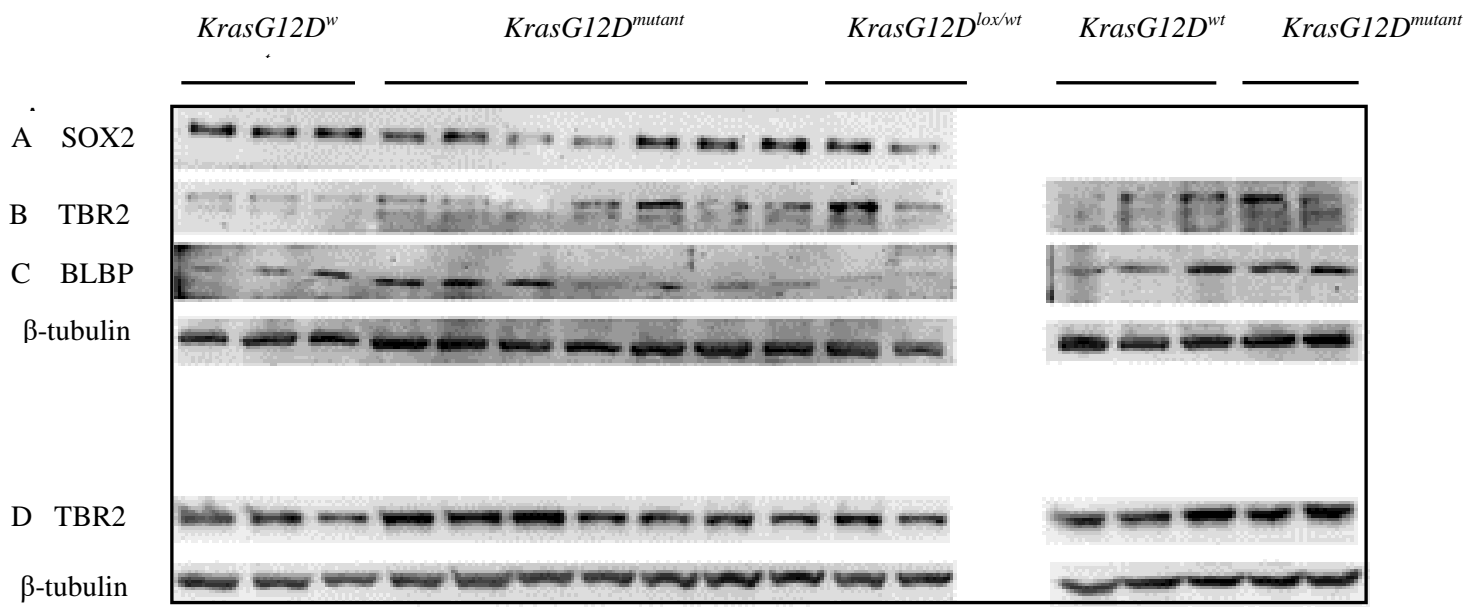


**Figure 5.18. Expression of neural markers in E14.5 *KrasG12D<sup>mutant</sup>*.** Western blotting was conducted on E14.5 brain lysate for the expression of neural progenitor marker SOX2, radial glia progenitor marker, BLBP, intermediate neural progenitor marker, TBR2, and post mitotic neuron marker, TBR1. The expression of neural markers SOX2 (A), TBR2 (B), BLBP (C) and TBR1 (D) was inconsistent for *KrasG12D<sup>mutant</sup>* and controls across the two litters. A total of 9 *KrasG12D<sup>mutant</sup>*, 4 *KrasG12D<sup>lox/wt</sup>* and 6 *KrasG12D<sup>wt</sup>* were used in this experiment.

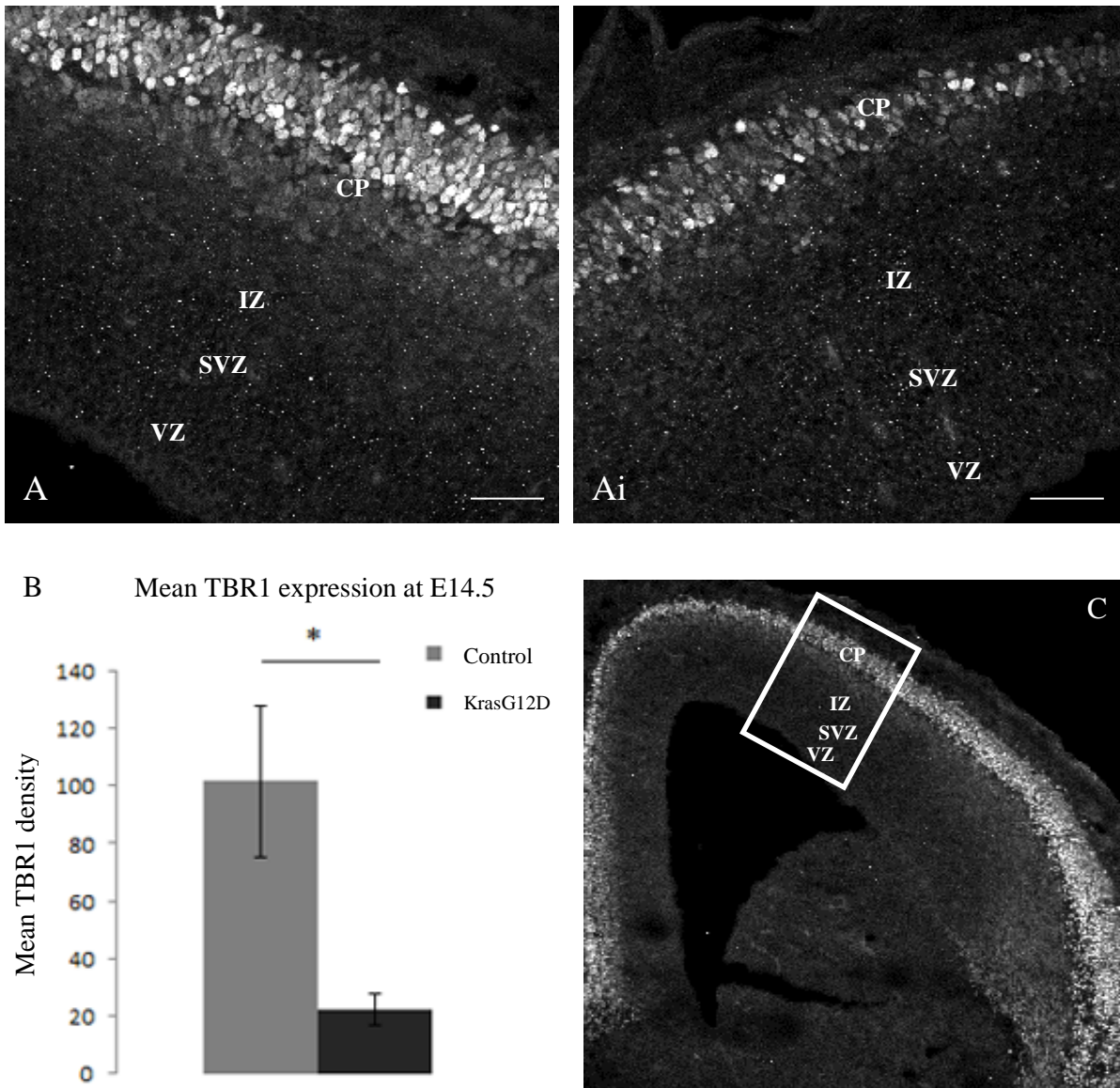


**Figure 5.19. Reduction in post-mitotic neurons at E14.5 in *KrasG12D*<sup>mutant</sup>** Immunofluorescence was conducted on E14.5 *KrasG12D*<sup>mutant</sup> (Ai) *KrasG12D*<sup>lox/wt</sup> or *KrasG12D*<sup>wt</sup> controls (A) for the expression of the post mitotic neuron marker, TBR1. (B) Graphical representation of the mean reduction in TBR1 expression in *KrasG12D*<sup>mutant</sup> compared to *KrasG12D* or *KrasG12D*<sup>wt</sup>. (C) Low magnification representative area of the higher magnifications in (A and Ai). Scale Bar represents 50µm. Each section was cut to 10µm thickness. A total of 3 *KrasG12D*<sup>mutant</sup> compared to 2 *KrasG12D*<sup>lox/wt</sup> or 3 *KrasG12D*<sup>wt</sup> controls were used in analysis. CP – cortical plate; IZ – intermediate zone; SVZ – subventricular zone; VZ – ventricular zone

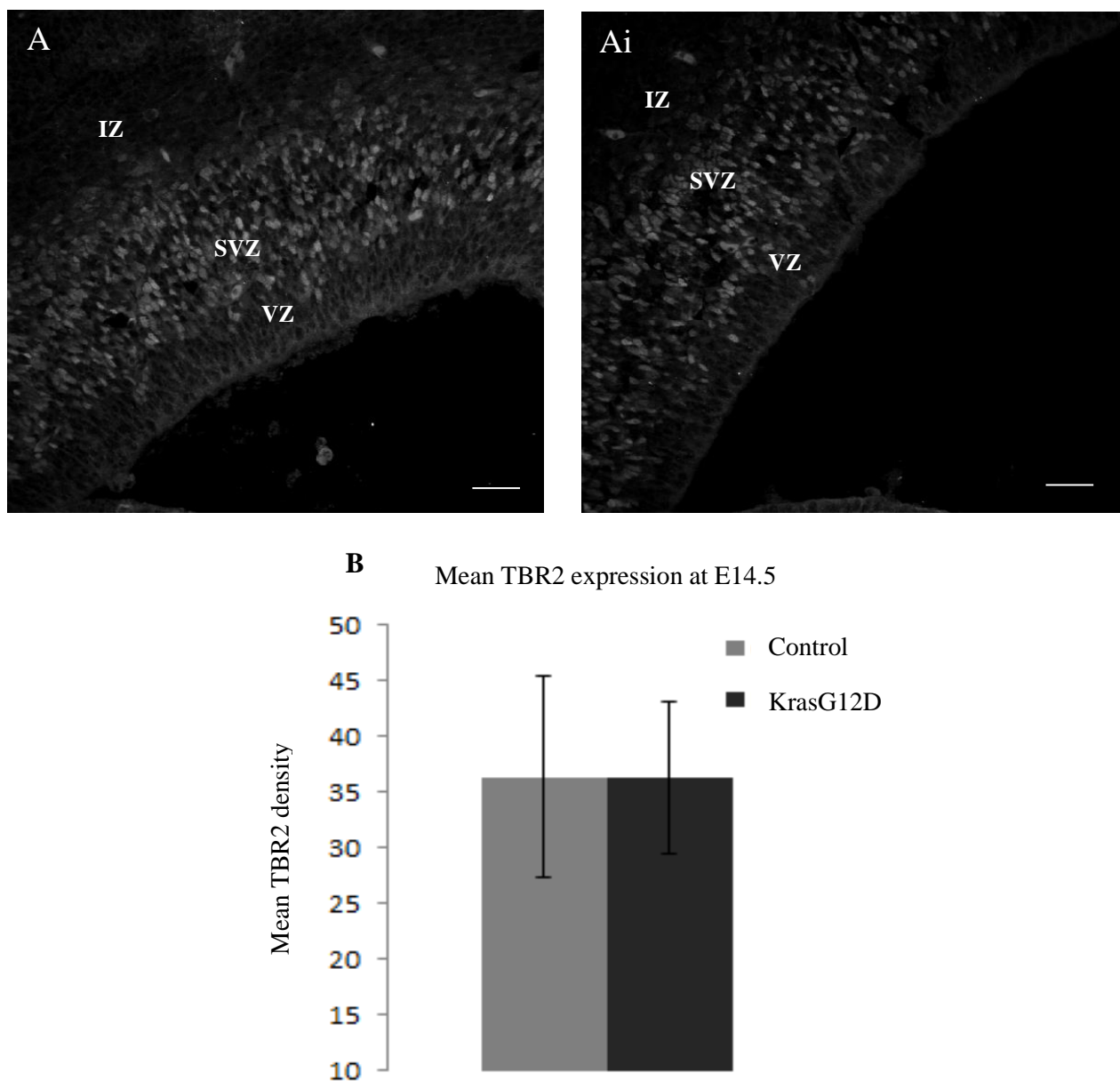


**Figure 5.20.** The number of intermediate progenitors at E14.5 in *KrasG12D<sup>mutant</sup>* is **unchanged**. Immunofluorescence was conducted on E14.5 *KrasG12D<sup>mutant</sup>* (Ai) and *KrasG12D<sup>lox/wt</sup>* of *KrasG12D<sup>wt</sup>* controls (A) for the expression of TBR2. TBR2 staining at the sub ventricular region of E14.5 control (A) and *KrasG12D<sup>mutant</sup>* (Ai) intermediate progenitors is unchanged. (B) Graphical representation of mean TBR2 expression as determine by the density of staining within the SVZ in the E14.5 cortex. Scale bar represent 50μm. A total of 3 *KrasG12D<sup>mutant</sup>*, 1 *KrasG12D<sup>lox/wt</sup>* and 2 *KrasG12D<sup>wt</sup>* were used in analysis. CP – cortical plate; IZ – intermediate zone; SVZ – subventricular zone; VZ – ventricular zone.

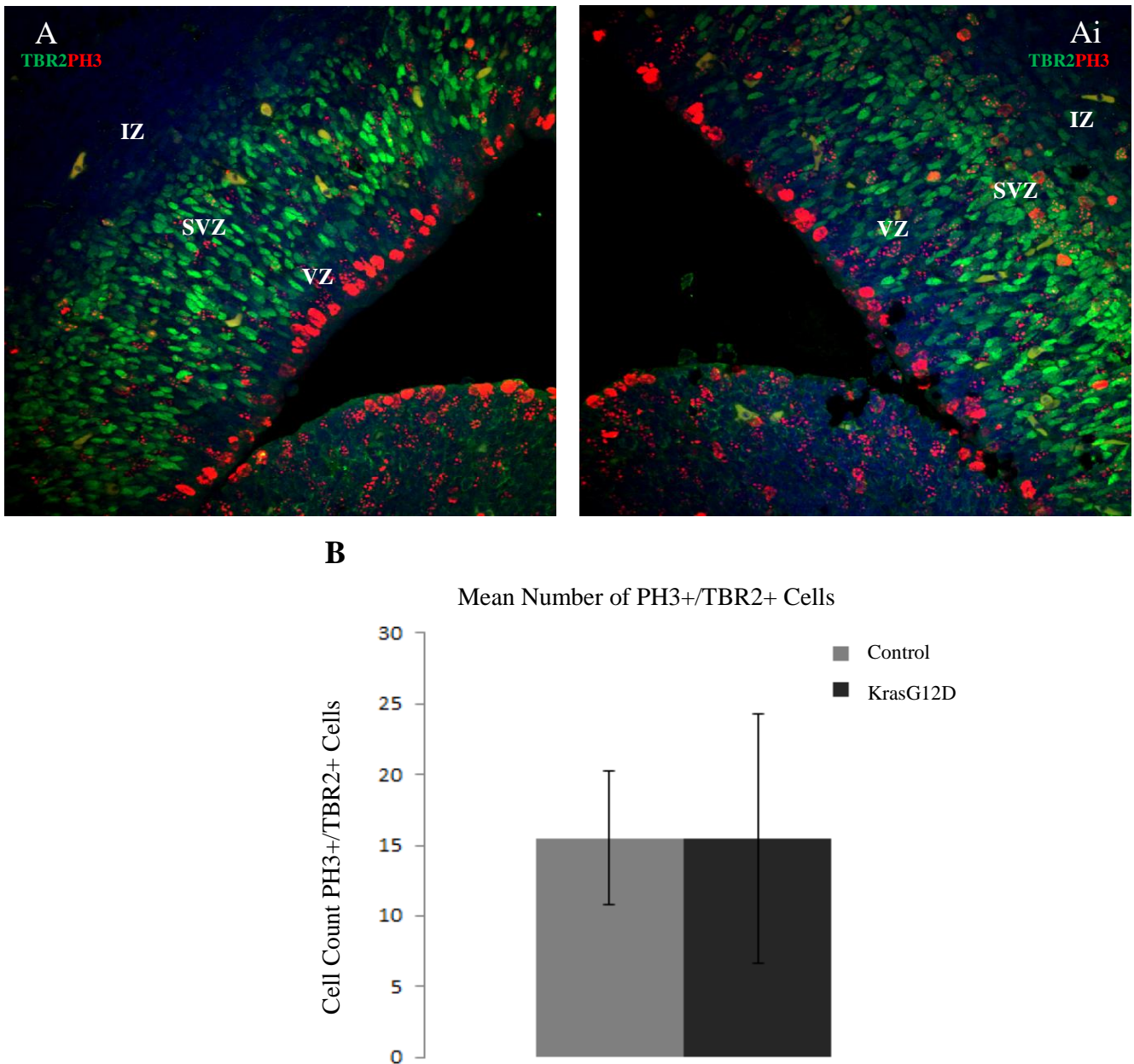


**Figure 5.21.** The number of mitotic intermediate progenitors in *E14.5 KrasG12D<sup>mutant</sup>* is **unchanged**. Immunofluorescent co-staining was conducted on *E14.5 KrasG12D<sup>lox/wt</sup>* (A) and *KrasG12D<sup>mutant</sup>* (Ai) with intermediate progenitor marker, TBR2, and mitotic marker, PH3 to determine the number of proliferating intermediate progenitors. There was no significant difference in the number of TBR2/PH3 co-expressing cells in *KrasG12D<sup>mutant</sup>* (Ai) compared to controls (A). (B) Graphical representation of the mean number of PH3+/TBR2+ cells within the VZ and SVZ region. There was no significant increase observed in *KrasG12D<sup>mutant</sup>* compared to controls. The number of PH3+/TBR2+ cells was counted by the resulting overlaid yellow (Red PH3+/ Green TBR2+). Scale bar represents 50µm.. A total of 3 *KrasG12D<sup>mutant</sup>*, 1 *KrasG12D<sup>lox/wt</sup>* and 2 *KrasG12D<sup>wt</sup>* were used in analysis. CP – cortical plate; IZ – intermediate zone; SVZ – subventricular zone; VZ – ventricular zone.

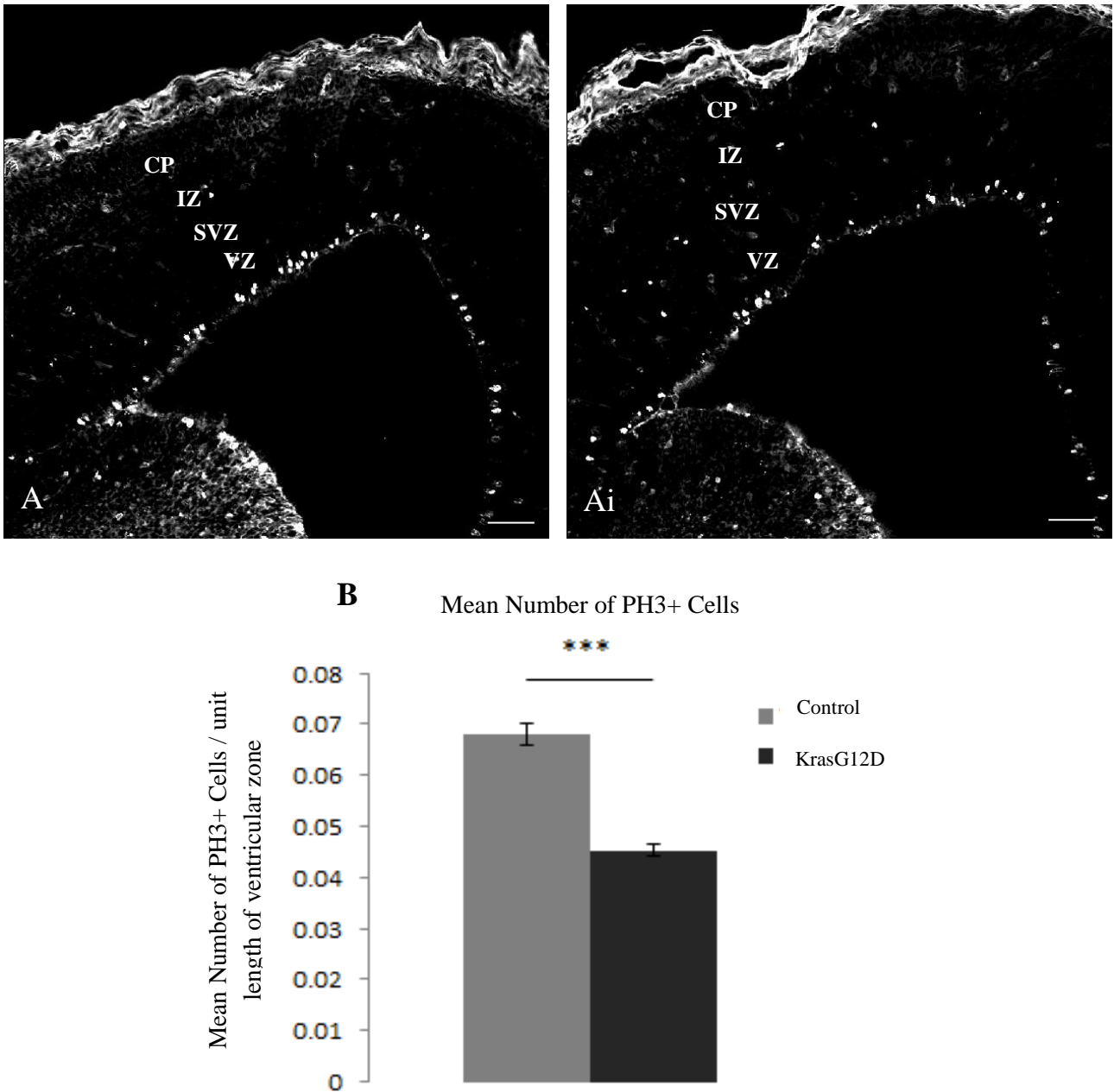


**Figure 5.22. Reduction in mitotic neural progenitors in E14.5 *KrasG12D*<sup>mutant</sup>.** Immunofluorescence was conducted on E14.5 *KrasG12D*<sup>mutant</sup> (Ai) and *KrasG12D*<sup>lox/wt</sup> of *KrasG12D*<sup>wt</sup> controls (A) for the expression of PH3. There was a significant reduction in the number of PH3+ mitotic neural progenitors at the ventricular zone lining the ventricles in E14.5 *KrasG12D*<sup>mutant</sup> (Ai). (B) Graphical representation of the number of PH3+ cells/unit length of the ventricular zone (cell#/μm) in *KrasG12D*<sup>mutants</sup>. High intensity PH3+ cells were counted along the length of the region lining the ventricular zone. Scale bars represent 50μm. A total of 4 *KrasG12D*<sup>mutant</sup>, 2 *KrasG12D*<sup>lox/wt</sup> and 3 *KrasG12D*<sup>wt</sup> were used in analysis. CP – cortical plate; IZ – intermediate zone; SVZ – subventricular zone; VZ – ventricular zone.

Interestingly, there was a reduction in the number of PH3 positive cells in *KrasG12D<sup>mutant</sup>* (Figure 5.22A and Ai).

The proliferative capacity of the progenitor cells within the *KrasG12D<sup>mutant</sup>* cortex at both E14.5 and E16.5 was further investigated using neurosphere assays (Azari, H et al 2011). In these assays the volume, the number of spheres, the number of cells/sphere, as well as the expression of neural cell markers were determined. Interestingly, 6hrs after dissecting E16.5 mutant cortex to propagated neurospheres, all *KrasG12D* mutant cells had died and no spheres were generated despite vigorous growth of neurospheres from *Kras<sup>wt</sup>* and *KrasG12D<sup>lox/wt</sup>* tissues (Figure 5.23). This result was consistent on three occasions, each from different litters. The ability to generate spheres from control tissue at the expected frequency indicated that the failure of spheres to grow from *KrasG12D<sup>mutant</sup>* tissue was not due to a technical problem. As spheres were not able to be propagated from this stage, the propagation of spheres from E14.5 was the next logical point of investigation.

Neurospheres were also generated from the cortices of E14.5 embryos. Unlike E16.5 neurospheres readily appeared and were passaged up to four times from all *Kras* genotypes. Sphere diameter and volume were analysed at each passage, and whole cell lysate was collected at passages zero, one, two and four for immunoblot analysis. A marked increase in sphere volume was apparent at each passage in *KrasG12D<sup>mutant</sup>* compared to controls (Figure 5.24A-D) but, by passage four there was a significant reduction in the size of the *KrasG12D<sup>mutant</sup>* spheres compared to controls, (Figure 5.24E and Figure 5.25). In addition there were fewer *KrasG12D<sup>mutant</sup>* spheres at passage 2 and 3 (Figure 5.25).

Neurospheres are composed of a heterogeneous population of cells including neural progenitors as well as their differentiated derivatives such as neuroblasts, neurons and astrocytes (Jensen and Parmar, 2006). Neural stem cells are the only cell type capable of initiating the formation of the neurospheres. Therefore, the observed increase in sphere volume may arise from alterations in cell proliferation rates as well as the balance of stem cell self-renewal versus differentiation. Therefore the next point of investigation was to determine which cell types were present, and in what proportion, in the E14.5 mutant spheres. To do this the expression of neural progenitor markers SOX2, PAX6, TBR2, and BLBP were investigated (Figure 5.26). SOX2, a marker of neural progenitors, increases with increasing passage number, peaking at passage two in controls, before decreasing at passage four. In

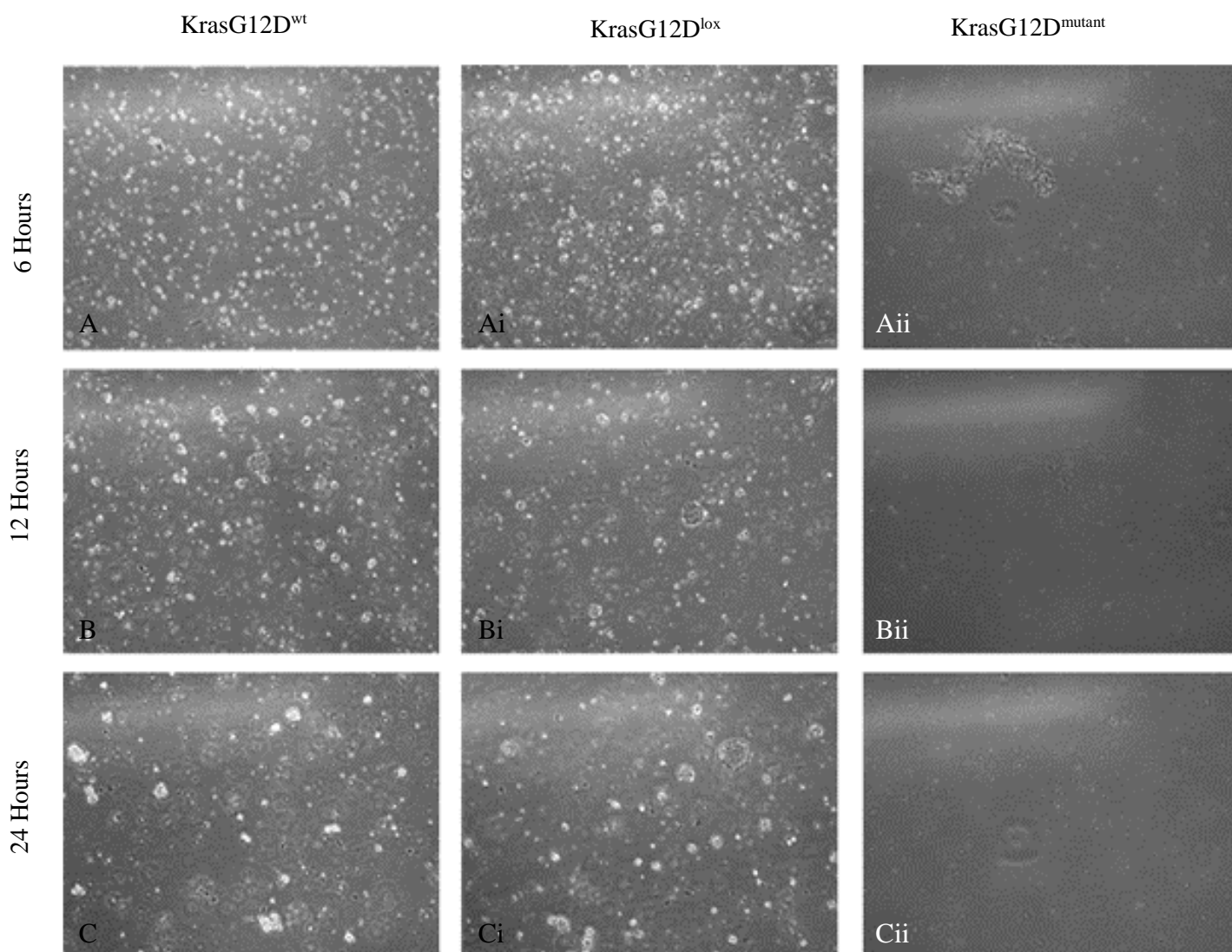


**Figure 5.23.** *No neurospheres form from E16.5 KrasG12D<sup>mutant</sup>. The cortex of E16.5 embryos was isolated and cultured for neurosphere formation. 6 hrs after dissection there was no neurosphere formation or any surviving cells for the (Aii) KrasG12D<sup>mutant</sup> compared to (A) KrasG12D<sup>wt</sup> and (Ai) KrasG12D<sup>lox/wt</sup> controls. There was also no evidence of cells or neurospheres either after (Bii) 12hours or (Cii) 24hrs. This was observed for a total 3 KrasG12D<sup>mutant</sup> 3 KrasG12D<sup>lox.wt</sup> and 4 KrasG12D<sup>wt</sup> across three separate litters*

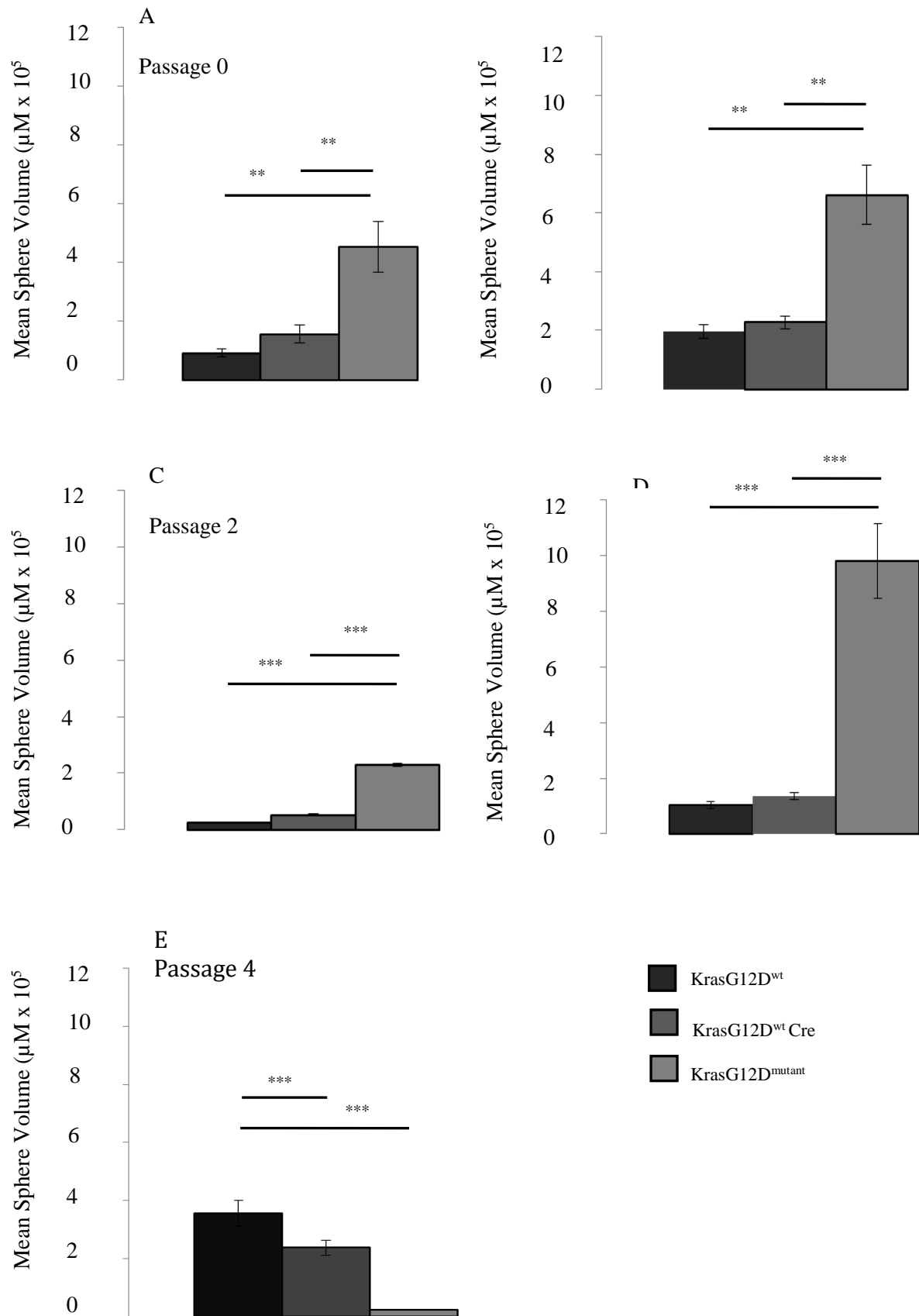


**Figure 5.24. Increased mean volume of neurospheres in E14.5 KrasG12D<sup>mutant</sup>.** Isolation of murine cortices was performed on E14.5 and neurospheres were generated. The volume of

neurospheres was calculated from the diameter of each sphere across at least 3 fields of view. Images (at least three fields of view per culture dish) of spheres were taken prior to each passage, and the diameter of each sphere was used to calculate the sphere volume in the equation:  $\text{volume} = (4/3)\pi r^3$ , where  $r = \text{diameter} / 2$ . There was a significant increase in the mean sphere volume for E14.5 propagated *KrasG12D<sup>mutant</sup>* spheres compared to controls, over three passages. (A) Mean sphere volume for passage zero (A)  $p < 0.001$ , passage one (B)  $p < 0.001$ , passage two (C)  $p < 0.0001$ , passage three (D)  $p < 0.000$  and passage four (E)  $**P < 0.001$ . Significant increase in *KRasG12D<sup>mutant</sup>* volume compared to controls,  $n = 2(\text{KrasG12D<sup>mutant</sup>})$ ,  $2(\text{KrasG12D<sup>wt</sup> Cre})$ ,  $1(\text{KrasG12D<sup>wt</sup> No Cre})$ . Controls: *KrasG12D<sup>wt</sup> No Cre* (*Cre*<sup>-</sup>/*Kras*<sup>-</sup>), *KrasG12D<sup>wt</sup> Cre* (*Cre*<sup>+</sup>/*Kras*<sup>-</sup>) Mutants: *KrasG12D<sup>mutant</sup>* (*Cre*<sup>+</sup>/*Kras*<sup>+</sup>).



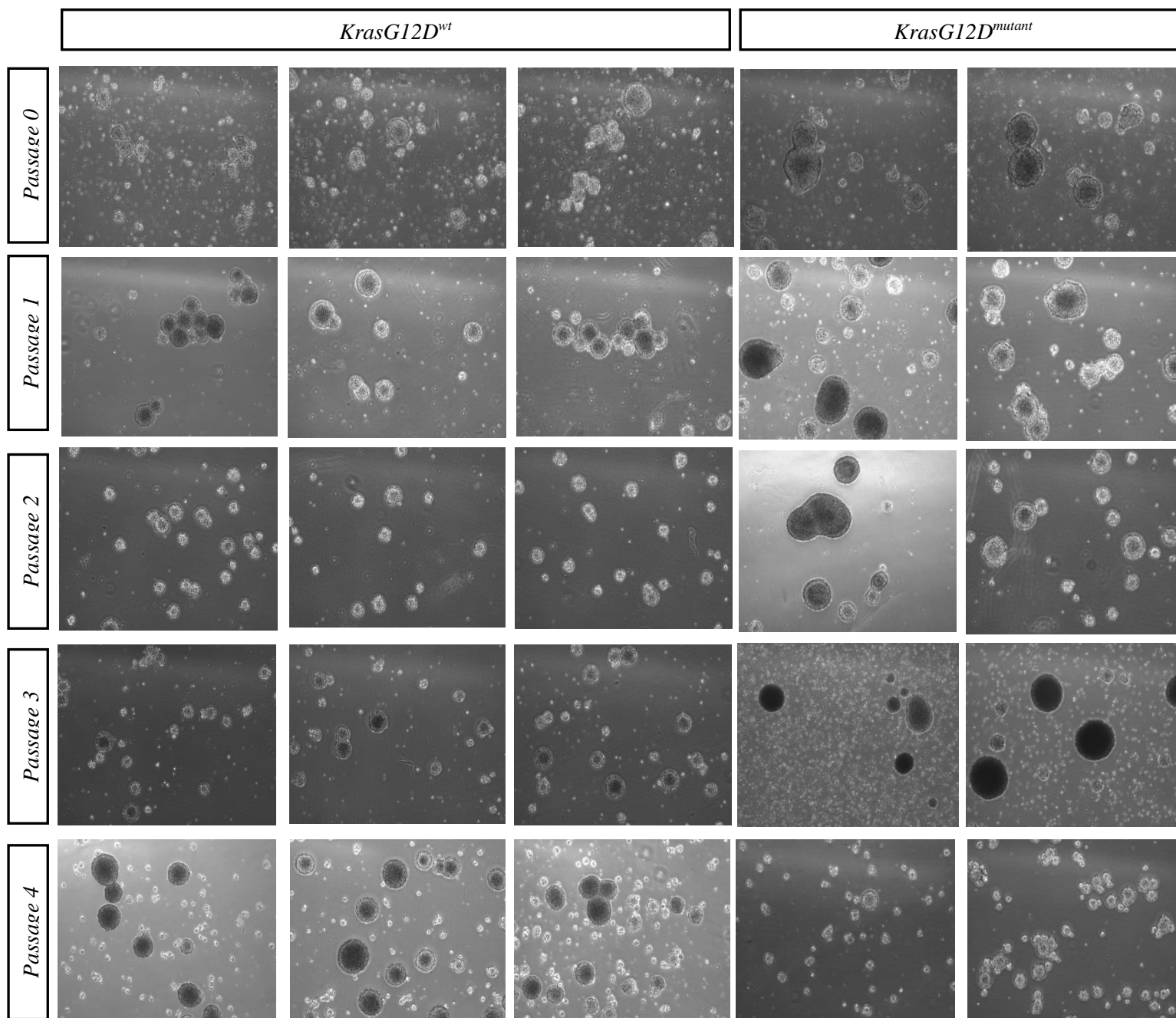


**Figure 5.25. *KrasG12D<sup>mutant</sup>* neurosphere volume is initially increased.** Significant increase in neurosphere volume of *KrasG12D* mutant neurospheres compared to controls from passage zero to passage three. Reduction in *KrasG12D* mutant neurosphere size after passage four compared to controls. Representative bright field microscopy of *KrasG12D<sup>mutant</sup>* neurospheres compared to *KrasG12D<sup>wt</sup>* control neurospheres over four passages. 2(*KrasG12D<sup>mutant</sup>*), 2(*KrasG12D<sup>wt</sup>* Cre), 1(*KrasG12D<sup>wt</sup>* No Cre)

*KrasG12D<sup>mutant</sup>* however, SOX2 expression remained high at passage four (Figure 5.26C). There was no obvious change in another marker of neural progenitors, PAX6 (Figure 5.26A). This suggests that the proportion of neural progenitors increases in later passages for *KrasG12D<sup>mutant</sup>*, whilst they decline in controls. To investigate the overall proliferation in the E14.5 mutant neurospheres at passage four, Ki67 expression was investigated and a reduction was detected in the *KrasG12D<sup>mutant</sup>* neurospheres at passage four (Figure 2.27). This suggested that the neurospheres had slowed in proliferation and may have also entered the G0 phase, which is the only part of the cell cycle not to express Ki67. Thus the response of neurospheres to growth factors may also be impaired such that the *KrasG12D<sup>mutant</sup>* spheres can't be stimulated out of G0. To investigate this possibility, the status of mTORC1 signalling was investigated after EGF and FGF stimulation (Figure 5.28). To do this, the neurospheres were spun down at passage four and resuspended and grown for 24hrs without EGF and FGF. The neurospheres were then stimulated with EGF+ and FGF+ media for 0, 10, 20 and 30mins and mTORC1 activity determined by analysing phospho-S6 (S235/236) expression (Figure 5.28). Twenty and 30mins after EGF and FGF stimulation a decline in p-S6 expression was observed in *KrasG12D<sup>mutant</sup>* (Figure 5.28) suggesting that mTORC1 activity was in fact impaired. This provides further evidence that proliferation of the spheres after passage four becomes impaired in the presence of activate *KrasG12D* whereby the neural progenitors, are not responding to growth factor signals and may be transitioning into intermediate progenitors and neuroblasts.

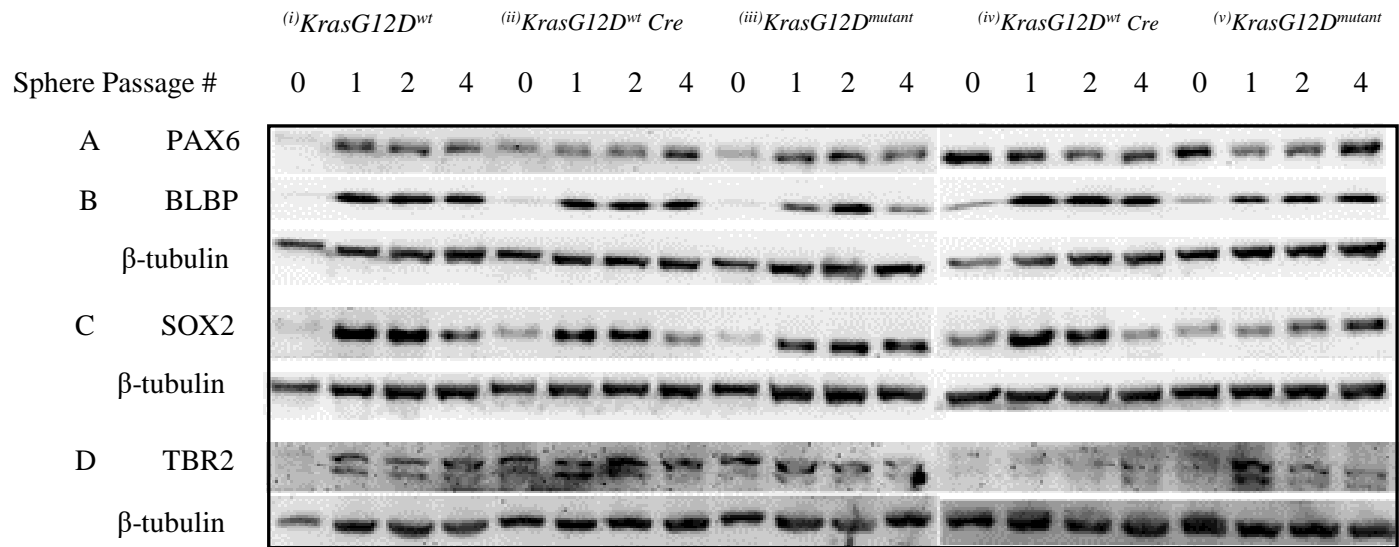


**Figure 5.26. Increase in SOX2 expression in E14.5 *KrasG12D<sup>mutant</sup>* neurospheres.** Expression of neural markers in E14.5 neurosphere lysates over four passages. Pax6 (A) and SOX2 (C) are markers of NPs, BLBP (B) and TBR2 (D) are markers of intermediate progenitors. (A) Pax6 expression was high in passage zero and four in *KrasG12D<sup>mutant</sup>* (v) but low in *KrasG12D<sup>mutant</sup>* (iii), and in two *KrasG12D<sup>wt</sup>* controls (i and ii) was low at zero and four, but high for *KrasG12D<sup>wt</sup>* (iv) and was therefore inconsistent overall. (B) BLBP expression in *KrasG12D<sup>mutant</sup>* (iii and v) was slightly lower than *KrasG12D<sup>wt</sup>* controls (i, ii and iv). (C) SOX2 expression increases with passage number to both *KrasG12D<sup>wt</sup>* (i, ii, iv) and *KrasG12D<sup>mutant</sup>* (iii, v) but expression remains high at passage four for *KrasG12D<sup>mutant</sup>* (iii, v), which declines in *KrasG12D<sup>wt</sup>* (i, ii, iv). (D) TBR2 expression was largely inconclusive. Beta-tubulin expression was used as a loading control. Controls: *KrasG12D<sup>wt</sup>* No Cre (Cre-/Kras-), *KrasG12D<sup>wt</sup>* Cre (Cre+/Kras-) Mutants: *KrasG12D<sup>mutant</sup>* (Cre+/Kras+).

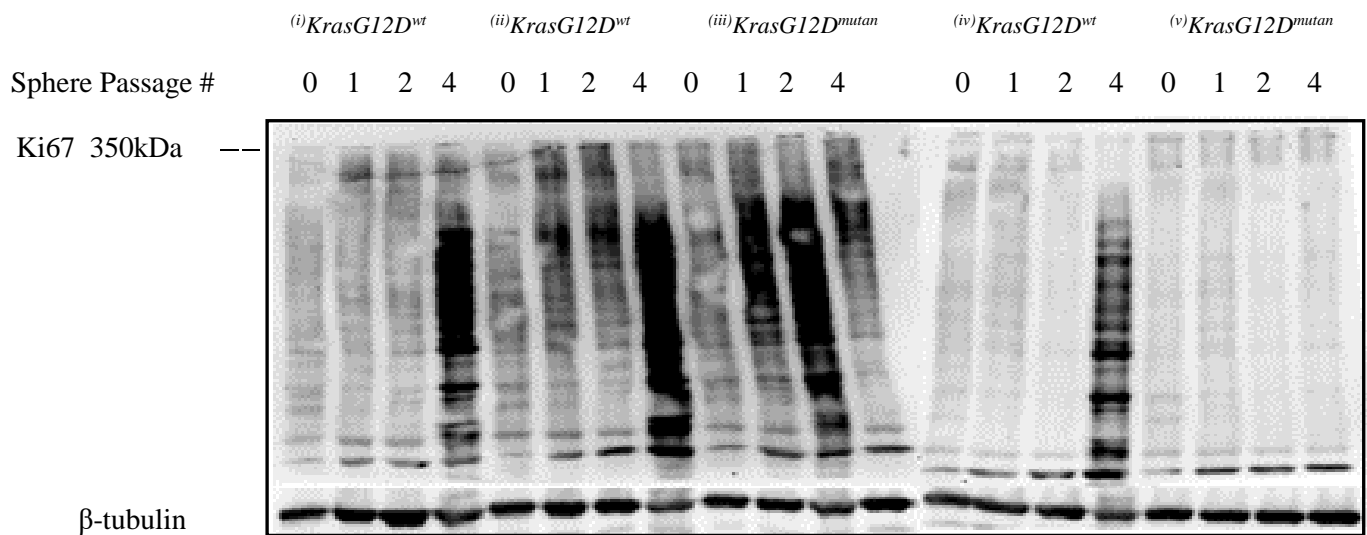


**Figure 5.27. Reduced Ki67 in E14.5 *KrasG12D<sup>mutant</sup>* neurospheres.** Immunoblot for the proliferative marker, Ki67, in E14.5 neurospheres. Expression was low in *KrasG12D<sup>mutant</sup>* (iii, v) E14.5 neurosphere lysates after passage zero, one, two and four in comparison with three controls (i, ii, iv). Beta-tubulin expression was used as a loading control. Controls: *KrasG12D<sup>wt</sup>* No Cre (Cre-/Kras-), *KrasG12D<sup>wt</sup>* Cre (Cre+/Kras-) Mutants: *KrasG12D<sup>mutant</sup>* (Cre+/Kras+)

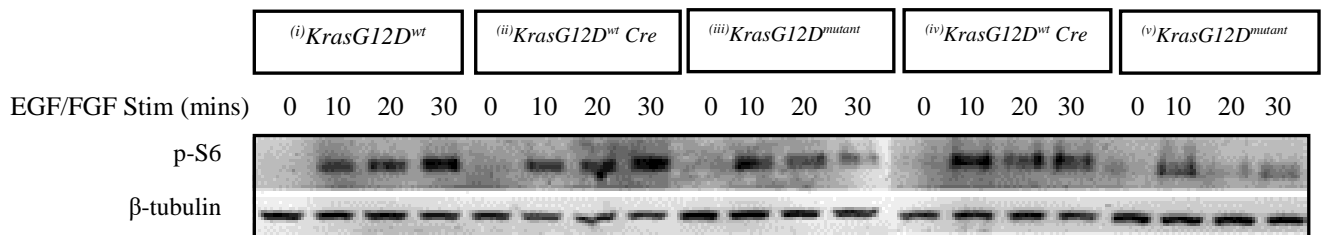


**Figure 5.28. Reduction in mTORC1 activity in E14.5 *KrasG12D<sup>mutant</sup>* neurospheres.** Immunoblot for the expression of the mTORC1 activity marker, p-S6 (S235/236), on passage four neurospheres lysates after 0, 10, 20, 30mins stimulation with EGF/FGF. There is a reduction in mTORC1 activity after 30mins EGF/FGF stimulation in *KrasG12D<sup>mutant</sup>* (iii, v) compared to *KrasG12D<sup>wt</sup>* (i, ii, iv) Phospho-S6 expression is used as a measurement of mTORC1 activity. Beta-tubulin expression as a loading control. Controls: (Cre-/Kras-), (Cre+/Kras-) Mutants: Cre+/Kras+

## 5.2 Discussion

The data presented here demonstrates that the activation of the KrasG12D mutation in neural progenitors results in embryonic lethality (Figure 5.3-5.6) altering brain morphology dramatically (Figure 5.7-5.12) in later stage embryos. The presence of the KrasG12D mutation and cre recombinase was 100% associated with brains swollen in size, displaying little recognisable neocortical tissue architecture or structure. Molecular and cellular analyses suggested this was associated with expansion of a neural progenitor population. It was concluded that the dominating cell type at E16.5 was the intermediate neural progenitors, as the majority of cells expressed neural progenitor markers such as SOX2 and TBR2 (Figure 5.16) but no post-mitotic neuron (TBR1) expression (Figure 5.17). This suggests that KrasG12D activation promoted intermediate progenitor expansion at the expense of differentiation into neurons. The reduction in (TBR1) neurons could already be observed by immunofluorescence at E14.5, (Figure 5.19Ai and B). The proliferation of the apical neural progenitors was also already diminished at this earlier time (Figure 5.22Ai and B). However, the propagation of neurospheres from E14.5 mutant cortex resulted in significantly larger spheres initially, implicating that the mitotic capacity of neural progenitors could be re-established *ex-vivo* resulting in rapid proliferation of progenitors (Figure 5.23-5.25). After four passages, however, the volume of mutant spheres was dramatically reduced, with majority of the spheres in quiescence based on reduced Ki67 (Figure 5.27) and mTORC1 activity (Figure 5.28), indicating that there was a decline in neural progenitor self-renewal capacity and the spheres were likely undergoing transition into intermediate progenitors. *In vivo*, at E14.5, the only cell type that was not reduced, was the (TBR2) intermediate progenitor population, (Figure 5.20Ai and B), providing evidence that the mutant intermediate progenitors are stabilised at E14.5, which go on to become expanded in E16.5 leading to the altered brain morphology observed in Nissl staining at E17.5.

### 5.2.1 Mutant neural progenitors are sacrificed in vivo, in favour of intermediate progenitor expansion.

By immunofluorescence, there was a reduction in post-mitotic TBR1 positive neurons, (Figure 5.19A and Ai) indicating that there is either less differentiation into neurons or these cells are deteriorating prior to E14.5. Considering that intermediate progenitors by E16.5, at which point there is little post-mitotic neuron expression, this result at E14.5, was not surprising. However, the reduction in PH3 positive cells at the ventricular zone at E14.5 was,

and indicated there were less mitotic neural progenitors at this stage. This was unexpected, as two embryonic days later, at E16.5, there is an obvious expansion of a homogenous population of undifferentiated cells. During the process of neural progenitor / radial glia division to produce intermediate progenitors, the length of the cell cycle is increased (García-García et al., 2012, Martíñez-Cerden et al., 2006) it seemed logical to assume that an increase in mitotic neural progenitors may be observed at E14.5. The only population of cells that does not decrease at E14.5, that is the (TBR2) intermediate progenitors (Figure 5.20A and Ai) and we know that hyperproliferation of this subtype is obvious two days later at E16.5. Therefore, the decline of mitotic neural progenitors may indicate their sacrifice in favour for the pre-expansion of the intermediate progenitors which occurs by E16.5. Upon the propagation of neurospheres from E14.5 mutants, evidence that there was a decline in neural stem cell/ neural progenitor population in favour of intermediate progenitor expansion was partially established.

Originally the propagation of neurospheres was attempted from E16.5 cortex, however no spheres or cells survived beyond 6 hours in culture as there was either not enough viable neural progenitors at this stage to initiate sphere formation, the dissociated cells had poor cell-cell adhesion or there was a lot of necrosis and apoptosis. From the immunoblot data, it has been established that the remaining cell populations at E16.5 in mutants are intermediate progenitors (TBR2 and SOX2 positive). If these are the only existing cell type in E16.5 mutants, these cells would not be able to propagate themselves as neurospheres over multiple passages (Xiong et al., 2011). The fact that the cells do not survive in part provides evidence that the mutant cells isolated cannot sustain themselves. However, there is also the possibility of poor cell-cell and cell-matrix adhesion, as the cells that were isolated did not congregated together, nor did they attach to the flasks. *KrasG12D* transformation often causes poor cell adhesion as a result of the cytoskeletal remodelling, which also promotes their motility in cancers (Pollock et al., 2004). Poor attachment to cells or other tissues would explain the tissue fragility of the mutant cortex at this stage. Lastly, there may be a substantial amount of cell death or apoptosis as a result of the mutation, and the cells are unable to survive as in previous studies, the *KrasG12D* mutation has shown to increased apoptosis and necrosis in patient derived colorectal cancers (Liu et al., 2015). Considering the severity of the mutation in the brain, by which animals die at birth and the neural tissue deformations that occur, it is not unreasonable to expect that there would be a substantial amount of apoptosis, however

this was not investigated in this study. As little data could be obtained from the mutant E16.5 spheres, E14.5 neurospheres were next investigated.

Unlike E16.5, the mutant E14.5 cortex enabled the establishment of neurospheres, despite the reduction in mitotic cells at the VZ *in vivo* (Figure 5.21). Therefore, it was expected that spheres may be smaller and have less proliferative capacity, based on the reduced mitotic cells at the VZ. Instead, the KrasG12D mutant spheres had significantly larger volumes, initially during early passages, (Figure 5.23 - 5.25), which indicated an expansion of either neural or intermediate progenitors (Zanni et al., 2015) within the KrasG12D mutant spheres contributing to the increased sphere volume. It is likely that the dominant population in KrasG12D mutants at E14.5 was intermediate progenitors; as they were sufficiently established and able to propagate neurospheres providing an initial proliferative advantage. However, by the fourth passage, the sphere volume decreased which occurs in neurospheres derived from intermediate progenitors, (Figure 5.24E) (Xiong et al., 2011). Intermediate progenitors are able to generate spheres for up to four or five passages before declining, whereas spheres derived from neural stem cells and neural progenitors are able to propagate spheres for greater than 7 passages (Xiong et al., 2011). Evidence for this is in the declined sphere volume in the KrasG12D mutants and, their reduced proliferation determined by Ki67 expression (Figure 5.27). During which point, the majority of the spheres may be in quiescence, based on both the reduced Ki67 expression (Gerdes et al., 1984) and reduced mTORC1 activity (phospho-S6 expression) (Figure 5.28) (Rodgers et al., 2014). Therefore, passage four was likely to be the point in which the mutant sphere intermediate progenitors were unable to continue the propagation of neurospheres.

### **5.2.2 *mTORC1 activity and KrasG12D<sup>mutant</sup> signalling***

Interplay between mTOR and Ras signalling has been previously reported (Chung et al., 1994, Carriere et al., 2011). For example, the activation of Ras/MAPK via growth factor (PDGF/IGF) stimulation, resulted in increased mTORC1 activity, due to enhanced Raptor phosphorylation (Carriere et al., 2011). Both Ras/MAPK and mTORC1 pathways are known to be upregulated during oncogenesis and in a variety of human cancers. However, the way in which the pathways integrate is disease specific. The pathways can integrate in direct proportion (synergistically) whereby the activation/inactivation of one pathway can enhance/inhibit the effect of the other to mediate its tumorigenic transformation or proliferative capacity. This has been shown to occur in T-cell lymphoblastic leukaemia,

whereby the inactivation of the mTORC1 component, Raptor, inhibited oncogenic Kras-induced proliferation of murine T-cells (Hoshii et al., 2014). This has also been shown in lung cancer progression, in which the hyper activation of mTORC1, via TSC1 deletion, results in increased oncogenic Kras transformation, *in vivo* (Liang et al., 2010), indicating that mTORC1 activity enhances Kras mediated transformation. Integration can also occur in an indirectly proportional manner, whereby down regulation of either pathway results in increased activity of the other. For instance, the inhibition of mTORC1 in patient tumours, by Rapamycin administration, led to an up regulation of Ras-MAPK pathway in a variety of human cancers (Carracedo et al., 2008). In our KrasG12D<sup>mutant</sup> neurosphere assay, after starving E14.5 mutant KrasG12D<sup>mutant</sup> spheres of EGF/FGF and stimulating the spheres 24hrs later, it was found that mTORC1 activity was indirectly proportional to Kras activation, with a reduction in phospho-S6 induction noticeable after twenty and thirty minutes after stimulation. This counter balance may be due to the cells in the neurosphere entering quiescence. During passage four, the sizes of the mutant spheres were a lot smaller than previous passages, implicating a decline in their proliferative capacity. It is likely that the KrasG12D mutant spheres were derived from intermediate progenitors, have reached their propagative capacity by the fourth passage and have entered quiescence, as they also displayed reduced Ki67 expression which is typical of G0 phase cells.

### 5.2.3 Previous studies of *KrasG12D* activation in neural progenitors

Previous investigations into the capacity of the *KrasG12D* mutation to cause tumourigenesis in the mouse, have all driven mutant *KrasG12D* expression from restricted later stage lineages, including the neural-glial lineage using GFAP-Cre and the radial-glial lineage using BLBP-Cre. Some of these models have incorporated extra temporal control by the use Tet-R induction of GFAP-Cre at varying stages in both embryonic and post-partum development to determine if tumourigenesis is impaired with later onset, which can be a great model for brain cancer progression in adults. This study was not designed to challenge the current mouse models used to mimic brain cancer, but rather to investigate the effect of inducing *KrasG12D* mutation from early neural progenitors (NPs), not at a later restricted lineage. In this study we found that KrasG12D activation resulted in no surviving postnatal offspring (Figure 5.2- 5.4). In embryos there was a distinct whole body paleness and cerebral swelling.

The majority of previous studies activated *KrasG12D* in later stage progenitors, targeting it to neuro-glia/astrocytic precursor cells expressing either GFAP-Cre or BLBP-Cre expressing.

Further studies have developed inducible mutation incorporating tetracycline inducible GFAP-Cre, in which the activation of the *KrasG12D* mutation can be induced in both later or early stage neuro-glial subtypes (Muñoz and Hawkins, 2014). For GFAP-Cre the earliest time the mutation can be activate is E12 (Mamber et al., 2012) and for BLBP-Cre, E10 (Anthony and Heintz, 2008). There has yet to be targeting to earlier stage neural progenitors to a specific region of the developing brain, despite it being discovered that early stage induction of the mutation with GFAP- and BLBP-Cre enhances tumour transformation and proliferation. Early *KrasG12D* activation from neuro-glial lineages causes tumour formation within weeks, which can be advanced to higher grade tumours within days post-partum, when in conjunction with tumour suppressor deletion. Here we have utilised Emx-1-Cre to drive the expression of *KrasG12D* to early stage neural progenitors at E9.5 *in utero*, which is earlier than previous studies (Anthony and Heintz, 2008, Holland et al., 2000, Mamber et al., 2012, Marumoto et al., 2009, Muñoz and Hawkins, 2014).

Activation of *KrasG12D* in conjunction with tumour suppressor deletion from glial-progenitor populations has previously resulted in viable progeny post partum (Ghazi, S et al 2012), with survival extending beyond weeks. Similarly, the activation of *KRASG12D* alone in glial-progenitor populations using the same GFAP-Cre didn't result in tumours until 4 weeks post-partum. Hence, it was anticipated that at least the mutant progeny would survive for a few weeks post-partum. If *USP9x* were acting as tumour suppressor, as in the development of PDA from PanIN (Pérez-Mancera et al 2012), then it may have been expected that embryos died *in utero*. However, in our system, activating *KRASG12D* alone from early neural progenitors resulted in embryonic lethality. As to whether the *USP9x* deletion has an effect in this is unclear, as the embryos with the genotype *Kras/Uspx*<sup>mutant</sup> (Figure 5.5) had the same phenotype as those with *KrasG12D*<sup>mutant</sup> (Figure 5.6) If *USP9x* were acting as an oncogene, its deletion is clearly not enough to rescue the embryo. It would be difficult to study *USP9x* as a tumour suppressor in this system, as the *KRASG12D* activation is already quite severe.

#### 5.2.4 *KrasG12D*<sup>mutant</sup> non-neural defects

Paleness and cerebral swelling were consistent phenotypes in all of the mutant embryos, from stage E15.5 onwards. At E14.5, although there was paleness, cerebral swelling was not prominent at this stage. This phenotype has been originally reported in both an ES cell generated *Kras* gene deletion (Johnson et al., 1997) study, and in *KrasG12D* mutant studies

(Tang et al., 2013, Tuveson et al., 2004). Similarly to us, the deletion of *Kras* gene yielded no viable full term offspring (Johnson et al., 1997), indicating that at least one healthy copy of the *Kras* gene is critical for embryonic survival.

The embryonic deletion (Johnson et al., 1997) and mutation of *Kras* (Tuveson et al., 2004) resulted in growth delay, superficial vasculature, reduced size and paleness evident from E11.5, with no embryo surviving past E14.5. However, no dramatic effect on the brain occurred until *N-ras* deletion was coupled with the *Kras* mutation, resulting in cell death in the forebrain and neural axis, at E9.5 (Johnson et al., 1997). Indicating that in isolation, a *Kras* deletion (Johnson et al., 1997) from the whole embryo is not sufficient to perturb brain tissue, unless another Ras protein is also affected.

*KrasG12D* activation in the fetal liver cells, using Vav-iCre induction was used to study childhood leukaemia in a foetal haematopoietic mouse model (Tang et al., 2013). Vav-iCre was thought to be expressed exclusively in the haematopoietic cells of the foetal liver. However poor vascularisation and systemic haemorrhage was observed within the entire embryo at E14.5 and brain haemorrhage became noticeable at E15.5. It was argued that brain haemorrhaging may be a result of leaky *Kras* expression in these tissues. This raises the possibility that the Vav-iCre induction may not be as specific for liver tissues as anticipated. Thus, it is not the leakiness of the *Kras* expression in tissues, but rather the leakiness of the Cre driven expression: Vav-i or *Emx-1* (in our case). No further investigation into side effect on the brain tissue after induction with Vav-iCre was investigated further in this study (Tang et al., 2013).

Spontaneous recombination between the wildtype and mutant *KrasG12D* allele has been reported in the transformation of somatic cells, of the whole animal, into tumorigenic tissue types. This phenomenon occurs at low frequencies but is quite virulent and has resulted in the development of skin papilloma, thymic lymphoma as well as hyperplasia and carcinoma of the lungs (Johnson et al., 2001). However, no spontaneous activation is reported in neural tissues. This may be responsible for the whole body phenotype that we observed in each of the *KrasG12D*<sup>mutant</sup> embryos, but should not contribute to the phenotype observed in the brain tissue.

We have induced *KrasG12D* activation with Emx1-Cre. Emx1 expression during embryonic development has been reported from E9.5. Although it has been shown to be restricted to the diencephalic/telencephalic regions, trigeminal ganglionic neural crest cells and front-nasal process (Gorski et al., 2002), it is also expressed in the first branchial arches, cranial ganglia as well as the developing limb bud during this stage. Expression in the branchial arches and developing limb bud, may have contributed to the paleness and poor vascularisation of the embryo, as occurred for the Vav-iCre induction of *KrasG12D*, which was thought to be restricted to the foetal liver cells.

### 5.3 Supplementary Figures

A Number of <i>Kras/Usp9x</i> <sup>mutant</sup> weaned mice						
Litter	Number of pups	Expected	Expected %	Number of <i>Kras/Usp9x</i> <sup>mutant</sup> Obtained	Ratio of Obtained	% of Ratio Obtained
1	8	2	25	0	0	0
2	10	2.5	25	0	0	0
3	10	2.5	25	0	0	0
4	10	2.5	25	0	0	0
5	10	2.5	25	0	0	0
6	10	2.5	25	0	0	0
7	11	2.75	25	0	0	0
8	9	2.25	25	0	0	0
9	9	2.25	25	0	0	0
10	10	2.5	25	0	0	0
Average	9.7	2.425	25	0	0	0
Total	97	24.25		0	0	

B Number of <i>KrasG12D</i> <sup>mutant</sup> weaned mice						
Litter	Number of pups	Expected	Expected %	Number <i>KrasG12D</i> <sup>lox</sup> obtained	Ratio of Obtained	% of Ratio Obtained
1	8	4	50	0	0	0
2	10	5	50	0	0	0
3	10	5	50	0	0	0
4	10	5	50	0	0	0
5	10	5	50	0	0	0
6	10	5	50	0	0	0
7	11	5.5	50	0	0	0
8	9	4.5	50	0	0	0
9	9	4.5	50	0	0	0
10	10	5	50	0	0	0
Average	9.7	4.85	50	0	0	0
Total	97	48.5		0	0	

C Number of <i>KrasG12D</i> <sup>lox</sup> / <i>Usp9x</i> <sup>lox</sup> weaned mice						
Litter	Number of pups	Expected	Expected %	Number of <i>KrasG12D</i> <sup>lox</sup> / <i>Usp9x</i> <sup>lox</sup> Obtained	Ratio of Obtained	% of Ratio Obtained
1	8	4	50	0	0	0
2	10	5	50	0	0	0
3	10	5	50	0	0	0
4	10	5	50	0	0	0
5	10	5	50	0	0	0
6	10	5	50	2	0.2	20
7	11	5.5	50	0	0	0
8	9	4.5	50	0	0	0
9	9	4.5	50	0	0	0
10	10	5	50	3	0.3	30
Average	9.7	4.85	50	0.5	0.05	5
Total	97	48.5		5.0	0.5	

D Number of <i>KrasG12D</i> <sup>lox</sup> weaned mice						
Litter	Number of pups	Expected	Expected %	Number <i>KrasG12D</i> <sup>lox</sup> obtained	Ratio of Obtained	% of Ratio Obtained
1	8	4	50	0	0	0
2	10	5	50	1	0.1	10
3	10	5	50	0	0	0
4	10	5	50	1	0.1	10
5	10	5	50	0	0	0
6	10	5	50	1	0.1	10
7	11	5.5	50	2	0.181818	18.18182
8	9	4.5	50	0	0	0
9	9	4.5	50	0	0	0
10	10	5	50	1	0.1	10
Average	9.7	4.85	50	0.6	0.4818	28.181
Total	97	48.5		6	0.04818	

E Number of <i>Usp9x</i> <sup>lox</sup> / <i>Emx-1-Cre</i> weaned mice						
Litter	Number of pups	Expected	Expected %	Number Obtained	Ratio of Obtained	% of Ratio Obtained
1	8	4	50	4	0.5	50
2	10	5	50	7	0.7	70
3	10	5	50	3	0.3	30
4	10	5	50	3	0.3	30
5	10	5	50	3	0.3	30
6	10	5	50	3	0.3	30
7	11	5.5	50	5	0.45	45
8	9	4.5	50	9	1.0	100
9	9	4.5	50	7	0.78	78
10	10	5	50	2	0.2	20
Average	9.7	2.425	50	4.6	4.83	48.3
Total	97	24.25		46	48.3	

F Number of <i>Emx-1-Cre</i> weaned mice						
Litter	Litter Embryos	Expected Numbers	Expected Percentage	Number Obtained	Ratio of Obtained	% of Ratio Obtained
1	8	4	50	2	0.25	25
2	10	5	50	0	0.0	0
3	10	5	50	2	0.2	20
4	10	5	50	3	0.4	40
5	10	5	50	5	0.5	50
6	10	5	50	2	0.2	20
7	11	5.5	50	4	0.273	27.3
8	9	4.5	50	0	0.0	0
9	9	4.5	50	0	0.0	0
10	10	5	50	0	0.0	0
Average	9.7	2.425	50	1.8	0.182	18.2
Total	97	24.25		18	1.82	

G Number of <i>Usp9x</i> <sup>lox</sup> weaned mice						
Litter	Litter Embryos	Expected Numbers	Expected Percentage	Number Obtained	Ratio of Obtained	% of Ratio Obtained
1	8	8	100	2	0.25	25
2	10	10	100	2	0.2	20
3	10	10	100	2	0.2	20
4	10	10	100	2	0.2	20
5	10	10	100	0	0.0	0
6	10	10	100	0	0.0	0
7	11	11	100	1	0.09	9
8	9	9	100	0	0.0	0
9	9	9	100	1	0.11	11
10	10	10	100	1	0.3	30
Average	9.7	9.7	100	1.1	0.135	13.5
Total	97	97		11	1.35	

H Number of <i>Negative</i> weaned mice						
Litter	Litter Embryos	Expected Numbers	Expected Percentage	Number Obtained	Ratio of Obtained	% of Ratio Obtained
1	8	0	0	0	0.25	25
2	10	0	0	0	0.2	20
3	10	0	0	3	0.2	20
4	10	0	0	1	0.2	20
5	10	0	0	0	0.0	0
6	10	0	0	4	0.0	0
7	11	0	0	0	0.09	9
8	9	0	0	0	0.0	0
9	9	0	0	1	0.11	11
10	10	0	0	30	0.3	30
Average	9.7	0	0	1.2	0.135	13.5
Total	97	0		12	1.35	

**Supplementary Figure 5.1. *Kras/Usp9x<sup>mutant</sup>* genotype is not observed in offspring.** The obtained numbers and percentages of ***Kras/Usp9x<sup>mutant</sup>*** (Table A), ***KrasG12D<sup>mutant</sup>*** (Table B), ***KrasG12D<sup>lox</sup>/Usp9x<sup>lox</sup>*** (Table C) and ***KrasG12D<sup>lox</sup>*** (Table D) are significantly lower than expected. Each table shows the total number of pups obtained in each litter for the first ten weaned litters as well as the expected numbers and percentage of those within each litter inheriting either: (1) all three alleles *KrasG12D<sup>lox</sup>*, *Usp9x<sup>lox</sup>* and *Emx-1-Cre* for ***Kras/Usp9x<sup>mutant</sup>***, (2) two alleles: *KrasG12D<sup>lox</sup>* and *Emx-1-Cre*, for ***KrasG12D<sup>mutant</sup>*** (3) *KrasG12D<sup>lox</sup>* and *Usp9x<sup>lox</sup>* for ***KrasG12D<sup>lox</sup>/Usp9x<sup>lox</sup>***, or (4) *KrasG12D<sup>lox</sup>* allele only for ***KrasG12D<sup>lox</sup>***. The actual obtained number, ratio and percentage of mice inheriting each allele is shown for each litter. (A) The average percentage of *Kras/Usp9x<sup>mutant</sup>* mice obtained per litter was zero, compared to the expected 25%. (B) The average percentage of *KrasG12D<sup>mutant</sup>* mice obtained per litter was zero, compared to the expected 50% (C) *KrasG12D<sup>lox</sup>/Usp9x<sup>lox</sup>* mice obtained per litter was 5%, compared to the expected 50%. (D) The average percentage of *KrasG12D<sup>lox</sup>* mice obtained per litter was 8.82%, compared to the expected 50%. (E, F, G).

## 6.0 CHAPTER SIX – CONCLUSIONS AND FUTURE DIRECTIONS

Here we provide further evidence that the regulation of neural progenitor proliferation is dependent on the presence of USP9x in human cells, *in vitro* and in murine neurosphere cultures *ex vivo*. Absence of Usp9x from cultured NPs did not result in their differentiation into neuronal or glial subtypes, as might be expected from *Usp9x in vivo* expression pattern which decreases as differentiation proceeds (Wood et al., 1997). Rather NPs accumulated in the quiescent phase of the cell cycle for both human neural progenitors and in murine neurospheres correlating with the downregulation of mTORC1 signalling. Previous studies in murine derived NSCs have shown that modest over-expression of USP9x promotes self-renewal and enhances proliferation (Jolly et al., 2009). The evidence provided here shows the counter situation where Usp9x depletion reduced NP proliferation, and identified a molecular mechanisms behind this. Co-immunoprecipitation of endogenous proteins identified Raptor as a Usp9x binding partner in murine lysates, and also that Raptor protein is reduced when USP9x is depleted, indicating the likely mechanism behind the reduced proliferation is reduced mTORC1 signalling. Previous studies had identified an interaction with mTORC1 components and USP9x, but relied on exogenous over-expression (Agrawal et al., 2012). By elucidating the region of Raptor to which USP9x binds, we could confirm the association of the two proteins as a direct interaction, without concluding that they are simply in a complex together. There are many ways to achieve this, but the best way would be to establish mutants of Raptor domains (or cut the Raptor gene into domains) and ligate these into a tagged vector. After over expressing these mutants in HEK 293 or ReNcells VM (as the interaction was established in E16.5 neural lysate from tissue, not a specific cell line), an immunoprecipitation assay can be conducted using the vector (into which the Raptor mutants are inserted) tag antibody to precipitate proteins bound to each of the Raptor mutants. From there, the precipitate can be assessed for mutant which fails to yield USP9x protein in the precipitate. It would be this region to which USP9x binds, therefore the sequence of this region could be established. This would unequivocally establish Raptor as a direct binding partner of USP9x.

The reduction in proliferation of neural stem cells implicates Usp9x as an oncogene. We investigated it as a candidate target to stop the uncontrolled proliferation of diseased neural stem cells that arise in diseases such as GBM. After obtaining GBM cells with uncontrolled proliferative capacity and depleting USP9x from them, the anticipated reduction in cellular

density did not occur, as had been previously described (Cox et al., 2013). Instead an increase in mTORC1 activity was observed in some of the GBM lines analysed our studies, which not only contradicts past literature (Cox et al., 2013) but also our observations of the mTORC1 activity in the USP9x depleted ReNcells VM. These data suggest USP9x might act as a tumour suppressor in some GBM cells, similar to its role in pancreatic cancer (Pérez-Mancera et al., 2012). Hence, targeting USP9x in GBM tumours in patients may result in the increased proliferation and expansion of the diseased cells, which could be detrimental to patient survival. This also applies to the recent proposal to use inhibitors of Usp9x function as a therapeutic approach in the treatment of lymphoma (Peterson et al., 2015)

The role of USP9x as a tumour suppressor in cancer has been recently established (Pérez-Mancera et al., 2012, Sun et al., 2011), and we aimed to provide further evidence for (or against) this *in vivo* by studying the activation of KrasG12D in conjunction with a Usp9x deletion from the forebrain. Interestingly, the effect of expressing the KrasG12D<sup>mutant</sup> alone on the forebrain was quite severe, so much so, that the added effect of Usp9x deletion was indistinguishable. Previous studies have revealed the importance of the Kras allele in mouse development, where knockout or mutation of the gene result in embryonic lethality (Johnson et al., 1997), but can be rescued by replacement of H-ras into the Kras locus (Potenza et al., 2005). The deletion of other Ras genes H-ras and N-ras does not have such a detrimental effect (Westcott and To, 2013). Here we provide further evidence that a healthy Kras allele is required for embryonic survival, but also that expression of the G12D mutation in the forebrain results in severe neural defects. In these mice, there was a mass expansion of intermediate progenitors by E16.5 during which stage there was severe deformation of the neural architecture. There were no post mitotic neurons present, indicating an impairment in neuronal differentiation which is most likely caused from the mass expansion of the progenitors. Strikingly, only two days prior, at E14.5, neural architecture appeared normal, although there was a reduction in post mitotic neurons and mitotic progenitors, with the only unchanged population being the intermediate progenitors. For neural development, this indicates that controlled tightly controlled Kras mediated signalling is important for intermediate progenitor differentiation (into post-mitotic neurons) especially between E14.5 and E16.5.

Although these findings largely contribute to the knowledge of Kras in neural development, they may be relevant to early neural tumour development. No studies on prenatal human

brain tumours have identified Kras as a contributor, however, mutations in the Kras allele have been identified in childhood brain tumours (Maltzman et al., 1997), albeit not the KrasG12D mutation specifically. Failure to identify Kras mutations in prenatal neural tumours may be because they don't occur, or because they result in early termination due to the severity of the mutation on embryonic development.

Overall, this thesis aimed to contribute further knowledge about the role of USP9x in neural stem cell proliferation, in the hope of elucidating some of the molecular mechanisms behind the changes in proliferation. Also, it was aimed to provide some insight into the interplay between Usp9x and KrasG12D in the development of neural tumours, considering the recent implication for Usp9x as a tumour suppressor in KrasG12D mediated pancreatic cancer transformation. Although Usp9x were abandoned from this second project, and a postnatal brain tumour model did not evolve due the severity of the mutation, hopefully some insight into the KrasG12D mediated effect on neural development was successful.

## 7.0 BIBLIOGRAPHY

- ABEL, T. W., CLARK, C., BIERIE, B., CHYTIL, A., AAKRE, M., GORSKA, A. & MOSES, H. L. 2009. GFAP-Cre-Mediated Activation of Oncogenic K-ras Results in Expansion of the Subventricular Zone and Infiltrating Glioma. *Molecular cancer research : MCR*, 7, 645-653.
- ABRAHAM, R. & CHIANG, C. 2005. Phosphorylation of mammalian target of rapamycin (mTOR) at Ser-2448 is mediated by p70S6 kinase. *J. Biol. Chem* 280, 25485-25490.
- ADACHI, K., MIRZADEH, Z., SAKAGUCHI, M., YAMASHITA, T., NIKOLCHEVA, T., GOTOH, Y., PELTZ, G., GONG, L., KAWASE, T., ALVAREZ-BUYLLA, A., OKANO, H. & SAWAMOTO, K. 2007. Beta-catenin signaling promotes proliferation of progenitor cells in the adult mouse subventricular zone. *Stem Cells*, 25, 2827-36.
- AGRAWAL, P., CHEN, Y.-T., SCHILLING, B., GIBSON, B. W. & HUGHES, R. E. 2012. Ubiquitin-specific Peptidase 9, X-linked (USP9X) Modulates Activity of Mammalian Target of Rapamycin (mTOR). *Journal of Biological Chemistry*, 287, 21164-21175.
- AGUIRRE, A., RUBIO, M. & GALLO, V. 2010. Notch and EGFR pathway interaction regulates neural stem cell number and self-renewal. *Nature*, 467, 323-327.
- AIGNER, L. & BOGDAHN, U. 2008. TGF-beta in neural stem cells and in tumors of the central nervous system. *Cell and Tissue Research*, 331, 225-241.
- AL-HAKIM, A. K., ZAGORSKA, A., CHAPMAN, L., DEAK, M., PEGGIE, M. & ALESSI, D. R. 2008. Control of AMPK-related kinases by USP9X and atypical Lys(29)/Lys(33)-linked polyubiquitin chains. *Biochem J*, 411, 249-60.
- ALBERT, L., KARSY, M., MURALI, R. & JHANWAR-UNIYAL, M. 2009. Inhibition of mTOR Activates the MAPK Pathway in Glioblastoma Multiforme. *Cancer Genomics - Proteomics*, 6, 255-261.
- AMADOR, V., GE, S., SANTAMARIA, P., GUARDAVACCARO, D. & PAGANO, M. 2007. APC/C(cdc20) controls the ubiquitin mediated degradation of p21 in prometaphase. *Mol Cell*, 27, 462-473.
- ANNOVAZZI, L., MELLAI, M., CALDERA, V., VALENTE, G. & SCHIFFER, D. 2011. SOX2 expression and amplification in gliomas and glioma cell lines. *Cancer Genomics Proteomics*, 8, 139-147.
- ANTHONY, T. E. & HEINTZ, N. 2008. Genetic lineage tracing defines distinct neurogenic and gliogenic stages of ventral telencephalic radial glial development. *Neural Development*, 3, 30-30.
- ARCELLA, A., BIAGIONI, F., ANTONIETTA OLIVA, M., BUCCI, D., FRATI, A., ESPOSITO, V., CANTORE, G., GIANCASPERO, F. & FORNAI, F. 2013. Rapamycin inhibits the growth of glioblastoma. *Brain Research*, 1495, 37-51.
- BABCOCK, J. T., NGUYEN, H. B., HE, Y., HENDRICKS, J. W., WEK, R. C. & QUILLIAM, L. A. 2013. Mammalian Target of Rapamycin Complex 1 (mTORC1) Enhances Bortezomib-induced Death in Tuberous Sclerosis Complex (TSC)-null Cells by a c-MYC-dependent Induction of the Unfolded Protein Response. *The Journal of Biological Chemistry*, 288, 15687-15698.
- BALGI, A., DIERING, G., DONOHUE, E., LAM, K., BRUNO, F., ZIMMERMAN, C., NUMATA, M. & ROBERGE, M. 2011. Regulation of mTORC1 signalling by pH. *PlosOne*.
- BALTUS, G. A., KOWALSKI, M. P., ZHAI, H., TUTTER, A. V., QUINN, D., WALL, D. & KADAM, S. 2009. Acetylation of Sox2 Induces its Nuclear Export in Embryonic Stem Cells. *STEM CELLS*, 27, 2175-2184.
- BEDFORD, L., LOWE, J., DICK, L. R., MAYER, R. J. & BROWNELL, J. E. 2011. Ubiquitin-like protein conjugation and the ubiquitin-proteasome system as drug targets. *Nat Rev Drug Discov*, 10, 29-46.
- BEGHINI, A., MAGNANI, I., ROVERSI, G., PIEPOLI, T., TERLIZZI, S. D., MORONI, R. F., POLLO, B., FUHRMAN CONTI, A. M., COWELL, J. K., FINOCCHIARO, G. & LARIZZA, L. 2003. The neural progenitor-restricted isoform of the MARK4 gene in 19q13.2

- is upregulated in human gliomas and overexpressed in a subset of glioblastoma cell lines. *Oncogene*, 22, 2581-2591.
- BEHAR, F. M., CIUREA, A. V., CHIVU, M., ZARNESCU, O., RADULESCU, R. & DRAGU, D. 2008. The development of xenograft glioblastoma implants in nude mice brain. *Journal of Medicine and Life*, 1, 275-286.
- BERTOLI, C., SKOTHEIM, J. M. & DE BRUIN, R. A. M. 2013. Control of cell cycle transcription during G1 and S phases. *Nature reviews. Molecular cell biology*, 14, 518-528.
- BIERNAT, W., TOHMA, Y., YONEKAWA, Y., KLEIHUES, P. & OHGAKI, H. 1997. Alterations of cell cycle regulatory genes in primary (de novo) and secondary glioblastomas. *Acta Neuropathologica*, 94, 303-309.
- BIRNBOIM, H. C. & DOLY, J. 1979. A rapid alkaline extraction procedure for screening recombinant plasmid DNA. *Nucleic Acids Research*, 7, 1513-1523.
- BLOMEN, V. A. & BOONSTRA, J. 2007. Cell fate determination during G1 phase progression. *Cellular and Molecular Life Sciences*, 64, 3084-3104.
- BREGYA, A., WONGA, T., SHAHA, A., JOHN, M., GOLDBERGB, J. & KOMOTAR, R. 2013. Active immunotherapy using dendritic cells in the treatment of glioblastoma multiforme. *Cancer Treatment Reviews*, 39, 891-907.
- BRETT, M., MCPHERSON, J., ZANG, Z. J., LAI, A., TAN, E.-S., NG, I., ONG, L.-C., CHAM, B., TAN, P., ROZEN, S. & TAN, E.-C. 2014. Massively Parallel Sequencing of Patients with Intellectual Disability, Congenital Anomalies and/or Autism Spectrum Disorders with a Targeted Gene Panel. *PloS one*, 9, e93409.
- BROADLEY, K. W. R., HUNN, M. K., FARRAND, K. J., PRICE, K. M., GRASSO, C., MILLER, R. J., HERMANS, I. F. & MCCONNELL, M. J. 2011. Side Population is Not Necessary or Sufficient for a Cancer Stem Cell Phenotype in Glioblastoma Multiforme. *Stem Cells*, 29, 452-461.
- BROWN, A., BORGMANN-WINTER, K., HAHN, C.-G., ROLE, L., TALMAGE, D., GUR, R., CHOW, J., PRADO, P., MCCLOSKEY, T., BAO, Y., BULINSKI, C. & DWORK, A. 2014. Increased stability of microtubules in cultured olfactory neuroepithelial cells from individuals with schizophrenia. *Progress in Neuro-psychopharmacology and Biological Psychiatry*, 48, 252-258.
- BROWN, C. Y., SADLON, T., GARGETT, T., MELVILLE, E., ZHANG, R., DRABSCH, Y., LING, M., STRATHDEE, C. A., GONDA, T. J. & BARRY, S. C. 2010. Robust, Reversible Gene Knockdown Using a Single Lentiviral Short Hairpin RNA Vector. *Human Gene Therapy*, 21, 1005-1017.
- CALEGARI, F. & HUTTNER, W. B. 2003. An inhibition of cyclin-dependent kinases that lengthens, but does not arrest, neuroepithelial cell cycle induces premature neurogenesis. *Journal of Cell Science*, 116, 4947-4955.
- CARRACEDO, A., MA, L., TERUYA-FELDSTEIN, J., ROJO, F., SALMENA, L., ALIMONTI, A., EGIA, A., SASAKI, A. T., THOMAS, G., KOZMA, S. C., PAPA, A., NARDELLA, C., CANTLEY, L. C., BASELGA, J. & PANDOLFI, P. P. 2008. Inhibition of mTORC1 leads to MAPK pathway activation through a PI3K-dependent feedback loop in human cancer. *The Journal of Clinical Investigation*, 118, 3065-3074.
- CARRIERE, A., ROMEO, Y., ACOSTA-JAQUEZ, H. A., MOREAU, J., BONNEIL, E., THIBAUT, P., FINGAR, D. C. & ROUX, P. P. 2011. ERK1/2 Phosphorylate Raptor to Promote Ras-dependent Activation of mTOR Complex 1 (mTORC1). *The Journal of Biological Chemistry*, 286, 567-577.
- CARTER, A., COLE, C., PLAYLE, A., RAMSAY, E. & SHERVINGTON, A. 2008. GPR26: A Marker for Primary Glioblastoma? *Mol. and Cell. Probes*, 22, 133-137.
- CASTELLANO, E. & DOWNWARD, J. 2011. RAS Interaction with PI3K: More Than Just Another Effector Pathway. *Genes & Cancer*, 2, 261-274.
- CASTILHO, R. M., SQUARIZE, C. H., CHODOSH, L. A., WILLIAMS, B. O. & GUTKIND, J. S. 2009. mTOR Mediates Wnt-Induced Epidermal Stem Cell Exhaustion and Aging. *Cell Stem Cell*, 5, 279-289.

- CHANDRIKA, G., NATESH, K., RANADE, D., CHUGH, A., SHASTRY, P. 2016. Suppression of the invasive potential of Glioblastoma cells by mTOR inhibitors involves modulation of NFkB and PKC-alpha signalling. *Scientific Reports*, 6,
- CHAU, V., TOBIAS, J. W., BACHMAIR, A., MARRIOTT, D., ECKER, D. J., GONDA, D. K. & VARSHAVSKY, A. 1989. A Multiubiquitin Chain Is Confined to Specific Lysine in a Targeted Short-Lived Protein. *Science*, 243, 1576-1583.
- CHEN, J., LI, Y., YU, T.-S., MCKAY, R. M., BURNS, D. K., KERNIE, S. G. & PARADA, L. F. 2012. A restricted cell population propagates glioblastoma growth after chemotherapy. *Nature*, advance online publication.
- CHOI, S., MAENG, Y., KIM, K., KIM, T. & KIM, E. 2014. Autophagy is induced by raptor degradation via the ubiquitin/proteasome system in granular corneal dystrophy type 2. *Biochem. Biophys. Res. Commun.*, 450, 1505-1511.
- CHUNG, J., GRAMMAR, T. C., LEMON, K. P., KAZLAUSKAS, A. & BLENIS, J. 1994. PDGF- and insulin-dependent pp70S6k activation mediated by phosphatidylinositol-3-OH kinase. *Nature*, 370, 71-75.
- CIAMMELLA, P., GALEANDRO, M., D'ABBIERO, N., PODGORNII, A., PISANELLO, A., BOTTI, A., CAGNI, E., IORI, M. & IOTTI, C. 2013. Hypo-fractionated IMRT for patients with newly diagnosed glioblastoma multiforme: A 6 year single institutional experience. *Clinical Neurology and Neurosurgery*, 115, 1609-1614.
- CLARK, M. J., HOMER, N., O'CONNOR, B. D., CHEN, Z., ESKIN, A., LEE, H., MERRIMAN, B. & NELSON, S. F. 2010. U87MG Decoded: The Genomic Sequence of a Cytogenetically Aberrant Human Cancer Cell Line. *PLoS Genet*, 6, 1-16.
- CLOËTTA, D., THOMANETZ, V., BARANEK, C., LUSTENBERGER, R. M., LIN, S., OLIVERI, F., ATANASOSKI, S. & RÜEGG, M. A. 2013. Inactivation of mTORC1 in the Developing Brain Causes Microcephaly and Affects Gliogenesis. *The Journal of Neuroscience*, 33, 7799-7810.
- COLLAND, F. 2010. The therapeutic potential of deubiquitinating enzyme inhibitors. *Biochem Soc Trans*, 38, 137-43.
- COLLER, H. A., SANG, L. & ROBERTS, J. M. 2006. A New Description of Cellular Quiescence. *PLoS Biol*, 4, e83.
- CORBIN, J. G., GAIANO, N., JULIANO, S. L., POLUCH, S., STANCIK, E. & HAYDAR, T. F. 2008. Regulation of Neural Progenitor Cell Development in the Nervous System. *Journal of neurochemistry*, 106, 2272-2287.
- COX, J., WILDER, P., GILMORE, J., WUEBBEN, E., WASHBURN, M. & RIZZINO, A. 2013. The SOX2-Interactome in Brain Cancer Cells Identifies the Requirement of MSI2 and USP9X for the Growth of Brain Tumor Cells. *PloS One*, 8, e62857.
- COX, J. L., WILDER, P. J., WUEBBEN, E. L., OUELLETTE, M. M., HOLLINGSWORTH, M. A. & RIZZINO, A. 2014. Context-dependent function of the deubiquitinating enzyme USP9X in pancreatic ductal adenocarcinoma. *Cancer Biology & Therapy*, 15, 1042-1052.
- CRESCENZI, M., SODDU, S. & TATÒ, F. 1995. Mitotic cycle reactivation in terminally differentiated cells by adenovirus infection. *Journal of Cellular Physiology*, 162, 26-35.
- DENNY, B. J., WHEELHOUSE, R. T., STEVENS, M. F. G., TSANG, L. L. H. & SLACK, J. A. 1994. NMR and Molecular Modeling Investigation of the Mechanism of Activation of the Antitumor Drug Temozolomide and Its Interaction with DNA. *Biochemistry*, 33, 9045-9051.
- DEY, J. H., BIANCHI, F., VOSHOL, J., BONENFANT, D., OAKELEY, E. J. & HYNES, N. E. 2010. Targeting Fibroblast Growth Factor Receptors Blocks PI3K/AKT Signaling, Induces Apoptosis, and Impairs Mammary Tumor Outgrowth and Metastasis. *Cancer Research*, 70, 4151-4162.
- DIBBENS, L. M., DE VRIES, B., DONATELLO, S., HERON, S. E., HODGSON, B. L., CHINTAWAR, S., CROMPTON, D. E., HUGHES, J. N., BELLOW, S. T., KLEIN, K. M., CALLENBACH, P. M. C., CORBETT, M. A., GARDNER, A. E., KIVITY, S., IONA, X., REGAN, B. M., WELLER, C. M., CRIMMINS, D., O'BRIEN, T. J., GUERRERO-LOPEZ, R., MULLEY, J. C., DUBEAU, F., LICCHETTA, L., BISULLI, F., COSSETTE, P., THOMAS, P. Q., GECZ, J., SERRATOSA, J., BROUWER, O. F., ANDERMANN, F., ANDERMANN, E., VAN DEN MAAGDENBERG, A. M. J. M., PANDOLFO, M.,

- BERKOVIC, S. F. & SCHEFFER, I. E. 2013. Mutations in DEPDC5 cause familial focal epilepsy with variable foci. *Nat Genet*, 45, 546-551.
- DIBBLE, C. C. & MANNING, B. D. 2013. Signal integration by mTORC1 coordinates nutrient input with biosynthetic output. *Nat Cell Biol*, 15, 555-564.
- DIEHL, J. A., CHENG, M., ROUSSEL, M. F. & SHERR, C. J. 1998. Glycogen synthase kinase-3 $\beta$  regulates cyclin D1 proteolysis and subcellular localization. *Genes & Development*, 12, 3499-3511.
- DILLY, A. K. & RAJALA, R. V. S. 2008. Insulin Growth Factor 1 Receptor/PI3K/AKT Survival Pathway in Outer Segment Membranes of Rod Photoreceptors. *Investigative Ophthalmology & Visual Science*, 49, 4765-4773.
- DONATO, R., MILJAN, E., HINES, S., AOUABDI, S., POLLOCK, K., PATEL, S., EDWARDS, F. & SINDEN, J. 2007. Differential development of neuronal physiological responsiveness in two human neural stem cell lines. *BMC Neuroscience*, 8, 36.
- DRABSCH, Y., HUGO, H., ZHANG, R., DOWHAN, D. H., MIAO, Y. R., GEWIRTZ, A. M., BARRY, S. C., RAMSAY, R. G. & GONDA, T. J. 2007. Mechanism of and requirement for estrogen-regulated MYB expression in estrogen-receptor-positive breast cancer cells. *Proceedings of the National Academy of Sciences*, 104, 13762-13767.
- DUPONT, S., MAMIDI, A., CORDENONSI, M., MONTAGNER, M., ZACCHIGNA, L., ADORNO, M., MARTELLO, G., STINCHFIELD, M. J., SOLIGO, S., MORSUT, L., INUI, M., MORO, S., MODENA, N., ARGENTON, F., NEWFELD, S. J. & PICCOLO, S. 2009. FAM/USP9x, a Deubiquitinating Enzyme Essential for TGF $\beta$  Signaling, Controls Smad4 Monoubiquitination. *Cell*, 136, 123-135.
- ELLIS, P., FAGAN, B., MAGNESS, S., HUTTON, S., TARANOVA, O., HAYASHI, S., MCMAHON, A., RAO, M. & PEVNY, L. 2004. SOX2, a persistent marker for multipotential neural stem cells derived from embryonic stem cells, the embryo or adult. *Dev Neurosci*, 26, 148-165.
- ESHLEMAN, J. S., CARLSON, B. L., MLADEK, A. C., KASTNER, B. D., SHIDE, K. L. & SARKARIA, J. N. 2002. Inhibition of the Mammalian Target of Rapamycin Sensitizes U87 Xenografts to Fractionated Radiation Therapy. *Cancer Research*, 62, 7291-7297.
- FANG, S., LORICK, K. L., JENSEN, J. P. & WEISSMAN, A. M. 2003. RING finger ubiquitin protein ligases: implications for tumorigenesis, metastasis and for molecular targets in cancer. *Seminars in Cancer Biol.*, 13, 5-14.
- FINGAR, D. C., RICHARDSON, C. J., TEE, A. R., CHEATHAM, L., TSOU, C. & BLENIS, J. 2004. mTOR Controls Cell Cycle Progression through Its Cell Growth Effectors S6K1 and 4E-BP1/Eukaryotic Translation Initiation Factor 4E. *Molecular and Cellular Biology*, 24, 200-216.
- FISHER, G. H., WELLEN, S. L., KLIMSTRA, D., LENCZOWSKI, J. M., TICHELAAR, J. W., LIZAK, M. J., WHITSETT, J. A., KORETSKY, A. & VARMUS, H. E. 2001. Induction and apoptotic regression of lung adenocarcinomas by regulation of a K-Ras transgene in the presence and absence of tumor suppressor genes. *Genes & Development*, 15, 3249-3262.
- FLEMING, H. E., JANZEN, V., LO CELSO, C., GUO, J., LEAHY, K. M., KRONENBERG, H. M. & SCADDEN, D. T. 2008. Wnt Signaling in the Niche Enforces Hematopoietic Stem Cell Quiescence and Is Necessary to Preserve Self-Renewal In Vivo. *Cell Stem Cell*, 2, 274-283.
- FOSTER, K., ACOUSTA-JAQUEZ, H., ROMEO, Y., EKIM, B., SOLIMAN, G., ROUX, P., BALLIF, B. & FINGAR, D. 2010. Regulation of mTOR complex 1 by raptor Ser863 and multisite phosphorylation. *J. Biol. Chem*, 285, 80-94.
- FRIEDMAN, H. S., KERBY, T. & CALVERT, H. 2000. Temozolomide and Treatment of Malignant Glioma. *Clinical Cancer Research*, 6, 2585-2597.
- FRIOCOURT, G., KAPPELER, C., SAILLOUR, Y., FAUCHEREAU, F., RODRIGUEZ, M. S., BAHI, N., VINET, M.-C., CHAFEY, P., POIRIER, K., TAYA, S., WOOD, S. A., DARGEMONT, C., FRANCIS, F. & CHELLY, J. 2005. Doublecortin interacts with the ubiquitin protease DFFRX, which associates with microtubules in neuronal processes. *Molecular and Cellular Neuroscience*, 28, 153-164.
- FROGER, A. & HALL, J. E. 2007. Transformation of Plasmid DNA into E. coli Using the Heat Shock Method. *Journal of Visualized Experiments : JoVE*, 253.

- FRUMAN, D. A., MEYERS, R. E. & CANTLEY, L. C. 1998. PHOSPHOINOSITIDE KINASES. *Annual Review of Biochemistry*, 67, 481-507.
- GALAN-MOYA, E. M., LE GUELTE, A., LIMA-FERNANDES, E., THIRANT, C., DWYER, J., BIDERE, N., COURAUD, P.-O., SCOTT, M. G. H., JUNIER, M.-P., CHNEIWEISS, H. & GAVARD, J. 2011. Secreted factors from brain endothelial cells maintain glioblastoma stem-like cell expansion through the mTOR pathway. *EMBO Rep*, 12, 470-476.
- GALANTI, G. F. T., I, K., SHOHAM, J., GALLILY, R., MECHOULAM, R., LAVIE, G., N, A., G, R. & A, T. 2008. Delta 9-tetrahydrocannabinol inhibits cell cycle progression by downregulation of E2F1 in human glioblastoma multiforme cells. *Acta Oncol*, 47, 1062-1067.
- GARCÍA-GARCÍA, E., PINO-BARRIO, M., LÓPEZ-MEDINA, L. & MARTÍNEZ-SERRANO, A. 2012. Intermediate progenitors are increased by lengthening of the cell cycle through calcium signaling and p53 expression in human neural progenitors. *Molecular Biology of the Cell*, 12, 1167-1180.
- GERDES, J., LEMKE, H., BAISCH, H., WACKER, H., SCHWAB, U. & STEIN, H. 1984. Cell cycle analysis of a cell proliferation-associated human nuclear antigen defined by the monoclonal antibody Ki-67. *Journal of Immunology*, 133, 1710-5.
- GERMAIN, D., RUSSELL, A., THOMPSON, A. & HENDLEY, J. 2000. Ubiquitination of Free Cyclin D1 Is Independent of Phosphorylation on Threonine 286. *Journal of Biological Chemistry*, 275, 12074-12079.
- GHAZI, S. O., STARK, M., ZHAO, Z., MOBLEY, B. C., MUNDEN, A., HOVER, L. & ABEL, T. W. 2012. Cell of Origin Determines Tumor Phenotype in an Oncogenic Ras/p53 Knockout Transgenic Model of High-Grade Glioma. *Journal of neuropathology and experimental neurology*, 71, 729-740.
- GHOSH P, WU M, ZHANG H & SUN H 2008. mTORC1 signaling requires proteasomal function and the involvement of CUL4-DDB1 ubiquitin E3 ligase. . *Cell Cycle*, 7, 373-381.
- GORSKI, J. A., TALLEY, T., QIU, M., PUELLES, L., RUBENSTEIN, J. L. R. & JONES, K. R. 2002. Cortical Excitatory Neurons and Glia, But Not GABAergic Neurons, Are Produced in the Emx1-Expressing Lineage. *The Journal of Neuroscience*, 22, 6309-6314.
- GÖTZ, M. & HUTTNER, W. B. 2005. The cell biology of neurogenesis. *Nature Reviews*, 6, 777-788.
- GUHA, A., FELDKAMP, M., LAU, N., BOSS, G. & PAWSON, A. 1997. Proliferation of human malignant astrocytomas is dependent on Ras activation. *Onogene*, 15, 2755-2765.
- GULATI, N., KARSY, M., ALBERT, L., MURALI, R. & JHANWAR-UNIYAL, M. 2009. Involvement of mTORC1 and mTORC2 in regulation of glioblastoma multiforme growth and motility. *International Journal of Oncology*, 35, 731-740.
- GUO, H., HONG, S., JIN, X.-L., CHEN, R.-S., AVASTHI, P. P., TU, Y.-T., IVANCO, T. L. & LI, Y. 2000. Specificity and Efficiency of Cre-Mediated Recombination in Emx1-cre Knock-in Mice. *Biochemical and Biophysical Research Communications*, 273, 661-665.
- GWALTER, J., WANG, M. L. & GOUT, I. 2009. The ubiquitination of ribosomal S6 kinases is independent from the mitogen-induced phosphorylation/activation of the kinase. *The International Journal of Biochemistry & Cell Biology*, 41, 828-833.
- HAGLUND, K. & DIKIC, I. 2005. Ubiquitylation and cell signaling. *Embo Journal*, 24, 3353-3359.
- HARA, K., MARUKI, Y., LONG, X., YOSHINO, K., OSHIRO, N., HIDAYAT, S., TOKUNAGA, C., AVRUCH, J. & YONEZAWA, K. 2002. Raptor, a Binding Partner of Target of Rapamycin (TOR), Mediates TOR Action. *Cell*, 110, 177-189.
- HARA, K., YONEZAWA, K., WENG, Q.-P., KOZLOWSKI, M. T., BELHAM, C. & AVRUCH, J. 1998. Amino Acid Sufficiency and mTOR Regulate p70 S6 Kinase and eIF-4E BP1 through a Common Effector Mechanism. *Journal of Biological Chemistry*, 273, 14484-14494.
- HAYAKAWA, Y., HIRATA, Y., NAKAGAWA, H., SAKAMOTO, K., HIKIBA, Y., KINOSHITA, H., NAKATA, W., TAKAHASHI, R., TATEISHI, K., TADA, M., AKANUMA, M., YOSHIDA, H., TAKEDA, K., ICHIJO, H., OMATA, M., MAEDA, S. & KOIKE, K. 2010. Apoptosis signal-regulating kinase 1 and cyclin D1 compose a positive feedback loop contributing to tumor growth in gastric cancer. *Proceedings of the National Academy of Sciences*, 108, 780-785.
- HAYFLICK, L. 1965. The limited in vitro lifetime of human diploid cell strains. *Experimental Cell Research*, 37, 614-636.

- HERSHKO, A. & CIECHANOVER, A. 1998. The Ubiquitin System. *Ann. Review of Biochem.*, 67, 425-479.
- HOGARTY, M. 2010. Mcl1 becomes ubiquitin-ous: new opportunities to antagonize a pro-survival protein. *Cell Research*, 4, 391-393.
- HOLLAND, E. C., CELESTINO, J., DAI, C., SCHAEFER, L., SAWAYA, R. E. & FULLER, G. N. 2000. Combined activation of Ras and Akt in neural progenitors induces glioblastoma formation in mice. *Nat Genet*, 25, 55-57.
- HOLMEN, S. L. & WILLIAMS, B. O. 2005. Essential Role for Ras Signaling in Glioblastoma Maintenance. *Cancer Research*, 65, 8250-8255.
- HOMAN, C. C., KUMAR, R., NGUYEN, L. S., HAAN, E., RAYMOND, F. L., ABIDI, F., RAYNAUD, M., SCHWARTZ, C. E., WOOD, S. A., GECZ, J. & JOLLY, L. A. 2014. Mutations in USP9X Are Associated with X-Linked Intellectual Disability and Disrupt Neuronal Cell Migration and Growth. *American Journal of Human Genetics*, 94, 470-478.
- HOSHII, T., KASADA, A., HATAKEYAMA, T., OHTANI, M., TADOKORO, Y., NAKA, K., IKENOUE, T., IKAWA, T., KAWAMOTO, H., FEHLING, H. J., ARAKI, K., YAMAMURA, K.-I., MATSUDA, S. & HIRAO, A. 2014. Loss of mTOR complex 1 induces developmental blockage in early T-lymphopoiesis and eradicates T-cell acute lymphoblastic leukemia cells. *Proceedings of the National Academy of Sciences of the United States of America*, 111, 3805-3810.
- HOSHII, T., TADOKORO, Y., NAKA, K., OOSHIO, T., MURAGUCHI, T., SUGIYAMA, N., SOGA, T., ARAKI, K., YAMAMURA, K.-I. & HIRAO, A. 2012. mTORC1 is essential for leukemia propagation but not stem cell self-renewal. *The Journal of Clinical Investigation*, 122, 2114-2129.
- HUSE, J. T. & HOLLAND, E. C. 2010. Targeting brain cancer: advances in the molecular pathology of malignant glioma and medulloblastoma. *Nat Rev Cancer*, 10, 319-331.
- HUSSAIN, S., FELDMAN, A., DAS, C., ZIESMER, S., ANSELL, S. & GALARDY, P. 2013. Ubiquitin hydrolase UCH-L1 destabilises mTOR complex 1 by antagonising DDB-CUL4-mediated ubiquitination of Raptor. *Mol. Cell. Biol.*, 33, 1188-1197.
- INOKI, K., LI, Y., ZHU, T., WU, J. & GUAN, K.-L. 2002. TSC2 is phosphorylated and inhibited by Akt and suppresses mTOR signalling. *Nat Cell Biol*, 4, 648-657.
- INOSHITA, S., TERADA, Y., NAKASHIMA, O., KUWAHARA, M., SASAKI, S. & MARUMO, F. 1999. Regulation of the G1/S transition phase in mesangial cells by E2F1. *Kidney Int*, 56, 1238-1241.
- JACKSON, E. L., WILLIS, N., MERCER, K., BRONSON, R. T., CROWLEY, D., MONTOYA, R., JACKS, T. & TUVESON, D. A. 2001. Analysis of lung tumor initiation and progression using conditional expression of oncogenic K-ras. *Genes & Development*, 15, 3243-3248.
- JACOBS, V., VALDES, P., HICKEY, W., DE-LEO, J. Current review of in vivo GBM rodent models: emphasis on the CNS-1 Tumour Model. *ASN Neuro*. 3, 171-181.
- JEFFERIES, H. B. J., FUMAGALLI, S., DENNIS, P. B., REINHARD, C., PEARSON, R. B. & THOMAS, G. 1997. Rapamycin suppresses 5[prime]TOP mRNA translation through inhibition of p70s6k. *EMBO J*, 16, 3693-3704.
- JENSEN, J. & PARMAR, M. 2006. Strengths and limitations of the neurosphere culture system. *Molecular Neurobiology*, 34, 153-161.
- JIN, K., PEEL, A. L., MAO, X. O., XIE, L., COTTRELL, B. A., HENSHALL, D. C. & GREENBERG, D. A. 2004. Increased hippocampal neurogenesis in Alzheimer's disease. *Proceedings of the National Academy of Sciences of the United States of America*, 101, 343-347.
- JOHNSON, L., GREENBAUM, D., CICHOWSKI, K., MERCER, K., MURPHY, E., SCHMITT, E., BRONSON, R. T., UMANOFF, H., EDELMANN, W., KUCHERLAPATI, R. & JACKS, T. 1997. K-ras is an essential gene in the mouse with partial functional overlap with N-ras. *Genes & Development*, 11, 2468-2481.
- JOHNSON, L., MERCER, K., GREENBAUM, D., BRONSON, R. T., CROWLEY, D., TUVESON, D. A. & JACKS, T. 2001. Somatic activation of the K-ras oncogene causes early onset lung cancer in mice. *Nature*, 410, 1111-1116.

- JOLLY, L. A., TAYLOR, V. & WOOD, S. A. 2009. USP9X Enhances the Polarity and Self-Renewal of Embryonic Stem Cell-derived Neural Progenitors. *Mol. Biol. Cell*, 20, 2015-2029.
- KAHN, J., HAYMAN, T., JAMAL, M., RATH, B., KRAMP, T., CAMPHAUSEN, K., TOFILON, P. & CELLS, T. M. M. I. A. E. T. R. S. O. G. S.-L. 2014. The mTORC1/mTORC2 inhibitor AZD2014 enhances the radio sensitivity of glioblastoma stem-like cells. *Neuro Oncology*, 16, 29-37.
- KALDIS, P. & PAGANO, M. 2009. Wnt Signaling in Mitosis. *Developmental Cell*, 17, 749-750.
- KAWASOME, H., PAPST, P., WEBB, S., KELLER, G. M., JOHNSON, G. L., GELFAND, E. W. & TERADA, N. 1998. Targeted disruption of p70s6k defines its role in protein synthesis and rapamycin sensitivity. *Proceedings of the National Academy of Sciences*, 95, 5033-5038.
- KHAPRE, R., PATEL, S., KONDRATOVA, A., CHAUDHARY, A., NIKKHIL, V., ANTOCH, M. & KONDRATOV, R. 2014. Metabolic clock generates nutrient anticipation rhythms in mTOR signalling. *Aging*, 6, 675-689.
- KINGSBURY, S. R., LODDO, M., FANSHAW, T., OBERMANN, E. C., PREVOST, A. T., STOEGER, K. & WILLIAMS, G. H. 2005. Repression of DNA replication licensing in quiescence is independent of geminin and may define the cell cycle state of progenitor cells. *Experimental Cell Research*, 309, 56-67.
- KIRSTETTER, P., ANDERSON, K., PORSE, B. T., JACOBSEN, S. E. W. & NERLOV, C. 2006. Activation of the canonical Wnt pathway leads to loss of hematopoietic stem cell repopulation and multilineage differentiation block. *Nat Immunol*, 7, 1048-1056.
- KNOWLES, M., PLATT, F., ROSS, R. & HURST, C. 2009. Phosphatidylinositol 3-kinase (PI3K) pathway activation in bladder cancer. *Cancer and Metastasis Reviews*, 28, 305-316.
- KOSO, H., TAKEDA, H., YEW, C. C. K., WARD, J. M., NARIAI, N., UENO, K., NAGASAKI, M., WATANABE, S., RUST, A. G., ADAMS, D. J., COPELAND, N. G. & JENKINS, N. A. 2012. Transposon mutagenesis identifies genes that transform neural stem cells into glioma-initiating cells. *Proceedings of the National Academy of Sciences*, 109, E2998-E3007.
- LAPLANTE, M. & SABATINI, D. M. 2009. mTOR signaling at a glance. *Journal of Cell Science*, 122, 3589-3594.
- LEONTIEVA, O., DEMIDENKO, Z. & MV, B. 2014. Rapamycin reverses insulin resistance (IR) in high-glucose medium without causing IR in normoglycemic medium. *Cell Death and Disease*, 5, e1214.
- LEONTIEVA, O. V., PASZKIEWICZ, G. M. & BLAGOSKLONNY, M. V. 2012. Mechanistic or mammalian target of rapamycin (mTOR) may determine robustness in young male mice at the cost of accelerated aging *Aging*, 4, 899-916.
- LI, L. & BHATIA, R. 2011. Stem Cell Quiescence. *Clinical Cancer Research*, 17, 4936-4941.
- LI, M. & ZHANG, P. 2009. The function of APC/CCdh1 in cell cycle and beyond. *Cell Division*, 4, 2.
- LI, Q. R., XING, X. B., CHEN, T. T., LI, R. X., DAI, J., SHENG, Q. H., XIN, S. M., ZHU, L. L., JIN, Y., PEI, G., KANG, J. H., LI, Y. X. & ZENG, R. 2011. Large Scale Phosphoproteome Profiles Comprehensive Features of Mouse Embryonic Stem Cells. *Molecular & Cellular Proteomics*, 10, -.
- LIANG, M.-C., MA, J., CHEN, L., KOZLOWSKI, P., QIN, W., LI, D., SHIMAMURA, T., THOMAS, R. K., HAYES, D. N., MEYERSON, M., KWIATKOWSKI, D. J. & WONG, K.-K. 2010. TSC1 loss synergizes with KRAS activation in lung cancer development in the mouse and confers rapamycin sensitivity. *Oncogene*, 29, 1588-1597.
- LIN, D., BARBASH, O., SURESH KUMAR, K., WEBER, J., WADE HARPER, J., KLEIN-SZANTO, A., RUSTGI, A., FUCHS, S. & DIEHL, A. 2006. Phosphorylation-dependent ubiquitination of cyclin D1 by the SCF-FBX4-acrystallin complex. *Mol Cell*, 24, 355-366.
- LINARES, JUAN F., DURAN, A., YAJIMA, T., PASPARAKIS, M., MOSCAT, J. & DIAZ-MECO, MARIA T. 2014. K63 Polyubiquitination and Activation of mTOR by the p62-TRAF6 Complex in Nutrient-Activated Cells. *Molecular Cell*, 51, 283-296.
- LIU, X., JAKUBOWSKI, M. & HUNT, J. 2015. KRAS Gene Mutation in Colorectal Cancer Is Correlated With Increased Proliferation and Spontaneous Apoptosis. *Journal of clinical pathology*, 68.

- LU, W., LAN, F., HE, Q., LEE, A., TANG, C., DONG, L., LAN, B., MA, X., WU, J. & SHEN, L. 2011. Inducible expression of stem cell associated intermediate filament nestin reveals an important role in glioblastoma carcinogenesis. *Int J Cancer*, 128, 343-351.
- MA, Y., WEI, S., LIN, Y., LUNG, J., CHANG, T., WHANG-PENG, J., LIU, J. M., YANG, D., YANG, W. & SHEN, C. 2000. PIK3CA as an oncogene in cervical cancer. *Oncogene*, 19, 2739-2744.
- MAGRI, L. & GALLI, R. 2012. mTOR signaling in neural stem cells: from basic biology to disease. *Cellular and Molecular Life Sciences*, 1-12.
- MAGRI, L. & GALLI, R. 2013. mTOR signaling in neural stem cells: from basic biology to disease. *Cellular and Molecular Life Sciences*, 70, 2887-2898.
- MALATESTA, P., HARTFUSS, E. & GÖTZ, M. 2000. Isolation of radial glial cells by fluorescent-activated cell sorting reveals a neuronal lineage. *Development*, 127, 5253-5263.
- MALTZMAN, T., MUELLER, B., SCHROEDER, J., RUTLEDGE, J., PATTERSON, K., PRESTON-MARTIN, S. & FAUSTMAN, E. 1997. Ras oncogene mutations in childhood brain tumors. *Cancer Epidemiol Biomarkers Prev*, 6, 239-43.
- MAMBER, C., KAMPHUIS, W., HARING, N. L., PEPRAH, N., MIDDELDORP, J. & HOL, E. M. 2012. GFAP $\delta$  Expression in Glia of the Developmental and Adolescent Mouse Brain. *PLoS ONE*, 7, e52659.
- MARKIEWICZ-ZUKOWSKA, R., BORAWSKA, M., FIEDOROWICZ, A., NALIWAJKO, S., SAWICKA, D. & CAR, H. 2013. Propolis changes the anticancer activity of temozolomide in U87MG human glioblastoma cell line. *BMC Complementary and Alternative Medicine*, 13, 50.
- MARTÍNEZ-CERDEN, V., NOCTOR, S. & KRIEGSTEIN, A. 2006. The Role of Intermediate Progenitor Cells in the Evolutionary Expansion of the Cerebral Cortex. *Cerebral Cortex*, 16.
- MARTINEZ, R. & ESTELLER, M. 2010. The DNA methylome of glioblastoma multiforme. *Neurobiol Dis*, 39, 40-6.
- MARUMOTO, T., TASHIRO, A., FRIEDMANN-MORVINSKI, D., SCADENG, M., SODA, Y., GAGE, F. & VERMA, I. 2009. Development of a novel mouse glioma model using lentiviral vectors. *Nature Medicine*, 15, 110-116.
- MENG, L., MOHAN, R., KWOK, B. H. B., ELOFSSON, M., SIN, N. & CREWS, C. M. 1999. Epoxomicin, a potent and selective proteasome inhibitor, exhibits in vivo antiinflammatory activity. *Proceedings of the National Academy of Sciences*, 96, 10403-10408.
- MERTZ, J., TAN, H., PAGALA, V., BAI, B., CHEN, P., LI, Y., CHO, J., SHAW, T., WANG, X., PENG, J. & OUTGROWTH, S. E. I. A. O. T. M. B. U. L. R. A. N. R. I. D. S. 2015. Sequential elution interactome analysis of the Mind bomb 1 ubiquitin ligase reveals a novel role in dendritic spine outgrowth. *Mol Cell Proteomics*, 14, 1898-910.
- MEULMEESTER, E. & DIJKE, P. 2011. The dynamic roles of TGF- $\beta$  in cancer. *The Journal of Pathology*, 223, 206-219.
- MITTNACHT, S. P., H & OLSON, M. M., C 1997. Ras signalling is required for inactivation of the tumour suppressor pRb cell-cycle control protein. *Curr Biol*, 7, 219-220.
- MOLINA, J. R. & ADJEI, A. A. 2006. The Ras/Raf/MAPK Pathway. *Journal of Thoracic Oncology*, 1, 7-9.
- MOON, B.-S., JEONG, W.-J., PARK, J., KIM, T. I., MIN, D. S. & CHOI, K.-Y. 2014. Role of Oncogenic K-Ras in Cancer Stem Cell Activation by Aberrant Wnt/ $\beta$ -Catenin Signaling. *Journal of the National Cancer Institute*, 106.
- MORTON, J. P., TIMPSON, P., KARIM, S. A., RIDGWAY, R. A., ATHINEOS, D., DOYLE, B., JAMIESON, N. B., OIEN, K. A., LOWY, A. M., BRUNTON, V. G., FRAME, M. C., EVANS, T. R. J. & SANSOM, O. J. 2010. Mutant p53 drives metastasis and overcomes growth arrest/senescence in pancreatic cancer. *Proceedings of the National Academy of Sciences of the United States of America*, 107, 246-251.
- MOUCHANTAF, R., AZAKIR, B., MCPHERSON, P., MILLARD, S., WOOD, S. & ANGERS, A. 2006. The Ubiquitin Ligase Itch Is Auto-ubiquitylated in Vivo and in Vitro but Is Protected from Degradation by Interacting with the Deubiquitylating Enzyme FAM/USP9X. *Journal of Biochemistry*, 281, 38738-38747.

- MUÑOZ, D. M. & HAWKINS, C. 2014. Developmental stage-specific transformation of neural progenitors. *Cell Cycle*, 13, 343-344.
- MURTAZA, M., JOLLY, L. A., GECZ, J. & WOOD, S. A. 2015. La FAM fatale: USP9X in development and disease. *Cellular and Molecular Life Sciences*, 72, 2075-2089.
- NAGAI, H., NOGUCHI, T., HOMMA, K., KATAGIRI, K., TAKEDA, K., MATSUZAWA, A. & ICHIJO, H. 2009. Ubiquitin-like Sequence in ASK1 Plays Critical Roles in the Recognition and Stabilization by USP9X and Oxidative Stress-Induced Cell Death. *Molecular Cell*, 36, 805-818.
- NOGUEIRA, L., RUIZ-ONTANON, P., VAZQUEZ-BARQUERO, A., LAFARGA, M., BERCIANO, M., ALDAZ, B., GRANDE, L., CASAFONT, I., SEGURA, V., ROBLES, E., SUAREZ, D., GARCIA, L., MARTINEZ-CLIMENT, J. & FERNANDEZ-LUNA, J. 2011. Blockade of the NFkB pathway drives differentiating glioblastoma initiating cells into senescence both in vitro and in vivo. *Oncogene*, 30, 3537-48.
- NOJIMA, H., TOKUNAGA, C., EGUCHI, S., OSHIRO, N., HIDAYAT, S., YOSHINO, K., HARA, K., TANAKA, N., AVRUCH, J. & YONEZAWA, K. 2003. The Mammalian Target of Rapamycin (mTOR) Partner, Raptor, Binds the mTOR Substrates p70 S6 Kinase and 4E-BP1 through Their TOR Signaling (TOS) Motif. *Journal of Biological Chemistry*, 278, 15461-15464.
- OHGAKI, H. & KLEIHUES, P. 2007. Genetic pathways to primary and secondary glioblastoma. *American Journal of Pathology*, 170.
- PALIOURAS, G. N., HAMILTON, L. K., AUMONT, A., JOPPÉ, S. E., BARNABÉ-HEIDER, F. & FERNANDES, K. J. L. 2012. Mammalian Target of Rapamycin Signaling Is a Key Regulator of the Transit-Amplifying Progenitor Pool in the Adult and Aging Forebrain. *The Journal of Neuroscience*, 32, 15012-15026.
- PAMARTHY, D., TAN, M., WU, M., CHEN, J., YANG, D., WANG, S., ZHANG, H. & SUN, Y. 2007. p27 degradation by an ellipticine series of compound via ubiquitin-proteasome pathway. *Cancer Biol Ther*, 6, 360-366.
- PARDEE, A. 1974. A restriction point for control of normal animal cell proliferation. *Proc Natl Acad Sci USA*, 71, 1286-90.
- PARK, Y., JIN, H.-S. & LIU, Y.-C. 2013. Regulation of T cell function by the ubiquitin-specific protease USP9X via modulating the Carma1-Bcl10-Malt1 complex. *Proceedings of the National Academy of Sciences*, 110, 9433-9438.
- PAVON, L. F., MARTI, L. C., SIBOV, T. T., MALHEIROS, S. M. F., BRANDT, R. A., CAVALHEIRO, S., & GAMARRA, L. F. (2013). In vitro Analysis of Neurospheres Derived from Glioblastoma Primary Culture: A Novel Methodology Paradigm. *Frontiers in Neurology*, 4, 214.
- PÉREZ-MANCERA, P. A., RUST, A. G., VAN DER WEYDEN, L., KRISTIANSEN, G., LI, A., SARVER, A. L., SILVERSTEIN, K. A. T., GRÜTZMANN, R., AUST, D., RÜMMELE, P., KNÖSEL, T., HERD, C., STEMPLE, D. L., KETTLEBOROUGH, R., BROSNAN, J. A., LI, A., MORGAN, R., KNIGHT, S., YU, J., STEGEMAN, S., COLLIER, L. S., TEN HOEVE, J. J., DE RIDDER, J., KLEIN, A. P., GOGGINS, M., HRUBAN, R. H., CHANG, D. K., BIANKIN, A. V., GRIMMOND, S. M., APGI, WESSELS, L. F. A., WOOD, S. A., IACOBUZIO-DONAHUE, C. A., PILARSKY, C., LARGAESPADA, D. A., ADAMS, D. J. & TUVESON, D. A. 2012. The deubiquitinase USP9X suppresses pancreatic ductal adenocarcinoma. *Nature*, 486, 266-270.
- PEREZ-MANCERA, P. A., RUST, A. G., VAN DER WEYDEN, L., KRISTIANSEN, G., LI, A., SARVER, A. L., SILVERSTEIN, K. A. T., GRUTZMANN, R., AUST, D., RUMMELE, P., KNOSEL, T., HERD, C., STEMPLE, D. L., KETTLEBOROUGH, R., BROSNAN, J. A., LI, A., MORGAN, R., KNIGHT, S., YU, J., STEGEMAN, S., COLLIER, L. S., TEN HOEVE, J. J., DE RIDDER, J., KLEIN, A. P., GOGGINS, M., HRUBAN, R. H., CHANG, D. K., BIANKIN, A. V., GRIMMOND, S. M., WESSELS, L. F. A., WOOD, S. A., IACOBUZIO-DONAHUE, C. A., PILARSKY, C., LARGAESPADA, D. A., ADAMS, D. J. & TUVESON, D. A. 2012. The deubiquitinase USP9X suppresses pancreatic ductal adenocarcinoma. *Nature*, advance online publication.

- PETERSON, L. F., SUN, H., LIU, Y., POTU, H., KANDARPA, M., ERMANN, M., COURTNEY, S. M., YOUNG, M., SHOWALTER, H. D., SUN, D., JAKUBOWIAK, A., MALEK, S. N., TALPAZ, M. & DONATO, N. J. 2015. *Targeting deubiquitinase activity with a novel small-molecule inhibitor as therapy for B-cell malignancies.*
- PICKART, C. M. & FUSHMAN, D. 2004. Polyubiquitin chains: polymeric protein signals. *Current Opinion in Chem. Biol.*, 8, 610-616.
- PIETRAS, E., WARR, M. & PASSEGUE, E. 2011. Cell cycle regulation in hematopoietic stem cells. *The Journal of Cell Biology*, 195, 709-720.
- PIVA, R., CANCELLI, I., CAVALLA, P., BORTOLOTTI, S., DOMINGUEZ, J., DRAETTA, G. & SCHIFFER, D. 1999. Proteasome-dependent degradation of p27/kip1 in gliomas. *Journal of Neuropathol Exp Neurol*, 58, 691-696.
- POLLOCK, C., SHIRASAWA, S., SASAZUKI, T., KOLCH, W. & DHILLON, A. 2004. Oncogenic K-RAS Is Required to Maintain Changes in Cytoskeletal Organization, Adhesion, and Motility in Colon Cancer Cells. *Journal of Cancer research*.
- POLO, S. E., THEOCHARIS, S. E., KLIJANIENKO, J., SAVIGNONI, A., ASSELAINE, B., VIELH, P. & ALMOUZNI, G. 2004. Chromatin Assembly Factor-1, a Marker of Clinical Value to Distinguish Quiescent from Proliferating Cells. *Cancer Research*, 64, 2371-2381.
- POTENZA, N., VECCHIONE, C., NOTTE, A., DE RIENZO, A., ROSICA, A., BAUER, L. & DI LAURO, R. 2005. Replacement of K-Ras with H-Ras supports normal embryonic development despite inducing cardiovascular pathology in adult mice. *EMBO Reports*, 6, 432-437.
- QIANG, L., YANG, Y., MA, Y.-J., CHEN, F.-H., ZHANG, L.-B., LIU, W., QI, Q., LU, N., TAO, L., WANG, X.-T., YOU, Q.-D. & GUO, Q.-L. 2009. Isolation and characterization of cancer stem like cells in human glioblastoma cell lines. *Cancer Letters*, 279, 13-21.
- QIAO, G., LI, Q., PENG, G., MA, J., FAN, H. & LI, Y. 2013. Similarity on neural stem cells and brain tumor stem cells in transgenic brain tumor mouse models. *Neural Regeneration Research*, 8, 2360-2369.
- RAMAKRISHNA, S., SURESH, B. & BAEK, K. H. 2011. The role of deubiquitinating enzymes in apoptosis. *Cell. and Mol. Life Sci.*, 68, 15-26.
- REIF, A., FRITZEN, S., FINGER, M., STROBEL, A., LAUER, M., SCHMITT, A. & LESCH, K. P. 2006. Neural stem cell proliferation is decreased in schizophrenia, but not in depression. *Mol Psychiatry*, 11, 514-522.
- REYNOLDS, BA, WEISS, S. 1992. Generation of neurons and astrocytes from isolated cells of the adult mammalian central nervous system. *Science*. 27, 255.
- RODGERS, J. T., KING, K. Y., BRETT, J. O., CROMIE, M. J., CHARVILLE, G. W., MAGUIRE, K. K., BRUNSON, C., MASTHEY, N., LIU, L., TSAI, C.-R., GOODELL, M. A. & RANDO, T. A. 2014. mTORC1 controls the adaptive transition of quiescent stem cells from G0 to GAlert. *Nature*, 510, 393-396.
- RUSSELL, R. C., FANG, C. & GUAN, K.-L. 2011. An emerging role for TOR signaling in mammalian tissue and stem cell physiology. *Development*, 138, 3343-3356.
- SAMBROOK, J., FRITSCH, E. F. & MANIATIS, T. 1989. *Molecular Cloning: A Laboratory Manual*, Cold Spring Harbor, Cold Spring Harbor Laboratory Press.
- SANDBERG, C. J., ALTSCHULER, G., JEONG, J., STRØMME, K. K., STANGELAND, B., MURRELL, W., GRASMO-WENDLER, U.-H., MYKLEBOST, O., HELSETH, E., VIKMO, E. O., HIDE, W. & LANGMOEN, I. A. 2013. Comparison of glioma stem cells to neural stem cells from the adult human brain identifies dysregulated Wnt- signaling and a fingerprint associated with clinical outcome. *Experimental Cell Research*, 319, 2230-2243.
- SASAKI, H., HIKOSAKA, Y., KAWANO, O., MORIYAMA, S., YANO, M. & FUJII, Y. 2011. Evaluation of Kras Gene Mutation and Copy Number Gain in Non-small Cell Lung Cancer. *Journal of Thoracic Oncology*, 6, 15-20.
- SATO, A., SUNAYAMA, J., MATSUDA, K.-I., TACHIBANA, K., SAKURADA, K., TOMIYAMA, A., KAYAMA, T. & KITANAKA, C. 2010. Regulation of neural stem/progenitor cell maintenance by PI3K and mTOR. *Neuroscience Letters*, 470, 115-120.
- SCHEFFER, I. E., HERON, S. E., REGAN, B. M., MANDELSTAM, S., CROMPTON, D. E., HODGSON, B. L., LICCHETTA, L., PROVINI, F., BISULLI, F., VADLAMUDI, L., GECZ,

- J., CONNELLY, A., TINUPER, P., RICOS, M. G., BERKOVIC, S. F. & DIBBENS, L. M. 2014. Mutations in mammalian target of rapamycin regulator DEPDC5 cause focal epilepsy with brain malformations. *Annals of Neurology*, 75, 782-787.
- SCHIFFER, D., CAVALLA, P., FIANO, V., GHIMENTI, C. & PIVA, R. 2002. Inverse relationship between p27/Kip.1 and F-box protein Skp2 in human astrocytoma gliomas by immunohistochemistry and western blot. *Neurosci Lett*, 328, 125-128.
- SCHWICKART, M., HUANG, X., LILL, J. R., LIU, J., FERRANDO, R., FRENCH, D. M., MAECKER, H., O'ROURKE, K., BAZAN, F., EASTHAM-ANDERSON, J., YUE, P., DORNAN, D., HUANG, D. C. S. & DIXIT, V. M. 2010. Deubiquitinase USP9X stabilizes MCL1 and promotes tumour cell survival. *Nature*, 463, 103-107.
- SHAH, B. H., NEITHARDT, A., CHU, D. B., SHAH, F. B. & CATT, K. J. 2006. Role of EGF receptor transactivation in phosphoinositide 3-kinase-dependent activation of MAP kinase by GPCRs. *Journal of Cellular Physiology*, 206, 47-57.
- SHAN, J., ZHAO, W. & GU, W. 2009. Suppression of Cancer Cell Growth by Promoting Cyclin D1 Degradation. *Molecular Cell*, 36, 469-476.
- SHAYESTEH, L., LU, Y., KUO, W.-L., BALDOCCHI, R., GODFREY, T., COLLINS, C., PINKEL, D., POWELL, B., MILLS, G. B. & GRAY, J. W. 1999. PIK3CA is implicated as an oncogene in ovarian cancer. *Nat Genet*, 21, 99-102.
- SHI, S. R., CHAIWUN, B., YOUNG, L., COTE, R. J. & TAYLOR, C. R. 1993. Antigen retrieval technique utilizing citrate buffer or urea solution for immunohistochemical demonstration of androgen receptor in formalin-fixed paraffin sections. *Journal of Histochemistry & Cytochemistry*, 41, 1599-604.
- SHI, Z., QIAN, X., LI, L., ZHANG, J., ZHU, S., ZHU, J., CHEN, L., ZHANG, K., HAN, L., YU, S., PU, P., JIANG, T. & KANG, C. 2012. Nuclear Translocation of  $\beta$ -catenin is Essential for Glioma Cell Survival. *Journal of Neuroimmune Pharmacology*, 7, 892-903.
- SHIN, I., YAKES, F. M., ROJO, F., SHIN, N.-Y., BAKIN, A. V., BASELGA, J. & ARTEAGA, C. L. 2002. PKB/Akt mediates cell-cycle progression by phosphorylation of p27Kip1 at threonine 157 and modulation of its cellular localization. *Nat Med*, 8, 1145-1152.
- SHINOZAKI, K., YOSHIDA, M., NAKAMURA, M., AIZAWA, S. & SUDA, Y. 2004. Emx1 and Emx2 cooperate in initial phase of archipallium development. *Mechanisms of Development*, 121, 475-489.
- SHTUTMAN, M., ZHURINSKY, J., SIMCHA, I., ALBANESE, C., D'AMICO, M., PESTELL, R. & BEN-ZE'EV, A. 1999. The cyclin D1 gene is a target of the  $\beta$ -catenin/LEF-1 pathway. *PNAS*, 96, 5522-5527.
- SIERRA, A., MARTÍN-SUÁREZ, S., VALCÁRCEL-MARTÍN, R., PASCUAL-BRAZO, J., AELVOET, S.-A., ABIEGA, O. & ENCINAS, J. M. 2015. Neuronal Hyperactivity Accelerates Depletion of Neural Stem Cells and Impairs Hippocampal Neurogenesis. *Cell Stem Cell*, 16, 488-503.
- SMITH, E. J., LEONE, G., DEGREGORI, J., JAKOI, L. & NEVINS, J. R. 1996. The accumulation of an E2F-p130 transcriptional repressor distinguishes a G0 cell state from a G1 cell state. *Molecular and Cellular Biology*, 16, 6965-76.
- SNOOK, A. & WALDMAN, S. 2013. Advances in Cancer Immunotherapy. *Discovery Medicine*, 15, 120-125.
- STEGEMAN, S., JOLLY, L. A., PREMARATHNE, S., GECZ, J., RICHARDS, L. J., MACKAY-SIM, A. & WOOD, S. A. 2013. Loss of Usp9x Disrupts Cortical Architecture, Hippocampal Development and TGF $\beta$ -Mediated Axonogenesis. *PLoS ONE*, 8, e68287.
- STRAUSS, R., HAMERLIK, P., LIEBER, A. & BARTEK, J. 2012. Regulation of Stem Cell Plasticity: Mechanisms and Relevance to Tissue Biology and Cancer. *Mol Ther*, 20, 887-897.
- STUPP, R., MASON, W., BENT, M., WELLER, M., FISHER, B., TAPHOORN, M., BELANGER, K., BRANDES, A., MAROSI, C., BOGDAHN, U., CURSCHMANN, J., JANZER, R., LUDWIN, S., GORLIA, T., ALLGEIER, A., LACOMBE, D., CAIRNCROSS, G., EISENHAUR, E., MIRIMANOFF, R. 2005. Radiotherapy plus Concomitant and Adjuvant Temozolomide for Glioblastoma. *New England Journal of Medicine*, 352, 987-986.
- SUN, H., KAPURIA, V., PETERSON, L. F., FANG, D., BORNMANN, W. G., BARTHOLOMEUSZ, G., TALPAZ, M. & DONATO, N. J. 2011. Bcr-Abl ubiquitination and

- Usp9x inhibition block kinase signaling and promote CML cell apoptosis. *Blood*, blood-2010-03-276477.
- TAKAHASHI, T., NOWAKOWSKI, R. S. & CAVINESS, V. S. 1995. The cell cycle of the pseudostratified ventricular epithelium of the embryonic murine cerebral wall. *J. Neurosci*, 15, 6046-6057.
- TAKANAGA, H., TSUCHIDA-STRAETEN, N., NISHIDE, K., WATANABE, A., ABURATANI, H. & KONDO, T. 2009. Gli2 Is a Novel Regulator of Sox2 Expression in Telencephalic Neuroepithelial Cells. *STEM CELLS*, 27, 165-174.
- TAMAI, H., SHINOHARA, H., MIYATA, T., SAITO, K., NISHIZAWA, Y., NOMURA, T. & OSUMI, N. 2007. Pax6 transcription factor is required for the interkinetic nuclear movement of neuroepithelial cells. *Genes to Cells*, 12, 983-996.
- TANG, P., GAO, C., LI, A., ASTER, J., SUN, L. & CHAI, L. 2013. Differential roles of Kras and Pten in murine leukemogenesis. *Leukemia*, 27, 1210-1214.
- TAURIELLO, D. V. & MAURICE, M. M. 2010. The various roles of ubiquitin in Wnt pathway regulation. *Cell Cycle*, 9, 3700-9.
- TAY, D. L., BHATHAL, P. S. & FOX, R. M. 1991. Quantitation of G0 and G1 phase cells in primary carcinomas. Antibody to M1 subunit of ribonucleotide reductase shows G1 phase restriction point block. *The Journal of Clinical Investigation*, 87, 519-527.
- TAYA, S., YAMAMOTO, T., KANAI-AZUMA, M., WOOD, S. A. & KAIBUCHI, K. 1999. The deubiquitinating enzyme Fam interacts with and stabilizes  $\beta$ -catenin. *Genes to Cells*, 4, 757-767.
- THE CANCER GENOME ATLAS RESEARCH, N. 2008. Comprehensive genomic characterization defines human glioblastoma genes and core pathways. *Nature*, 455, 1061-1068.
- TOHYAMA, T., LEE, V., RORKE, L., MARVIN, M., MCKAY, R. & TROJANOWSKI, J. 1992. Nestin expression in embryonic human neuroepithelium and in human neuroepithelial tumor cells. *Lab Invest*, 66, 303-13.
- TOUIL, Y., ZULIANI, T., WOLOWCZUK, I., KURANDA, K., PROCHAZKOVA, J., ANDRIEUX, J., LE ROY, H., MORTIER, L., VANDOMME, J., JOUY, N., MASSELOT, B., SÉGARD, P., QUESNEL, B., FORMSTECHE, P. & POLAKOWSKA, R. 2013. The PI3K/AKT Signaling Pathway Controls the Quiescence of the Low-Rhodamine123-Retention Cell Compartment Enriched for Melanoma Stem Cell Activity. *Stem Cells*, N/A-N/A.
- TRIVIGNO, D., ESSMANN, F., HUBER, S. & RUDNER, J. 2012. Deubiquitinase USP9x confers radioresistance through stabilization of Mcl-1. *Neoplasia*, 14, 893-904.
- TUVESON, D. A., SHAW, A. T., WILLIS, N. A., SILVER, D. P., JACKSON, E. L., CHANG, S., MERCER, K. L., GROCHOW, R., HOCK, H., CROWLEY, D., HINGORANI, S. R., ZAKS, T., KING, C., JACOBETZ, M. A., WANG, L., BRONSON, R. T., ORKIN, S. H., DEPINHO, R. A. & JACKS, T. 2004. Endogenous oncogenic K-rasG12D stimulates proliferation and widespread neoplastic and developmental defects. *Cancer Cell*, 5, 375-387.
- UEKI, K., ONO, Y., HENSON, J. W., EFIRD, J. T., VON DEIMLING, A. & LOUIS, D. N. 1996. CDKN2/p16 or RB Alterations Occur in the Majority of Glioblastomas and Are Inversely Correlated. *Cancer Research*, 56, 150-153.
- UHRBOM, L., KASTEMAR, M., JOHANSSON, F. K., WESTERMARK, B. & HOLLAND, E. C. 2005. Cell Type-Specific Tumor Suppression by Ink4a and Arf in Kras-Induced Mouse Gliomagenesis. *Cancer Research*, 65, 2065-2069.
- VAN HOOFF, D., PASSIER, R., WARD-VAN OOSTWAARD, D., PINKSE, M. W. H., HECK, A. J. R., MUMMERY, C. L. & KRIJGSVELD, J. 2006. A Quest for Human and Mouse Embryonic Stem Cell-specific Proteins. *Molecular & Cellular Proteomics*, 5, 1261-1273.
- VARA, J. Á. F., CASADO, E., DE CASTRO, J., CEJAS, P., BELDA-INIESTA, C. & GONZÁLEZ-BARÓN, M. 2004. PI3K/Akt signalling pathway and cancer. *Cancer Treatment Reviews*, 30, 193-204.
- VAULEON E, A. T., COLLET B, MOSSER J, QUILLIEN V 2010. Overview of Cellular Immunotherapy for Patients with Glioblastoma. *Clinical and Developmental Immunology*, 2010.

- VAULEON, E., AVRIL, T., COLLET, B., MOSSER, J. & QUILLIEN, V. 2010. Overview of Cellular Immunotherapy for Patients with Glioblastoma. *Clinical and Developmental Immunology*, 2010, 689171.
- VERHAAK, R. G. W., HOADLEY, K. A., PURDOM, E., WANG, V., QI, Y., WILKERSON, M. D., MILLER, C. R., DING, L., GOLUB, T., MESIROV, J. P., ALEXE, G., LAWRENCE, M., O'KELLY, M., TAMAYO, P., WEIR, B. A., GABRIEL, S., WINCKLER, W., GUPTA, S., JAKKULA, L., FEILER, H. S., HODGSON, J. G., JAMES, C. D., SARKARIA, J. N., BRENNAN, C., KAHN, A., SPELLMAN, P. T., WILSON, R. K., SPEED, T. P., GRAY, J. W., MEYERSON, M., GETZ, G., PEROU, C. M. & HAYES, D. N. 2010. Integrated Genomic Analysis Identifies Clinically Relevant Subtypes of Glioblastoma Characterized by Abnormalities in PDGFRA, IDH1, EGFR, and NF1. *Cancer Cell*, 17, 98-110.
- VIGLIETTO, G., MOTTI, M. L., BRUNI, P., MELILLO, R. M., D'ALESSIO, A., CALIFANO, D., VINCI, F., CHIAPPETTA, G., TSICHLIS, P., BELLACOSA, A., FUSCO, A. & SANTORO, M. 2002. Cytoplasmic relocalization and inhibition of the cyclin-dependent kinase inhibitor p27Kip1 by PKB/Akt-mediated phosphorylation in breast cancer. *Nat Med*, 8, 1136-1144.
- VLACHOSTERGIOS, P. J., VOUTSADAKIS, I. A. & PAPANDREOU, C. N. 2012. The ubiquitin-proteasome system in glioma cell cycle control. *Cell Division*, 7, 18-18.
- VOSKAS, D., LING, L. S. & WOODGETT, J. R. 2010. Does GSK-3 provide a shortcut for PI3K activation of Wnt signalling? *F1000 biology reports*, 2, 82.
- WALDAU, B. & SHETTY, A. K. 2008. Behaviour of neural stem cells in Alzheimer brain. *Cell Mol Life*, 65, 2372-2384.
- WANG, J., WANG, Q., CUI, Y., LIU, Z., ZHAO, W., WANG, C., DONG, Y., HOU, L., HU, G., LUO, C., CHEN, J. & LU, Y. 2012. Knockdown of cyclin D1 inhibits proliferation, induces apoptosis, and attenuates the invasive capacity of human glioblastoma cells. *Journal of Neuro-Oncology*, 106, 473-484.
- WANG, M., PANASYUK, G., GWALTER, J., NEMAZANY, I., FENTON, T., FILONENKO, V. & GOUT, I. 2008. Regulation of ribosomal S6 kinases by ubiquitylation. *Biochemical and Biophysical Research Communications*, 369, 382-387.
- WANG, Q., VON, T., BRONSON, R., RUAN, M., MU, W., HUANG, A., MAIRA, S.-M. & ZHAO, J. J. 2013. Spatially distinct roles of class Ia PI3K isoforms in the development and maintenance of PTEN hamartoma tumor syndrome. *Genes & Development*, 27, 1568-1580.
- WANG, S. I., PUC, J., LI, J., BRUCE, J. N., CAIRNS, P., SIDRANSKY, D. & PARSONS, R. 1997. Somatic Mutations of PTEN in Glioblastoma Multiforme. *Cancer Research*, 57, 4183-4186.
- WARD, A. F., BRAUN, B. S. & SHANNON, K. M. 2012. Targeting oncogenic Ras signaling in hematologic malignancies. *Blood*, 120, 3397-3406.
- WESTCOTT, P. & TO, M. 2013. The genetics and biology of KRAS in lung cancer. *Chinese Journal of Cancer*, 32, 63-70.
- WOLFF, N., VEGA-RUBIN-DE-CELIS, S., XIE, X., CASTRILLON, D., KABBANI, W. & BRUGAROLAS, J. 2011. Cell-type-dependent regulation of mTORC1 by REDD1 and the Tumor Suppressors TSC1/TSC2 and LKB1 in response to Hypoxia. *Molecular and Cellular Biology*, 31.
- WOOD, S. A., PASCOE, W. S., RU, K., YAMADA, T., HIRCHENHAIN, J., KEMLER, R. & MATTICK, J. S. 1997. Cloning and expression analysis of a novel mouse gene with sequence similarity to the Drosophila fat facets gene. *Mechanisms of Development*, 63, 29-38.
- WU, Y. & ZHOU, B. P. 2007. Kinases meet at TSC. *Cell Res*, 17, 971-973.
- XIE, Y., AVELLO, M., SCHIRLE, M., WHINNIE, E. M., FENG, Y., BRIC-FURLONG, E., WILSON, C., NATHANS, R., ZHANG, J., KIRSCHNER, M. W., HUANG, S.-M. A. & CONG, F. 2012. Deubiquitinase FAM/USP9X interacts with the E3 ubiquitin ligase SMURF1 and protects it from ligase activity-dependent self-degradation. *Journal of Biological Chemistry*.
- XIONG, F., GAO, H., ZHEN, Y., CHEN, X., LIN, W., SHEN, J., YAN, Y., WANG, X., LIU, M. & GAO, Y. 2011. Optimal time for passaging neurospheres based on primary neural stem cell cultures. *Cytotechnology*, 63, 621-631.
- XU, X., STOCKHAMMER, F. & SCHMITT, M. 2012. Cellular-Based Immunotherapies for Patients with Glioblastoma Multiforme. *Clinical and Developmental Immunology*, 2012, 764213.

- YAMADA, D., HOSHII, T., TANAKA, S., HEGAZY, A. M., KOBAYASHI, M., TADOKORO, Y., OHTA, K., UENO, M., ALI, M. A. E. & HIRAO, A. 2014. Loss of Tsc1 accelerates malignant gliomagenesis when combined with oncogenic signals. *Journal of Biochemistry*, 155, 227-233.
- YAMAZAKI, S., IWAMA, A., TAKAYANAGI, S.-I., ETO, K., EMA, H. & NAKAUCHI, H. 2009. TGF- $\beta$  as a candidate bone marrow niche signal to induce hematopoietic stem cell hibernation. *Blood*, 113, 1250-1256.
- YUAN, X., CURTIN, J., XIONG, Y., LIU, G., WASCHSMANN-HOGIU, S., FARKAS, D. L., BLACK, K. L. & YU, J. S. 2004. Isolation of cancer stem cells from adult glioblastoma multiforme. *Oncogene*, 23, 9392-9400.
- ZANNI, G., MARTINO, E., OMELIANENKO, A., ANDÄNG, M., DELLE, U., ELMROTH, K. & BLOMGREN, K. 2015. Lithium increases proliferation of hippocampal neural stem/progenitor cells and rescues irradiation-induced cell cycle arrest in vitro. *Oncotarget*.
- ZHANG, J., GRINDLEY, J. C., YIN, T., JAYASINGHE, S., HE, X. C., ROSS, J. T., HAUG, J. S., RUPP, D., PORTER-WESTPFAHL, K. S., WIEDEMANN, L. M., WU, H. & LI, L. 2006. PTEN maintains haematopoietic stem cells and acts in lineage choice and leukaemia prevention. *Nature*, 441, 518-522.
- ZHOU, B. P., LIAO, Y., XIA, W., SPOHN, B., LEE, M.-H. & HUNG, M.-C. 2001. Cytoplasmic localization of p21Cip1/WAF1 by Akt-induced phosphorylation in HER-2/neu-overexpressing cells. *Nat Cell Biol*, 3, 245-252.
- ZOHRABIAN, V. M., FORZANI, B., CHAU, Z., MURALI, R. & JHANWAR-UNIYAL, M. 2009. Rho/ROCK and MAPK Signaling Pathways Are Involved in Glioblastoma Cell Migration and Proliferation. *Anticancer Research*, 29, 119-123.